Doctoral Dissertation
Doctoral Program in Civil and Environmental Engineering (38th Cycle)

Identification of nonlinear and time-varying systems under dynamic and seismic excitation

Linda Scussolini
* * * * * *

Supervisors
Prof. Rosario Ceravolo, Supervisor
Prof. Giuseppe Andrea Ferro, Co-Supervisor

Doctoral Examination Committee:
Prof. Anatoliy Bovsunovsky, National Technical University of Ukraine 'Igor Sikorsky Kyiv Polytechnic Institute'
Prof. Martin Dalgaard Ulriksen, Aarhus University
Prof. Luis David Avendaño-Valencia, University of Southern Denmark

Politecnico di Torino
2026

I hereby declare that, the contents and organisation of this dissertation constitute my own original work and does not compromise in any way the rights of third parties, including those relating to the security of personal data.

…….....
Linda Scussolini
Turin, January 31, 2026

Abstract

Over the last decades, a change of paradigm toward advanced numerical simulations and virtual prototyping has encouraged the exploration of nonlinear techniques for system identification (SI). In its broadest sense, nonlinear SI concerns the determination of nonlinear models by combining information from data with those coming from a priori knowledge of the system. In structural applications, systems inherently exhibit nonlinear behaviour due to the presence of elements such as joints, innovative energy absorption devices, and degrading components, whose behaviour can be difficult to predict, understand, and monitor. In that case, nonlinear SI plays a significant role for understanding the structural response and can achieve high levels of efficiency with reduced computational effort if the identification problem is properly constructed by considering convenient variables and relationships. Despite this potential, the modelling and identification of nonlinear behaviour of structures under seismic, or more generally, dynamic excitation is still an open issue to date, mainly due to the complexity of model formulation and parameter definition.

The present thesis addresses these issues by developing and applying instantaneous identification tools for the characterisation of nonlinear and time-varying dynamical systems. The proposed approaches aim at estimating nonlinear parameters from non-stationary responses by exploiting the time localisation of spectral components, thus extending the concept of local stationarity to nonlinear and time-varying dynamical systems. While the first part of the thesis introduces the problem of identifying nonlinear and time-varying models in earthquake engineering and structural dynamics, the subsequent chapters propose novel methodologies, validated through numerical benchmarks and experimental testing on nonlinear dynamical systems.

The main original contributions of this thesis can be summarised as follows: (i) an instantaneous identification method for nonlinear and time-varying

structural systems under random excitation is formulated using Volterra-based modelling and linear time-frequency representations and validated numerically on Duffing-type systems; (ii) the energetic nature of quadratic time-frequency transforms, in particular the Wigner-Ville distribution, is exploited in combination with perturbative Volterra approaches to generalise the identification problem to markedly non-stationary responses, including those typical of bistable dynamics; (iii) experimental identification is carried out on a bistable seismic energy dissipation device using a dedicated prototype testing machine and instantaneous probabilistic formulations under both perfectly elastic and Bouc-Wen modelling assumptions, demonstrating robust parameter estimation even at large response amplitudes.

The advantage of these methods is twofold. On the one hand, they provide practical and easily scalable tools to identify nonlinear parameters from non-stationary data. On the other, they can be directly combined with efficient and specifically designed experimental tests, allowing reliable characterisation of structural behaviour under realistic conditions.

Acknowledgements

My deepest gratitude goes to my supervisor, Prof. Rosario Ceravolo, for his patient guidance during these years, both on a scientific and human level. I would also like to thank my co-supervisor, Prof. Giuseppe Ferro, for his support throughout this path. I am profoundly grateful to Prof. Giuseppe Abbiati for hosting me at Aarhus University during my PhD. Those months of inspiring discussions and invaluable advice have been of paramount importance for my research. A special thanks goes to Prof. Andrea De Marchi for his indispensable support with experiments, which were fundamental to this thesis work. Finally, a huge thank you goes to Gaetano, Giorgia, and Stefania, who have provided constant support while sharing this journey with me from the very beginning, and to Valeria (my bistable counterpart), Alessio, and Cristian, who joined along the way: thank you for all the time shared together.

To conclude, I will switch to my mother tongue to address those closest to me. Mamma, ringraziarti per tutto sarebbe impossibile: in questi anni mi hai insegnato che la leggerezza non è mai una debolezza, ma un punto di forza. Sergio, grazie per essere il mio 'secondo papà'. Grazie a zio Rudy e a Valentina (con Gius), che in questi anni hanno sempre trovato il tempo per chiamarmi ogni sera per sapere come stessi. Grazie anche a Nicola, zio Ivano, zia Francesca, Chiara, e Vittoria: si dice che la famiglia non si possa scegliere, ma io non avrei potuto fare scelta migliore. La mia forza siete tutti voi.

Elisabetta, grazie per avermi camminato accanto in un altro capitolo della mia vita. Sei la certezza che per quanto la strada sia in salita, non dovrò mai percorrerla da sola (anche se con qualche lamentela). Grazie a Pietro, amico 'con la a maiuscola', da sempre.

Davide, tu sei il mio punto fermo. Grazie per il tuo supporto costante, in tutto, e la tua pazienza infinita, che mi hanno aiutato a non perdere mai di vista l'obiettivo. Un grazie enorme anche a Tiziana, Mario, e Chiara, per farmi sempre sentire a casa.

Infine, un pensiero va al mio papà: grazie per avermi insegnato a non avere paura di camminare '*sempre in direzione ostinata e contraria'*. Sei in ogni mio traguardo.

A mio papà

How to read this thesis

The thesis is structured as follows.

Chapter 1 introduces the reader to the definition and the role of system identification in structural dynamics, with particular attention on defining the motivations and challenges behind its nonlinear counterpart.

Chapter 2 presents an extensive overview of the nonlinear identification techniques and their different classifications.

Chapter 3 reports on identification techniques for signals whose statistical properties change over time and admitting a time-localisation of their spectral components. Limitations of existing identification strategies are also pointed out.

Chapter 4 proposes a novel identification technique based on the combination of a Volterra series approach with linear time-frequency transforms for time-varying systems under random excitation. This is benchmarked numerically on single- and multi-degree-of-freedom Duffing oscillators.

Chapter 5 employs a Wigner-Ville transform for the identification of a classical and bistable Duffing oscillator without relying on explicit analytical expressions, as done in Chapter 4. More specifically, the procedure proposed here exploits the energetic information coming from quadratic transforms for parameter estimation.

Chapter 6 exploits the bistable dynamics introduced in Chapter 5 for seismic energy absorption purposes. An instantaneous probabilistic identification technique is proposed for validating the experimental data gathered from a tailored prototype testing machine, also for dealing with uncertainties.

Chapter 7 extends the numerical investigation and experimental validation to the case of bistable systems presenting a not perfectly elastic behaviour by employing the prototype testing machine described in Chapter 6.

Contents

List of Tables

List of Figures

List of Acronyms

ABC	Approximate Bayesian computation
ALEs	Associated linear equations
ARMA	Autoregressive moving average
BBW	Bistable Bouc-Wen
CSB	Cosine-shaped beam
CRP	Conditioned reverse path
DoF	Degree-of-freedom
DPE	Direct parameter estimation
EnKF	Ensemble Kalman filter
EKF	Extended Kalman filter
FE	Finite element
FRF	Frequency response function
HFRF	Higher-order frequency response function
IRF	Impulse response function
KDE	Kernel density estimation
KF	Kalman filter
MCMC	Markov Chain Monte Carlo
MDoF	Multi-degrees-of-freedom
NARMAX	Nonlinear autoregressive moving average with exogenous input
NES	Nonlinear energy sink
NIFO	Nonlinear identification through feedback of the output
NNM	Nonlinear normal modes
PSD	Power spectral density
P-WVD	Pseudo Wigner-Ville distribution
RFS	Restoring force surface
RMSE	Root mean squared error
RP	Reverse path
SCAL	Scalogram
SDoF	Single-degree-of-freedom
SHM	Structural health monitoring
SI	System identification
SNR	Signal-to-noise ratio

SPEC	Spectrogram
STFT	Short-time Fourier transform
S-WVD	Smoothed pseudo-Wigner-Ville distribution
TF	Transfer function
TMD	Tuned mass damper
UKF	Unscented Kalman filter
WL	Window length
WT	Wavelet transform
WVD	Wigner-Ville distribution

Chapter 1

Nonlinear models in structural dynamics and earthquake engineering

1.1 Introduction

Although the concept of nonlinearity is nothing but a tautology, from a practical point of view, it implies the loss of the most important property of linear systems, namely the principle of superposition of effects. It is also true, however, that the variety of nonlinear behaviours makes it unfeasible to provide a single description encompassing all possible nonlinear systems (Worden, 2019).

The impossibility of formulating a unique definition of nonlinearity has important consequences. In particular, estimating the parameters describing a nonlinear behaviour is not a straightforward task, and the choice of an appropriate estimation technique is strictly case-dependent. While, in many cases, it is a convenient alternative to assume that a linear model is sufficient to describe the dynamic behaviour of a system, the fact remains that the world we live in is nonlinear and time-varying. Hence, the accurate identification of nonlinear, and eventually time-varying, behaviours in structural systems is of paramount importance, as it allows a more reliable prediction of how real-world structures behave when the nonlinearity is activated, e.g., when subject to extreme events such as earthquakes. This advances the field beyond the limitations of traditional linear models.

Focusing more on our field of investigation, a natural question arises: if linearisation often produces acceptable results, why are nonlinear models necessary in many structural engineering problems, particularly to interpret the

seismic response of structures? An equally natural answer is that strong earthquakes push buildings to their limits of resistance and deformability. Another reason can be found in the fact that it is precisely thanks to the nonlinearity of some elements, or anti-seismic devices, that structures resist earthquakes.

Some relevant examples of nonlinear behaviour can be found in structures having constraints with variable stiffness, materials, and devices with responses that depend on the magnitude of the stresses (e.g., vibration isolation components), and the presence of structural joints allowing relative movement between connected parts. Particularly, when subject to earthquakes, the presence of joints can lead to the phenomenon of seismic pounding. Indeed, during earthquakes, structural bodies separated by joints (e.g., adjacent structures, bridges) can exhibit out-of-phase vibrations. If the dynamic properties, such as fundamental frequencies, damping ratio, and lateral stiffness, of the parts composing the jointed systems are different, then the seismic pounding can be more pronounced (Anagnostopoulos, 1996).

Nonlinearity reveals itself in a series of characteristic phenomena, none of which can be interpreted using a linear model (Branstetter et al., 1988). The *bifurcation of equilibrium* (Pellicano and Vestroni, 2000), possibly linked to the onset of self-excited oscillations (Doelman and Verhulst, 1994), the appearance of higher harmonics, namely *super-harmonics*, and/or lower harmonics, namely *sub-harmonics* (Bovsunovsky and Surace, 2005), the transfer of energy from one mode of vibration to other modes (Romeo et al., 2015), the dependence of the steady-state response on initial conditions (Natsiavas, 1992), and chaotic vibrations (Chen and Dong, 1993; Mosekilde et al., 1988) are only some of the phenomena that find description and justification in the field of nonlinear dynamic systems theory. The number of publications related to nonlinear dynamics makes it impossible to provide an exhaustive list: a general and extended discussion of the theoretical aspects can be found in the classical books of (Drazin, 1992; Nayfeh and Mook, 1995; Thompson and Stewart, 2002).

The challenge in providing a unified definition of nonlinearity directly impact the so-called system identification (SI) process. Since the behaviour of a nonlinear system cannot be expressed as a simple combination of its inputs, traditional linear identification techniques are no longer applicable. This indicates that the identification task must explicitly consider the nonlinear nature of the system, requiring specific mathematical formulations and/or approaches. As a result, the parameter estimation process becomes problem-dependent and computationally demanding, making the identification of nonlinear systems a central and ongoing issue in structural dynamics, and consequently in the characterisation of structures subject to seismic motions. References to the nonlinear parameter identification task as well as basic methods (e.g., gradient-based methods, nonlinear filtering)

can be found in (Billings, 2013; Haber and Unbehauen, 1990; Kerschen et al., 2006; Noël and Kerschen, 2017; Schoukens and Ljung, 2019; Strejc, 1981).

Generally, dynamic identification consists of estimating the parameters of a structural model based on measurements of forcing and response (displacements, velocities, accelerations). In the case of nonlinear structures, this process requires a much larger amount of experimental data than that required for linear identification (Pearson, 1979). In structural engineering applications, however, this condition is difficult to meet, especially when tests must be performed in situ. Since it is rarely possible to interrupt the operation of the structure (as in the case of railway or motorway bridges, for example), testing must be carried out in a short time frame, which is often insufficient to collect an adequate amount of data for nonlinear identification. In addition, there are economic considerations that influence the planning of monitoring activities and the timing of tests.

The excitation conditions of the structure represent a further discriminating factor in dynamic identification procedures. The choice between using known forcing functions and analysing the response due to environmental excitations (such as traffic or wind) depends on the state of conservation of the structure, as well as on the level of accessibility and the possibilities for installing the instrumentation. In the case of nonlinear structures, it is common to use known deterministic (e.g. stepped-sine tests) or stochastic forcing functions. In both cases, the vibration of the structure must be analysed across a wide range of operating conditions, as the excitation level above which nonlinearity becomes observable is not known a priori.

1.2 System identification: definition and objectives

Generally, SI can be defined as the research domain where models are fitted into measured data (Ljung, 1987) and takes shape as the treatment of the second-order inverse problem (Tarantola, 2005). In structural dynamics, the SI problem resolution amounts to the dynamical parameters estimation of a structure based on input and/or output measurements (e.g., displacements, velocities, accelerations), acquired through sensing devices (Ewins, 2009; Maia and Montalvão e Silva, 1997). The possibility of correctly identifying the parameters of the structure and the estimation reliability strongly depend on the quantity and quality of the available experimental data.

The process of dynamic SI is characterised by four basic ingredients (Ljung, 1998): (i) design of experimental setup and experimental signals acquisition; (ii) hypothesis on the model for the description of the system dynamics; (iii) signal processing and parameter estimation; (iv) validation and choice of the most suitable model for the description of the input/output relationship.

The third aspect, i.e., parameter estimation, applied to nonlinear systems, is the main focus of this thesis work. For what concerns linear systems, the techniques employed for parameter estimation are numerous, and usually classified based on the domain they are performed in (Ljung, 2004): *time-domain* (Ibrahim and Mikulcik, 1977; Juang and Pappa, 1984; Overschee and de Moor, 1996; Petsounis and Fassois, 2001) and *frequency-domain* (Brincker et al., 2001; Pintelon and Schoukens, 2012; Richardson and Formenti, 1982). A third joint domain is given by the *time-frequency domain* (Bonato et al., 2000; Kijewski-Correa, 2003; Nagarajaiah and Basu, 2009; Perez-Ramirez et al., 2016). On the other hand, they can be grouped into direct methods, if the matrices of the system model are identified, and indirect if the modal parameters are estimated based on the frequency response function (FRF) (Maia and Montalvão e Silva, 1997). Another typical classification is based on the number of input channels, i.e., type of excitation used, and output channels, i.e., number of sensors available (Reynders, 2012).

In the case of indirect methods, the identification results, usually depicted in terms of natural frequencies, mode shapes, and damping ratios, can be employed for the calibration of models to reflect the identified modal parameters for other scopes (Mottershead and Friswell, 1993; Sinha and Friswell, 2002). Dynamic SI is especially valuable for the monitoring, diagnosis, and control of civil structures (Ormando et al., 2021). Indeed, the experimental data obtained from dynamic testing can be employed to calibrate numerical models, such as surrogate or finite element (FE) models, predict the response under dynamic loading, assess the overall safety conditions of the structure, and design control systems to enhance the structural response under extreme excitations, such as earthquakes. Frequently, these objectives are not independent of each other, but are intertwined, as they are not mutually exclusive.

In particular, a comprehensive number of applications of linear SI to existing civil structures can be found, with the final aim of: (i) understanding their structural behaviour, by recording the phenomena that may influence it (Gentile et al., 2019); (ii) assessing the efficacy of structural or seismic interventions, by comparing the dynamic properties, i.e., natural frequencies and mode shapes, before and after structural restoration works, and planning new strengthening and retrofitting interventions (Bayraktar et al., 2018); (iii) monitoring the evolution of potential damage (Gres et al., 2018; Sarhosis et al., 2021) and the effect of human and/or environmental phenomena (Ceravolo et al., 2021).

Evaluation of the structural behaviour

One of the first objectives following the SI task is the evaluation of the structural behaviour under static and dynamic conditions. This objective is twofold. On the one hand, it allows the validation of the global features or modes

of the structure; on the other, it permits the understanding of some local behaviours, including high order vibration modes, which sometimes are the sentinel for the presence of damage or anomalies in structure.

An interesting example of structural diagnosis is given by the bell tower of the dome of Fossano (Ceravolo et al., 2016). The bell tower has been subject to a one-time dynamic identification campaign during September 2011, which allowed the successful identification of the vibration modes of the structures, confirming the presence of two translational modes and one torsional mode as global ones. A mechanical model was then built and experimentally calibrated on the basis of the SI results. Bi-dimensional elements, i.e., shell elements, were employed to perform the mesh. The structure was assumed to be fixed at the base, and soil-structure interaction was neglected. More importantly for this discussion, the experimentally calibrated mechanical values of material properties highlighted a substantial difference in the quality of the material on the different levels of the bell tower. The bell tower as well as the calibrated FE model with the corresponding values of elastic modulus are reported in Figure 1.1.

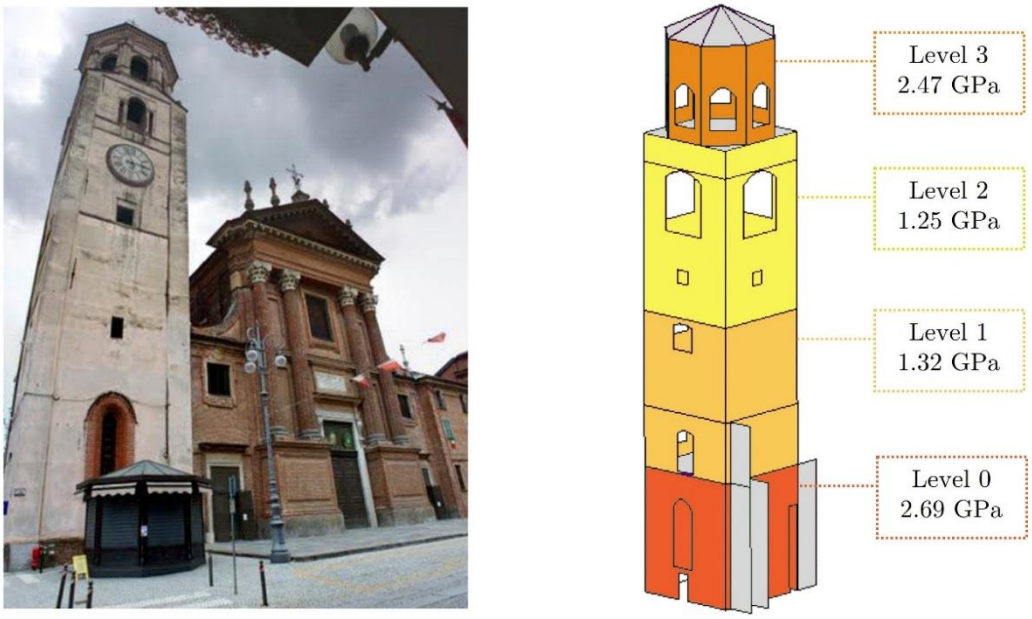

Figure 1.1. Fossano bell tower: (a) picture of the bell tower and (b) FE model calibrated experimentally on the basis of SI results (Ceravolo et al., 2016).

The heterogeneity within the elastic modulus values along the different macro-elements of the structure provided a suggestion on the presence of anomalies affecting structural behaviour, such as local weakening in the connections and cracks. In particular, the experimentally calibrated FE model highlighted the presence of some local modes between 5-10 Hz involving the bulging of masonry at the middle and higher levels of the tower. These local modes are depicted in Figure 1.2. As a result, and in conjunction with core sampling carried out at various levels of the bell tower, it was concluded that the

material deteriorated as the level of the bell tower increased. This ultimately led to the installation of a temporary intervention, which, also following a more recent long-term monitoring campaign, proved effective for the last decade.

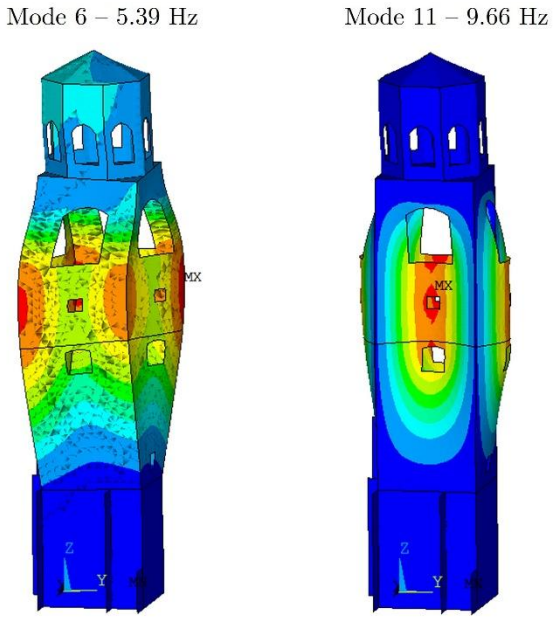

Figure 1.2. Local modes of Fossano bell tower (Ceravolo et al., 2016).

Design and/or assessment of seismic improvement intervention

The models calibrated using data from SI can be employed for the design and/or the assessments of seismic improvement interventions on structures. One very recent example is given by the Church of Santa Maria delle Grazie, better known as Santa Caterina, in Casale Monferrato (AL), which represents one of the most important examples of baroque religious architecture of its territory. The church was subject to several dynamic campaigns with the aim of identifying its modal properties. A first extensive testing campaign took place in September 2010 (Ceravolo et al., 2016). This led to the experimental calibration of a FE model, as in the case of Fossano bell tower. In particular, the experimentally calibrated FE model showed that the second and third vibration modes, instead of involving the whole structure, were mainly characterised by local mechanisms involving the cantilever façade and the lantern. This, combined with thorough visual inspections and a preliminary definition of the crack pattern, allowed the recognition of these two components as distinct vulnerable elements. Based on these results, two different interventions were planned, designed, and built. Going into greater detail, in the case of the facade, the intervention consisted in a metal frame properly connected to the tympanum. Conversely, in the case of the lantern, the intervention consisted of sixteen *L*-shaped profiles along the columns, aligned with the interior corners of the windows. Figure 1.3 shows a global view of the church of Santa Caterina as well as the interventions on the lantern and on the façade.

(a) (b) (c)

Figure 1.3. Church of Santa Caterina: (a) global view, (b) intervention on the lantern, and (c) intervention of the façade.

A further experimental campaign, carried out in December 2022, allowed the assessment of the seismic improvement interventions (Ceravolo et al., 2024). The subsequent calibration of the model with the two interventions implemented showed that the vibrations modes did not change remarkably after the strengthening of the vulnerable portions of the church, due to the fact that they do not directly affect the mass and/or the stiffness of the church. More interestingly, an additional mode at 3.88 Hz was detected on the model with the interventions. The interventions were removed to confirm their impact on the structural response. This situation is depicted in Figure 1.4. In such case that mode corresponds to the first numerical mode of the model (i.e., the mode at 2.87 Hz, which is lower than the frequency corresponding to the first global mode), while in the case of the model with the interventions implemented, it corresponds to the third numerical mode.

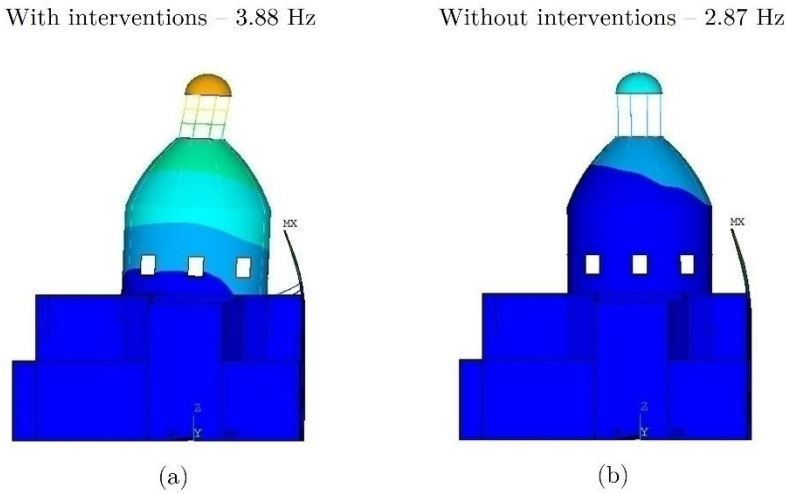

(a) (b)

Figure 1.4. (a) Additional mode at 3.88 Hz on the model with interventions and (b) verification on the church with intervention removed (Ceravolo et al., 2024).

Diagnosis of structural anomalies and damage

A third objective associated with SI is to determine the most damage-sensitive features of a structure, which allow to clearly detect anomalies in the structure and to assess its health state. If this task is integrated in long-term monitoring systems, it also allows the detection of damage before and after extreme events, such as earthquakes. This is the case of the Arena of Verona, permanently monitored during the Emilia earthquake of 2012 (Lorenzoni et al., 2013). Figure 1.5 shows the Arena of Verona as well as the sensors layout employed for the experimental modal analysis with the earthquake base acceleration as external excitation.

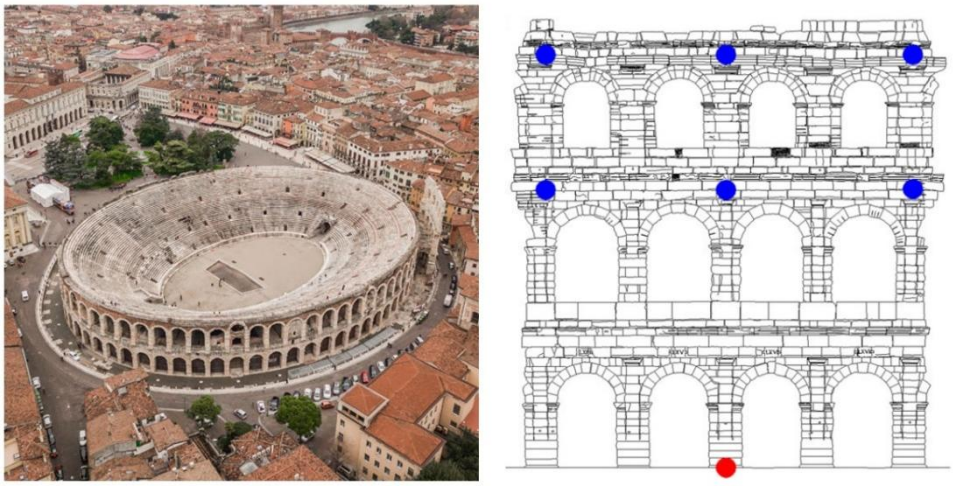

(a) (b)

Figure 1.5. Arena of Verona: (a) aerial view and (b) location of the input and output channels (in red and blue, respectively) employed for SI during the 2012 earthquake (Lorenzoni et al., 2013).

The characterisation of a structure requires a thorough analysis of the dynamic response both under operating conditions and during earthquakes, as high-amplitude vibrations can significantly affect the behaviour of the structure. In the case of the Arena of Verona, the comparison of measurements taken before and after the earthquake showed a slight decrease in frequencies, not associated with visible structural damage, as also confirmed by post-earthquake inspections. This reduction was attributed to a change in the interaction between the stone blocks and thus a slightly nonlinear behaviour of the structure, resulting in small permanent residual deformations (Lorenzoni et al., 2013).

1.3 From linear to nonlinear: motivations and challenges

Despite the several advantages of linear SI, as observed in the case of the Arena of Verona, even slight nonlinearities can affect the fundamental dynamic properties of a structure, i.e., natural frequencies and damping ratios, revealing the limitations of purely linear identification approaches, as they cannot describe more complex dynamic phenomena (e.g., contact interactions, monolater behaviours, plasticisation, buckling, etc.). In order to take into account these

phenomena, one should add nonlinear terms to the model employed for SI (Sjöberg et al., 1995). Nevertheless, finding a mathematical model which could predict the behaviour of a nonlinear system implies two main issues (Hong et al., 2008): (i) the determination of the model structure which describes the input-output relationship is often not unique; (ii) the estimation of the parameters of the model structure is not trivial, and requires high computational effort.

In the case of existing buildings, a fundamental aspect is given by the definition of a target knowledge level, related to the availability of information on the considered structure, e.g., geometric and material characteristics (Binda et al., 2000; Ceravolo et al., 2019). From a practical perspective, this intuitively implies that the number of parameters to be estimated in the SI task should increase according to the desired knowledge level. Depending on that, one may decide to evaluate the fundamental frequencies only, or the complete modal model of structure, or, finally, the nonlinear behaviour. However, the parameters estimated are usually linear, thus leading to a linear model. Afterwards, the linear model is employed as a basis for further analyses (such as static and dynamic nonlinear analyses), see for instance (D'Ambrisi et al., 2012), without considering nonlinearity as an intrinsic property of the model employed for SI. Therefore, the presence of nonlinear terms is not usually concerned for SI of existing structures.

Besides the elevated computational complexity, the lack of consideration of nonlinear terms in the SI process is also due to the fact that structural responses are often approximately linear under operational conditions (Lorenzoni et al., 2013), unless of environmental effects which can be removed with dedicated tools (Sohn, 2007). To appreciate nonlinear effects, it would be necessary to resort to forced tests, capable of stressing the structure at higher excitation levels. Nevertheless, in order to observe the symptoms of nonlinearity in the response, it is necessary to achieve excitation amplitudes that are difficult to obtain under real operating conditions. Consequently, applications on full-scale structures that take nonlinearity into account are still limited to the analysis and simulation of the response to strong natural excitations.

In order to analyse nonlinearity, one may exploit data from structures under seismic excitations. This could happen on structures subject to a long-term monitoring, as seen for the Arena of Verona, which is crucial for assessing the structural health and ensuring the preservation of a structure, but also to acquire data under different types of excitations, rather than ambient vibrations. One example is given by the town hall of Pizzoli, subject to a permanent monitoring system. The building is part of the Italian Seismic Observatory of Structures (Cattari et al., 2019; Ceravolo et al., 2017; Sivori et al., 2025; Spina et al., 2011). The monitoring system recorded the seismic response and input during some seismic events. In particular, the building experienced significant damage from an October 2016 event and a subsequent one in January 2017. These data were used

in a nonlinear identification task (Ceravolo et al., 2020; Miraglia et al., 2020). The building, depicted in Figure 1.6(a), exhibited a global box-like behaviour, also confirmed by on-site inspections that verified good connections between walls and floor-walls before the seismic events, and from previous analyses on a linearly calibrated model. This allowed an important simplification of the building into a two degrees-of-freedom system, as shown in Figure 1.6(b). Specifically, this was achieved by using the acceleration recordings from channels 4, 10, 15, 5, 11, and 16, as they were considered most representative of the floor behaviour.

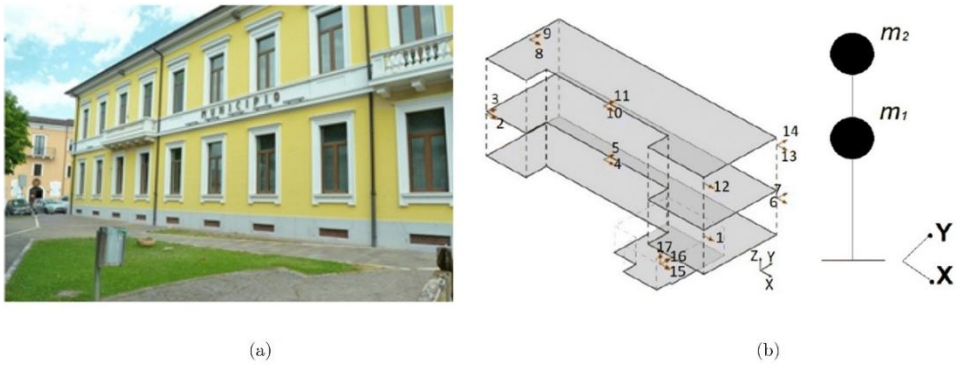

Figure 1.6. Pizzoli town hall: (a) view of the building and (b) schematic of the sensors with the associated simplified model (Miraglia et al., 2020).

Another example of application of nonlinear identification is given by the Vincent Thomas bridge, a major transportation connection located in San Pedro, California. It is a cable-suspension bridge, completed in 1964, and extensively instrumented in 1980 with 26 accelerometers, as depicted in Figure 1.7.

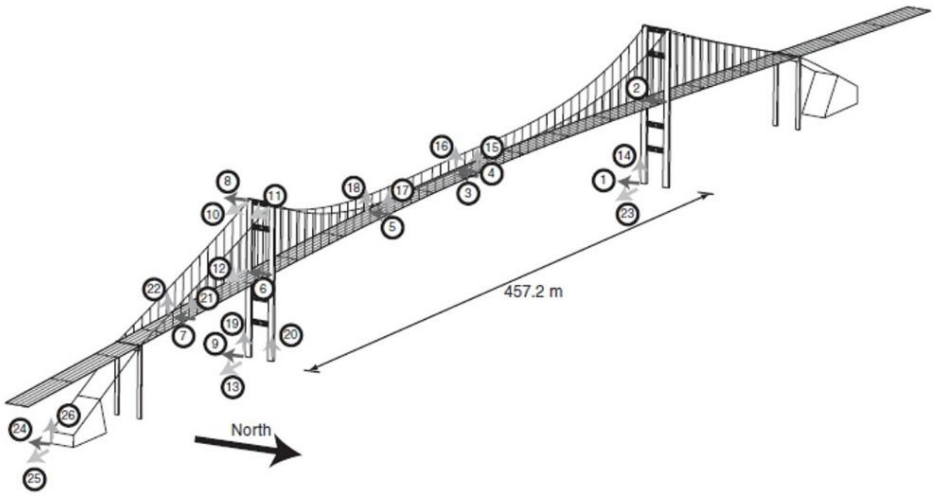

Figure 1.7. Vincent Thomas bridge: locations of the accelerometers (Smyth et al., 2003).

Owing to this extensive instrumentation, the bridge has been the object of several linear SI campaigns, see for instance (He et al., 2008; Luş et al., 1999). Recently, an investigation on a passive control system effectiveness on the same bridge has been performed (Haseli et al., 2023). More importantly for this thesis

work, Smyth et al. proposed a combined linear and nonlinear identification task on the same bridge (Smyth et al., 2003). The authors exploited two seismic events occurred between 1985 and 2000, namely, the Whittier-Narrows earthquake of 1987, and the Northridge earthquake of 1994. As main result, they observed the presence of residual components in the measured response when compared to the one estimated using a linear SI procedure. They concluded that the latter where attributable to some unmodelled linear dynamics and/or measurement noise.

These examples have in common the implementation of a monitoring system during extreme events. Nonetheless, the adoption of such systems necessitates a thorough evaluation of the costs involved, since it requires a significant number of resources, both in economic terms and in terms of the expertise needed for their management and maintenance. Thus, not many structures are permanently monitored, complicating the acquisition of data under seismic excitation for existing structures. Conventionally, laboratory-controlled tests are preferred to simulate real-world scenarios of nonlinearities.

1.4 The route of nonlinear system identification

The previous section reported only some of the reasons why the analysis of structures through nonlinear identification techniques in earthquake engineering and dynamics constitutes a specific sector. In order to accomplish this task, specific models and techniques should be employed, more demanding than linear ones. In general, nonlinear system identification can be described as a route, with three main steps to accomplish (Kerschen et al., 2006), as described by Figure 1.8. While the final step involves determining the model parameters from the data collected from experiments or numerical simulations, the first two steps can be handled using specific techniques or prior system knowledge.

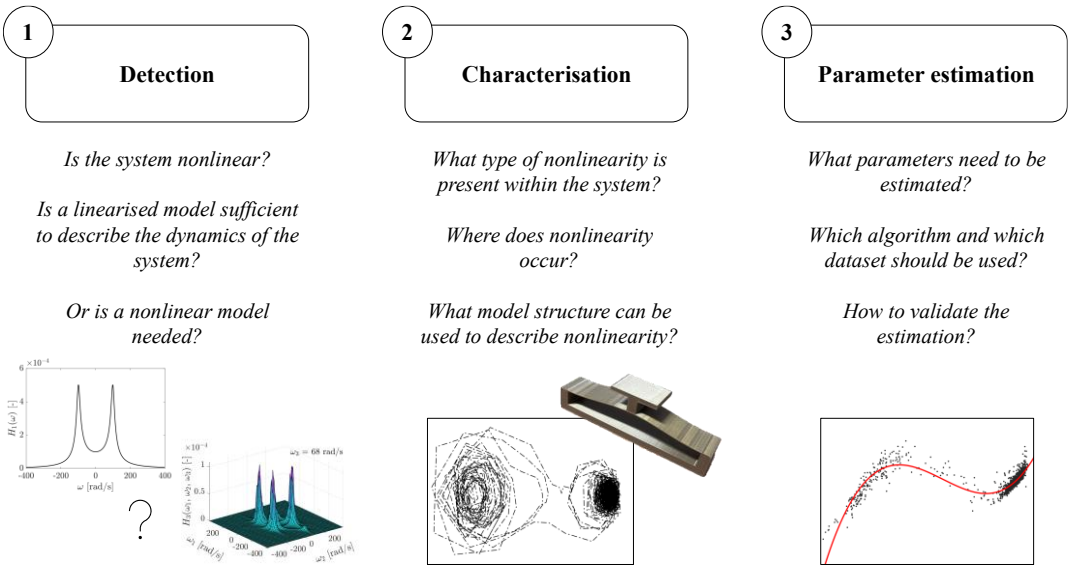

Figure 1.8. Nonlinear identification route.

1.4.1 Detection

The *detection* step involves nonlinearity testing, by answering the following questions:

- Is the system nonlinear?
- Do I need a nonlinear model, or a linearised one is enough?

To obtain a proper answer, one may first define what does *nonlinear* mean. As a first tentative, one may refer to the definition introduced at the beginning of this thesis, according to which a nonlinear system is a system that does not respect the superposition principle. From a practical point of view, however, this definition provides little help in identifying whether a system should be modelled in a linear or nonlinear manner, making it necessary to refer to more sophisticated techniques for detecting nonlinearity (Worden and Tomlinson, 2019).

Among others, the nonlinearity may be seen as a *distortion* from linearity. The Hilbert transform can be employed to diagnose this distortion using FRF data. This is because the FRF of a linear system remains invariant under the Hilbert transformation (Simon and Tomlinson, 1984). Once the Hilbert transform has been computed, it is possible to represent the FRF of the original signal, here intended as the signal which did not undergo any transformation, and the FRF of the Hilbert transform of signal (i.e., the modulus of the imaginary part of the analytical signal). Figure 1.9 shows the comparison of FRF in the linear and nonlinear case, in order to visualise what distortion actually means. A predominant peak around 1.7 Hz, representing the natural frequency of the system, can be observed. However, in the nonlinear case, additional peaks arise at other frequencies representing the clearly not negligible combination of nonlinear phenomena in the total response of the system.

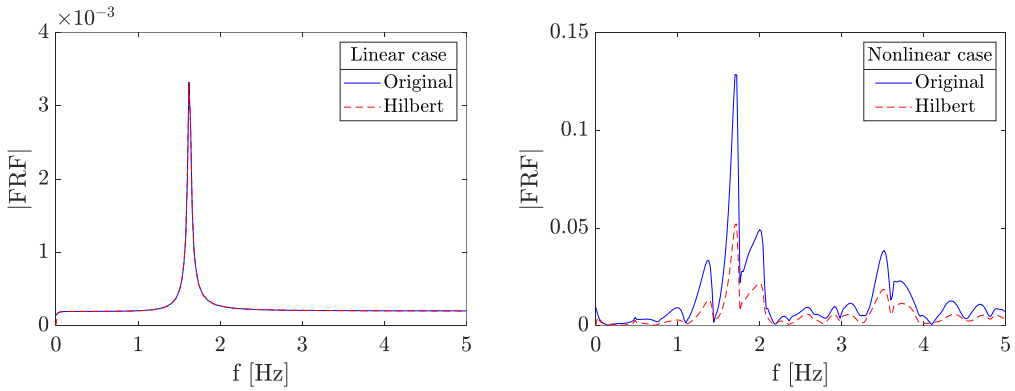

Figure 1.9. Representation of the FRF before and after Hilbert transformation of the signal in a linear and a nonlinear case.

Thus, if one should answer to the two questions raised at the beginning for the case of the system reported in Figure 1.9:

- The system is nonlinear, if nonlinearity is quantified as a deviation from linearity.

- A linearised model would not be enough to represent the response of the system, since it would underestimate the nonlinear components, which are not predominant but at the same time not negligible part of the response.

The nonlinearity quantified as a deviation from linearity raised some nonlinear indicators. In particular, given an output $y(t)$ and an input $u(t)$, a nonlinear indicator, namely coherence, is given by (Newland, 1993):

$$\gamma(\omega)^2 = \frac{|S_{yu}(\omega)|^2}{S_{yy}(\omega)S_{uu}(\omega)} \tag{1.1}$$

where $S_{yu}(\omega)$ is the input-output cross-spectrum, $S_{uu}(\omega)$ is the input auto-spectrum, and $S_{yy}(\omega)$ is the output auto-spectrum. On the one hand, if the quantity $\gamma(\omega)^2$ is equal to 1, then the system is inherently linear. On the other hand, if $0 < \gamma(\omega)^2 < 1$, then the system is nonlinear. The main drawback of this indicator is that it can be used as a noise detector. Therefore, it could be difficult to unravel nonlinearity from noise. Based on the Hilbert transform, a further indicator, namely Rauch's corehence function λ^2, is calculated as (Rauch, 1992):

$$\lambda(\omega)^2 = \frac{\left|E\left\{\mathcal{H}\left(G(\omega)\right)G(\omega)^*\right\}\right|^2}{E\left\{\left|\mathcal{H}\left(G(\omega)\right)\right|^2\right\}E\{|G(\omega)|^2\}} \tag{1.2}$$

where $\mathcal{H}\left(G(\omega)\right)$ is the Hilbert transform of the generic FRF $G(\omega)$, and $E\{\cdot\}$ stands for expected value. Corehence has the main advantage over the well-known coherence of allowing a distinction between nonlinearity and noise effects, making it a more sensitive indicator (Rauch, 1992).

1.4.2 Characterisation

As done for the detection, one can draw up a series of questions for the second step of the nonlinear identification route, namely *characterisation*:

- What is nonlinear?

- Where is the nonlinearity located?

- What model structure can be used?

The determination and the location of nonlinearity is generally linked to the experimental configuration adopted. In many systems of engineering interest, the

nonlinear behaviour is not distributed throughout the entire structure, but is concentrated in specific regions, often intentionally designed. A typical case is that of a predominantly linear main structure coupled with a more flexible secondary element, responsible for the onset of nonlinear effects in the presence of large displacements.

An example is given by the steel laboratory beam used within the framework of the European research project COST Action F3 (Golinval et al., 2003). In particular, two benchmarks have been proposed: one by the Ecole Centrale de Lyon (ECL), reported in Figure 1.10 (Bellizzi and Defilippi, 2003; Thouverez, 2003), and one from the University of Liege (ULg). The two beams, characterised by a local nonlinearity, differed in the coupling element, which, conversely to the case of the ECL beam, is not present in the ULg beam. The localisation of nonlinearity in a precise point of the beam allowed its exploitation for several works to validate different identification techniques, see (Chen et al., 2012; Demarie et al., 2011; Fasana et al., 2004; Kerschen et al., 2003; Lenaerts et al., 2003; Renjith and Praveen Krishna, 2024).

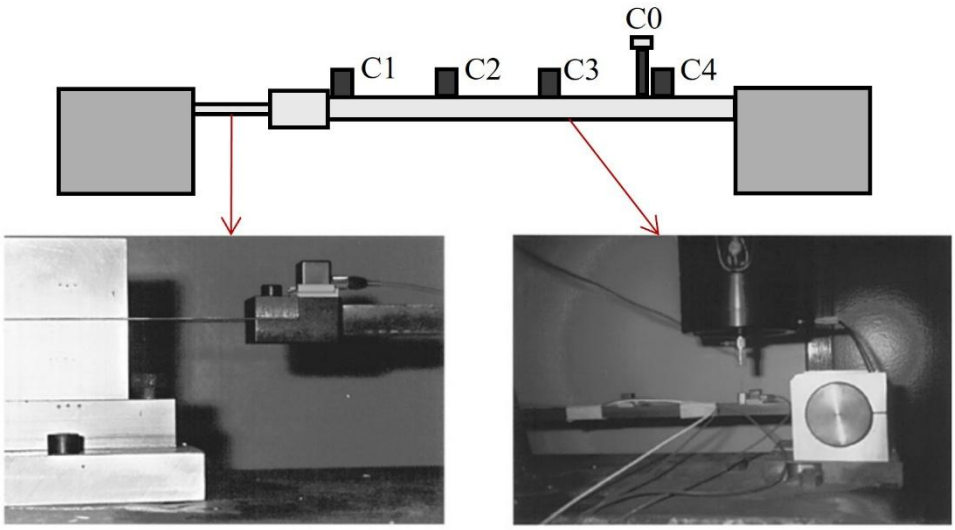

Figure 1.10. ECL experimental setup of a beam with localised nonlinearities (Thouverez, 2003).

After localisation, the main issue is to identify the most proper model to represent nonlinearity. In such configurations, nonlinearity can be interpreted as a localised stiffness contribution, mainly of a geometric nature, which can be represented, as a first approximation, by polynomial terms added to the equations of motion of a reduced model. Accordingly, the most common types of nonlinearities encountered in structures can be attributed to *stiffness*, especially if connected to large deformations (Nayfeh, 2024), and/or *damping* effects (Al-Hababi et al., 2020). For nonlinear identification purposes, it is common practice to reduce them to simplified models, in which the nonlinear contribution is expressed as a damping force $f_{r,d}(\dot{y})$ and/or stiffness $f_{r,s}(y)$, added to the

equation of motion of the classical oscillator, characterised by a displacement y and a velocity $\dot{y}$ (Worden and Tomlinson, 2019).

Stiffness nonlinearity

One of the most common cases for describing nonlinearities is given by the stiffness nonlinearity. If the stiffness assumes a cubic form, the restoring force can be written as $f_{r,s}(y) = k_1 y + k_3 y^3$. Any oscillator characterised by such restoring force is said to be a Duffing oscillator (Duffing, 1918). The coefficient k_3 can assume both positive and negative values (Kovacic and Brennan, 2011). If $k_3 > 0$, the restoring force will be higher than the one predicted by the linear term only, especially at high levels of excitation. These systems are said to be of *hardening* type. Conversely, if $k_3 < 0$ the stiffness decreases for increasing levels of excitation, and the systems are defined as *softening*. It is important to highlight that a purely softening cubic stiffness does not guarantee global stability of the system (Nayfeh and Sanchez, 1989). In that case, higher-order polynomial terms are implicitly required. Figure 1.11 depicts the restoring force and the potential energy for a linear, hardening, and softening oscillator.

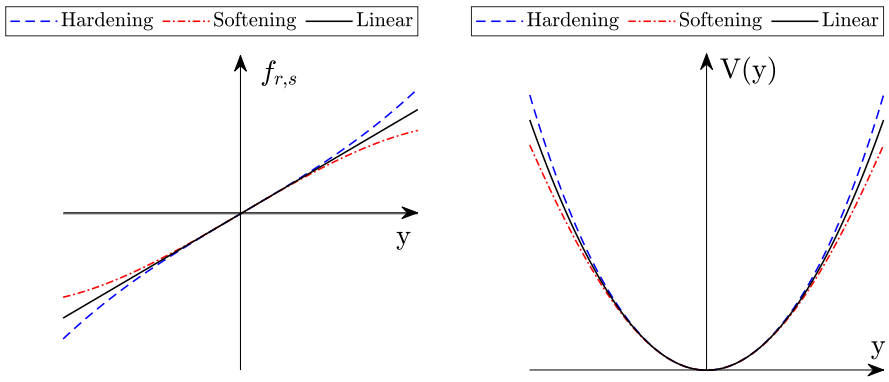

Figure 1.11. Hardening and softening type of cubic stiffness: restoring force (on the left) and potential energy (on the right).

Even though the classical symmetric Duffing oscillator implies a linear stiffness $k_1 > 0$, there are cases where it is convenient to assume that term as negative. Figure 1.12 represents the variation of the shape of the potential energy when the stiffness k_1 assumes negative and positive values. In particular, in the case $k_1 < 0$, one has a specific phenomenon, called bistability, characterised by a double-well potential (Harne and Wang, 2017). Such mathematical property is convenient for describing several physical phenomena and in recent years a change of paradigm in its exploitation took place for energy absorption and dissipation purposes (Vakakis, 2017). Among the most prominent applications, there are nonlinear energy sinks (NES) relying on the bistable behaviour for targeted energy transfer in the mitigation of vibrations (Habib and Romeo, 2018;

Vakakis, 2001). More generally, a review on the exploitation of geometric nonlinearities can be found in (Gatti et al., 2019).

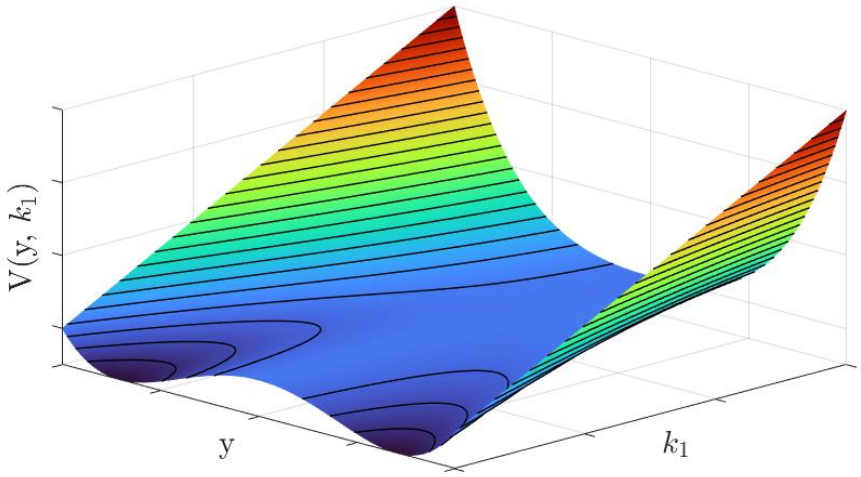

Figure 1.12. Potential energy as function of linear stiffness k_1.

Damping nonlinearity

One common form of polynomial damping is quadratic and writes $f_{r,d}(\dot{y}) = c_{NL}\dot{y}|\dot{y}|$, where the dissipative force depends as a polynomial on the velocity (Ruzicka and Derby, 1971). The absolute value term ensures that the force is always opposite to the velocity. Unlike linear viscous damping $f_{r,d}(\dot{y}) = c\dot{y}$, here the intensity of the force increases more rapidly with the amplitude of the velocity, making damping particularly effective at high excitation levels. Another form of nonlinear damping is Coulomb friction, in which the dissipative force is approximated as constant in modulus and always opposite to the direction of motion $f_{r,d}(\dot{y}) = c_F \text{sign}(\dot{y})$, where c_F is the value of the friction force. These nonlinearities are represented in Figure 1.13. There may be cases where the damping nonlinearity can have a bilinear shape, such as in the case of automotive shock absorbers. Since it overcomes the scope of the thesis, the interested reader is referred to (Surace et al., 1992).

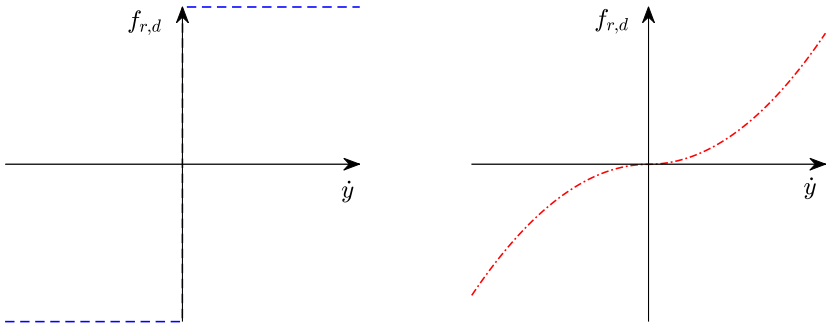

Figure 1.13. Types of nonlinear damping: Coulomb friction (on the left) and quadratic (on the right).

1.4.3 Parameter estimation

Parameter estimation, namely the last step of the system identification route, is nothing else than the identification of the model coefficients describing the nonlinear behaviour, therefore the core of nonlinear SI. In particular, the following questions should be addressed:

- What parameters are estimated?
- What algorithm?
- What dataset?
- How to validate the estimation?

This step highly depends on the algorithm used for performing the nonlinear system identification, as also is the interpretation of the estimated coefficients. A variety of methods exist in the literature to perform this task.

1.5 Concluding remarks

The first chapter of this thesis aimed to pave the way to nonlinear identification tools. More specifically, these tools are not only user-oriented, but also case-dependent. In the linear domain, the dynamic behaviour of a structure can be generally described by its modal properties, and the same identification technique can be applied to structures which are vastly different in terms of materials, construction typologies, and boundary conditions. This is not inherently true for nonlinear models, which always require different parameters depending on the case under study.

Hence, aside from the obvious consideration that nonlinear SI is much more complex than its linear counterpart, other critical issues must be considered: designing experiments require greater attention, choosing the model structure is more demanding, and estimating parameters is often more challenging, both computationally and experimentally. Ultimately, one should keep in mind that '*all models are wrong, but some are useful*' (Box, 1979). It is thus worth emphasising that the role of nonlinear identification in the field of structural and earthquake engineering is not to increase model complexity, but to find a balance between accuracy and usability.

References

Al-Hababi, T., Cao, M., Saleh, B., Alkayem, N.F., Xu, H., 2020. A critical review of nonlinear damping identification in structural dynamics: Methods, applications, and challenges. Sensors 20, 7303.

Anagnostopoulos, S.A., 1996. Building pounding re-examined: how serious a problem is it, in: Eleventh World Conference on Earthquake Engineering. Pergamon, Elsevier Science Oxford, UK, p. 2108.

Bayraktar, A., Calik, I., Türker, T., Ashour, A., 2018. Restoration effects on experimental dynamic characteristics of masonry stone minarets. Materials and Structures 51, 141.

Bellizzi, S., Defilippi, M., 2003. Non-linear mechanical systems identification using linear systems with random parameters. Mechanical Systems and Signal Processing 17, 203–210.

Billings, S.A., 2013. Nonlinear system identification: NARMAX methods in the time, frequency, and spatio-temporal domains. John Wiley & Sons.

Binda, L., Saisi, A., Tiraboschi, C., 2000. Investigation procedures for the diagnosis of historic masonries. Construction and Building materials 14, 199–233.

Bonato, P., Ceravolo, R., De Stefano, A., Molinari, F., 2000. Use of cross-time–frequency estimators for structural identification in non-stationary conditions and under unknown excitation. Journal of Sound and vibration 237, 775–791.

Bovsunovsky, A.P., Surace, C., 2005. Considerations regarding superharmonic vibrations of a cracked beam and the variation in damping caused by the presence of the crack. Journal of Sound and Vibration 288, 865–886.

Box, G.E.P., 1979. Robustness in the Strategy of Scientific Model Building, in: Robustness in Statistics. Elsevier, pp. 201–236. https://doi.org/10.1016/B978-0-12-438150-6.50018-2

Branstetter, L.J., Jeong, G.D., Yao, J.T., Wen, Y.K., Lin, Y.K., 1988. Mathematical modelling of structural behaviour during earthquakes. Probabilistic engineering mechanics 3, 130–145.

Brincker, R., Zhang, L., Andersen, P., 2001. Modal identification of output-only systems using frequency domaindecomposition. Smart materials and structures 10, 441.

Cattari, S., Degli Abbati, S., Ottonelli, D., Marano, C., Camata, G., Spacone, E., da Porto, F., Modena, C., Lorenzoni, F., Magenes, G., 2019. Discussion on data recorded by the Italian structural seismic monitoring network on three masonry structures hit by the 2016–2017 Central Italy earthquake, in: Proceedings of the 7th International Conference on Computational Methods in Structural Dynamics and Earthquake Engineering (COMPDYN), Crete, Greece.

Ceravolo, R., Coletta, G., Miraglia, G., Palma, F., 2021. Statistical correlation between environmental time series and data from long-term monitoring of buildings. Mechanical Systems and Signal Processing 152, 107460.

Ceravolo, R., De Lucia, G., Lenticchia, E., Miraglia, G., 2019. Seismic Structural Health Monitoring of Cultural Heritage Structures, in: Limongelli, M.P., Çelebi, M. (Eds.), Seismic Structural Health Monitoring, Springer Tracts in Civil Engineering. Springer International Publishing, Cham, pp. 51–85. https://doi.org/10.1007/978-3-030-13976-6_3

Ceravolo, R., Faraci, A., Miraglia, G., 2020. Bayesian calibration of hysteretic parameters with consideration of the model discrepancy for use in seismic structural health monitoring. Applied Sciences 10, 5813.

Ceravolo, R., Lenticchia, E., Miraglia, G., Scussolini, L., 2024. Improving the dynamic behaviour of historic buildings using experimental data: application to a Baroque church. J Civil Struct Health Monit 14, 1575–1594. https://doi.org/10.1007/s13349-024-00804-x

Ceravolo, R., Matta, E., Quattrone, A., Zanotti Fragonara, L., 2017. Amplitude dependence of equivalent modal parameters in monitored buildings during earthquake swarms. Earthq Engng Struct Dyn 46, 2399–2417. https://doi.org/10.1002/eqe.2910

Ceravolo, R., Pistone, G., Fragonara, L.Z., Massetto, S., Abbiati, G., 2016. Vibration-Based Monitoring and Diagnosis of Cultural Heritage: A Methodological Discussion in Three Examples. International Journal of Architectural Heritage 10, 375–395. https://doi.org/10.1080/15583058.2013.850554

Chen, G., Dong, X., 1993. From chaos to order—perspectives and methodologies in controlling chaotic nonlinear dynamical systems. International Journal of Bifurcation and Chaos 3, 1363–1409.

Chen, Y., Yaghoubi, V., Linderholt, A., Abrahamsson, T., 2012. Model calibration of locally nonlinear structures using information from sub and super harmonic responses, in: The Proceedings of the International Conference on Noise and Vibration Engineering, ISMA.

D'Ambrisi, A., Mariani, V., Mezzi, M., 2012. Seismic assessment of a historical masonry tower with nonlinear static and dynamic analyses tuned on ambient vibration tests. Engineering Structures 36, 210–219. https://doi.org/10.1016/j.engstruct.2011.12.009

Demarie, G.V., Ceravolo, R., Sabia, D., Argoul, P., 2011. Experimental identification of beams with localized nonlinearities. Journal of Vibration and Control 17, 1721–1732.

Doelman, A., Verhulst, F., 1994. Bifurcations of strongly non-linear self-excited oscillations. Mathematical Methods in the applied sciences 17, 189–207.

Drazin, P.G., 1992. Nonlinear systems. Cambridge University Press.

Duffing, G., 1918. Erzwungene Schwingungen bei veränderlicher Eigenfrequenz und ihre technische Bedeutung. Vieweg.

Ewins, D.J., 2009. Modal testing: theory, practice and application. John Wiley & Sons.

Fasana, A., Garibaldi, L., Marchesiello, S., 2004. Performances analysis of frequency domain nonlinear identification techniques, in: ISMA 2004. ISMA, pp. 2115–2128.

Gatti, G., Brennan, M.J., Tang, B., 2019. Some diverse examples of exploiting the beneficial effects of geometric stiffness nonlinearity. Mechanical Systems and Signal Processing 125, 4–20.

Gentile, C., Ruccolo, A., Canali, F., 2019. Continuous monitoring of the Milan Cathedral: dynamic characteristics and vibration-based SHM. Journal of Civil Structural Health Monitoring 9, 671–688.

Golinval, J.C., Kerschen, G., Lenaerts, V., Thouverez, F., Argoul, P., 2003. WORKING GROUP 3—IDENTIFICATION OF NON-LINEAR SYSTEMS. Mechanical Systems and Signal Processing 17, 177–178. https://doi.org/10.1006/mssp.2002.1549

Gres, S., Andersen, P., Johansen, R.J., Ulriksen, M.D., Damkilde, L., 2018. A Comparison of Damage Detection Methods Applied to Civil Engineering Structures, in: Conte, J.P., Astroza, R., Benzoni, G., Feltrin, G., Loh, K.J., Moaveni, B. (Eds.), Experimental Vibration Analysis for Civil Structures, Lecture Notes in Civil Engineering. Springer International Publishing, Cham, pp. 306–316. https://doi.org/10.1007/978-3-319-67443-8_26

Haber, R., Unbehauen, H., 1990. Structure identification of nonlinear dynamic systems—a survey on input/output approaches. Automatica 26, 651–677.

Habib, G., Romeo, F., 2018. Comparative analysis of NES and TMD performance via high-dimensional invariant manifolds, in: IUTAM Symposium on Exploiting Nonlinear Dynamics for Engineering Systems. Springer, pp. 143–153.

Harne, R.L., Wang, K.-W., 2017. Harnessing bistable structural dynamics: for vibration control, energy harvesting and sensing. John Wiley & Sons.

Haseli, B., Homami, P., Nouri, G., 2023. Optimal design of TMDs to reduce the longitudinal seismic response of the suspension bridges. Int. J. Dynam. Control 11, 1465–1479. https://doi.org/10.1007/s40435-022-01062-9

He, X., Moaveni, B., Conte, J.P., Elgamal, A., Masri, S.F., 2008. Modal Identification Study of Vincent Thomas Bridge Using Simulated Wind-Induced Ambient Vibration Data. Computer aided Civil Eng 23, 373–388. https://doi.org/10.1111/j.1467-8667.2008.00544.x

Hong, X., Mitchell, R.J., Chen, S., Harris, C.J., Li, K., Irwin, G.W., 2008. Model selection approaches for non-linear system identification: a review. International Journal of Systems Science 39, 925–946. https://doi.org/10.1080/00207720802083018

Ibrahim, S.R., Mikulcik, E.C., 1977. A method for the direct identification of vibration parameters from the free response. The Shock and Vibration Inform. Ctr. Shock and Vibration Bull. Part. 4: Sep. 1977.

Juang, J.N., Pappa, R., 1984. An Eigensystem Realization Algorithm (ERA) for Modal Parameter Identification, NASA, in: JPL Workshop on Identification and Control of Flexible Space Structures, Pasadena, CA, USA.

Kerschen, G., Lenaerts, V., Golinval, J.-C., 2003. Identification of a continuous structure with a geometrical non-linearity. Part I: Conditioned reverse path method. Journal of Sound and Vibration 262, 889–906.

Kerschen, G., Worden, K., Vakakis, A.F., Golinval, J.-C., 2006. Past, present and future of nonlinear system identification in structural dynamics. Mechanical systems and signal processing 20, 505–592.

Kijewski-Correa, T.L., 2003. Full-scale measurements and system identification: A time-frequency perspective. University of Notre Dame.

Kovacic, I., Brennan, M.J., 2011. The Duffing equation: nonlinear oscillators and their behaviour. John Wiley & Sons.

Lenaerts, V., Kerschen, G., Golinval, J.-C., 2003. Identification of a continuous structure with a geometrical non-linearity. Part II: Proper orthogonal decomposition. Journal of Sound and vibration 262, 907–919.

Ljung, L., 2004. State of the art in linear system identification: Time and frequency domain methods, in: Proceedings of the 2004 American Control Conference. IEEE, pp. 650–660.

Ljung, L., 1998. System Identification, in: Procházka, A., Uhlíř, J., Rayner, P.W.J., Kingsbury, N.G. (Eds.), Signal Analysis and Prediction, Applied and Numerical Harmonic Analysis. Birkhäuser Boston, Boston, MA, pp. 163–173. https://doi.org/10.1007/978-1-4612-1768-8_11

Ljung, L., 1987. Theory for the user. System identification.

Lorenzoni, F., Casarin, F., Modena, C., Caldon, M., Islami, K., Da Porto, F., 2013. Structural health monitoring of the Roman Arena of Verona, Italy. J Civil Struct Health Monit 3, 227–246. https://doi.org/10.1007/s13349-013-0065-0

Luş, H., Betti, R., Longman, R.W., 1999. Identification of linear structural systems using earthquake-induced vibration data. Earthquake Engineering & Structural Dynamics 28, 1449–1467.

Maia, N.M.M., Montalvão e Silva, J.M., 1997. Theoretical and experimental modal analysis. (No Title).

Miraglia, G., Lenticchia, E., Surace, C., Ceravolo, R., 2020. Seismic damage identification by fitting the nonlinear and hysteretic dynamic response of monitored buildings. Journal of Civil Structural Health Monitoring 10, 457–469.

Mosekilde, E., Aracil, J., Allen, P.M., 1988. Instabilities and chaos in nonlinear dynamic systems. System Dynamics Review 4, 14–55.

Mottershead, J.E., Friswell, M.I., 1993. Model updating in structural dynamics: a survey. Journal of sound and vibration 167, 347–375.

Nagarajaiah, S., Basu, B., 2009. Output only modal identification and structural damage detection using time frequency & wavelet techniques. Earthquake Engineering and Engineering Vibration 8, 583–605.

Natsiavas, S., 1992. Steady state oscillations and stability of non-linear dynamic vibration absorbers. Journal of Sound and Vibration 156, 227–245.

Nayfeh, A.H., 2024. Linear and nonlinear structural mechanics. John Wiley & Sons.

Nayfeh, A.H., Mook, D.T., 1995. Nonlinear oscillations, Wiley classics library. J. Wiley & sons, New York Chichester Brisbane.

Nayfeh, A.H., Sanchez, N.E., 1989. Bifurcations in a forced softening Duffing oscillator. International Journal of Non-Linear Mechanics 24, 483–497.

Newland, D.E., 1993. An introduction to random vibrations. Sprctral & Wavelet Analysis.

Noël, J.-P., Kerschen, G., 2017. Nonlinear system identification in structural dynamics: 10 more years of progress. Mechanical Systems and Signal Processing 83, 2–35.

Ormando, C., Raeisi, F., Clemente, P., Mufti, A., 2021. The SHM as higher level inspection in the evaluation of structures, in: International Conference of the European Association on Quality Control of Bridges and Structures. Springer, pp. 452–461.

Overschee, P.V., de Moor, B.L., 1996. Subspace identification for linear systems: theory-implementation-applications.

Pearson, A.E., 1979. Nonlinear system identification with limited time data. Automatica 15, 73–84.

Pellicano, F., Vestroni, F., 2000. Nonlinear dynamics and bifurcations of an axially moving beam. J. Vib. Acoust. 122, 21–30.

Perez-Ramirez, C.A., Amezquita-Sanchez, J.P., Adeli, H., Valtierra-Rodriguez, M., Romero-Troncoso, R. de J., Dominguez-Gonzalez, A., Osornio-Rios, R.A., 2016. Time-frequency techniques for modal parameters identification of civil structures from acquired dynamic signals. Journal of Vibroengineering 18, 3164–3185.

Petsounis, K.A., Fassois, S.D., 2001. Parametric time-domain methods for the identification of vibrating structures—a critical comparison and assessment. Mechanical Systems and Signal Processing 15, 1031–1060.

Pintelon, R., Schoukens, J., 2012. System identification: a frequency domain approach. John Wiley & Sons.

Rauch, A., 1992. Corehence: A powerful estimator of nonlinearity theory and application. Presented at the PROCEEDINGS OF THE INTERNATIONAL MODAL ANALYSIS CONFERENCE, SEM SOCIETY FOR EXPERIMENTAL MECHANICS INC, pp. 784–784.

Renjith, A.R., Praveen Krishna, I.R., 2024. A semi-analytical solution in time domain for evaluating the nonlinear normal modes of a cantilever beam

with a tip nonlinearity. Nonlinear Dyn 112, 16037–16059. https://doi.org/10.1007/s11071-024-09899-9

Reynders, E., 2012. System identification methods for (operational) modal analysis: review and comparison. Archives of Computational Methods in Engineering 19, 51–124.

Richardson, M.H., Formenti, D.L., 1982. Parameter estimation from frequency response measurements using rational fraction polynomials, in: Proceedings of the 1st International Modal Analysis Conference. Union College Schenectady, NY, pp. 167–186.

Romeo, F., Manevitch, L.I., Bergman, L.A., Vakakis, A., 2015. Transient and chaotic low-energy transfers in a system with bistable nonlinearity. Chaos: An Interdisciplinary Journal of Nonlinear Science 25.

Ruzicka, J.E., Derby, T.F., 1971. Influence of damping in vibration isolation.

Sarhosis, V., Dais, D., Smyrou, E., Bal, I.E., Drougkas, A., 2021. Quantification of damage evolution in masonry walls subjected to induced seismicity. Engineering Structures 243, 112529.

Schoukens, J., Ljung, L., 2019. Nonlinear system identification: A user-oriented road map. IEEE Control Systems Magazine 39, 28–99.

Simon, M., Tomlinson, G.R., 1984. Use of the Hilbert transform in modal analysis of linear and non-linear structures. Journal of Sound and Vibration 96, 421–436.

Sinha, J.K., Friswell, M.I., 2002. Model updating: a tool for reliable modeling, design modification and diagnosis. The Shock and Vibration Digest 34, 27–35.

Sivori, D., Merani, M.G.B., Bocchi, F., Spina, D., Cattari, S., 2025. Environmental effects on the experimental modal parameters of masonry buildings: experiences from the Italian Seismic Observatory of Structures (OSS) network. J Civil Struct Health Monit 15, 307–331. https://doi.org/10.1007/s13349-024-00847-0

Sjöberg, J., Zhang, Q., Ljung, L., Benveniste, A., Delyon, B., Glorennec, P.-Y., Hjalmarsson, H., Juditsky, A., 1995. Nonlinear black-box modeling in system identification: a unified overview. Automatica 31, 1691–1724.

Smyth, A.W., Pei, J.-S., Masri, S.F., 2003. System identification of the Vincent Thomas suspension bridge using earthquake records. Earthquake Engineering & Structural Dynamics 32, 339–367.

Sohn, H., 2007. Effects of environmental and operational variability on structural health monitoring. Philosophical Transactions of the Royal Society A: Mathematical, Physical and Engineering Sciences 365, 539–560.

Spina, D., Lamonaca, B.G., Nicoletti, M., Dolce, M., 2011. Structural monitoring by the Italian Department of Civil Protection and the case of 2009 Abruzzo seismic sequence. Bull Earthquake Eng 9, 325–346. https://doi.org/10.1007/s10518-010-9232-4

Strejc, V., 1981. Trends in identification. Automatica 17, 7–21. https://doi.org/10.1016/0005-1098(81)90081-9

Surace, C., Worden, K., Tomlinson, G.R., 1992. On the non-linear characteristics of automotive shock absorbers. Proceedings of the Institution of Mechanical Engineers, Part D: Journal of Automobile Engineering 206, 3–16.

Tarantola, A., 2005. Inverse problem theory and methods for model parameter estimation. SIAM.

Thompson, J.M.T., Stewart, H.B., 2002. Nonlinear dynamics and chaos. John Wiley & Sons.

Thouverez, F., 2003. Presentation of the ECL benchmark. Mechanical Systems and Signal Processing 17, 195–202.

Vakakis, A.F., 2017. Intentional utilization of strong nonlinearity in structural dynamics. Procedia Engineering 199, 70–77.

Vakakis, A.F., 2001. Inducing passive nonlinear energy sinks in vibrating systems. J. Vib. Acoust. 123, 324–332.

Worden, K., 2019. Nonlinearity in structural dynamics: detection, identification and modelling. CRC Press.

Worden, K., Tomlinson, G.R., 2019. Nonlinearity in Structural Dynamics: Detection, Identification and Modelling, 1st ed. CRC Press. https://doi.org/10.1201/9780429138331

Chapter 2

Different approaches and classifications of nonlinear system identification techniques

Throughout the last years several techniques have been proposed to solve the identification problem for nonlinear systems (Kerschen et al., 2006; Noël and Kerschen, 2017; Quaranta et al., 2020). Although a general consensus within the scientific community about the existing definitions has not been reached, and finding a unique categorisation of nonlinear techniques is difficult, some criteria for classifying nonlinear identification techniques can be established. Such classifications may depend on the domain the identification is performed in, or on the model structure (white-box, black-box, or grey-box), or on the computational intelligence methods employed.

2.1 Classifications of nonlinear identification techniques

A first classification criterion for nonlinear techniques relies on the model structure, which can assume a white-box, black-box, or grey-box representation (Kerschen et al., 2006; Quaranta et al., 2020; Sjöberg et al., 1995). In particular, the methods exploiting a grey-box representation are typically referred to as *parametric* approaches, as they require prior knowledge of the physical characteristics of the system to formulate the mathematical model. The reason why parametric methods are not purely white-box models is that they require the measured response of the system as well as the excitation input in order to estimate some of the parameters describing the system. Conversely, black-box models are the basis of *non-parametric* approaches. The latter do not include

hypotheses on the type and location of nonlinearities, and the estimated quantities are not directly linked to the physical characteristics of the system.

Going into greater detail for each of the two categories, the parametric identification problem is generally formulated as a minimisation problem. The latter has been classically solved through estimation techniques mostly based on the least square method (Golub and Van Loan, 1980) and optimisation algorithms (Fletcher, 1987). The choice of the optimisation algorithm strongly depends on the system model and the objectives of the minimisation problem, as well as on its physical boundaries. In particular, one may rely on approaches based on penalty functions, which indirectly enforce constraints by adding terms to the cost function, or methods based on Lagrange multipliers, which explicitly account for constraints in the minimisation problem through appropriate multipliers (Andrei, 2022; Bertsekas, 1976; Boukari and Fiacco, 1995).

Parametric methods can be furtherly classified on the basis of the domain they are performed in, which can be time-dependent or frequency-dependent. The time-domain methods are the eldest nonlinear identification methods, such as the direct parameter estimation (DPE) (Gifford and Tomlinson, 1989; Mohammad et al., 1992) and the nonlinear autoregressive models with moving average and exogenous input (NARMAX) method (Billings, 2013; Leontaritis and Billings, 1985a, 1985b). The latter represents an extension to the nonlinear field of the autoregressive moving average models (ARMA) widely used in linear identification. The NARMAX model holds as main advantage the versatility of describing the input-output relationship in any nonlinear system, but its use in structural engineering is limited, due to the difficulty of validating it experimentally. Frequency-domain methods are, for instance, the Reverse Path (RP) method (Bendat et al., 1992; Rice and Fitzpatrick, 1991) or the Conditioned Reverse Path (CRP) method (Richards and Singh, 1998). Specifically, RP and CRP methods allow the identification of the parameters in the frequency domain starting from the response to stochastic excitations, exploiting the dynamic stiffness matrix to invert the input-output representation.

On the other hand, non-parametric methods consist in searching a model which could minimise an error describing the distance between the measured and the predicted response of the system. It is completely based on the availability of the experimental data only, without knowing any physics of the system. Non-parametric methods can be based on a polynomial representation, such as the restoring force surface (RFS) method, introduced by Masri & Caughey (Masri and Caughey, 1979), and consisting of determining a three-dimensional surface, defined in the phase plane (Nayfeh and Mook, 1995), characteristic of the internal restoring forces to which the system is subject during vibration.

Another popular non-parametric approach is given by neural networks (Pei et al., 2004; Walczak and Cerpa, 1999), i.e., computing systems consisting of multiple connected computational units, calibrated on experimental measurements and able to learn the functional input-output relationship (training the network). The versatility of neural networks lies in their generalisation capability, allowing their application in the structural field to the problem of identification and diagnosis (Chen et al., 1990). Other identification methods are based on the Hilbert transform (Feldman, 1994a, 1994b). Their conceptual simplicity allowed the application of those methods to real structures, as demonstrated by (Spina et al., 1996). An extension known as Hilbert-Huang transform has been proposed in (Huang et al., 1998). Additionally, numerous identification techniques are based on the Volterra series representation of the system input/output relationship and consist of determining the higher-order characteristic functions of the system (Collis et al., 1998; Tawfiq and Vinh, 2003).

Alternative approaches interpret nonlinearities as unmeasured internal forces, such as the nonlinear identification through feedback of the outputs (NIFO) proposed by Adams & Allemang (Adams and Allemang, 1999a, 1999b). Building on this idea, other authors developed an efficient method exploiting subspace algorithms, called nonlinear subspace identification (NSID) (Marchesiello and Garibaldi, 2008; Noël et al., 2014). Similarly, an approach has been proposed for distributed systems (Anastasio et al., 2019). Continuation methods, based on the combination of feedback control with path controlling, have been also proposed as a viable alternative for the identification and tracking of parameters under steady-state response (Renson et al., 2016). Figure 2.1 depicts the classification into parametric and non-parametric approaches.

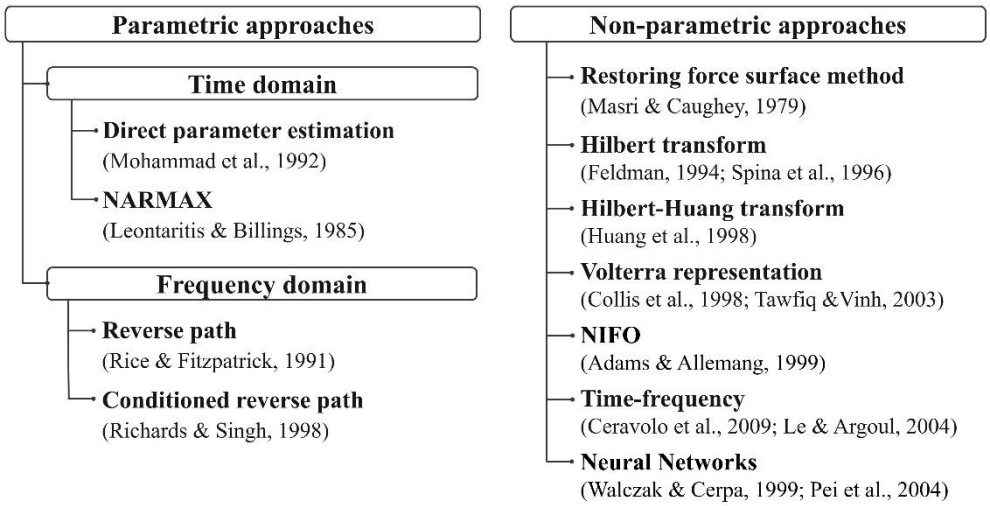

Figure 2.1. Classification into parametric and non-parametric approaches.

A further classification criterion, which is more interesting for the scope of this thesis, brings to the distinction into instantaneous and non-instantaneous approaches. An *instantaneous* approach allows extracting the quantities to be

identified instant by instant. This is particularly useful in the field of structural health monitoring (SHM), where often one should look for a change in parameters during a time window in order to detect damage or degradation. Instantaneous methods can be furtherly divided into online, such as the extended Kalman filter (EKF) (Ribeiro, 2004) and unscented Kalman filter (UKF) (Chatzi et al., 2010; Wu and Smyth, 2007), and offline methods, which mainly involve the Hilbert transform (Feldman, 1994a, 1994b). Another category, which could be performed both online and offline, is represented by the time-frequency methods, which exploits the representations of the signals in the time-frequency domain (e.g., wavelets) (Bonato et al., 2000; Bursi et al., 2010; Ceravolo, 2009; Ceravolo et al., 2007; Le and Argoul, 2004; Spina et al., 1996). Figure 2.2 depicts the classification into instantaneous and non-instantaneous approaches.

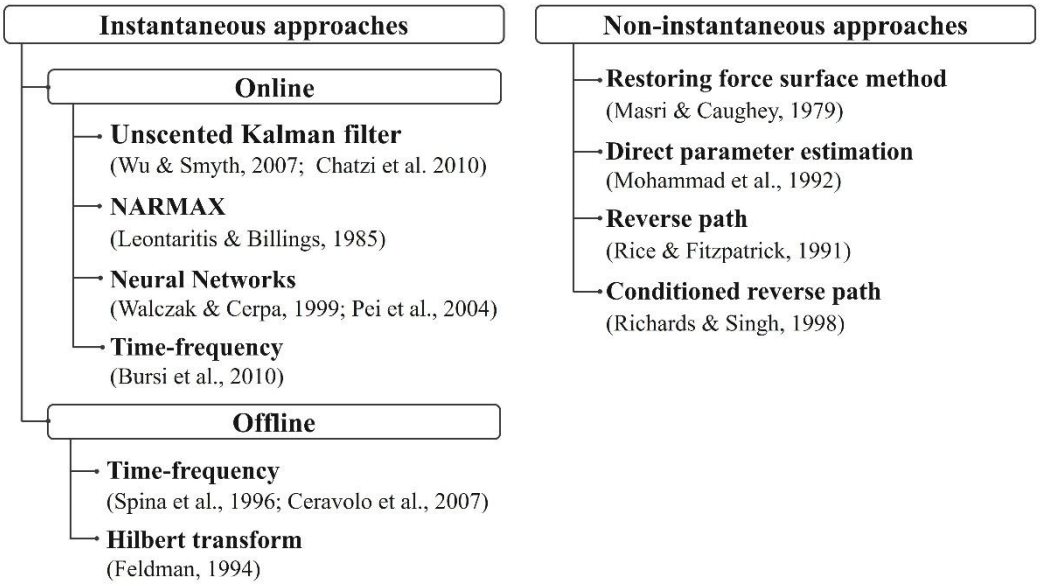

Figure 2.2. Classification into instantaneous and non-instantaneous approaches.

A more recent classification has been proposed by Quaranta et al. (Quaranta et al., 2020) based on *computational intelligence* algorithms. In particular, parametric and non-parametric approaches have been furtherly divided by detailing this classification: (i) evolutionary computing, with attention on genetic algorithms, differential evolution, and genetic programming; (ii) swarm intelligence, with particle swarm optimisation as key technique; (iii) neurocomputing (e.g., artificial neural networks).

More recently, additional methods have been developed, complementing the existing classification schemes. For instance, nonlinear normal modes (NNM), which can be defined as the extension of the linear modes into the nonlinear field, first introduced by (Rosenberg, 1962) and extensively studied in (Shaw and Pierre, 1993; Vakakis, 2001), have been exploited with the aim of identifying the parameters of nonlinear models (Pai, 2011). The major drawback of this technique lies in the fact that NNMs can be observed during impulses as the modes arising

near the natural frequencies of the system, which make this technique extremely peculiar and case-dependent.

Another technique which has been developed in the scientific literature on the basis of the work of Beck (Beck and Katafygiotis, 1998) is represented by the Bayesian approaches. The advantage of this kind of approaches lies in the probabilistic nature of the method, which not only allows the consideration of the uncertainty of the system, but also the selection of the most plausible class of models for a structural or mechanical system within some specified set of model classes, based on system response data, on the basis of a model parsimony principle which can be stated as '*simpler models are to be preferred over unnecessarily complicated ones*' (Beck and Yuen, 2004).

It is worth highlighting that these classifications are not mutually exclusive. For example, Bayesian inference represents a transversal framework that can be applied both to time, frequency, and time-frequency domain, and both to parametric and non-parametric approaches, depending on the formulation. This section aimed to give a brief overview of the most relevant classifications, while the following subchapters will provide a more detailed discussion on the methods which served as the basis for this thesis.

2.2 State-of-the-art methods

2.2.1 Restoring force surface method

The RFS method was first introduced in 1979 by Masri and Caughey (Masri and Caughey, 1979). A parallel approach, called force-state mapping, was developed by Crawley and O'Donnel (Crawley and O'Donnell, 1986) and Crawley and Aubert (Crawley and Aubert, 1984). The RFS method does not require any assumption on the type of nonlinearity, being therefore a non-parametric method. In this case, the generic equation of motion for a single-degree-of-freedom (SDoF) system writes:

$$m\ddot{y} + f_r(y, \dot{y}) = u \tag{2.1}$$

where m is the mass, u is the generic external excitation, f_r is the generic restoring force, containing both the linear and the nonlinear description of the system, and y, $\dot{y}$, and $\ddot{y}$ are the displacement, velocity, and acceleration response, respectively. The basic idea below the RFS method is to exploit a representation of the restoring force f_r in the Cartesian plane $(y, \dot{y}, f_r)$, where the plane $(y, \dot{y})$ is nothing else than the state-space. If the mass m is known, then the restoring force f_r can be extrapolated experimentally as:

$$f_{r,i}(y_i, \dot{y}_i) = u_i - m\ddot{y}_i \tag{2.2}$$

with y_i, $\dot{y}_i$, and $\ddot{y}_i$ as the measured values of displacement, velocity, and acceleration at the time instant t_i. Given that if either of these three variables is known, the remaining two are always inferable, then the quantity $(y_i, \dot{y}_i, f_{r,i})$ is known at every time step t_i. A convenient model of the restoring force f_r was introduced by Masri by exploiting the Chebyshev polynomials of i-th and j-th order T_i and T_j (Masri and Caughey, 1979):

$$f_r(y, \dot{y}) \approx \hat{f}_r(\bar{y}, \dot{\bar{y}}) = \sum_{i=0}^{m} \sum_{j=0}^{n} C_{ij} T_i(y) T_j(\dot{y}) \tag{2.3}$$

with C_{ij} as the unknown coefficients to be determined by using least-squares fitting. The values $\bar{y}$ and $\dot{\bar{y}}$ are the displacement and the velocity normalised to the region of existence of the Chebyshev polynomials, i.e., [-1, +1], respectively.

The latter equation has a series of advantages: (i) the Chebyshev polynomials are orthogonal (i.e., each order of polynomial is independent of the others), with the desirable property that the coefficients do not need to be recalculated if a lower order model is acceptable (the higher-order coefficients can simply be omitted); (ii) these polynomials can be easily evaluated through numerical integration due to the domain of existence of their coefficients with all the advantages that follow; (iii) every Chebyshev polynomial is intrinsically a minimax polynomial (i.e., the polynomial with the minimum value of the maximum error from the function to be approximated), due to its equal-ripple property (the Chebyshev expansion oscillates between almost equal upper and lower bounds), making it a favourable choice in functions approximation. However, this procedure requires a huge amount of displacement, velocity, and acceleration data, making complex instrumentation and numerical analyses needed, and suffers from bias unless the identification is iterated, making it computationally inefficient.

A simple application of the RFS method is reported in Figure 2.3. The method, implemented in Matlab®, is applied to a symmetric Duffing oscillator, with mass $m = 1$ kg, damping $c = 0.15$ Ns/m, linear stiffness $k_1 = 1$ N/m and cubic stiffness $k_3 = 5$ N/m^3. The system is excited by a single-harmonic excitation as $A_1 \sin(\omega_1 t)$ with A_1 equal to 5 and $\omega_1 = 1$ rad/s. The displacement response y has been obtained by numerical integration in Matlab®. Figure 2.3(a) represents the Cartesian plane $(y, \dot{y}, f_r)$ with f_r calculated accordingly to Equation (2.2), from which it is straightforward to obtain the stiffness and damping restoring force. A polynomial fitting can be used to obtain $f_{r,s}$ and $f_{r,d}$, see Figure 2.3(b).

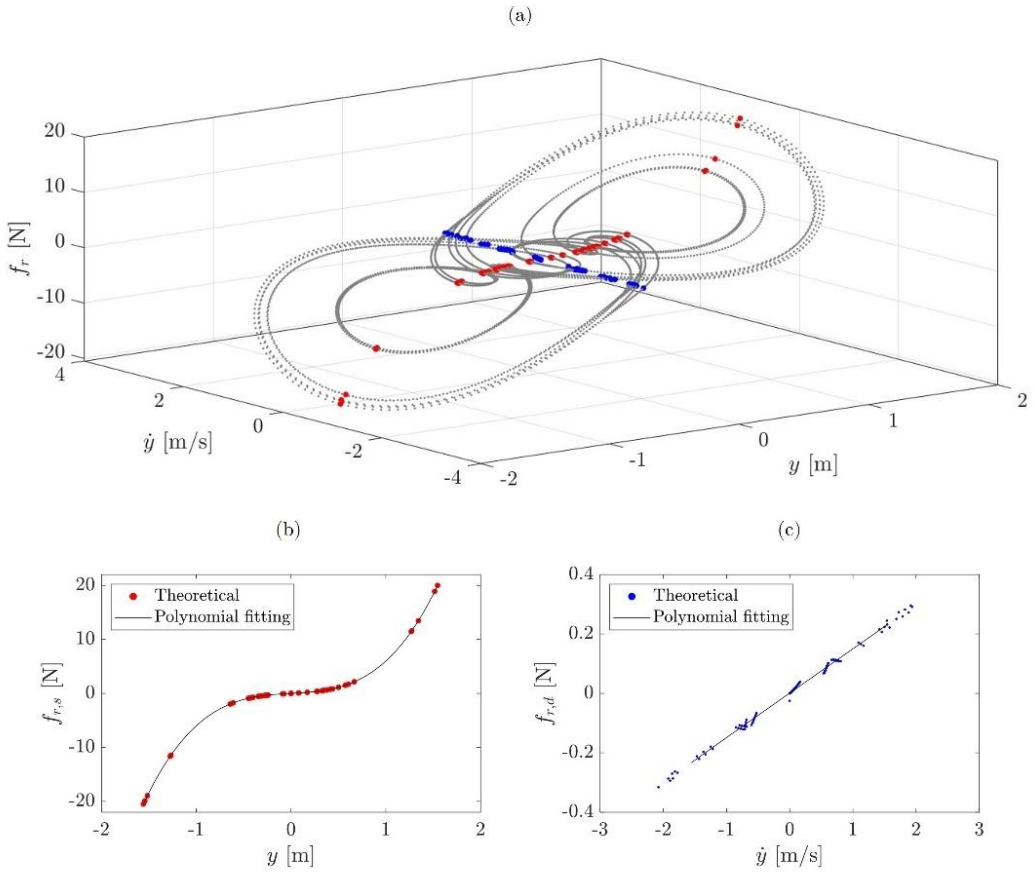

Figure 2.3. Application of RFS method on a symmetric Duffing oscillator: (a) restoring force f_r in the Cartesian plane $(y, \dot{y}, f_r)$, (b) theoretical vs. fitted stiffness restoring force $f_{r,s}$, and (c) theoretical vs. fitted damping restoring force $f_{r,d}$.

If ordinary polynomials are used instead of Chebyshev polynomials (Crawley and Aubert, 1984; Crawley and O'Donnell, 1986; Yang and Ibrahim, 1985), the restoring force formulation becomes:

$$f_r(y, \dot{y}) \approx \hat{f}_r(\bar{y}, \dot{\bar{y}}) = \sum_{i=0}^{m} \sum_{j=0}^{n} A_{ij} y_i \dot{y}_j \tag{2.4}$$

where A_{ij} are ordinary unknown coefficients. The main disadvantage of using ordinary polynomials instead of Chebyshev ones lies in the fact that they do not hold the orthogonality property. However, it was demonstrated that the computation of ordinary polynomials was faster than the Chebyshev one, leading to the unnecessity of the orthogonality property. The most important consequence of lack of orthogonality lays in the possibility of an ill-conditioned problem when the number of terms is particularly large. Another important aspect is given by the possibility of these equations to represent only polynomial type nonlinearities (e.g., Duffing, Helmholtz-Duffing, etc.). For these reasons, a more general and convenient form of Equation (2.4) was proposed as (Al-Hadid and Wright, 1989):

$$f_r(y,\dot{y}) \approx \hat{f}_r(\bar{y},\dot{\bar{y}}) = \sum_{i=0}^{N} B_i F(y_i,\dot{y}_i) \tag{2.5}$$

where B_i are ordinary unknown coefficients and $F(y_i,\dot{y}_i)$ are ordinary basis functions including also non-polynomial nonlinear representation. Starting from this more general form, other Authors proposed the extension to hysteretic systems (Benedettini et al., 1995). In such a case, Equation (2.4) is completed by adding a second equation:

$$\dot{f}_r = g(\dot{y},f_r) = \sum_{i=1}^{n}\sum_{j=1}^{m} A_{ij}\dot{y}_i f_{r,j} \tag{2.6}$$

The model reported in Equation (2.6) allows a representation of the derivative of the restoring force f_s in the plane $(\dot{y},f_s)$. A further generalisation of this model leads to its dependence on displacement:

$$\dot{f}_r = g(y,\dot{y},f_r) \tag{2.7}$$

where the considered model is a Duhem hysteretic model. A similar extension of RFS method to hysteretic systems was provided by Masri in (Masri et al., 2004), also considering its dependence on the external excitation. Equations (2.6)-(2.7) were successfully applied to the identification of degrading hysteretic systems in (Ceravolo et al., 2013). The simplicity of representation given by Equation (2.1) allowed a direct extension of the method to multi-degrees-of-freedom (MDoF) by the same Authors (Masri et al., 1987). In particular, the following equation of motion is considered:

$$\mathbf{M}\ddot{\mathbf{y}} + \mathbf{f}_r(\mathbf{y},\dot{\mathbf{y}}) = \mathbf{u}(t) \tag{2.8}$$

where $\mathbf{M}$ is the mass matrix of the MDoF system, $\mathbf{f}_r(\mathbf{y},\dot{\mathbf{y}})$ is the restoring force for the different degrees-of-freedom (DoFs), $\mathbf{y}$, $\dot{\mathbf{y}}$, and $\ddot{\mathbf{y}}$ are the displacement, velocity, and acceleration vectors, respectively.

2.2.2 Direct parameter estimation

The DPE scheme lays its grounds on the basic concept of using a physical coordinate system rather than a modal coordinates one, as happens in the case of the RFS method for MDoF systems, coupled with the least-squares estimation theory (Mohammad et al., 1992). For a generic MDoF system with N DoFs, a concentrated mass m_i is considered, and each i-th point is considered to be linked to the j-th point with a link l_{ij}. These masses are restored to equilibrium by internal forces in the links, which depend only on the relative displacements $\delta_{ij} = y_i - y_j$ and velocities $\delta_{ij} = \dot{y}_i - \dot{y}_j$ of the masses. Moreover, the mass m_i

interacts with the ground through the force l_{ii}, which depends on δ_{ii} and $\dot{\delta}_{ii}$. If the relationship $l_{ij} = l_{ji}$ holds, then:

$$f_{ij}(\delta_{ij}, \delta_{ij}) = -f_{ji}(\delta_{ji}, \delta_{ji}) = -f_{ji}(\delta_{ij}, \delta_{ij}) \tag{2.9}$$

As a consequence, the equation of motion becomes:

$$m_i \ddot{y}_i + \sum_{j=1}^{N} f_{ij}(\delta_{ij}, \dot{\delta}_{ij}) = u_i \qquad i = 1, \dots, N \tag{2.10}$$

with u_i as the generic i-th external excitation. In practical application, the measured quantities are given by the accelerations and the input forces at the N points. Then, a differencing operation yields to the relative accelerations $\ddot{\delta}_{ij}$, and, as a consequence, through simple numerical integrations, to the relative velocities and displacements $\dot{\delta}_{ij}$ and δ_{ij}. If a polynomial representation is used for the representation of the force f_{ij}, then Equation (2.10) becomes:

$$m_i \ddot{y}_i + \sum_{j=1}^{N} \sum_{k=0}^{p} \sum_{l=0}^{q} a_{(ij)kl} (\delta_{ij})^k (\dot{\delta}_{ij})^l = u_i \qquad i = 1, \dots, N \tag{2.11}$$

The main advantage of Equation (2.11) lies in the possibility of using classical least-squares estimation to determine the best fitting of parameters m_i and $a_{(ij)kl}$. Another possibility is to use the singular value decomposition. Moreover, a priori estimation of the mass is not needed for this kind of method. The identification is accomplished in two steps: (i) the parameters of the equations of motion where the external excitation u_i is applied are calculated; (ii) the parameters of the other equations of motion are identified. Let's consider the case where the excitation u_1 is applied only to the mass m_1. The two steps write:

$$\begin{cases} m_1 \ddot{y}_1 + \sum_{j=1}^{N} \sum_{k=0}^{p} \sum_{l=0}^{q} a_{(1j)kl} (\delta_{1j})^k (\dot{\delta}_{1j})^l = u_1 & i = 1 \text{ (first step)} \\ \sum_{j=1}^{N} \sum_{k=0}^{p} \sum_{l=0}^{q} a'_{(ij)kl} (\delta_{ij})^k (\dot{\delta}_{ij})^l = -\ddot{y}_i & i = 2, \dots, N \text{ (second step)} \end{cases} \tag{2.12}$$

with $a'_{(ij)kl} = a_{(ij)kl}/m_i$. The main disadvantage of this method, similarly to the case of RFS method, is that it requires all data to be measured in all degrees of freedom and a full model of the system to be known, making it impractical to use.

2.2.3 Hilbert-transform based methods

The Hilbert transform is a powerful tool for nonlinearity detection. However, methods based on Hilbert transform are also generally considered to be reliable time-domain identification methods and relatively accurate compared with other ones. In particular, its use in nonlinear identification has been proposed by Feldman, with two specific methods depending on the system response to the input excitation: FREEVIB (Feldman, 1994a) if the response is a free decay, and FORCEVIB (Feldman, 1994b) if the response is a forced vibration. Basically, these methods exploit analytical signals calculated starting from the response of the system $y(t)$. In this form, the analytic signal $Y(t)$ can be represented as function of two different components, the envelope $A(t)$ and the phase $\Psi(t)$, and it writes:

$$Y(t) = y(t) - \mathcal{H}[y(t)] = y(t) - \tilde{y}(t) = A(t)e^{j\Psi(t)} \tag{2.13}$$

with $\tilde{y}(t)$ as the Hilbert transform of $y(t)$. The envelope and the phase are defined as, respectively:

$$\begin{aligned} A(t) &= \sqrt{y^2(t) - \tilde{y}^2(t)} \\ \Psi(t) &= \operatorname{atan}\left(\frac{\tilde{y}(t)}{y(t)}\right) \end{aligned} \tag{2.14}$$

The Hilbert transform operates in the same domain and can be defined as:

$$\mathcal{H}[y(t)] = \tilde{y}(t) = -\frac{1}{j\pi} PV \int_{-\infty}^{+\infty} \frac{y(\tau)}{t-\tau} d\tau \tag{2.15}$$

The main advantage of using the Hilbert transform is the possibility to easily retrieve the instantaneous frequency $\omega(t)$ starting from the instantaneous phase $\Psi(t)$ as:

$$\omega(t) = \dot{\Psi}(t) = \frac{y(t)\,\dot{\tilde{y}}(t) - \dot{y}(t)\tilde{y}(t)}{y^2(t) - \tilde{y}^2(t)} = \operatorname{Im}\left[\frac{\dot{Y}(t)}{Y(t)}\right] \tag{2.16}$$

In order to demonstrate the concepts of FREEVIB method, in the case of a SDOF system subject to free oscillations one has:

$$\ddot{y} + h(A)\dot{y} + \omega_0^2(A)y = 0 \tag{2.17}$$

where $h(A)$ and $\omega_0^2(A)$ are two functions introduced by the method of Feldman, defined as nonlinear damping and nonlinear stiffness functions, respectively. These do not represent the real values of damping and stiffness but

are mathematical escamotages to obtain the system's damping and stiffness curves. The main hypothesis about this method lies in the fact that $h(A)$ and $\omega_0^2(A)$ do not have overlapping spectra with $y(t)$, thus $h(A)$ and $\omega_0^2(A)$ are invariant under the Hilbert operator $\mathcal{H}$. This leads to:

$$\ddot{\tilde{y}} + h(A)\dot{\tilde{y}} + \omega_0^2(A)\tilde{y} = 0 \tag{2.18}$$

By substituting the analytic signal, one has:

$$\ddot{Y} + h(A)\dot{Y} + \omega_0^2(A)Y = 0 \tag{2.19}$$

By resorting Eq. (2.14) one has:

$$\begin{aligned} \dot{Y}(t) &= Y(t)\left[\frac{\dot{A}(t)}{A(t)} + j\omega(t)\right] \\ \ddot{Y}(t) &= Y(t)\left[\frac{\ddot{A}(t)}{A(t)} + \omega^2(t) + \frac{2j\left(\dot{A}(t)\omega(t)\right)}{A(t)} + j\ \dot{\omega}(t)\right] \end{aligned} \tag{2.20}$$

Consequently:

$$\begin{aligned} h(t) &= -2\frac{\dot{A}(t)}{A(t)} - \frac{\dot{\omega}(t)}{\omega(t)} \\ \omega_0^2(t) &= \omega^2(t) - \frac{\ddot{A}(t)}{A(t)} + 2\left(\frac{\dot{A}(t)}{A(t)}\right)^2 + \frac{\dot{A}(t)\dot{\omega}(t)}{A(t)\omega(t)} \end{aligned} \tag{2.21}$$

In the case of free damped vibrations, the amplitude $A(t)$ decreases monotonically over time. This property allows for the definition of its inverse function, $t(A)$, which expresses time as a function of amplitude. Using this inverse relationship, it becomes possible to express both the instantaneous damping and the instantaneous frequency as functions of the amplitude $h(A) = h(t(A))$ and $\omega_0^2(A) = \omega_0^2(t(A))$.

A common way to visualise this relationship is through a plot of amplitude versus instantaneous frequency, commonly referred to as the backbone diagram, particularly useful for identifying stiffness nonlinearities. Figure 2.4 reports the typical results of a FREEVIB procedure, implemented in Matlab®, for a symmetric Duffing oscillator with softening behaviour. The numerical values of the parameters can be retrieved from the stiffness and damping forces $f_{r,s}$ and $f_{r,d}$ through a least-squares fitting procedure.

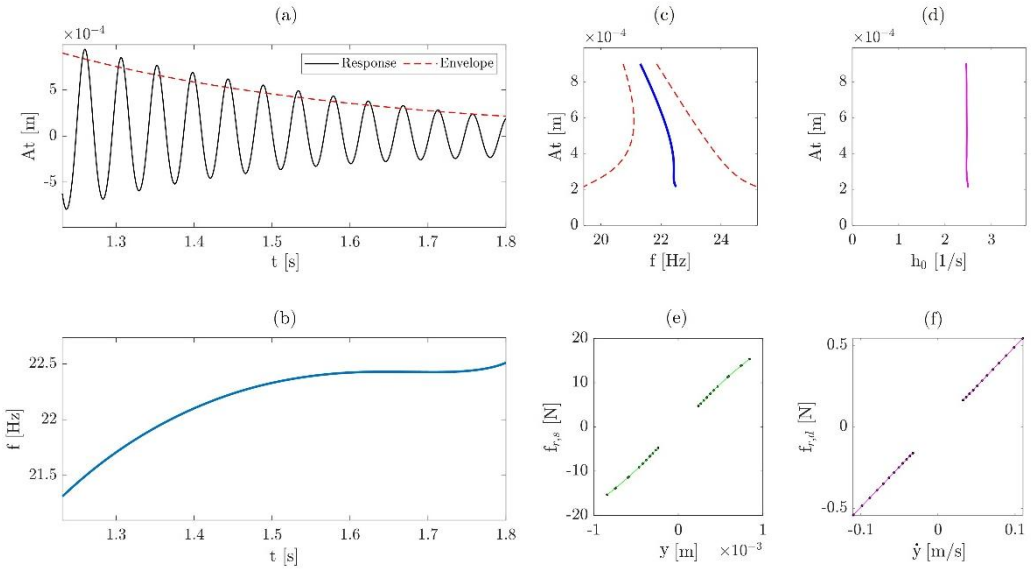

Figure 2.4. FREEVIB results for a Duffing oscillator with softening behaviour: (a) response and amplitude of the Hilber transform, (b) instantaneous frequency, (c) backbone curve, (d) damping factor curve, (e) stiffness restoring force, and (f) damping force.

Similarly, in the forced vibration $u(t)/m$ case, one has:

$$\ddot{Y} + h(A)\dot{Y} + \omega_0^2(A)Y = U(t)/m \tag{2.22}$$

with $U(t)$ as the analytic signal of the input excitation $u(t)$, and consequently:

$$\begin{aligned} h(t) &= \frac{\beta(t)}{m\omega(t)} - 2\frac{\dot{A}(t)}{A(t)} - \frac{\dot{\omega}(t)}{\omega(t)} \\ \omega_0^2(t) &= \omega^2(t) + \frac{\alpha(t)}{m} - \frac{\beta(t)\dot{A}(t)}{mA(t)\omega(t)} - \frac{\ddot{A}(t)}{A(t)} + 2\left(\frac{\dot{A}(t)}{A(t)}\right)^2 + \frac{\dot{A}(t)\dot{\omega}(t)}{A(t)\omega(t)} \\ \frac{U(t)}{X(t)} &= \alpha(t) + j\beta(t) = \frac{u(t)y(t) + \tilde{u}(t)\tilde{y}(t)}{y^2(t) + \tilde{y}^2(t)} + j\frac{\tilde{u}(t)y(t) - u(t)\tilde{y}(t)}{y^2(t) + \tilde{y}^2(t)} \end{aligned} \tag{2.23}$$

with $\alpha(t) = \mathrm{Re}[U(t)/Y(t)]$ and $\beta(t) = \mathrm{Im}[U(t)/Y(t)]$. The case $\alpha(t) = \beta(t) = 0$ corresponds to the FREEVIB method, thus being a particular case of the FORCEVIB one.

2.2.4 Reverse path and conditioned reverse path

The RP method is based on the extension of the '*H1*' and '*H2*' estimation techniques to nonlinear systems. The quantities H_1 and H_2 can be described as:

$$H_1(\omega) = \frac{S_{yu}(\omega)}{S_{uu}(\omega)}, H_2(\omega) = \frac{S_{yy}(\omega)}{S_{yu}(\omega)} \tag{2.24}$$

with the quantities $S_{yu}(\omega)$, $S_{uu}(\omega)$, and $S_{yy}(\omega)$ describing the cross-power spectral density (PSD) between the input and the output, and the auto-PSD of these two quantities, respectively. However, the direct estimation of these quantities cannot be used since the underlying linear characteristics of the system, and as a consequence, of the response are corrupted by the nonlinearities.

As implicitly contained in the definition, the RP approach is based on an inversion of the meaning of input and output. The approach was first introduced by Rice and Fitzpatrick (Rice and Fitzpatrick, 1991), and Bendat et al. (Bendat et al., 1995). In the RP method, the equations of motion for a MDoF should be written as follows:

$$\mathbf{M}\ddot{\mathbf{y}} + \mathbf{C}\dot{\mathbf{y}} + \mathbf{K}\mathbf{y} + \sum_{j=1}^{n} \mathbf{A}_j \, \mathbf{z}_j = u(t) \tag{2.25}$$

where $\mathbf{M}$, $\mathbf{C}$, and $\mathbf{K}$ are the mass, damping and stiffness matrices, $\mathbf{y}$ is the vector of displacements (the single- and double-dots indicates single and double differentiation), $u(t)$ is the external excitation, and $\mathbf{z}_j$ is the j-th term of the nonlinear function vector with the corresponding coefficients $\mathbf{A}_j$. In the case of a quadratic and cubic stiffness at the i-th DoF the vector is given by $\mathbf{z}(t) = [0, \dots, y_i^2(t), y_i^3(t), \dots, 0\,]^{\mathrm{T}}$. By Fourier transforming Equation (2.25) one has:

$$\mathbf{B}(\omega)\mathbf{Y}(\omega) + \sum_{j=1}^{n} \mathbf{A}_j \, \mathbf{Z}_j(\omega) = \mathbf{U}(\omega) \tag{2.26}$$

with $\mathbf{B}(\omega) = -\omega^2\mathbf{M} + i\omega\mathbf{C} + \mathbf{K}$ as the dynamic stiffness matrix. From the latter equation, it discerns the RP terminology: the external excitation is now seen as output, caused by the application of the input constituted by the displacement vector. Exploiting this formulation, the definition of the cross-PSD of the linear term can be written as:

$$\mathbf{S}_{YU}(\omega) = \frac{2}{T}\mathbb{E}[\mathbf{Y}^*(\omega)\mathbf{U}(\omega)] = \mathbf{S}_{YY}(\omega)\mathbf{B}^{\mathrm{T}} + \sum_{j=1}^{n} \mathbf{S}_{YZ_j}(\omega)\,\mathbf{A}_j^{\mathrm{T}} \tag{2.27}$$

In analogous way, the j-th cross-PSD of the nonlinear term can be written as:

$$\mathbf{S}_{Z_jU}(\omega) = \frac{2}{T}\mathbb{E}\left[\mathbf{Z}_j^*(\omega)\mathbf{U}(\omega)\right] = \mathbf{S}_{Z_jY}(\omega)\mathbf{B}^{\mathrm{T}} + \sum_{j=1}^{n}\mathbf{S}_{Z_jZ_j}(\omega)\,\mathbf{A}_j^{\mathrm{T}} \tag{2.28}$$

In Equations (2.27)-(2.28), $\mathbb{E}$ indicates the expectation operator, and T is the length of the temporal measurement window. By reorganising in matrix form, one has:

$$\boldsymbol{\Gamma} = \boldsymbol{\Xi}\boldsymbol{\Psi}^{\mathrm{T}} \tag{2.29}$$

$$\boldsymbol{\Gamma} = \left[\mathbf{S}_{YU}(\omega)^{\mathrm{T}}, \mathbf{S}_{Z_1U}(\omega)^{\mathrm{T}}, \dots, \mathbf{S}_{Z_jU}(\omega)^{\mathrm{T}}, \dots, \mathbf{S}_{Z_nU}(\omega)^{\mathrm{T}}\right]^{\mathrm{T}} \tag{2.30}$$

$$\boldsymbol{\Xi} = \begin{bmatrix} \mathbf{S}_{YY}(\omega) & \mathbf{S}_{Z_1U}(\omega) & \dots & \mathbf{S}_{Z_jU}(\omega) & \dots & \mathbf{S}_{Z_nU}(\omega) \\ \mathbf{S}_{Z_1Y}(\omega) & \mathbf{S}_{Z_1Z_1}(\omega) & \dots & \mathbf{S}_{Z_1Z_j}(\omega) & \dots & \mathbf{S}_{Z_1Z_n}(\omega) \\ \dots & \dots & \dots & \dots & \dots & \dots \\ \mathbf{S}_{Z_jY}(\omega) & \mathbf{S}_{Z_jZ_1}(\omega) & \dots & \mathbf{S}_{Z_jZ_j}(\omega) & \dots & \mathbf{S}_{Z_jZ_n}(\omega) \\ \dots & \dots & \dots & \dots & \dots & \dots \\ \mathbf{S}_{Z_nY}(\omega) & \mathbf{S}_{Z_nZ_1}(\omega) & \dots & \mathbf{S}_{Z_nZ_j}(\omega) & \dots & \mathbf{S}_{Z_nZ_n}(\omega) \end{bmatrix} \tag{2.31}$$

$$\boldsymbol{\Psi} = [\mathbf{B}, \dots, \mathbf{A}_1, \dots, \mathbf{A}_j, \dots, \mathbf{A}_n] \tag{2.32}$$

The main issue associated to this kind of formulation is that the matrix $\boldsymbol{\Xi}$ can be determined by inversion only if the number of external inputs acting on the system is equal to the total number of measured DoFs. Since in experimental measurements this hypothesis is rarely true, that formulation allows the determination of the rows of $\boldsymbol{\Xi}$ corresponding to the DoFs where the external input acts. Moreover, the formulation is characterised by a numerical ill-conditioning. To overcome these limitations, the same Authors proposed a conditioned version of the method (CRP), which relies on determining a set of mutually uncorrelated input forces through the estimation of conditioned PSD. The main drawback of the conditioned version lies in its computational burden.

2.2.5 Volterra approaches

Volterra series (Volterra, 1959) approaches are an interesting method for establishing a non-parametric model for a nonlinear input-output process. For a generic nonlinear dynamical system associated with a single attractor at the zero state and differentiable and smooth nonlinearity, the Volterra series expresses the time-domain response in the following form (Storer, 1991; Storer and Tomlinson, 1993; Tawfiq and Vinh, 2003; Worden, 2019):

$$y(t) \approx \sum_{p=0}^{m} y^{(p)}(t) \tag{2.33}$$

where $y^{(0)}$ is a constant, and the components $y^{(1)}, \dots, y^{(m)}$ are defined as:

$$y^{(1)}(t) = \int_{-\infty}^{+\infty} h^{(1)}(\tau_1) u(t-\tau_1) d\tau_1 \tag{2.34}$$

$$y^{(2)}(t) = \int_{-\infty}^{+\infty} \int_{-\infty}^{+\infty} h^{(2)}(\tau_1, \tau_2) u(t-\tau_1) u(t-\tau_2) d\tau_1 d\tau_2 \tag{2.35}$$

$$\vdots$$

$$y^{(m)}(t) = \int_{-\infty}^{+\infty} \dots \int_{-\infty}^{+\infty} h^{(m)}(\tau_1, \dots, \tau_m) u(t-\tau_1) \dots u(t-\tau_m) d\tau_1 \dots d\tau_m \tag{2.36}$$

with m being the chosen truncation order of the series, $y^{(p)}(t)$ the p-th component of the response of the system, $h^{(m)}(\tau_1, \dots, \tau_m)$ the m-th order Volterra kernel, and $u(t)$ the external excitation. In its infinite, convergent form, the series provides an exact representation of the system output. However, in any practical scenario, the series is truncated resulting in an approximation. Noteworthy, $h^{(m)}(\tau_1, \dots, \tau_m)$ is symmetric with respect to the sorting of the input arguments. This means that for $m = 2$, the symmetry entails that $h^{(2)}(\tau_1, \tau_2) = h^{(2)}(\tau_2, \tau_1)$. Also, it generalises the concept of the linear impulse response function (IRF) to account for higher order interactions in the system. It follows that truncation of the Volterra series at the first order provides an exact representation for linear systems. The m-th order Volterra kernel transform $H^{(m)}(\omega_1, \dots, \omega_m)$, here referred to as higher order frequency response function (HFRF) is defined as:

$$\begin{aligned} H^{(m)}(\omega_1, \dots, \omega_m) = & \int_{-\infty}^{+\infty} \dots \int_{-\infty}^{+\infty} d\tau_1 \dots d\tau_m \\ & \times h^{(m)}(\tau_1, \dots, \tau_m) \\ & \times e^{-j(\omega_1 \tau_1 + \dots + \omega_m \tau_m)} \end{aligned} \tag{2.37}$$

By Fourier transforming Equation (2.36), and exploiting the kernel definition of Equation (2.37), one has:

$$Y^{(m)}(\omega) = \frac{1}{(2\pi)^{m-1}} \int_{-\infty}^{+\infty} \dots \int_{-\infty}^{+\infty} d\omega_1 \dots d\omega_{m-1} \times H^{(m)}(\omega_1, \dots, \omega_{m-1}, \omega - \omega_1 - \dots - \omega_{m-1}) \times U(\omega_1) \dots U(\omega_{m-1}) U(\omega - \omega_1 - \dots - \omega_{m-1}) \tag{2.38}$$

Consequently, Equation (2.33) can be written in the frequency domain as:

$$Y(\omega) \approx \sum_{p=0}^{m} Y^{(p)}(\omega) \tag{2.39}$$

An example of Volterra kernels calculated as in Equation (2.37) for an oscillator with quadratic stiffness k_2 can be found in Figure 2.5. The kernels have been calculated for an oscillator with mass $m = 1$ kg, damping $c = 0.377$ Ns/m, linear stiffness $k_1 = 39.5$ N/m and quadratic stiffness $k_2 = 100$ N/m^2.

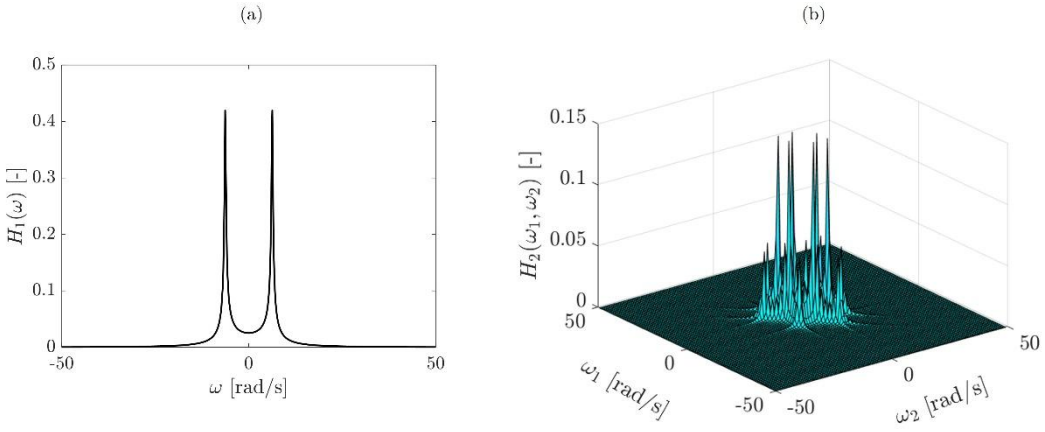

Figure 2.5. (a) Linear and (b) quadratic Volterra kernels.

Volterra system identification has been used for several decades and represents perhaps one of the most well-established frameworks for nonlinear system identification. Examples of instantaneous applications on systems presenting polynomial and hysteretic behaviour can be found in (Ceravolo et al., 2010; Demarie et al., 2005a, 2005b). One of its main advantages lies in the possibility of constructing a direct analytic form of the HFRF for nonlinear systems, especially under specific classes of external excitations (e.g., random) (Worden, 2019). More recently, machine learning techniques have been combined with classical Volterra series approaches (Worden et al., 2025). The applicability of Volterra series is limited by the existence and the convergence of the series (Brockett, 1976) which is still an open challenge (Jing and Xiao, 2017).

Many nonlinearities of practical interest (e.g., bistable Duffing oscillators or hysteretic systems) are characterised by discontinuous or non-smooth

nonlinearities, and the corresponding systems do not strictly admit a Volterra representation. As a consequence, the series convergence may be restricted, and low-order truncations of the series may provide an inaccurate representation of the system dynamics. However, for the Volterra series to be meaningful, two conditions must hold, namely, existence and converge.

Existence and convergence of the Volterra series

The existence condition basically should answer the following question (Lesiak and Krener, 2003; Worden, 2019): when a system response admit being written as a series of functionals? This issue requires fairly extended and complicated mathematical formulations, which can be found in (Palm and Poggio, 1977; Palm and Pöpel, 1985), leading to the following conclusion: "*The class of Volterra-like representable systems is only restricted by a kind of smoothness condition*". This statement becomes more intuitive if one recalls the definition of Volterra series as expansion from functions to functionals. In this sense, a Volterra series-type model expresses the input-output relationship of a system as a functional Taylor series with polynomials of increasing degree (Flake, 1963; Gripenberg et al., 1990). If the input-output relationship is sufficiently smooth in the Fréchet sense (Palm and Poggio, 1977; Xu, 1996), meaning that small perturbations of the input produce correspondingly small variations in the output, then each polynomial term can be written as part of a Volterra series. Thus, Volterra series exists for any nonlinear system whose input-output relationship is smooth. The main drawback of this kind of conclusion is that existence does not imply convergence, which should be carefully verified as separate criterion.

The form of Volterra series as an infinite expansion immediately raises the problem of convergence as the following question (Rugh, 1981): for which time intervals and inputs do the series converge? Usually, answering this question involves finding the radius of convergence the Volterra series, i.e., defining bounds on the external input $u(t)$ on a specific time interval (Hélie and Laroche, 2010; Thouverez, 2000). The calculations required for finding suitable bounds to the problem of convergence are often difficult and impractical to implement. Several attempts have been made in the literature to propose some convergence criteria (Cheng et al., 2017). For instance, for a Duffing oscillator the convergence of its Volterra series can be assessed by defining a ratio involving the magnitude of the spectrum (Li and Billings, 2011; G. Tomlinson et al., 1996). Another appealing idea for establishing a closed-form solution for convergence bounds lies its basis on perturbation approaches (Bullo, 2002). Parametric analyses, which overcome the difficulties coming from analytical formulations, have also been employed to verify the convergence of the Volterra series (Carassale and Kareem, 2010). However, in many cases these criteria are valid for systems subject to harmonic excitation only (Chatterjee and Vyas, 2000; Li and Billings, 2011; Peng and Lang, 2007). More recently, criteria involving a general class of nonlinear

systems subject to either harmonic or general input excitations have been proposed (Zhu and Lang, 2020).

Although convergence can be rigorously addressed from a mathematical perspective, such analyses are often impractical and provide limited applicability (Worden, 2019). Thus, the initial question can be modified as (G. R. Tomlinson et al., 1996): how many terms of the series need to be included to obtain a required accuracy in the representation? In this sense, the convergence issue is mainly related to the fact that the series is required to be truncated at a finite number of terms in all practical computations, possibly leading to large errors. However, it is worth to underline that there does not exist still a uniform approach to the problem of convergence, which should be addressed independently for each nonlinear system under consideration (Cheng et al., 2017).

Associated linear equations for Volterra operators

The method of associated linear equations (ALEs) was first introduced by Vazquez Feijoo et al. (Vazquez Feijoo et al., 2005, 2004). This approach is particularly valuable for increasing the computational efficiency in the calculation of the response of nonlinear systems, being basically a system composed of linear differential equations, and for its applicability (Argoul et al., 2010; Vazquez Feijoo et al., 2010). The basic idea of the ALEs method involves solving a series of linear equations to determine the response of the system. Each equation corresponds to a specific term in the Volterra series expansion, avoiding the direct computation of multiple convolution integrals.

Let's consider a generic dynamical system with input and output polynomial nonlinearity described by the following second-order differential equation:

$$m\ddot{y}(t) + c\dot{y}(t) + \sum_{j=1}^{N} k_j y^j(t) = u(t) \tag{2.40}$$

with m as the mass, c as the linear damping, k as the linear stiffness, k_j as the generic j-th polynomial stiffness, and a_j the generic j-th polynomial nonlinear input coefficient. If the system holds a Volterra series representation, and rearranging Equation (2.40) by leaving on the left hand-side only the linear elements, one has:

$$m\sum_{p=0}^{+\infty} \ddot{y}^{(p)}(t) + c\sum_{p=0}^{+\infty} \dot{y}^{(p)}(t) + k\sum_{p=0}^{+\infty} y^{(p)}(t) = u(t) - \sum_{j=2}^{N} k_j \left[\sum_{p=0}^{+\infty} y^{(p)}(t)\right]^j \tag{2.41}$$

with $y^{(p)}(t)$ representing a specific order term in the Volterra series, and where the series is considered in its infinite form, thus, the truncation order m is

not considered at this stage of mathematical treatment. The polynomial terms in the right-hand side of Equation (2.41) can be interpreted as additional inputs applied to the linear system. The second term in the right hand-side can be developed in powers, thus having a series of terms linear in the parameters. By expanding and rearranging these terms, one has:

$$m\sum_{p=0}^{+\infty}\ddot{y}^{(p)}(t)+c\sum_{p=0}^{+\infty}\dot{y}^{(p)}(t)+k\sum_{p=0}^{+\infty}y^{(p)}(t)=u(t)-\sum_{j=2}^{N}k_j\sum_{i_1=1}^{+\infty}\dots\sum_{i_j=1}^{+\infty}y_{i_1}(t)\dots y_{i_j}(t) \quad (2.42)$$

When using the harmonic probing method, the p-th term of the Volterra series $y^{(p)}(t)$ is nothing else than a harmonic of pulsation $p\Omega$. This property, along with the explicit expression reported in Equation (2.42), suggests expressing p-th term of the Volterra series $y^{(p)}(t)$ as the response of the linear system to a fictitious harmonic input of pulse $p\Omega$. This fictitious external force can be obtained by collecting all the products $y_{i_1}(t)\dots y_{i_j}(t)$ on the right-hand side of Equation (2.42) as a common factor. As a consequence, it is straightforward to assume a series of differential equations with the following form:

$$\begin{aligned} &m\ddot{y}^{(1)}+c\dot{y}^{(1)}+ky^{(1)}=u \\ &m\ddot{y}^{(p)}+c\dot{y}^{(p)}+ky^{(p)}=-\sum_{l=2}^{p}k_l\sum_{i_1}^{p-l+1}\dots\sum_{i_{j-1}}^{p-j+j-i_1-\dots-i_{j-1}}\dots\sum_{l_l}^{p-i_1-\dots-i_{l-1}}y_{i_1}\dots y_{i_j}\dots y_{i_l} \end{aligned} \quad (2.43)$$

where $-\sum_{l=2}^{p}k_l\sum_{i_1}^{p-l+1}\dots\sum_{i_{j-1}}^{p-j+j-i_1-\dots-i_{j-1}}\dots\sum_{l_l}^{p-i_1-\dots-i_{l-1}}y_{i_1}\dots y_{i_j}\dots y_{i_l}$ is the fictitious external force, function of the $p-1$ terms of the Volterra series, and acting on the linear system (i.e., the real one). The differential equations can be described by the differential operator *L* as:

$$L\left[y^{(p)}(t)\right]=f[u(t),y^{(1)}(t),y^{(2)}(t),\dots,y^{(p-1)}(t)] \quad (2.44)$$

with $y^{(p)}(t)$ and L defined as:

$$y^{(p)}(t)=\int_{-\infty}^{+\infty}h^{(1)}(t-\tau)f[y^{(1)}(t),y^{(2)}(t),\dots,y^{(p-1)}(t)]d\tau \quad (2.45)$$

$$L=m\frac{d^2}{dt^2}+c\frac{d}{dt}+k \quad (2.46)$$

where h_1 is the Green's function of the L operator, equal to the IRF. Thus, as general form for a SDoF polynomial system, introducing the truncation order m, the following linear differential equations can be solved:

$$\begin{cases} m\ddot{y}^{(1)} + c\dot{y}^{(1)} + k_1 y^{(1)} = u \\ m\ddot{y}^{(2)} + c\dot{y}^{(2)} + k_1 y^{(2)} = g_2\left[y^{(1)}\right] \\ m\ddot{y}^{(3)} + c\dot{y}^{(3)} + k_1 y^{(3)} = g_3\left[y^{(1)}, y^{(2)}\right] \\ \vdots \\ m\ddot{y}^{(m)} + c\dot{y}^{(m)} + k_1 y^{(m)} = g_j\left[y^{(1)}, y^{(2)}, \dots, y^{(m-1)}\right] \end{cases} \tag{2.47}$$

where g_j is the generic form of nonlinearity, defining the fictitious external force to be applied on the linear system.

2.2.6 NARMAX

The NARMAX term originated as a model formulation, but now it represents a nonlinear identification technique. In particular, it consists of the following steps: (i) structure detection; (ii) parameter estimation; (iii) model validation; (iv) prediction; (v) analysis. The NARMAX approach was introduced in 1981 by the work of Billings (Billings, 1981), and furtherly developed in (Leontaritis and Billings, 1985c, 1985d). A NARMAX model can be written as a discrete approximation of the equation of motion as:

$$\begin{aligned} y(k) = F[&y(k-1), y(k-2), \dots, y\left(k-n_y\right), \\ &u(k-1), u(k-2), \dots, u(k-n_u), \\ &\xi(k-1), \xi(k-2), \dots, \xi\left(k-n_\xi\right)] \end{aligned} \tag{2.48}$$

where $y(k)$, $u(k)$, and $\xi(k)$ are the system response, input excitation, and noise at the discrete time instant k, while F is the generic nonlinear function. The quantities n_y, n_u, and n_ξ represent the time lags in the output, input, and noise.

The NARMAX approach is based on an explicit model structure selection with the aim of obtaining parsimonious and interpretable representations, making the step of structure detection central. In the case of a polynomial system Equation (2.48) can approximate the model adequately for different excitation levels. It is possible to easily extend Equation (2.48) to the case of non-polynomial nonlinearity, bypassing the sensitivity to the input due to the Weierstrass approximation theorem, by adding additional non-polynomial terms (Billings and Chen, 1989). An extensive survey of NARMAX methods for nonlinear identification can be found in (S. A. Billings, 2013).

Compared to the classical Volterra series approach, the main difference is that the Volterra series expresses the current output exclusively as a nonlinear function of past inputs. Although theoretically elegant, this formulation becomes inefficient for systems whose dynamics depend nonlinearly on the output, requiring a large number of terms for an accurate representation. NARMAX partially overcomes this limitation by allowing the inclusion of nonlinear terms of

the delayed output. Therefore, the Volterra series, and more generally block models, can be interpreted as special cases of the NARMAX.

2.3 Concluding remarks

This chapter has introduced some state-of-the-art nonlinear identification techniques, which will serve, either directly or indirectly, as a basis for the development of the methods adopted in this thesis. It is worth noting that there is no universal identification method that is optimal for all classes of systems and all operating conditions. Indeed, the development and implementation of techniques intended for real-world application often depend on the specific characteristics of the problem they seek to solve. For this reason, Chapter 3 will focus on techniques and approaches specifically conceived for addressing some of the issues related to time-varying and nonlinear systems.

References

Adams, Allemang, R.J., 1999a. A NEW DERIVATION OF THE FREQUENCY RESPONSE FUNCTION MATRIX FOR VIBRATING NON-LINEAR SYSTEMS. Journal of Sound and Vibration 227, 1083–1108. https://doi.org/10.1006/jsvi.1999.2396

Adams, Allemang, R.J., 1999b. Characterization of Nonlinear Vibrating Systems Using Internal Feedback and Frequency Response Modulation. Journal of Vibration and Acoustics 121, 495–500. https://doi.org/10.1115/1.2894008

Ajjan Al-Hadid, M., Wright, J.R., 1989. Developments in the force-state mapping technique for non-linear systems and the extension to the location of non-linear elements in a lumped-parameter system. Mechanical Systems and Signal Processing 3, 269–290. https://doi.org/10.1016/0888-3270(89)90053-8

Anastasio, D., Marchesiello, S., Kerschen, G., Noël, J.P., 2019. Experimental identification of distributed nonlinearities in the modal domain. Journal of Sound and Vibration 458, 426–444. https://doi.org/10.1016/j.jsv.2019.07.005

Andrei, N., 2022. Penalty and augmented Lagrangian methods, in: Modern Numerical Nonlinear Optimization. Springer, pp. 475–519.

Argoul, P., Ceravolo, R., Demarie, G.V., Sabia, D., 2010. Instantaneous identification of localized non-linearities in steel framed structures. Mécanique & Industries 11, 105–116. https://doi.org/10.1051/meca/2010022

Beck, J.L., Katafygiotis, L.S., 1998. Updating Models and Their Uncertainties. I: Bayesian Statistical Framework. J. Eng. Mech. 124, 455–461. https://doi.org/10.1061/(ASCE)0733-9399(1998)124:4(455)

Beck, J.L., Yuen, K.-V., 2004. Model Selection Using Response Measurements: Bayesian Probabilistic Approach. J. Eng. Mech. 130, 192–203. https://doi.org/10.1061/(ASCE)0733-9399(2004)130:2(192)

Bendat, J.S., Coppolino, R.N., Palo, P.A., 1995. Identification of physical parameters with memory in non-linear systems. International Journal of Non-Linear Mechanics 30, 841–860. https://doi.org/10.1016/0020-7462(95)00023-2

Bendat, J.S., Palo, P.A., Coppolino, R.N., 1992. A general identification technique for nonlinear differential equations of motion. Probabilistic Engineering Mechanics 7, 43–61.

Benedettini, F., Capecchi, D., Vestroni, F., 1995. Identification of Hysteretic Oscillators under Earthquake Loading by Nonparametric Models.

Bertsekas, D.P., 1976. On penalty and multiplier methods for constrained minimization. SIAM Journal on Control and Optimization 14, 216–235.

Billings, Stephen A, 2013. Nonlinear System Identification: NARMAX Methods in the Time, Frequency, and Spatio–Temporal Domains, 1st ed. Wiley. https://doi.org/10.1002/9781118535561

Billings, S. A., 2013. Nonlinear system identification: NARMAX methods in the time, frequency, and spatio-temporal domains. John Wiley & Sons.

Billings, S.A., 1981. Identification of nonlinear systems using parameter estimation techniques, in: Institute of Electrical Engineers Conference. pp. 183–190.

Billings, S.A., Chen, S., 1989. Extended model set, global data and threshold model identification of severely non-linear systems. International Journal of Control 50, 1897–1923.

Bonato, P., Ceravolo, R., De Stefano, A., Molinari, F., 2000. USE OF CROSS-TIME–FREQUENCY ESTIMATORS FOR STRUCTURAL IDENTIFICATION IN NON-STATIONARY CONDITIONS AND UNDER UNKNOWN EXCITATION. Journal of Sound and Vibration 237, 775–791. https://doi.org/10.1006/jsvi.2000.3097

Boukari, D., Fiacco, A.V., 1995. Survey of penalty, exact-penalty and multiplier methods from 1968 to 1993. Optimization 32, 301–334. https://doi.org/10.1080/02331939508844053

Brockett, R.W., 1976. Volterra series and geometric control theory. Automatica 12, 167–176.

Bullo, F., 2002. Series expansions for analytic systems linear in control. Automatica 38, 1425–1432.

Bursi, O.S., Ceravolo, R., Demarie, G.V., Erlicher, S., Molinari, M., ZANOTTI FRAGONARA, L., 2010. Non-linear identification of a benchmark steel-concrete composite structure subjected to pseudo-dynamic tests, in: Proc. 14th European Conference on Earthquake Engineering. MKD.

Carassale, L., Kareem, A., 2010. Modeling Nonlinear Systems by Volterra Series. J. Eng. Mech. 136, 801–818. https://doi.org/10.1061/(ASCE)EM.1943-7889.0000113

Ceravolo, R., 2009. Time–frequency analysis. Encyclopedia of Structural Health Monitoring.

Ceravolo, R., Demarie, G.V., Erlicher, S., 2010. Instantaneous identification of degrading hysteretic oscillators under earthquake excitation. Structural Health Monitoring 9, 447–464.

Ceravolo, R., Demarie, G.V., Erlicher, S., 2007. Instantaneous identification of Bouc-Wen-type hysteretic systems from seismic response data. Key Engineering Materials 347, 331–338.

Ceravolo, R., Erlicher, S., Zanotti Fragonara, L., 2013. Comparison of restoring force models for the identification of structures with hysteresis and degradation. Journal of Sound and Vibration 332, 6982–6999. https://doi.org/10.1016/j.jsv.2013.08.019

Chatterjee, A., Vyas, N.S., 2000. CONVERGENCE ANALYSIS OF VOLTERRA SERIES RESPONSE OF NONLINEAR SYSTEMS SUBJECTED TO HARMONIC EXCITATION. Journal of Sound and Vibration 236, 339–358. https://doi.org/10.1006/jsvi.2000.2967

Chatzi, E.N., Smyth, A.W., Masri, S.F., 2010. Experimental application of on-line parametric identification for nonlinear hysteretic systems with model uncertainty. Structural Safety 32, 326–337.

Chen, S., Billings, S.A., Grant, P.M., 1990. Non-linear system identification using neural networks. International Journal of Control 51, 1191–1214. https://doi.org/10.1080/00207179008934126

Cheng, C.M., Peng, Z.K., Zhang, W.M., Meng, G., 2017. Volterra-series-based nonlinear system modeling and its engineering applications: A state-of-the-art review. Mechanical Systems and Signal Processing 87, 340–364. https://doi.org/10.1016/j.ymssp.2016.10.029

Collis, W.B., White, P.R., Hammond, J.K., 1998. HIGHER-ORDER SPECTRA: THE BISPECTRUM AND TRISPECTRUM. Mechanical Systems and Signal Processing 12, 375–394. https://doi.org/10.1006/mssp.1997.0145

Crawley, E., Aubert, A., 1984. Identification of nonlinear structural elements by force-state mapping, in: 25th Structures, Structural Dynamics and Materials Conference. Presented at the 25th Structures, Structural Dynamics and Materials Conference, American Institute of Aeronautics and Astronautics, Palm Springs,CA,U.S.A. https://doi.org/10.2514/6.1984-992

Crawley, E., O'Donnell, K., 1986. Identification of nonlinear system parameters in joints using the force-state mapping technique, in: 27th Structures, Structural Dynamics and Materials Conference. Presented at the 27th Structures, Structural Dynamics and Materials Conference, American Institute of Aeronautics and Astronautics, San Antonio,TX,U.S.A. https://doi.org/10.2514/6.1986-1013

Demarie, Ceravolo, R., de Stefano, A., 2005a. Instantaneous identification of polynomial nonlinearity based on Volterra series representation. Key Engineering Materials 293, 703–710.

Demarie, Ceravolo, R., De Stefano, A., Li, O.D., 2005b. Instantaneous identification of rigid bodies on nonlinear support based on volterra series representation, in: Proc. of the 2nd International Conference on Structural Health Monitoring of Intelligent Infrastructure. pp. 16–18.

Feldman, M., 1994a. Non-linear system vibration analysis using Hilbert transform--I. Free vibration analysis method "Freevib." Mechanical Systems and Signal Processing 8, 119–127. https://doi.org/10.1006/mssp.1994.1011

Feldman, M., 1994b. Non-linear system vibration analysis using Hilbert transform--II. Forced vibration analysis method "Forcevib." Mechanical Systems and Signal Processing 8, 309–318. https://doi.org/10.1006/mssp.1994.1023

Flake, R.H., 1963. Volterra series representation of nonlinear systems. Transactions of the American Institute of Electrical Engineers, Part II: Applications and Industry 81, 330–335.

Fletcher, R., 1987. Practical methods of optimization, 2nd ed. ed. Wiley, Chichester New York Brisbane [etc.].

Gifford, S.J., Tomlinson, G.R., 1989. Recent advances in the application of functional series to non-linear structures. Journal of Sound and Vibration 135, 289–317. https://doi.org/10.1016/0022-460X(89)90727-X

Golub, G.H., Van Loan, C.F., 1980. An Analysis of the Total Least Squares Problem. SIAM J. Numer. Anal. 17, 883–893. https://doi.org/10.1137/0717073

Gripenberg, G., Londen, S.-O., Staffans, O., 1990. Volterra integral and functional equations. Cambridge University Press.

Hélie, T., Laroche, B., 2010. Computation of convergence bounds for Volterra series of linear-analytic single-input systems. IEEE Transactions on automatic control 56, 2062–2072.

Huang, N.E., Shen, Z., Long, S.R., Wu, M.C., Shih, H.H., Zheng, Q., Yen, N.-C., Tung, C.C., Liu, H.H., 1998. The empirical mode decomposition and the Hilbert spectrum for nonlinear and non-stationary time series analysis. Proceedings of the Royal Society of London. Series A: mathematical, physical and engineering sciences 454, 903–995.

Jing, X., Xiao, Z., 2017. On convergence of Volterra series expansion of a class of nonlinear systems. Asian Journal of Control 19, 1089–1102.

Kerschen, G., Worden, K., Vakakis, A.F., Golinval, J.-C., 2006. Past, present and future of nonlinear system identification in structural dynamics. Mechanical Systems and Signal Processing 20, 505–592. https://doi.org/10.1016/j.ymssp.2005.04.008

Le, T.-P., Argoul, P., 2004. Continuous wavelet transform for modal identification using free decay response. Journal of sound and vibration 277, 73–100.

Leontaritis, Billings, S.A., 1985a. Input-output parametric models for non-linear systems Part I: deterministic non-linear systems. International Journal of Control 41, 303–328. https://doi.org/10.1080/0020718508961129

Leontaritis, Billings, S.A., 1985b. Input-output parametric models for non-linear systems Part II: stochastic non-linear systems. International Journal of Control 41, 329–344. https://doi.org/10.1080/0020718508961130

Leontaritis, Billings, S.A., 1985c. Input-output parametric models for non-linear systems part II: stochastic non-linear systems. International journal of control 41, 329–344.

Leontaritis, Billings, S.A., 1985d. Input-output parametric models for non-linear systems part I: deterministic non-linear systems. International journal of control 41, 303–328.

Lesiak, C., Krener, A., 2003. The existence and uniqueness of Volterra series for nonlinear systems. IEEE transactions on automatic control 23, 1090–1095.

Li, L., Billings, S., 2011. Analysis of nonlinear oscillators using Volterra series in the frequency domain. Journal of Sound and Vibration 330, 337–355.

Marchesiello, S., Garibaldi, L., 2008. A time domain approach for identifying nonlinear vibrating structures by subspace methods. Mechanical Systems and Signal Processing 22, 81–101. https://doi.org/10.1016/j.ymssp.2007.04.002

Masri, S.F., Caffrey, J.P., Caughey, T.K., Smyth, A.W., Chassiakos, A.G., 2004. Identification of the state equation in complex non-linear systems. International Journal of Non-Linear Mechanics 39, 1111–1127. https://doi.org/10.1016/S0020-7462(03)00109-4

Masri, S.F., Caughey, T.K., 1979. A Nonparametric Identification Technique for Nonlinear Dynamic Problems. Journal of Applied Mechanics 46, 433–447. https://doi.org/10.1115/1.3424568

Masri, S.F., Miller, R.K., Saud, A.F., Caughey, T.K., 1987. Identification of Nonlinear Vibrating Structures: Part I—Formulation. Journal of Applied Mechanics 54, 918–922. https://doi.org/10.1115/1.3173139

Mohammad, K.S., Worden, K., Tomlinson, G.R., 1992. Direct parameter estimation for linear and non-linear structures. Journal of Sound and Vibration 152, 471–499. https://doi.org/10.1016/0022-460X(92)90482-D

Nayfeh, A.H., Mook, D.T., 1995. Nonlinear oscillations, Wiley classics library. J. Wiley & sons, New York Chichester Brisbane [etc.].

Noël, J.P., Kerschen, G., 2017. Nonlinear system identification in structural dynamics: 10 more years of progress. Mechanical Systems and Signal Processing 83, 2–35. https://doi.org/10.1016/j.ymssp.2016.07.020

Noël, J.P., Marchesiello, S., Kerschen, G., 2014. Subspace-based identification of a nonlinear spacecraft in the time and frequency domains. Mechanical Systems and Signal Processing 43, 217–236. https://doi.org/10.1016/j.ymssp.2013.10.016

Pai, P.F., 2011. Time–frequency characterization of nonlinear normal modes and challenges in nonlinearity identification of dynamical systems. Mechanical Systems and Signal Processing 25, 2358–2374. https://doi.org/10.1016/j.ymssp.2011.02.013

Palm, G., Poggio, T., 1977. The Volterra Representation and the Wiener Expansion: Validity and Pitfalls. SIAM J. Appl. Math. 33, 195–216. https://doi.org/10.1137/0133012

Palm, G., Pöpel, B., 1985. Volterra representation and Wiener-like identification of nonlinear systems: Scope and limitations. Quarterly reviews of biophysics 18, 135–164.

Pei, J.-S., Smyth, A.W., Kosmatopoulos, E.B., 2004. Analysis and modification of Volterra/Wiener neural networks for the adaptive identification of non-linear hysteretic dynamic systems. Journal of Sound and Vibration 275, 693–718. https://doi.org/10.1016/j.jsv.2003.06.005

Peng, Z.K., Lang, Z.Q., 2007. On the convergence of the Volterra-series representation of the Duffing's oscillators subjected to harmonic excitations. Journal of Sound and Vibration 305, 322–332.

Quaranta, G., Lacarbonara, W., Masri, S.F., 2020. A review on computational intelligence for identification of nonlinear dynamical systems. Nonlinear Dyn 99, 1709–1761. https://doi.org/10.1007/s11071-019-05430-7

Renson, L., Gonzalez-Buelga, A., Barton, D.A.W., Neild, S.A., 2016. Robust identification of backbone curves using control-based continuation.

Journal of Sound and Vibration 367, 145–158. https://doi.org/10.1016/j.jsv.2015.12.035

Ribeiro, M.I., 2004. Kalman and Extended Kalman Filters: Concept, Derivation and Properties.

Rice, H.J., Fitzpatrick, J.A., 1991. A procedure for the identification of linear and non-linear multi-degree-of-freedom systems. Journal of Sound and Vibration 149, 397–411. https://doi.org/10.1016/0022-460X(91)90444-O

Richards, C.M., Singh, R., 1998. IDENTIFICATION OF MULTI-DEGREE-OF-FREEDOM NON-LINEAR SYSTEMS UNDER RANDOM EXCITATIONS BY THE "REVERSE PATH" SPECTRAL METHOD. Journal of Sound and Vibration 213, 673–708. https://doi.org/10.1006/jsvi.1998.1522

Rosenberg, R.M., 1962. The Normal Modes of Nonlinear n-Degree-of-Freedom Systems. Journal of Applied Mechanics 29, 7–14. https://doi.org/10.1115/1.3636501

Rugh, W.J., 1981. Nonlinear system theory. Johns Hopkins University Press Baltimore.

Shaw, S.W., Pierre, C., 1993. Normal Modes for Non-Linear Vibratory Systems. Journal of Sound and Vibration 164, 85–124. https://doi.org/10.1006/jsvi.1993.1198

Sjöberg, J., Zhang, Q., Ljung, L., Benveniste, A., Delyon, B., Glorennec, P.-Y., Hjalmarsson, H., Juditsky, A., 1995. Nonlinear black-box modeling in system identification: a unified overview. Automatica 31, 1691–1724.

Spina, D., Valente, C., Tomlinson, G.R., 1996. A new procedure for detecting nonlinearity from transient data using the gabor transform. Nonlinear Dyn 11, 235–254. https://doi.org/10.1007/BF00120719

Storer, D.M., 1991. Dynamic analysis of non-linear structures using higher order frequency response functions. The University of Manchester (United Kingdom).

Storer, D.M., Tomlinson, G.R., 1993. Recent developments in the measurement and interpretation of higher order transfer functions from non-linear structures. Mechanical Systems and Signal Processing 7, 173–189.

Tawfiq, I., Vinh, T., 2003. CONTRIBUTION TO THE EXTENSION OF MODAL ANALYSIS TO NON-LINEAR STRUCTURE USING VOLTERRA FUNCTIONAL SERIES. Mechanical Systems and Signal Processing 17, 379–407. https://doi.org/10.1006/mssp.2002.1499

Thouverez, F., 2000. Analysis of the volterra series convergence, in: IUTAM/IFToMM Symposium on Synthesis of Nonlinear Dynamical Systems: Proceedings of the IUTAM/IFToMM Symposium Held in Riga, Latvia, 24–28 August 1998. Springer, pp. 247–255.

Tomlinson, G., Manson, G., Lee, G., 1996. A simple criterion for establishing an upper limit to the harmonic excitation level of the Duffing oscillator using the Volterra series. Journal of Sound and Vibration 190, 751–762.

Tomlinson, G.R., Manson, G., Lee, G.M., 1996. A simple criterion for establishing an upper limit to the harmonic excitation level of the Duffing oscillator using the Volterra series. Journal of Sound and Vibration 190, 751–762.

Vakakis, A.F. (Ed.), 2001. Normal Modes and Localization in Nonlinear Systems. Springer Netherlands, Dordrecht. https://doi.org/10.1007/978-94-017-2452-4

Vazquez Feijoo, J.A., Worden, K., Montes Garcia, P., Lagunez Rivera, L., Juarez Rodriguez, N., Pech Pérez, A., 2010. Analysis of MDOF nonlinear systems using associated linear equations. Mechanical Systems and Signal Processing 24, 2824–2843. https://doi.org/10.1016/j.ymssp.2010.04.008

Vazquez Feijoo, J.A., Worden, K., Stanway, R., 2005. Associated Linear Equations for Volterra operators. Mechanical Systems and Signal Processing 19, 57–69. https://doi.org/10.1016/j.ymssp.2004.03.003

Vazquez Feijoo, J.A., Worden, K., Stanway, R., 2004. System identification using associated linear equations. Mechanical Systems and Signal Processing 18, 431–455. https://doi.org/10.1016/S0888-3270(03)00078-5

Volterra, V., 1959. Theory of functionals and of integral and integro-differential equations Dover Publications. Inc., USA.

Walczak, S., Cerpa, N., 1999. Heuristic principles for the design of artificial neural networks. Information and Software Technology 41, 107–117. https://doi.org/10.1016/S0950-5849(98)00116-5

Worden, K., 2019. Nonlinearity in structural dynamics: detection, identification and modelling. CRC Press.

Worden, K., Rogers, T., Preston, O., 2025. Machine-learning perspectives on Volterra system identification. Philosophical Transactions of the Royal Society A: Mathematical, Physical and Engineering Sciences 383.

Wu, M., Smyth, A.W., 2007. Application of the unscented Kalman filter for real-time nonlinear structural system identification. Struct. Control Health Monit. 14, 971–990. https://doi.org/10.1002/stc.186

Xu, L.Y., 1996. Nonlinear dynamic systems, volterra series, and uniform approximations. The University of Texas at Austin.

Yang, Y., Ibrahim, S.R., 1985. A Nonparametric Identification Technique for a Variety of Discrete Nonlinear Vibrating Systems. Journal of Vibration and Acoustics 107, 60–66. https://doi.org/10.1115/1.3274717

Zhu, Y.-P., Lang, Z.-Q., 2020. A new convergence analysis for the Volterra series representation of nonlinear systems. Automatica 111, 108599.

Chapter 3

Identification of systems featuring a time localisation of spectral components

3.1 Motivations

System identification uses random data analysis techniques that are very well established and reliable when referring to linear and stationary systems (Bendat and Piersol, 2011; Castro, 2021; Gardner and Robinson, 1989; Kay, 1993; Marple Jr, 2019; Mitra, 2001; Oppenheim et al., 1989; Stoica and Moses, 2005). Nevertheless, models used in the field of earthquake engineering, as well as in various applications of structural dynamics, often cannot rely on simplifications such as linearity or time-invariance (Orozco et al., 2026). Correspondingly, the stochastic processes that describe the dynamic response signals of these systems are generally non-stationary (Hammond and White, 1996). For instance, in a first-order non-stationary signal $y(t)$, the expected value of the signal $\mathbb{E}[y(t)]$ depends on a time-varying mean $\mu(t)$; additionally, in a second-order non-stationary signal, also the variance changes with time $\sigma(t)$, and likewise for each successive order (Priestley, 1988). This notion is directly related to the definition of order for stationary processes (Priestley, 1982).

A very challenging situation arises when the realisations of a stochastic process are generated from a nonlinear dynamical system subject to non-stationary excitation, e.g., an earthquake. Indeed, when the task is SI, it is difficult to distinguish the effects of the system's nonlinearity from those of the excitation's non-stationarity within the dynamic response signals (Čačko et al., 1988; Hammond, 1968; Priestley, 1967, 1965). The frequent co-occurrence of

nonlinearity and non-stationarity sources in natural and engineered systems necessitates advanced techniques capable of handling both aspects simultaneously. Thus, the SI task will face difficulty when the time-varying system involves the nonlinearity, making the system solution have both the nonlinear and non-stationary components. Figure 3.1 shows a linear stationary signal compared to a nonlinear non-stationary one (a-c) with their corresponding phase portraits (b-d).

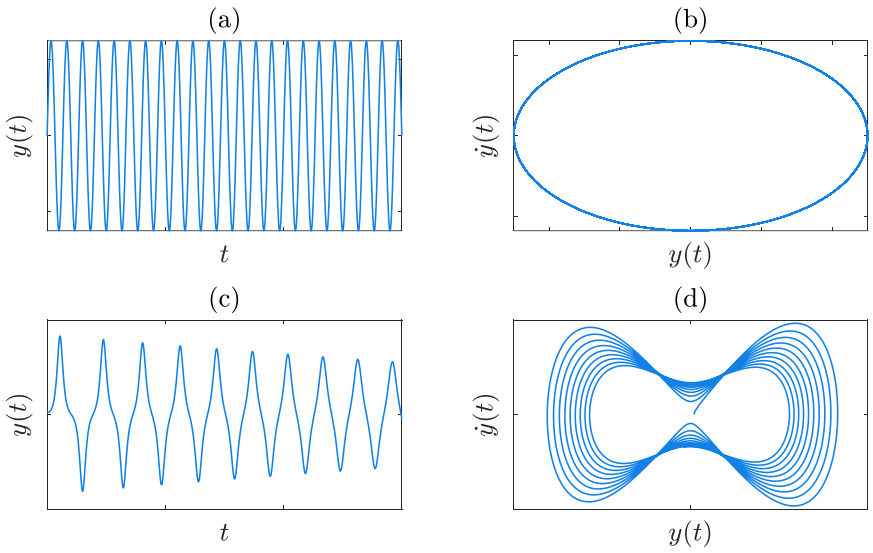

Figure 3.1. Stationary and linear signal (a) and non-stationary and nonlinear signal (c) with the corresponding phase portrait (b-d).

The instantaneous characteristics of the response are therefore closely related to both the nonlinear and non-stationary nature of the system. Under such conditions, nonlinear identification methods based on the assumption of system stationarity are often inadequate or inaccurate (Dimitriadis et al., 2004).

In particular, the main computational issues arising from the coupling of non-stationarity and nonlinearity can be summarised as follows (Cheng et al., 2015):

(i) establishing a quantitative relationship between the dynamic parameters of the system and the instantaneous characteristics of the response, such as frequency and amplitude, in order to interpret the observed variations in terms of physical changes in the system is not straightforward.

(ii) accurately *identifying* and *estimating* the temporal variations of these quantities from the measured signals require appropriate signal processing techniques.

3.2 Time localisation of spectral components

Unravelling nonlinearity from non-stationarity is one of the main challenges when dealing with signals which are both nonlinear and non-stationary (Argoul et al., 2000; Bonato et al., 2000a; Ceravolo, 2004; Priestley, 1965). In this context, time-frequency analysis represents an effective tool for characterising signals whose spectral components vary over time (Bradford, 2007; Dalianis et al., 1998; Hammond and White, 1996; Priestley, 1965; Spina et al., 1996). As an example, let us consider a linear chirp and a pulse as two distinct time-varying signals. The signals behave in a completely different way in the time domain, but they can have identical spectral estimates. Conversely, any type of time-frequency representation provides a three-dimensional space composed of time, frequency, and power that shows how the spectral content varies over time (Boashash, 2015; Ceravolo, 2008; Cohen, 1995; Flandrin, 1998). In this way, it becomes intuitively clear how two signals with the same frequency spectrum can have different temporal characteristics.

3.2.1 Linear time-frequency transforms

All linear time-frequency transforms satisfy the superposition principle (Hlawatsch and Boudreaux-Bartels, 2002), i.e., if the generic signal $y(t)$ can be considered as a combination of different components, then its time-frequency representation is the same linear combination of the single-component time-frequency representation. Some examples of linear time-frequency transforms are the short-time Fourier transform (STFT) (Allen and Rabiner, 2005; Baba, 2012; Nawab and Quatieri, 1987; Portnoff, 2003) and the wavelet transform (WT) (Chui, 1992; Debnath, 2003; Rioul and Vetterli, 1991).

Short-time Fourier transform

The most intuitive way to introduce the time localisation of the components of a signal relies on the concept of windowing (Bastiaans, 2003; Cohen, 1995; Oppenheim, 1978; Rabiner, 1978), which can be easily explained as follows. Instead of considering the entire signal, a short portion of the signal is isolated around a time instant t_i. This is achieved by multiplying the signal by a windowing function, i.e. a function with amplitude between 0 and 1 that is non-zero only in a small interval around t_i. As a result, only the part of signal falling within the window contributes to the analysis. This straightforward notion is represented in Figure 3.2. In particular, windowing can be applied both in time and frequency domain: if in time the operation is a simple multiplication (represented by the symbol $\times$), in frequency domain it becomes a convolution (represented by the symbol $*$).

Time-frequency approaches relying on windowing basically introduce the time localisation of frequency components by pre-windowing the signal around a

time instant t_i, calculating its Fourier transform, and doing that for each time instant. Thus, a frequency spectrum characterising the signal locally for each time instant is obtained. By repeating this transformation, it is possible to trace the evolution of the spectral content over time.

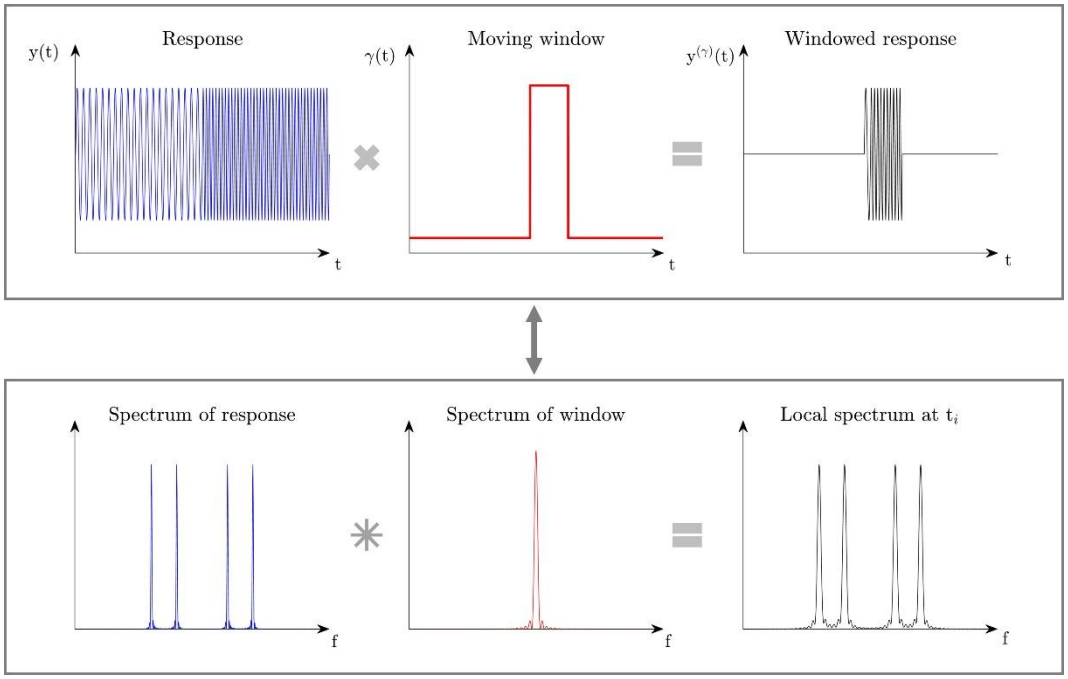

Figure 3.2. Windowing in time and frequency domain.

Accordingly, by introducing a short time analysis window $\gamma(t)$, the STFT of a generic signal $y(t)$ is defined as (Cohen, 1995; Hlawatsch and Boudreaux-Bartels, 2002):

$$\mathbf{STFT}_y^{(\gamma)}(t,\omega) = \int_{-\infty}^{+\infty} y(t')\gamma^*(t-t')e^{-j\omega t'}dt' \tag{3.1}$$

where the superscript * denotes complex conjugation. An advantageous property is given by the fact that the STFT can be also expressed in terms of signal and window spectra by exploiting the time-frequency duality (Hlawatsch and Boudreaux-Bartels, 2002):

$$\mathbf{STFT}_y^{(\gamma)}(t,\omega) = \int_{-\infty}^{+\infty} Y(\omega')\Gamma^*(\omega'-\omega)e^{j(\omega'-\omega)t}d\omega' \tag{3.2}$$

Thus, the STFT can be simply interpreted as the inverse Fourier transform of the windowed spectrum, as represented in Figure 3.2, in which the window spectrum $\Gamma^*(\omega)$ is nothing more than the Fourier transform of the short time analysis window $\gamma(t)$. The inverse FT of the windowed spectrum can be

interpreted as the result of passing the signal through a filter with frequency response $\Gamma^*(\omega' - \omega)$ and centred around the bandpass frequency ω (Nawab and Quatieri, 1987; Portnoff, 2003; Rabiner and Schafer, 2007).

Wavelet transforms

A second important linear transform is given by the WT defined as (Hlawatsch and Boudreaux-Bartels, 2002):

$$\mathbf{WT}_y^{(\psi)}(t,\omega) = \int_{-\infty}^{+\infty} Y(\omega') \sqrt{\frac{\omega}{\omega_0}} \psi^* \left(\frac{\omega}{\omega_0} (t' - t) \right) dt' \tag{3.3}$$

with $\psi(t)$ as the analysing wavelet, i.e., a real or complex bandpass function centred around $t = 0$ in the time-domain. The parameter ω_0 represents the center frequency of $\psi(t)$. The WT has been originally introduced as time-scale representation (Rioul and Vetterli, 1991) and indeed preserves the time shifts and the time scaling, however not the frequency shifts. There exists a similarity between the STFT and the WT. Indeed, like the STFT case, the WT can be interpreted as the result of filtering the signal with a bandpass filter, which, conversely to the STFT, is proportional to the center frequency ω. Also, both their time and frequency resolutions are related via the Heisenberg-Gabor inequality, also known as uncertainty principle (Cohen, 1995; Gabor, 1946). However, while in the case of STFT the resolution is the same for each analysis frequency, the WT analyses higher frequencies values with better time resolution but poorer frequency resolution (Rioul, 1990).

Uncertainty principle and best windowing

The Heisenberg-Gabor inequality, or uncertainty principle, has a main role in the time-frequency analysis (Loughlin and Cohen, 2004). In general, the uncertainty principle can be written as (Cohen, 1995; Gabor, 1946):

$$TB \geq \frac{1}{2} \tag{3.4}$$

where T and B are the duration and bandwidth defined as:

$$\begin{aligned} T^2 = \sigma_t^2 &= \int (t - < t >)^2 |y(t)|^2 dt \\ B^2 = \sigma_\omega^2 &= \int (\omega - < \omega >)^2 |Y(\omega)|^2 d\omega \end{aligned} \tag{3.5}$$

Thus, combining Equation (3.4) and (3.5), it follows that the uncertainty principle has 4 main ingredients: (i) the signal density in time $|y(t)|^2$; (ii) the signal density in frequency $|Y(\omega)|^2$; (iii) the Fourier pairs $y(t)$ and $Y(\omega)$; (iv) the

standard deviations of time and frequency T and B. Practically speaking, this principle states that one cannot have or construct a signal for which both T and B are simultaneously arbitrarily small and should always be respected. The fact that the higher is the resolution in frequency, the lower is the resolution in time, and vice versa, means that if the window $\gamma(t)$ is short in duration, the frequency window is broad. Conversely, if the window is long in duration, the frequency window is narrow, and one has a narrowband spectrum. There should always be a trade-off between time and frequency localisation, and the degree of trade-off depends on the window, signal, time, and frequency. The uncertainty principle defines these trade-off dependencies. A crucial aspect is given by the impossibility of finding the perfect window. Studies on the influence of the window on the identification task have been conducted in (Ceravolo, 2008). Table 3.1 shows the most common types of windows, then depicted in Figure 3.3.

Table 3.1. Common types of windows.

Type	Definition	
Rectangular	$\gamma(t) = \begin{cases} 1 \\ 0 \end{cases}$	for $0 \le t \le T$ otherwise
Bartlett (triangular)	$\gamma(t) = \begin{cases} \frac{2t}{T} \\ 2 - \frac{2t}{T} \\ 0 \end{cases}$	for $0 \le t \le \frac{T}{2}$ for $\frac{T}{2} \le t \le T$ otherwise
Hanning	$\gamma(t) = \begin{cases} 0.5 - 0.5\cos\left(\frac{2\pi t}{T}\right) \\ 0 \end{cases}$	for $0 \le t \le T$ otherwise
Hamming	$\gamma(t) = \begin{cases} 0.54 - 0.46\cos\left(\frac{2\pi t}{T}\right) \\ 0 \end{cases}$	for $0 \le t \le T$ otherwise
Blackman	$\gamma(t) = \begin{cases} 0.42 - 0.5\cos\left(\frac{2\pi t}{T}\right) + 0.08\cos\left(\frac{4\pi t}{T}\right) \\ 0 \end{cases}$	for $0 \le t \le T$ otherwise

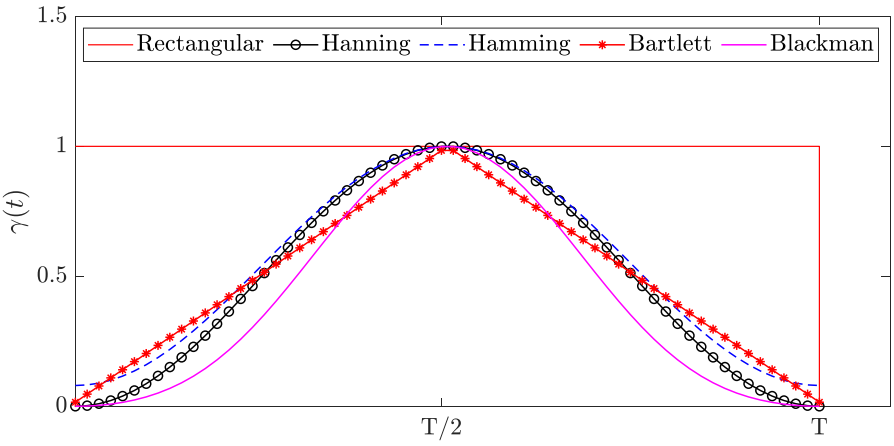

Figure 3.3. Types of windows as function of time.

Even if it is said that no window is applied to a signal, there is always a windowing effect in the discrete time computation of the signals (Oppenheim et al., 1989). Indeed, passing from continuous to discrete, the signal is convoluted with a rectangular window of uniform height. Therefore, 'no window' is often a uniform/rectangular window. Hanning and Hamming are remarkably similar, but Hanning touches the zero eliminating every discontinuity (Harris, 2005). An Hanning type of window is satisfactory for both harmonic and random signals, since it has good frequency resolution and reduces the spectral leakage (Wickramarachi, 2003).

If applied to a STFT, the windowing process has two main effects (Oppenheim et al., 1989): (i) reduced resolution, mainly affected by the width of the main lobe; (ii) leakage effect, which basically consists in an overlap between the frequencies (the component at one frequency leaks into the vicinity of another component due to the spectral smearing introduced by the window), and depends on the relative amplitude of the main lobe and the side lobes.

3.2.2 Quadratic time-frequency transforms

Linearity is a desirable property because it allows for the analysis of complex signals by breaking them down into simpler components. However sometimes it is most reasonable to assume a quadratic version of these transforms, especially when it is convenient to assume the time-frequency representation as energy distribution (Boashash and Ouelha, 2017; Grace, 1981; Rihaczek, 1968). By defining the instantaneous power of the signal $|y(t)|^2$ and the spectral energy density $|Y(f)|^2$, this energetic interpretation is conveniently expressed by the following marginal properties (Cohen, 1995; Loughlin et al., 2002; Wigner, 1932, 1971):

$$|y(t)|^2 = \int_{-\infty}^{+\infty} \mathbf{T}_y(t,\omega)d\omega \tag{3.6}$$

$$|Y(\omega)|^2 = \int_{-\infty}^{+\infty} \mathbf{T}_y(t,\omega)dt \tag{3.7}$$

with $\mathbf{T}_y(t,\omega)$ as the time-frequency transform of the signal $y(t)$. Consequently, the energy of the signal can be defined as (Rihaczek, 1968):

$$E_y = \int_{-\infty}^{+\infty} |y(t)|^2 dt = \int_{-\infty}^{+\infty} |Y(\omega)|^2 d\omega = \iint_{+\infty}^{-\infty} \mathbf{T}_y(t,\omega)dtd\omega \tag{3.8}$$

Generally, the marginal properties are not sufficient to define an energy density at every point of the time-frequency plane due to the uncertainty principle

(Loughlin, 1992), as reported in Equation (3.4). However, in some cases marginal properties can be overlooked, and it is possible to obtain an adequate energetic interpretation (Claasen and Mecklenbrauker, 1984). It is the case of the spectrogram (SPEC) and the scalogram (SCAL), i.e., the squared versions of the STFT and WT, respectively, that allow a qualitative overview of the energetic content of the signal (Cohen, 2002). In particular, they write:

$$\mathbf{SPEC}_y^{(\gamma)}(t,\omega) = \left|\mathbf{STFT}_y^{(\gamma)}(t,\omega)\right|^2 \tag{3.9}$$

$$\mathbf{SCAL}_y^{(\psi)}(t,\omega) = \left|\mathbf{WT}_y^{(\psi)}(t,\omega)\right|^2 \tag{3.10}$$

As a consequence, the linear superposition principle does not hold anymore, and in turn a quadratic superposition principle can be derived. For a two-components signal $y(t) = a_1 y_1(t) + a_2 y_2(t)$, the latter writes (Hlawatsch and Boudreaux-Bartels, 2002):

$$\mathbf{T}_y(t,\omega) = |a_1|^2 \mathbf{T}_{y_1}(t,\omega) + |a_2|^2 \mathbf{T}_{y_2}(t,\omega) + a_1 a_2 \mathbf{T}_{y_1 y_2}(t,\omega) + a_2 a_1 \mathbf{T}_{y_2 y_1}(t,\omega) \tag{3.11}$$

The last two terms are the cross or interference terms. In the specific case of SPEC and SCAL, if two signal components are sufficiently apart in the time-frequency plane, these terms are equal to zero (Jeong and Williams, 1992).

Wigner-Ville distribution and its smoothed version

The Wigner-Ville distribution (WVD), or transform, is obtained by a generalisation of the Wiener-Khinchine theorem, which states that the correlation function and the power spectrum generally form a Fourier pair (Cohen, 1998, 1992). By assuming a symmetric form of the instantaneous temporal and spectral autocorrelation as function of time and frequency lag τ and ν, one has (Cohen and Posch, 1985; Hlawatsch, 2002):

$$r_y(\tau,t) = y\left(t - \frac{\tau}{2}\right) y\left(t + \frac{\tau}{2}\right) \tag{3.12}$$

$$R_y(\nu,\omega) = Y\left(\omega - \frac{\nu}{2}\right) Y\left(\omega + \frac{\nu}{2}\right) \tag{3.13}$$

By transforming Equations (3.12) and (3.13), one obtains the WVD as (Cohen, 1995):

$$\mathbf{WVD}_y(t,\omega) = \int_{-\infty}^{+\infty} y\left(t+\frac{\tau}{2}\right) y^*\left(t-\frac{\tau}{2}\right) e^{-j\omega\tau} d\tau \tag{3.14}$$

$$= \int_{-\infty}^{+\infty} Y\left(\omega+\frac{\nu}{2}\right) Y^*\left(\omega-\frac{\nu}{2}\right) e^{jt\nu} d\nu \tag{3.15}$$

If one considers the cross-correlation between two distinct signals $y_1(t)$ and $y_2(t)$, the WVD assumes the following more general form:

$$\mathbf{WVD}_{y_1y_2}(t,\omega) = \int_{-\infty}^{+\infty} y_1\left(t+\frac{\tau}{2}\right) y_2^*\left(t-\frac{\tau}{2}\right) e^{-j\omega\tau} d\tau \tag{3.16}$$

$$= \int_{-\infty}^{+\infty} Y_1\left(\omega+\frac{\nu}{2}\right) Y_2^*\left(\omega-\frac{\nu}{2}\right) e^{jt\nu} d\nu \tag{3.17}$$

The WVD satisfies a large number of desirable properties, among them, the shift-invariance, and the possibility of assuming real values only (Cohen, 2002). Being based on a correlative structure, however, it does not allow an online implementation in time-frequency identification tasks (Carmona et al., 1998). The WVD is particularly important in the case of signals with time-varying properties, since it highlights the so-called ridge, i.e. the instantaneous frequency variation over time. An evaluation of the performance of the WVD in the estimation of time-varying instantaneous frequency is reported in (Ivanovic et al., 2003).

Although WVD is theoretically remarkably interesting due to its mathematical properties, its practical use is often limited by the presence of interference terms (Hlawatsch, 1984). Since these terms are oscillatory in nature, they can be attenuated by applying a smoothing operation (e.g., low-pass filtering). Basically, the smoothed-pseudo WVD (herein after defined as S-WVD) is obtained by introducing two distinct smoothing windows in time and frequency domain, $w(t)$ and $W(\omega)$, as (Flandrin and Rioul, 1990):

$$\mathbf{S-WVD}_y^{(w,W)}(t,\omega) = \int_{-\infty}^{+\infty} w(t)W(\omega) y_1\left(t+\frac{\tau}{2}\right) y_2^*\left(t-\frac{\tau}{2}\right) e^{-j\omega\tau} d\tau \tag{3.18}$$

The windows effective lengths determine independently the time and frequency smoothing spread, resulting in increasing computational efficiency and flexibility. If the time-smoothing is omitted, then the distribution is referred to as pseudo WVD (P-WVD), which is nothing more than a short-time WVD (Flandrin and Escudié, 1984).

It is worth noting that this reduction of the interference terms results in a dispersion in the time-frequency domain, because smoothing tends to broaden the signal terms in the WVD. This effect is illustrated in Figure 3.4 in the case of a chirp varying linearly between 100 Hz and 400 Hz.

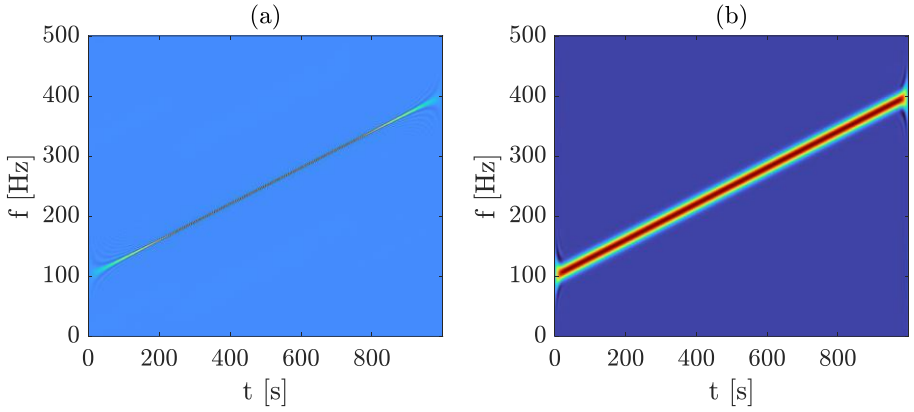

Figure 3.4. Chirp signal: (a) WVD and (b) S-WVD.

It is therefore clear that there should be a fundamental trade-off between good interference attenuation and good time-frequency concentration: a broad smoothing function in the WVD domain effectively reduces interference but worsens the time-frequency concentration of the signal. A further negative consequence of smoothing is the possible loss of some desirable properties of the time-frequency representation (Hlawatsch and Flandrin, 1997).

Cohen class of transform

The Cohen class of transforms is composed by the quadratic time-frequency transforms which hold the time-frequency shift-invariance, i.e., if the signal $y(t)$ is delayed in time and/or shifted in frequency, then its time-frequency transform will be shifted with the same delay (Claasen and Mecklenbraüker, 1980). Basically, Cohen demonstrated that each member of this class can be viewed as a filtered WVD. In particular, one has a following general formula, which can be written in four different domains: time-frequency domain, temporal correlation domain, spectral correlation domain, and ambiguity function domain (Cohen, 1995, 1966). In the temporal correlation domain, one has:

$$\mathbf{T}_y(t,f) = \int_{-\infty}^{+\infty}\int_{-\infty}^{+\infty} r_y(t',\tau)\psi(t-t',\tau)e^{-j2\pi f\tau}dt'd\tau \tag{3.19}$$

$$\psi(t,\tau) = \int_{-\infty}^{+\infty}\int_{-\infty}^{+\infty} \theta(\nu,\tau)e^{-j2\pi\nu\tau}d\nu \tag{3.20}$$

where θ is the kernel function, different for each transform (in the case of the WVD, it is equal to 1). An overview of the kernels for several quadratic time-frequency transforms can be found in (Cohen, 2002). The concept of kernel in Cohen class of transforms intuitively recalls the one found in the case of Volterra series approaches, described in Chapter 2. A close analogy between Cohen's class and a second-order double Volterra series representation has been reported from a systemic interpretation point of view in (Nam and Powers, 2003).

3.3 Instantaneous parameter estimation

3.3.1 Time-frequency domain identification

Locally stationary processes

To approach non-stationary problems, it is possible to start from the concept of spectral density, which is well-consolidated in the case of stationary processes, and extend it to locally stationary processes (Barbato and Conte, 2008; Hammond and White, 1996; Priestley, 1965; Shields and Deodatis, 2013; Wang et al., 2022).

Let us consider a generic process F. In the case of WVD, the spectral density $S_{\mathbf{WVD}}$ can be calculated as (Carmona et al., 1998; Martin and Flandrin, 2003):

$$S_{\mathbf{WVD}} = \mathbb{E}[\mathbf{WVD}_F(t,\omega)] = \int_{-\infty}^{+\infty} \mathbb{E}[r_F(t,\tau)]e^{-j\omega\tau}d\tau \tag{3.21}$$

with $\mathbb{E}[r_F(t,\tau)]$ as the covariance function, defined as the expected value of the auto-correlation function. It is clear that in the case of a stationary process, $S_{\mathbf{WVD}}$ is independent of time and reduces to the usual spectral density $S_F(\omega)$ (Carmona et al., 1998; Martin and Flandrin, 2003). In the case of non-stationary process, the main issue is to deal with the fact that, usually, only a limited number of realisations of the process is available. However, if the process is ergodic (e.g., ideal Gaussian white noise), then an estimate of Equation (3.21) can be obtained from a single realisation $y(t)$ of the process by averaging over instantaneous spectra of finite bandwidth B as (Flandrin and Martin, 1997):

$$V_B(\omega) = \frac{1}{\mathrm{B}} \int_{-\mathrm{B}/2}^{+\mathrm{B}/2} \left|\mathbf{WVD}_y(t,\omega)\right| dt \tag{3.22}$$

In the case of the spectrogram, one has (Carmona et al., 1998):

$$S_{\mathbf{SPEC}} = \mathbb{E}[\mathbf{SPEC}_F^{(\gamma)}(t,\omega)] = \int_{-\infty}^{+\infty} |\Gamma(\omega' - \omega)|^2 S_F(\omega) d\omega' \tag{3.23}$$

with $S_F(\omega)$ as the spectral density associated with F. Equation (3.23) shows that the value of $S_{\mathbf{SPEC}}$ at ω is a weighted average of the spectral density. Again, assuming the ergodicity of the signal, also in the case of a non-stationary process one can define an estimate of SPEC as (Carmona et al., 1998):

$$V_B(\omega) = \frac{1}{\mathrm{B}} \int_{-\mathrm{B}/2}^{+\mathrm{B}/2} \left|\mathbf{SPEC}_y^{(\gamma)}(t,\omega)\right| dt \tag{3.24}$$

Equation (3.24) is a weighted average, thus the estimator is biased. A spectral function supporting this kind of operation can be defined also for the SCAL (Carmona et al., 1998).

The covariance operator can be defined as a convolution, known to be diagonalised by complex exponential functions. In general, when a process is non-stationary, the covariance operator assumes time-varying characteristics, making its estimation difficult due to the impossibility of a priori knowledge on diagonalisation. In such a case, one may approach non-stationary processes as locally stationary ones (Dahlhaus, 1996), whose covariance operators are convolutions in an approximate way. In the case of linear time-series, this extension is straightforward, see (Dahlhaus, 1997; Mallat et al., 1998). However, in the nonlinear case, the situation is more challenging and needs further investigation. A general theory for nonlinear locally stationary processes is presented in (Dahlhaus et al., 2019).

In time-frequency plane, it is difficult to provide a universal definition for local stationarity, but rather several formalisations around the idea that a process is nearly stationary over short intervals with evolving statistical properties (Dahlhaus, 2012). The most intuitive idea for visualising the notion of local stationarity refers to the WVD. The Wigner spectrum varies around a time instant $\bar{t}$ so that the interval of variation is $[\bar{t} - \delta, \bar{t} + \delta]$. The parameter δ is called stationarity length (Martin, 1984). The problem of defining a window (or kernel, in the case of Cohen class of transform) consistent with δ remains an open issue. Several techniques have been formulated, often based on optimisation procedures (Durak and Arikan, 2003; Kozek, 1992; Marx and Gryllias, 2023) or Monte Carlo strategies (Abbiati et al., 2015). However, these methods were designed to be applied to stochastic processes or to a sufficient number of sample realisations and are not adequate when only a single observation of the signal is available.

Time-frequency estimation

By retrieving the estimators reported in Equation (3.22) and (3.24), an appealing idea is to extend them to the case of a single realisation $y(t)$ of locally stationary processes by imposing $B = \delta$ as (Ceravolo, 2008):

$$V_y(t,\omega) = \left|\mathbf{T}_y(t,\omega)\right| \tag{3.25}$$

where $\mathbf{T}_y(t,\omega)$ is any quadratic time-frequency representation. Starting from Equation (3.25), it is possible to track the amplitude ratio and phase difference in multi-channel measurements (Bonato et al., 2000a, 2000b). In linear time-invariant systems, this can support dynamic identification procedures, since the stability of those estimators over time discriminates the modal components from exogenous frequency components. Modal signals exhibit time-invariant amplitude and phase relationships; thus, their modal shapes remain constant over time. Based on this notion, identifying the modal frequencies essentially consists of finding the values of frequencies for which the estimators remain constant in time.

In the case of nonlinear time-varying systems, one should retrieve to more sophisticated procedures, arising from signal synthesis, which basically involves designing a target time-frequency distribution that maps desired signal characteristics and then using inverse problem techniques to reconstruct the time-domain signal (Boashash, 1988). In the time-frequency plane, filtering can be envisaged by introducing a time-frequency mask $\Gamma(t,\omega)$ as (Boudreaux-Bartels and Parks, 2003; Mecklenbräuker and Hlawatsch, 1997):

$$\widetilde{\mathbf{T}}(t,\omega) = \Gamma(t,\omega)\mathbf{T}(t,\omega) \tag{3.26}$$

However, usually one should refer to optimisation techniques to find the time-frequency decomposition which best fits the time-frequency models, since in the masking approach not all two-dimensional functions are valid time-frequency representations. In particular, this problem can be written as the minimisation of an objective function J as (Boudreaux-Bartels and Parks, 2003; Mecklenbräuker and Hlawatsch, 1997):

$$J = \left\|\mathbf{T}_y(t,\omega) - \widetilde{\mathbf{T}}(t,\omega)\right\| \rightarrow \min_y J \tag{3.27}$$

In some applications, it convenient to solve Equation (3.27) on an online basis, by performing a *block-by-block* identification on finite intervals of the signal $y(t)$, whose length depends on the chosen window (or kernel, if the

transform belongs to the Cohen class). In such a case, one wants to find the optimal global vector of parameters **p** as:

$$J(t) = \left| \int_{-\infty}^{+\infty} \left[\mathbf{T}_y(t,\omega) - \widetilde{\mathbf{T}}(t,\omega) \right] d\omega \right| \rightarrow \min_{\mathbf{p}} J \tag{3.28}$$

The algorithm and type of transform chosen to solve Equation (3.28) depend on the specific problem to be solved. It should be noted that an online implementation is allowed only if causal transforms are employed and at the cost of accepting a small delay in the identification.

3.3.2 Bayesian filtering for online identification

Another convenient approach for localising in time spectral components of signals is given by Bayesian filters (Chen, 2003). Over the years, filter theory has provided a solid base for the instantaneous tracking of linear and nonlinear parameters over time by sequentially estimating the evolutionary state of a system based on measurements over time. In particular, Bayesian filters form the basis for dynamic state estimation (Rhodes, 2003; Simon, 2006). In the case of linear systems with Gaussian noise, Kalman filter, introduced by Kalman (Kalman, 1960), is widely used due to its optimality and computational efficiency. In particular, Gaussian white noise disturbances are hypothesised in both the system states and outputs. This method allows a sort of cleaning of the process, justifying its definition as filtering, and a determination of the optimal states of the system.

Different extensions of the Kalman filter can be found considering the nonlinear nature of the system, particularly, its ensemble, extended, and unscented versions. In Kalman filtering, the prior and posterior distributions are assumed to be Gaussian. However, when the state-propagation and observation models are nonlinear, they cannot be computed in closed form anymore (Simon, 2010). Depending on the approximation of the first and second order moments, i.e. mean and covariance, one can have: (i) Ensemble Kalman Filter (EnKF), employing a Montecarlo approximation (Evensen, 2003, 1994); (ii) EKF, which exploits a linearisation through a Taylor series approximation (Hoshiya and Saito, 1984; Ribeiro, 2004); (iii) UKF, which is based on the unscented transform, and propagates a set of sigma points (Julier and Uhlmann, 1997; Olivier and Smyth, 2017; Wan and Van Der Merwe, 2000).

Among these, the EKF is very popular owing to its simplicity: basically, the state equations are linearised around the current state estimation, making it possible the use of classical KF using the Jacobian of the nonlinear model instead of the constant matrices of linear model. This allows a constrained computational cost even in presence of nonlinearity, but the approximation error can become significant.

A more general approach, valid also in the case of highly nonlinear systems, is given by particle filtering, which, as in the case of UKF, transforms a set of points via known nonlinear equations and combines the results to estimate the mean and covariance of the state (Ristic et al., 2003). In contrast to the UKF, where the sigma points are deterministically selected, the particle filter relies on random sampling, and therefore typically requires a much larger number of points. Importantly, as the number of points increases, the estimation error can approach zero, at the cost of increasing computational effort (Simon, 2006). Figure 3.5 gives an overview of filters in the case of linear and nonlinear systems. By comparing UKF and EKF, it is clear that the choice of a series of sample points, i.e., sigma points, instead of a distribution allows the overpassing of the linearisation errors of the EKF simultaneously reducing the computational complexity. Indeed, it is intuitive that performing a nonlinear transformation on single points rather than an entire distribution is less computational expensive.

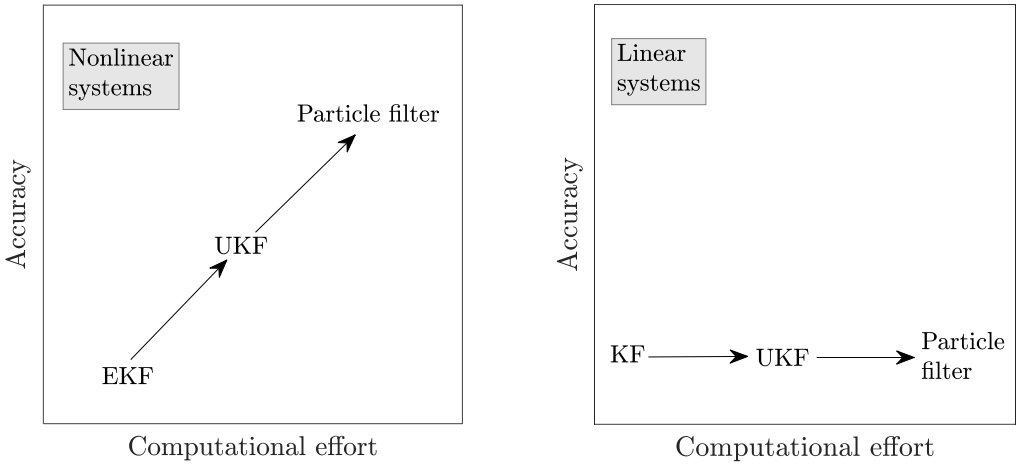

Figure 3.5. Overview of the Bayesian filters. *Reproduced from (Simon, 2006)*.

Going into greater detail in the UKF, sigma points should be chosen in order to capture the mean and the covariance of the current state estimate; then, they are passed through the nonlinear function to predict the next state and expected measurement. After the first step of choice of sigma points, UKF basically consists of two steps:

(i) prediction, where the sigma points are propagated through the nonlinear function to estimate the predicted mean and covariance of the state, and, consequently, of the measurement.

(ii) correction, where the UKF corrects the state estimate by updating its mean and covariance.

Finally, weighting is performed on the predicted state and measurement mean and covariance to prioritise the sigma points closer to the true distribution. Let us

consider a n-state discrete-time nonlinear system characterised by the following state-space and measurement equations:

$$\mathbf{x}_{k+1} = f(\mathbf{x}_k, \mathbf{u}_k, \mathbf{t}_k) + \mathbf{w}_k \tag{3.29}$$

$$\mathbf{y}_k = h(\mathbf{x}_k, \mathbf{t}_k) + \mathbf{v}_k \tag{3.30}$$

where $\mathbf{x}$ is the state vector of dimension $n \times 1$, $\mathbf{y}$ is the output vector, $\mathbf{u}$ is the input vector, $\mathbf{t}$ is the time vector, and $\mathbf{w}$ and $\mathbf{v}$ are the process and measurement noises, respectively. Both f and h are nonlinear functions. UKF is an iterative process whose steps are reported in the following table.

UKF algorithm (Julier et al., 2002)

$\hat{\mathbf{x}}_0^+ = E(\mathbf{x}_0)$ $\mathbf{P}_0^+ = E(\mathbf{x}_0 - \hat{\mathbf{x}}_0^+)(\mathbf{x}_0 - \hat{\mathbf{x}}_0^+)^T$	*Initialisation*
$\hat{\mathbf{x}}_{k-1}^{(i)} = \hat{\mathbf{x}}_{k-1}^{(i)} + \left(\sqrt{n\mathbf{P}_{k-1}^+}\right)_i^T \quad i = 1, \dots, n$ $\hat{\mathbf{x}}_{k-1}^{(i)} = \hat{\mathbf{x}}_{k-1}^{(i)} - \left(\sqrt{n\mathbf{P}_{k-1}^+}\right)_i^T \quad i = 1, \dots, n$	*Computation of sigma points*
$\hat{\mathbf{x}}_k^{(i)} = f\left(\hat{\mathbf{x}}_{k-1}^{(i)}, \mathbf{u}_k, \mathbf{t}_k\right)$	*Nonlinear propagation of sigma points through state equation*
$\hat{\mathbf{x}}_k^- = \sum_{i=1}^{2n} W_m^{(i)} \hat{\mathbf{x}}_k^{(i)}$	*A priori state vector prediction*
$\mathbf{P}_k^- = \sum_{i=1}^{2n} W_c^{(i)} \left(\hat{\mathbf{x}}_k^{(i)} - \hat{\mathbf{x}}_k^-\right)\left(\hat{\mathbf{x}}_k^{(i)} - \hat{\mathbf{x}}_k^-\right)^T + \mathbf{Q}_{k-1}$	*A priori state covariance prediction*
$\hat{\mathbf{y}}_k^{(i)} = h\left(\hat{\mathbf{x}}_k^{(i)}, \mathbf{t}_k\right)$	*Nonlinear propagation of sigma points through measurement equation*
$\hat{\mathbf{y}}_k = \sum_{i=1}^{2n} W_m^{(i)} \hat{\mathbf{y}}_k^{(i)}$	*Measurement vector prediction*
$\mathbf{P}_\mathbf{y} = \sum_{i=1}^{2n} W_c^{(i)} \left(\hat{\mathbf{y}}_k^{(i)} - \hat{\mathbf{y}}_k^-\right)\left(\hat{\mathbf{y}}_k^{(i)} - \hat{\mathbf{y}}_k^-\right)^T + \mathbf{R}_k$	*Measurement covariance prediction*
$\mathbf{P}_{\mathbf{xy}} = \sum_{i=1}^{2n} W_c^{(i)} \left(\hat{\mathbf{x}}_k^{(i)} - \hat{\mathbf{x}}_k^-\right)\left(\hat{\mathbf{y}}_k^{(i)} - \hat{\mathbf{y}}_k^-\right)^T + \mathbf{R}_k$	*Cross covariance prediction*
$\mathbf{K}_k = \mathbf{P}_{\mathbf{xy}}\mathbf{P}_\mathbf{y}^{-1}$ $\hat{\mathbf{x}}_k^+ = \hat{\mathbf{x}}_k^- + \mathbf{K}_k(\mathbf{y}_k - \hat{\mathbf{y}}_k)$ $\mathbf{P}_k^+ = \mathbf{P}_k^- - \mathbf{K}_k\mathbf{P}_y\mathbf{K}_k^T$	*Measurement update by using Kalman filter*

The weights of mean and covariance $W_m^{(i)}$ and $W_c^{(i)}$, respectively, can be positive or negative, but must obey the following condition:

$$\sum_{i=0}^{p} W^{(i)} = 1 \tag{3.31}$$

with p as the number of sigma points. A special attention should be devoted in the choice of the process and measurement noise, **Q** and **R**, respectively. The process noise **Q** directly affect the dispersion of sigma point $\hat{\mathbf{x}}_{k-1}^{(i)}$, thus the a priori state covariance prediction $\mathbf{P}_k^-$. Conversely, the measurement noise **R** quantifies the uncertainty linked to the observations, contributing to the covariance $\mathbf{P_y}$ and cross-covariance $\mathbf{P_{xy}}$, used in the measurement update. A convenient choice of **Q** and **R** is therefore crucial to guarantee an accurate and stable estimate of the desired parameters. To this end, a simplified sensitivity analysis on the role of **Q** and **R** in the estimation has been carried out and reported in Figure 3.6. In particular, a classical Duffing oscillator described by a linear and cubic stiffness k_1 and k_3 has been chosen as a model for this study.

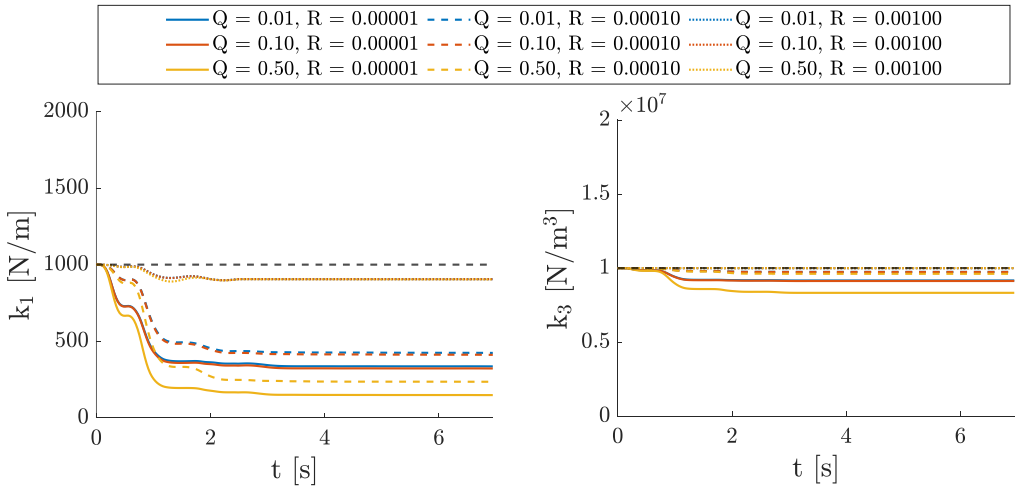

Figure 3.6. Sensitivity analysis on the process and measurement noise.

It is clear that both **Q** and **R** influence the estimation task. For this reason, procedures have been proposed to correctly tune these parameters. The tuning can be approached as a classical optimisation problem: to this aim, the methodology proposed by (Scardua and Da Cruz, 2017) wants to optimise a scalar goal function, designed to properly weight points in the UKF parameter domain, with the weight indicating the state estimation performance of the UKF when tuned with that specific point. The whole process is performed offline to avoid increasing the computational burden of the UKF during runtime. Nevertheless, an online tuning is possible by updating **Q** and **R** during the filtering procedure. A possible approach could rely on the use of a moving window, employed to

compute **Q** and **R** over continuous segments of residuals, i.e., the differences between the measured and estimated quantities (Ghorbani et al., 2025).

3.4 Applications and challenges in nonlinear time-varying parameter identification

Despite the promising capabilities of time-frequency transforms for tracking nonlinear time-varying parameters, they have rarely been applied to the characterisation of structural or non-structural components. A first category of applications concerns nonlinearity detection and, eventually, estimation. Recently, the numerical identification of a nonstationary, nonlinear, and damped mechanical system subject to white Gaussian noise was carried out in (Carpine et al., 2022). In that work, the nonlinearity was introduced as an additional stiffness restoring force and analysed using a continuous formulation of the WT. Another example concerning a beam with concentrated nonlinearity, whose first mode was used to simulate a Duffing oscillator, is given in (Argoul and Le, 2003; Demarie et al., 2011). In that case, the nonlinearity was visible in the after-shock accelerations after an impact hammer excitation. Significant variations in the WT representation, associated with nonlinearities, were observed in the case of a bridge in (Rospars et al., 2024). Furthermore, linear transforms, and in particular STFT, have been combined with other techniques, such as Volterra series based approaches, to instantaneously identify nonlinearities in cable-stayed footbridges (Kumar and Fragonara, 2013). Conversely, Bayesian filters have been largely applied, at least numerically, to identify structural nonlinear parameters (Ebrahimian et al., 2015). Examples concerning the adaptive online parametric identification algorithm of time-varying parameters simulating damage with different techniques from time-frequency and Bayesian filters can be found in (Lin et al., 2001).

More recently, an interesting class of application was introduced, regarding the case of nonlinear devices for energy absorption and/or dissipation. A recent benchmarking study on different polynomial nonlinearities has been proposed by (Zhao et al., 2024). Two MDOF models with varying numbers of magnetorheological dampers simulating nonlinearity have been employed used to numerically validate the effectiveness of the EKF slightly modified. Then, an experimental validation on a laboratory-controlled frame has been carried out. An experimental identification of the instantaneous parameters of a vibration control system has been carried out in (Niola et al., 2019) by introducing an augmented version of the UKF with boundaries constraints to take into account the nonlinear parameters describing the control system.

Nevertheless, several challenges arise and should be addressed when employing methods for tracking instantaneously the parameters of non-stationary signals. Many of these issues are related to the specific method employed. For

instance, when using a linear time-frequency transform, it has been said that an appealing idea is to make the signal locally stationary. In such a case, the issue of choosing an appropriate windowing function is of paramount importance, since it has been proved that its choice heavily influences the estimation results, with an associated bias. Also, when dealing with some specific classes of nonlinear systems, one may rely on simplified approaches reducing the computational burden, such as Volterra series approaches. However, the conditions of convergence of such series should be carefully addressed when dealing with systems for which several response states may co-exist. Finally, a more important challenge is related to dealing with experimental uncertainties. Some of these issues will be addressed, and potentially resolved, in the following chapters.

3.5 Concluding remarks

This chapter introduced different instantaneous identification techniques specifically suited for signals admitting a time localisation of spectral components. The latter represent the typology of signals analysed in the following chapters. When combined with the methodologies presented in Chapter 2, these techniques further enhance the effective estimation of parameters in nonlinear systems. In light of these considerations, the following chapters will aim to propose tailored strategies to solve specific challenges across several types of nonlinear models, useful in practical applications of earthquake engineering and structural dynamics.

References

Abbiati, G., Ceravolo, R., Surace, C., 2015. Time-dependent estimators for on-line monitoring of full-scale structures under ambient excitation. Mechanical Systems and Signal Processing 60, 166–181.

Allen, J.B., Rabiner, L.R., 2005. A unified approach to short-time Fourier analysis and synthesis. Proceedings of the IEEE 65, 1558–1564.

Argoul, P., Hans, S., Conti, F., Boutin, C., 2000. Time-frequency analysis of free oscillations of mechanical structures. Application to the identification of the mechanical behaviour of buildings under shocks, in: Proceeding of the COST F3 Conference: System Identification and Structural Health Monitoring, Madrid, Spain.,(283–292).

Argoul, P., Le, T.-P., 2003. INSTANTANEOUS INDICATORS OF STRUCTURAL BEHAVIOUR BASED ON THE CONTINUOUS CAUCHY WAVELET ANALYSIS. Mechanical Systems and Signal Processing 17, 243–250. https://doi.org/10.1006/mssp.2002.1557

Baba, T., 2012. Time-frequency analysis using short time Fourier transform. The Open Acoustics Journal 5, 32–38.

Barbato, M., Conte, J.P., 2008. Spectral characteristics of non-stationary random processes: Theory and applications to linear structural models. Probabilistic engineering mechanics 23, 416–426.

Bastiaans, M., 2003. On the sliding-window representation in digital signal processing. IEEE transactions on acoustics, speech, and signal processing 33, 868–873.

Bendat, J.S., Piersol, A.G., 2011. Random data: analysis and measurement procedures. John Wiley & Sons.

Boashash, B., 2015. Time-frequency signal analysis and processing: a comprehensive reference. Academic press.

Boashash, B., 1988. Time-Frequency Signal Analysis And Synthesis The Choice Of A Method And Its Application, in: Advanced Algorithms and Architectures for Signal Processing III. SPIE, pp. 164–185.

Boashash, B., Ouelha, S., 2017. An improved design of high-resolution quadratic time–frequency distributions for the analysis of nonstationary multicomponent signals using directional compact kernels. IEEE Transactions on Signal Processing 65, 2701–2713.

Bonato, P., Ceravolo, R., De Stefano, A., Molinari, F., 2000a. Use of cross-time–frequency estimators for structural identification in non-stationary conditions and under unknown excitation. Journal of Sound and vibration 237, 775–791.

Bonato, P., Ceravolo, R., De Stefano, A., Molinari, F., 2000b. Cross-time frequency techniques for the identification of masonry buildings. Mechanical Systems and Signal Processing 14, 91–109.

Boudreaux-Bartels, G., Parks, T., 2003. Time-varying filtering and signal estimation using Wigner distribution synthesis techniques. IEEE Transactions on Acoustics, Speech, and Signal Processing 34, 442–451.

Bradford, S.C., 2007. Time-frequency analysis of systems with changing dynamic properties.

Čačko, J., Bílý, M., Bukoveczky, J., 1988. Random processes: Measurement, analysis and simulation. (No Title).

Carmona, R., Hwang, W.-L., Torresani, B., 1998. Practical Time-Frequency Analysis: Gabor and wavelet transforms, with an implementation in S. Academic Press.

Carpine, R., Argoul, P., Rospars, C., 2022. Characterization of nonlinear, nonstationary systems in operational modal analysis using wavelet transform, in: ISMA-USD Noise and Vibration Engineering Conference 2022. p. .

Castro, I.P., 2021. An introduction to the digital analysis of stationary signals: a computer illustrated text. CRC Press.

Ceravolo, R., 2008. Time–Frequency Analysis, in: Boller, C., Chang, F., Fujino, Y. (Eds.), Encyclopedia of Structural Health Monitoring. Wiley. https://doi.org/10.1002/9780470061626.shm047

Ceravolo, R., 2004. Use of instantaneous estimators for the evaluation of structural damping. Journal of Sound and Vibration 274, 385–401. https://doi.org/10.1016/j.jsv.2003.05.025

Chen, Z., 2003. Bayesian filtering: From Kalman filters to particle filters, and beyond. Statistics 182, 1–69.

Cheng, C., Sa-Ngasoongsong, A., Beyca, O., Le, T., Yang, H., Kong, Z., Bukkapatnam, S.T., 2015. Time series forecasting for nonlinear and non-stationary processes: a review and comparative study. Iie Transactions 47, 1053–1071.

Chui, C.K., 1992. An introduction to wavelets. Academic press.

Claasen, T., Mecklenbraüker, W.F.G., 1980. The Wigner distribution. A tool for time-frequency analysis, Part III: Relations with other time frequency Continuous-time signal representations. Phillips journal of research 35, 373–389.

Claasen, T.A., Mecklenbrauker, W., 1984. On the time-frequency discrimination of energy distributions: Can they look sharper than Heisenberg?, in: ICASSP'84. IEEE International Conference on Acoustics, Speech, and Signal Processing. IEEE, pp. 278–281.

Cohen, L., 2002. Time-frequency distributions-a review. Proceedings of the IEEE 77, 941–981.

Cohen, L., 1998. The generalization of the Wiener-Khinchin theorem, in: Proceedings of the 1998 IEEE International Conference on Acoustics, Speech and Signal Processing, ICASSP'98 (Cat. No. 98CH36181). IEEE, pp. 1577–1580.

Cohen, L., 1995. Time frequency analysis, Prentice Hall signal processing series. Prentice Hall, Englewood Cliffs, NJ.

Cohen, L., 1992. Convolution, filtering, linear systems, the Wiener-Khinchin theorem: Generalizations, in: Advanced Signal Processing Algorithms, Architectures, and Implementations III. SPIE, pp. 378–393.

Cohen, L., 1966. Generalized Phase-Space Distribution Functions. Journal of Mathematical Physics 7, 781–786. https://doi.org/10.1063/1.1931206

Cohen, L., Posch, T., 1985. Generalized ambiguity functions, in: ICASSP'85. IEEE International Conference on Acoustics, Speech, and Signal Processing. IEEE, pp. 1033–1036.

Dahlhaus, R., 2012. Locally stationary processes, in: Handbook of Statistics. Elsevier, pp. 351–413.

Dahlhaus, R., 1997. Fitting time series models to nonstationary processes. The annals of Statistics 25, 1–37.

Dahlhaus, R., 1996. On the Kullback-Leibler information divergence of locally stationary processes. Stochastic processes and their applications 62, 139–168.

Dahlhaus, R., Richter, S., Wu, W.B., 2019. Towards a general theory for nonlinear locally stationary processes.

Dalianis, S.A., Hammond, J.K., White, P.R., Cambourakis, G.E., 1998. Simulation and identification of nonstationary systems using linear time-frequency methods. Journal of Vibration and Control 4, 75–91.

Debnath, L., 2003. Wavelets and signal processing. Springer Science & Business Media.

Demarie, G.V., Ceravolo, R., Sabia, D., Argoul, P., 2011. Experimental identification of beams with localized nonlinearities. Journal of Vibration and Control 17, 1721–1732. https://doi.org/10.1177/1077546310385287

Dimitriadis, G., Fassois, S.D., Poulimenos, A.G., Shi, D., 2004. Identification and model updating of a non-stationary vibrating system, in: Engineering Systems Design and Analysis. pp. 143–152.

Durak, L., Arikan, O., 2003. Short-time Fourier transform: two fundamental properties and an optimal implementation. IEEE Transactions on Signal Processing 51, 1231–1242.

Ebrahimian, H., Astroza, R., Conte, J.P., 2015. Extended Kalman filter for material parameter estimation in nonlinear structural finite element models using direct differentiation method. Earthquake Engineering & Structural Dynamics 44, 1495–1522.

Evensen, G., 2003. The ensemble Kalman filter: Theoretical formulation and practical implementation. Ocean dynamics 53, 343–367.

Evensen, G., 1994. Sequential data assimilation with a nonlinear quasi-geostrophic model using Monte Carlo methods to forecast error statistics. Journal of Geophysical Research: Oceans 99, 10143–10162.

Flandrin, P., 1998. Time-frequency/time-scale analysis. Academic press.

Flandrin, P., Escudié, B., 1984. An interpretation of the pseudo-Wigner-Ville distribution. Signal Processing 6, 27–36.

Flandrin, P., Martin, W., 1997. The Wigner-Ville spectrum of nonstationary random signals. The Wigner Distribution—Theory and Applications in Signal Processing 211–267.

Flandrin, P., Rioul, O., 1990. Affine smoothing of the Wigner-Ville distribution, in: International Conference on Acoustics, Speech, and Signal Processing. IEEE, pp. 2455–2458.

Gabor, D., 1946. Theory of communication. Part 1: The analysis of information. Journal of the Institution of Electrical Engineers-part III: radio and communication engineering 93, 429–441.

Gardner, W.A., Robinson, E.A., 1989. Statistical spectral analysis—A nonprobabilistic theory.

Ghorbani, E., Dollon, Q., Gosselin, F.P., 2025. PHYSICS-AWARE TUNING OF UNSCENTED KALMAN FILTER TO ESTIMATE PARAMETERS, QUANTIFY ABRUPT PARAMETER CHANGE, AND QUANTIFY UNCERTAINTY IN IDENTIFICATION OF A DYNAMIC SYSTEM WITH MANY DOFS. Authorea Preprints.

Grace, O.D., 1981. Instantaneous power spectra. The Journal of the Acoustical Society of America 69, 191–198.

Hammond, J.K., 1968. On the response of single and multidegree of freedom systems to non-stationary random excitations. Journal of Sound and Vibration 7, 393–416.

Hammond, J.K., White, P.R., 1996. The analysis of non-stationary signals using time-frequency methods. Journal of Sound and vibration 190, 419–447.

Harris, F.J., 2005. On the use of windows for harmonic analysis with the discrete Fourier transform. Proceedings of the IEEE 66, 51–83.

Hlawatsch, F., 2002. Duality and classification of bilinear time-frequency signal representations. IEEE Transactions on signal processing 39, 1564–1574.

Hlawatsch, F., 1984. Interference terms in the Wigner distribution. Proc. Dig. Sig. Proc. 363.

Hlawatsch, F., Boudreaux-Bartels, G.F., 2002. Linear and quadratic time-frequency signal representations. IEEE signal processing magazine 9, 21–67.

Hlawatsch, F., Flandrin, P., 1997. The interference structure of the Wigner distribution and related time-frequency signal representations, in: The Wigner Distribution-Theory and Applications in Signal Processing. Elsevier, pp. 59–133.

Hoshiya, M., Saito, E., 1984. Structural identification by extended Kalman filter. Journal of engineering mechanics 110, 1757–1770.

Ivanovic, V.N., Dakovic, M., Stankovic, L., 2003. Performance of quadratic time-frequency distributions as instantaneous frequency estimators. IEEE Transactions on Signal Processing 51, 77–89.

Jeong, J., Williams, W.J., 1992. Kernel design for reduced interference distributions. IEEE Transactions on Signal Processing 40, 402–412.

Julier, S., Uhlmann, J., Durrant-Whyte, H.F., 2002. A new method for the nonlinear transformation of means and covariances in filters and estimators. IEEE Transactions on automatic control 45, 477–482.

Julier, S.J., Uhlmann, J.K., 1997. New extension of the Kalman filter to nonlinear systems, in: Signal Processing, Sensor Fusion, and Target Recognition VI. Spie, pp. 182–193.

Kalman, R.E., 1960. A new approach to linear filtering and prediction problems.

Kay, S.M., 1993. Fundamentals of statistical signal processing: estimation theory. Prentice-Hall, Inc.

Kozek, W., 1992. Time-frequency signal processing based on the Wigner-Weyl framework. Signal Processing 29, 77–92.

Kumar, A., Fragonara, L.Z., 2013. Identification of weak non-linearities in cables of cable-stayed footbridges. IJLCPE 1, 292. https://doi.org/10.1504/IJLCPE.2013.058222

Lin, J.-W., Betti, R., Smyth, A.W., Longman, R.W., 2001. On-line identification of non-linear hysteretic structural systems using a variable trace approach. Earthquake engineering & structural dynamics 30, 1279–1303.

Loughlin, P.J., 1992. Time-frequency energy density functions: Theory and synthesis. University of Washington.

Loughlin, P.J., Cohen, L., 2004. The Uncertainty Principle: Global, Local, or Both? IEEE Trans. Signal Process. 52, 1218–1227. https://doi.org/10.1109/TSP.2004.826160

Loughlin, P.J., Pitton, J.W., Atlas, L.E., 2002. Bilinear time-frequency representations: New insights and properties. IEEE Transactions on signal processing 41, 750–767.

Mallat, S., Papanicolaou, G., Zhang, Z., 1998. Adaptive covariance estimation of locally stationary processes. Annals of Statistics 1–47.

Marple Jr, S.L., 2019. Digital spectral analysis. Courier Dover Publications.

Martin, W., 1984. Measuring the degree of non-stationarity by using the Wigner-Ville spectrum, in: ICASSP'84. IEEE International Conference on Acoustics, Speech, and Signal Processing. IEEE, pp. 262–265.

Martin, W., Flandrin, P., 2003. Wigner-Ville spectral analysis of nonstationary processes. IEEE Transactions on Acoustics, Speech, and Signal Processing 33, 1461–1470.

Marx, D.G., Gryllias, K., 2023. Differentiable short-time Fourier transform window length selection driven by cyclo-stationarity, in: Proceedings of the Annual Conference of the Prognostics and Health Management Society, PHM. PHM Society, pp. 1–10.

Mecklenbräuker, W.F., Hlawatsch, F., 1997. The Wigner distribution-theory and applications in signal processing. Elsevier.

Mitra, S.K., 2001. Digital signal processing: a computer-based approach. McGraw-Hill Higher Education.

Nam, S.-W., Powers, E.J., 2003. Volterra series representation of time-frequency distributions. IEEE transactions on signal processing 51, 1532–1537.

Nawab, S.H., Quatieri, T.F., 1987. Short-time Fourier transform, in: Advanced Topics in Signal Processing. pp. 289–337.

Niola, V., Palli, G., Strano, S., Terzo, M., 2019. Nonlinear estimation of the Bouc-Wen model with parameter boundaries: Application to seismic isolators. Computers & Structures 222, 1–9.

Olivier, A., Smyth, A.W., 2017. Review of nonlinear filtering for SHM with an exploration of novel higher-order Kalman filtering algorithms for uncertainty quantification. Journal of Engineering Mechanics 143, 04017128.

Oppenheim, A.V., 1978. Applications of digital signal processing. Englewood Cliffs.

Oppenheim, A.V., Oppenheim, A.V., Schafer, R.W., 1989. Discrete-time signal processing, Prentice Hall signal processing series. Prentice-Hall International, Englewoods Cliffs, NJ.

Orozco, J., Hernández, F., Astroza, R., 2026. Time-variant dynamic characterization and seismic response identification of base-isolated buildings. Journal of Building Engineering 117, 114768. https://doi.org/10.1016/j.jobe.2025.114768

Portnoff, M., 2003. Time-frequency representation of digital signals and systems based on short-time Fourier analysis. IEEE Transactions on Acoustics, Speech, and Signal Processing 28, 55–69.

Priestley, M.B., 1988. Non-linear and non-stationary time series analysis. London: Academic Press.

Priestley, M.B., 1982. Spectral Analysis and Time Series, Two-Volume Set: Volumes I and II. Elsevier Science.

Priestley, M.B., 1967. Power spectral analysis of non-stationary random processes. Journal of Sound and Vibration 6, 86–97.

Priestley, M.B., 1965. Evolutionary spectra and non-stationary processes. Journal of the Royal Statistical Society: Series B (Methodological) 27, 204–229.

Rabiner, L.R., 1978. Digital processing of speech signals. Pearson Education India.

Rabiner, L.R., Schafer, R.W., 2007. Introduction to digital speech processing. Foundations and Trends® in Signal Processing 1, 1–194.

Rhodes, I., 2003. A tutorial introduction to estimation and filtering. IEEE Transactions on Automatic Control 16, 688–706.

Ribeiro, M.I., 2004. Kalman and extended kalman filters: Concept, derivation and properties. Institute for Systems and Robotics 43, 3736–3741.

Rihaczek, A., 1968. Signal energy distribution in time and frequency. IEEE Transactions on information Theory 14, 369–374.

Rioul, O., 1990. A discrete-time multiresolution theory unifying octave-band filter banks, pyramid and wavelet transforms. IEEE Trans. ASSP.

Rioul, O., Vetterli, M., 1991. Wavelets and signal processing. IEEE signal processing magazine 8, 14–38.

Ristic, B., Arulampalam, S., Gordon, N., 2003. Beyond the Kalman filter: Particle filters for tracking applications. Artech house.

Rospars, C., Argoul, P., Carpine, R., 2024. Wavelet analysis to detect nonstationary and nonlinear behaviours in railway bridge. Procedia Structural Integrity 64, 716–723.

Scardua, L.A., Da Cruz, J.J., 2017. Complete offline tuning of the unscented Kalman filter. Automatica 80, 54–61. https://doi.org/10.1016/j.automatica.2017.01.008

Shields, M.D., Deodatis, G., 2013. Estimation of evolutionary spectra for simulation of non-stationary and non-Gaussian stochastic processes. Computers & Structures 126, 149–163.

Simon, D., 2010. Kalman filtering with state constraints: a survey of linear and nonlinear algorithms. IET control theory & applications 4, 1303–1318.

Simon, D., 2006. Optimal state estimation: Kalman, H infinity, and nonlinear approaches. John Wiley & Sons.

Spina, D., Valente, C., Tomlinson, G.R., 1996. A new procedure for detecting nonlinearity from transient data using the Gabor transform. Nonlinear Dynamics 11, 235–254.

Stoica, P., Moses, R.L., 2005. Spectral analysis of signals. Pearson Prentice Hall Upper Saddle River, NJ.

Wan, E.A., Van Der Merwe, R., 2000. The unscented Kalman filter for nonlinear estimation, in: Proceedings of the IEEE 2000 Adaptive Systems for Signal Processing, Communications, and Control Symposium (Cat. No. 00EX373). Ieee, pp. 153–158.

Wang, D., Yu, F., Kong, F., Xu, J., 2022. Simulation of fully nonstationary random processes using generalized harmonic wavelets. Mechanical Systems and Signal Processing 181, 109468. https://doi.org/10.1016/j.ymssp.2022.109468

Wickramarachi, P., 2003. Effects of windowing on the spectral content of a signal. Sound and vibration 37, 10–13.

Wigner, E., 1932. On the quantum correction for thermodynamic equilibrium. Physical review 40, 749.

Wigner, E.P., 1971. Quantum-mechanical distribution functions revisited, in: Part I: Physical Chemistry. Part II: Solid State Physics. Springer, pp. 251–262.

Zhao, Y., Xu, B., Deng, B., Dyke, S.J., 2024. Generality of nonparametric nonlinearity identification approach with improved extended Kalman filter using different polynomial models. Measurement 227, 114235.

Chapter 4

Identification of Volterra time-varying parameters in dynamical systems under random excitation

A key limitation of most time-frequency approaches for SI, as presented in Chapter 3, is the assumption that the input excitation is known. In principle, such approaches could be adapted to the case of unknown input by adopting a Monte Carlo strategy, where multiple input realisations are sampled to statistically infer the system behaviour. Nevertheless, this may be computationally demanding and often impractical for real-time and/or large-scale applications. A promising alternative arises when the system belongs to a specific subclass of nonlinear dynamical systems, characterised by certain properties, i.e., smooth nonlinearities, here intended as sufficiently differentiable (Palm and Poggio, 1977), and the presence of a stable attractor at zero. For such systems, it may be possible to estimate the spectral density of the output directly, without requiring knowledge of the input, by using a Volterra series-based approach.

Volterra series is an expansion technique that expresses a functional as an infinite sum, or series, of simpler functionals by introducing the concept of Volterra kernel, which can reflect either the higher-order IRF (Tawfiq and Vinh, 2003) or the higher-order transfer function (TF) of the system (Collis, 1996; Tick, 1961). The Volterra theory was extensively developed in 20th century for the theoretical analysis and kernel estimation for stochastic processes (Billings, 2013; Schetzen, 2006). Although several authors proposed methods for estimating higher-order time or frequency domain series during the second half of the last century, often without explicitly relying on Volterra theory (Brillinger, 1970; Tick, 1961), it was the work of Lee and Schetzen (Lee and Schetzen‡, 1965) that provided a concrete and experimentally tractable framework for identifying the

nonlinear characteristics of a system. Their approach was grounded in the Wiener series representation. Mathematically, the Wiener series represents an orthogonal reformulation of the Volterra series under the assumption of Gaussian white noise (Rugh, 1981). Palm and Poggio explicitly addressed the problem of relating Volterra and Wiener representation by revisiting the mathematical formulation of the Wiener-Lee-Schetzen algorithm (Palm and Poggio, 1977). Specifically, they demonstrated that Wiener kernels emerge from a statistical orthogonalisation of Volterra kernels.

The orthogonalisation transforms the Volterra series into distinct blocks (Mathews and Sicuranza, 2000). Wiener series are more immediate to interpret than Volterra ones due to their block-structured representation, expressed as a cascade of linear-nonlinear components, from an identification-oriented perspective (Schoukens and Tiels, 2017). Going into greater detail, Wiener models are built starting from two basic blocks, namely, a linear time-invariant system block followed by a static nonlinear block (Schetzen, 2005). Starting from this intuitive idea, several techniques have been proposed (Schoukens and Tiels, 2017), also based on the idea of separating linear and nonlinear components (S. A. Billings and Fakhouri, 1978).

However, one of the main reasons for the popularity of the approach proposed by Lee and Schetzen is that the leading Wiener kernels can be directly measured via the cross-correlation method, thus computing time-averaged cross-correlations between the system output and products of time-shifted input signals. The Wiener-Lee-Schetzen algorithm has led to different developments in cross-correlation techniques for nonlinear SI, for which a review can be found in (Simpson and Power, 1972).

Several developments of the cross-correlation method based on Wiener kernels can be found in literature, see for instance (S.A. Billings and Fakhouri, 1978; Goussard et al., 1985; Kim and Powers, 1988; Klein and Yasui, 1979). Despite its practical usefulness, the method suffers from the following flaws (Franz and Schölkopf, 2006). First, it requires a large amount of samples for estimating the higher-order kernels through cross-correlation (Papoulis, 1965). Second, the method, at least in principle, works only in the case the input is Gaussian white noise (Palm and Poggio, 1977). Some works attempted to mitigate this restriction by extending the method to the case of non-Gaussian excitation (Hawes and Langley, 2018). Third, the method assumes noise-free signals, limiting its applicability in experimental settings. Practically speaking, these limitations are correlated with the main assumption of the method, implying a stationary signal both in input and output (Wiener, 1949), hence not generally applicable to the case of time-varying parameters. A tentative of extension to some specific classes of time-varying systems is reported in (Nordsjo and Zetterberg, 2002).

Another important drawback of the block-structured (e.g., Wiener, Hammerstein, Uryson) formulation of the identification problem lies in the fact that it suffers from the restrictions given by the model definition (Billings, 2013). As a consequence, the computation of higher order FRF was extended to NARMAX models in a more general way (Billings and Tsang, 1989a, 1989b). In the last twenty years, several attempts have been made to employ Volterra series approaches in the identification of nonlinear systems, with special attention on the definition of reliable estimators of spectra (Doyle et al., 2002). Some methodologies employed harmonic probing through a recursive iteration approach (Chatterjee and Vyas, 2003) and/or an explicit definition of cross-cumulants for second- and third-order Volterra systems (Kalouptsidis and Koukoulas, 2000; Koukoulas and Kalouptsidis, 1997). Other approaches used state-space representation and Kalman filtering for effective SI in the case of time-varying Volterra systems (Weng and Barner, 2006).

Volterra-based approaches have been brought to the SHM community with the work of Worden (Chance et al., 1998; Worden et al., 2014, 1997; Worden and Tomlinson, 2019). In the context of SI of time-varying nonlinear dynamical systems, time-domain methods have been mainly exploited to instantaneously identify nonlinear parameters of dynamical systems. Luo and Billings (Luo and Billings, 1995) proposed a recursive orthogonal decomposition method based on a rectangular sliding window, capable of adaptively identifying model structure and parameters online with good numerical stability and limited memory usage, particularly suited for slowly time-varying systems. More recently, a stochastic approach where the Volterra model represents parameters as random variables and uses the maximum entropy principle yielding a robust description of the system's behaviour has been proposed by Villani et al. (Villani et al., 2022).

Other works exploited a joint time-frequency domain, with all the advantages that follow, as reported in Chapter 3. In particular, Demarie et al. (Demarie et al., 2011) employed the STFT combined with a truncated Volterra series to perform time-frequency identification of nonlinear systems, extracting instantaneous modal properties and nonlinearities. The STFT combined with a Volterra approach can be found also in Ceravolo et al. (Ceravolo et al., 2010), modelling the nonlinear restoring force through time-varying polynomial coefficients derived from the Volterra kernels with the aim of identifying degrading hysteretic behaviour over time. Others (Gkikas and Athanassoulis, 2014) used the Hilbert-Huang transform combined with the Volterra-Wiener theory by expressing the nonlinear system through Wiener-Hammerstein cascades whose polynomial coefficients and impulse responses are identified in a time-frequency framework.

These studies, and particularly the ones conducted by (Ceravolo et al., 2010; Demarie et al., 2011), highlighted some of the major challenges when performing instantaneous parameter estimation combined with Volterra series approaches,

which can be summarised as follows: (i) reducing the computational burden associated with the instantaneous estimation of Volterra-based models, (ii) dealing with the case of an input excitation which is not directly measurable, and (iii) mitigating the distortions introduced by time-frequency windowing. This chapter addresses these limitations by proposing a parameter estimation technique that does not require explicit knowledge of the input and accounts for windowing distortions, while preserving the advantages of time-frequency methods.

4.1 Definition of a Volterra series-based time-frequency estimator under unknown excitation

As anticipated in the previous chapters, nonlinear SI is generally an ill-posed problem, unless appropriate assumptions and simplifications are made. Furthermore, in applications to large-scale structures, the excitation cannot be fully measured, for instance due to the presence of unmeasured disturbances (e.g., those produced by wind), and consequently statistical assumptions are deemed necessary. When the input is assumed to be a Gaussian white noise, one can exploit the definition of spectral density for a wide-sense stationary random process as the Fourier transform of the autocorrelation function (Bendat and Piersol, 2011). In such a case, the even terms disappear (Laning and Battin, 1956; Sauder, 2021), and the cross input-output spectral density, S_{yu}, is given by the following expression (Worden and Manson, 1998):

$$S_{yu}(\omega) = \Lambda(\omega) S_{uu}(\omega) = \sum_{p=1}^{\frac{m+1}{2}} S_{y^{(2p-1)}u}(\omega) \tag{4.1}$$

where S_{uu} is the input spectral density, m is the truncation order of the Volterra series, $\Lambda(\omega)$ is referred to as composite FRF, and the index $2p-1$ is used to enforce the selection of odd terms only (Worden and Tomlinson, 2019). As a practical matter, Equation (4.1) basically extends the summation of different order terms, i.e., the core of classical Volterra series approaches, to the cross input-output spectral density. The p-th spectral density can be defined as:

$$\begin{aligned} S_{y^{(2p-1)}u}(\omega) = \frac{(2p)!\, S_{uu}(\omega)}{p!\, 2^p (2\pi)^{p-1}} & \int_{-\infty}^{+\infty} \dots \int_{-\infty}^{+\infty} d\omega_1 \dots d\omega_{p-1} \\ & \times H^{(2p-1)}\left(\omega_1, -\omega_1, \dots, \omega_{p-1}, -\omega_{p-1}, \omega\right) \\ & \times S_{uu}(\omega_1) \dots S_{uu}\left(\omega_{p-1}\right) \end{aligned} \tag{4.2}$$

If the spectral density of the input is constant and equal to $S_{uu} = P$, Equation (4.2) becomes:

$$S_{y^{(2p-1)}u}(\omega) = \frac{(2p)!\,P^p}{p!\,2^p(2\pi)^{p-1}} \int_{-\infty}^{+\infty} \dots \int_{-\infty}^{+\infty} d\omega_1 \dots d\omega_{p-1} \times H^{(2p-1)}\left(\omega_1, -\omega_1, \dots, \omega_{p-1}, -\omega_{p-1}, \omega\right) \tag{4.3}$$

Thus, the composite FRF $\Lambda(\omega)$ can be written as :

$$\Lambda(\omega) = \sum_{p=1}^{\frac{m+1}{2}} \frac{(2p)!\,P^{p-1}}{p!\,2^p(2\pi)^{p-1}} \int_{-\infty}^{+\infty} \dots \int_{-\infty}^{+\infty} d\omega_1 \dots d\omega_{p-1} \times H^{(2p-1)}\left(\omega_1, -\omega_1, \dots, \omega_{p-1}, -\omega_{p-1}, \omega\right) \tag{4.4}$$

As an example, the composite FRF is derived for the case of a classical Duffing oscillator, by considering a truncation order $m = 5$. In such a case, the cross input-output spectral density of Equation (4.1) writes:

$$S_{yu}(\omega) = S_{y^{(1)}u}(\omega) + S_{y^{(3)}u}(\omega) + S_{y^{(5)}u}(\omega) \tag{4.5}$$

where:

$$S_{y^{(1)}u}(\omega) = H^{(1)}(\omega)P \tag{4.6}$$

$$S_{y^{(3)}u}(\omega) = \frac{3P^2}{2\pi} \int_{-\infty}^{+\infty} H^{(3)}(\omega_1, -\omega_1, \omega) d\omega_1 \tag{4.7}$$

$$S_{y^{(5)}u}(\omega) = \frac{15P^3}{(2\pi)^2} \int_{-\infty}^{+\infty} \int_{-\infty}^{+\infty} H^{(5)}(\omega_1, -\omega_1, \omega_2, -\omega_2, \omega) d\omega_1 d\omega_2 \tag{4.8}$$

The terms corresponding to a truncation order higher than $m = 5$ have not been considered due to the increased complexity of the analytical expression. Equations (4.6)-(4.8) can be further simplified as (Worden and Manson, 1998):

$$S_{y^{(3)}u}(\omega) = -\frac{3k_3 H^{(1)}(\omega)^2}{2ck_1} P^2 \tag{4.9}$$

$$S_{y^{(5)}u}(\omega) = \left(\frac{9k_3^2 H^{(1)}(\omega)^3}{4c^2k_1^2} + \frac{9k_3^2 H^{(1)}(\omega)^2}{4c^2k_1^3} + \frac{9k_3^2 H^{(1)}(\omega)^2}{2\pi^2} I(\omega)\right) P^3 \tag{4.10}$$

with:

$$I(\omega) = \frac{-\pi^2\left(\omega^2 - 3\omega_d^2 - 10j\zeta\omega_n\omega - 27\zeta^2\omega_n^2\right)}{mc^2k_1^2(\omega - \omega_d - 3j\zeta\omega_n)(\omega + \omega_d - 3j\zeta\omega_n)(\omega - 3\omega_d - 3j\zeta\omega_n)(\omega + 3\omega_d - 3j\zeta\omega_n)} \tag{4.11}$$

In this case, the composite FRF expressed by Equation (4.4) becomes:

$$\begin{aligned}\Lambda(\omega) = H^{(1)}(\omega) - \frac{3k_3H^{(1)}(\omega)^2}{2ck_1}P + \cdots \\ \left(\frac{9k_3^2H^{(1)}(\omega)^3}{4c^2k_1^2} + \frac{9k_3^2H^{(1)}(\omega)^2}{4c^2k_1^3} + \frac{9k_3^2H^{(1)}(\omega)^2}{2\pi^2}I(\omega)\right)P^2\end{aligned} \tag{4.12}$$

It is clear that Equation (4.12) only depends on the linear kernel $H^{(1)}(\omega)$. This is an advantage in the identification task, where the calculation of the HFRF of the system can represent a not negligible computational burden, especially if the characteristics of the considered system are time-varying, as often happens in real-world situations.

4.1.1 Time-frequency estimation

The identification of non-stationary systems can be rigorously addressed by introducing the concept of local stationarity. Under this assumption, a stochastic process is regarded as approximately stationary within a sufficiently short time interval centred around a given time instant $\bar{t}$ so that its statistical properties vary slowly with time. This hypothesis allows the use of instantaneous time-frequency representations and naturally leads to local estimation procedures based on the minimisation of suitable cost functions in the time-frequency plane, as formalised in Equations (3.21)-(3.28) for linear systems.

In the case of linear systems, the extension from a stationary to a locally stationary process is ensured by the existence of a single FRF, which provides a complete spectral description of the system. One may exploit this advantageous property also in the nonlinear case, where, however, such a description is no longer sufficient, since the system response cannot be fully characterised by a single spectral density, but as a composite one, introduced from Equation (4.1). Consequently, the analytical expressions of the spectral density derived from Volterra theory remain valid within a local time interval around $\bar{t}$. This theoretical extension justifies the formulation of an instantaneous identification problem for nonlinear systems admitting a Volterra representation, in direct analogy with Equation (3.28).

More specifically, as seen in Section 3.3.1, the basic idea behind time-frequency identification is to minimise the distance between the time-frequency model $\mathbf{T}_y(t, \omega; \mathbf{p})$ and the time-frequency transform of the measured signal $\widetilde{\mathbf{T}}_y(t, \omega)$. The time-frequency model is defined in terms of the global vector of

parameters $\mathbf{p}$. Although the frequency content at a given time is a local, but not strictly instantaneous, property (Cohen, 1989), estimating parameters with temporal significance, such as in time-varying systems, requires performing an instantaneous minimisation to accurately determine the parameter vector $\mathbf{p}$ at each time instant t. Thus, the minimisation process yields an optimal vector of parameters $\mathbf{p}_{id}$ for each local time instant $\bar{t}$ as:

$$\mathbf{p}_{id}(\bar{t}) = \arg \min_{\mathbf{p}} J(\bar{t}; \mathbf{p}) \tag{4.13}$$

where $J(\bar{t}; \mathbf{p})$ is the distance to be minimised. The latter can be written with respect to the frequency variable ω as:

$$J(\bar{t}; \mathbf{p}) = \left\| \mathbf{T}_y(t, \omega; \mathbf{p}) - \widetilde{\mathbf{T}}_y(t, \omega) \right\|^2_{2,D_\omega} \tag{4.14}$$

The choice of the time-frequency transform is not unique and depends on the specific identification process. The advantages and main drawbacks for several types of transforms have been reported in Chapter 3 of this thesis.

The estimation methodology proposed here starts from the general formulation of Equation (4.1), but is specifically designed for white noise excitation, as for this special case an analytical expression of the spectral density is available from Volterra theory. Also, the analytical form of the Volterra kernel is known from the nonlinear model (e.g., the generic polynomial representation), and only the parameters entering these analytical expressions are estimated from the measured data. Similarly, since the excitation is white noise, the input spectrum S_{uu} corresponding to the variance P can be estimated as well, if not known.

In the special case where a STFT time-frequency representation is chosen, with γ as a short-time analysis window, the resulting model can be expressed by combining cross-spectral estimations over multiple windows. This approach allows the tracking in time of frequency components, with each window γ providing a localised time frame over which the output spectrum is estimated. If the system holds $y(t)$ and $u(t)$ as the measured output and input, respectively, then the time-frequency transform $\mathbf{T}_y(t, \omega; \mathbf{p})$ of the measured output subject to windowing centred at time instant $\bar{t}$ can be seen as the instantaneous Fourier spectrum of the signal. In such a case , the objective function to minimise writes:

$$J(\bar{t}; \mathbf{p}) = \left\| \mathbf{T}_{y_\gamma}(\bar{t}, \omega; \mathbf{p}) - \widetilde{\mathbf{T}}_{y_\gamma}(\bar{t}, \omega) \right\|^2_{2,D_\omega} \tag{4.15}$$

with $\mathbf{T}_{y_\gamma}(t, \omega; \mathbf{p})$ and $\widetilde{\mathbf{T}}_{y_\gamma}(t, \omega)$ as the time-frequency transforms of the measured signal. In this case, the transform of the measured signal writes:

$$\widetilde{\mathbf{T}}_{y_\gamma}(\bar{t},\omega) \coloneqq \mathbb{E}[Y_\gamma(\bar{t},\omega)Y_\gamma^*(\bar{t},\omega)] \tag{4.16}$$

where $Y_\gamma(\bar{t},\omega)$ is the Fourier transform of the signal windowed in time-domain $y_\gamma(\bar{t},t) = y(t)\gamma(t-\bar{t})$ and $\mathbb{E}$ represents the expectation operator, being the windowed spectral density an approximation of the analytical spectral density of the system, with all the distortions that follow.

If the windowing function is short, the distortions given by the effects of the window may be partially mitigated by convolving the spectral density of the output, $S_{yy}(\bar{t},\omega;\mathbf{p})$, with the one of the windowing function, $S_{\gamma\gamma}(\bar{t},\omega)$. In such a case, a possible time-frequency estimator is given by:

$$\mathbf{T}_{y_\gamma}(\bar{t},\omega;\mathbf{p}) \coloneqq \frac{S_{yy}(\bar{t},\omega;\mathbf{p}) * S_{\gamma\gamma}(\bar{t},\omega)}{Z} \approx S_{yy}^{\gamma}(\bar{t},\omega) \tag{4.17}$$

with Z as a normalisation constant, depending on window type, and the symbol $*$ as the convolution operator. The output auto-spectrum is defined as:

$$S_{yy}(\bar{t},\omega;\mathbf{p}) = \Lambda(\omega;\mathbf{p})S_{yu}(\bar{t},\omega;\mathbf{p}) \tag{4.18}$$

The quantities $\Lambda(\omega;\mathbf{p})$ and $S_{yu}(\bar{t},\omega;\mathbf{p})$ have been defined previously in Equations (4.1)-(4.4). The described identification procedure constitutes a simple, yet effective, approach for systems under white noise excitation.

4.1.2 Numerical implementation

The procedure described in Section 4.2 has been numerically implemented in Matlab®, in order to validate it on a benchmark oscillator. Time and frequency axes are discretised as:

$$t = \bar{t} + r\Delta t \tag{4.19}$$

$$\omega = s\Delta\omega \tag{4.20}$$

where the time index is $t \in [0,\dots,T/\Delta t]$ and the frequency index is $s \in [-T/2\Delta t,\dots,T/2\Delta t]$, being T the length of the window function γ and Δt the sampling period of the signals. The discretised sampled output and window function read:

$$y[r] = y(\bar{t} - T/2 + r\Delta t) \tag{4.21}$$

$$\gamma[r] = \gamma(r\Delta t) \tag{4.22}$$

and the sampled Volterra kernel and input spectral density:

$$H^{(p)}[s_1, \dots, s_p; \mathbf{p}] = H^{(p)}(s_1\Delta\omega, \dots, s_p\Delta\omega; \mathbf{p}) \tag{4.23}$$

$$S_{uu}[s] = S_{uu}(s\Delta\omega) \tag{4.24}$$

The implementation of the objective function as described in Equation (4.15) is reported in its discrete version in the pseudo-code below. The minimisation is carried out using a gradient-based optimisation, as implemented in *fmincon* function in Matlab®. A normalisation preprocessing step was performed on all the parameters such that their values lie within the [0, 1] interval to improve the convergence behaviour of the optimisation algorithm. Thus, a starting point of 0.1 was considered in the estimation process. Moreover, a tolerance value ε was added at the denominator of the objective function to avoid numerical stability issues. For each time window, the algorithm calculates the Fourier transform of the windowed output signal and estimates its local spectral density. This measured time-frequency transform is then compared with the model-based spectral density computed following Volterra theory. The distortions caused by the analysis window are included by performing a convolution between the model-based spectral density and the window spectrum. Finally, the objective function is evaluated by minimising the distance between the theoretical and measured spectral density.

Algorithm 1: Numerical implementation of the objective function for single γ

1: for $s \in [-T/2\Delta t, \dots, T/2\Delta t]$

2: $Y^{\gamma}[s] = \sum_r y[r]\gamma[r]e^{-j(s\Delta\omega)(r\Delta t)}\Delta t$

3: $\widetilde{\mathbf{T}}_{y_\gamma}[s] \coloneqq S^{\gamma}_{yy}[s] = |Y^{\gamma}[s]|^2$ *Measured*

4: $S_{yu}[s; \mathbf{p}] = \sum_{p=1}^{\frac{m+1}{2}} S_{y^{2p-1}u}[s; \mathbf{p}]$

5: $\Lambda[s; \mathbf{p}] = \sum_{p=1}^{\frac{m+1}{2}} \frac{(2p)!}{p!2^p(2\pi)^{p-1}} \sum_{s_1,\dots,s_{p-1}} H^{2p-1}[s_1, -s_1, \dots, s; \mathbf{p}]$
$\times S_{uu}[s_1] \dots S_{uu}[s_{p-1}]\Delta\omega^{p-1}$

6: $S_{yy}[s; \mathbf{p}] = \Lambda[s; \mathbf{p}]S_{yu}[s; \mathbf{p}]$

7: $\Gamma[s] = \sum_r \gamma[r]\, e^{-j(s\Delta\omega)(r\Delta t)}\Delta t$

8: $S_{\gamma\gamma}[s] = |\Gamma[s]|^2$

9: $\mathbf{T}_{y_\gamma}[s; \mathbf{p}] \coloneqq \frac{S_{yy}[s;\mathbf{p}] * S_{\gamma\gamma}[s]}{z}$ *Estimator*

10: end

11: $J(\mathbf{p}) = \frac{\sum_s \left(\mathbf{T}_{y_\gamma}[s;\mathbf{p}] - \widetilde{\mathbf{T}}_{y_\gamma}[s]\right)^2}{\sum_s \left(-\widetilde{\mathbf{T}}_{y_\gamma}[s]\right)^2 + \varepsilon}$

4.2 Benchmark: classical Duffing oscillator

Numerical benchmarking was carried out for the validation of the proposed time-frequency estimator. The reference case study is a Duffing oscillator due to its convenience of use and the availability of analytical equations for the HFRFs. Furthermore, the system is smooth because of the infinite differentiability of polynomial nonlinearities, which guarantees the existence of the Volterra series. The equation of motion for a symmetric Duffing oscillator described by mass m, linear damping c, linear stiffness k_1, and cubic stiffness k_3, and excited by a generic external excitation $u(t)$ writes:

$$m\ddot{y} + c\dot{y} + k_1 y + k_3 y^3 = u(t) \tag{4.25}$$

The first two HFRFs of the Duffing oscillator can be obtained via harmonic probing and write:

$$H^{(1)}(\omega) = \frac{1}{k_1 - m\omega^2 + jc\omega} \tag{4.26}$$

$$H^{(3)}(\omega_1, \omega_2, \omega_3) = \frac{1}{6} H^{(1)}(\omega_1 + \omega_2 + \omega_3)(6k_3 H^{(1)}(\omega_1) H^{(1)}(\omega_2) H^{(1)}(\omega_3)) \tag{4.27}$$

Equations (4.26)-(4.27) have been solved for a system with the numerical values reported in Table 4.1. The values were chosen to ensure a natural frequency f_n of 1 Hz, commonly adopted as a reference value in numerical benchmarks to facilitate the interpretation of the system dynamics. Both kernels $H^{(1)}(\omega)$ and $H^{(3)}(\omega_1, \omega_2, \omega_3)$ are depicted in Figure 4.1. In particular, $H^{(3)}(\omega_1, \omega_2, \omega_3)$ has been represented for three different values of ω_3. Figure 4.1(a) clearly shows that the linear kernel $H^{(1)}(\omega)$ is not a comprehensive representation of the system dynamics. The linear kernel $H^{(1)}(\omega)$ indicates the global maxima, corresponding to the fundamental frequency of the underlying linear system. However, the local maxima distributed among the $H^{(3)}$-plane indicate the presence of other peaks, corresponding to the other combinations of frequencies governing the nonlinear response of the system, see Figure 4.1(b-d). If the system is described by a polynomial of higher order than 3, then the combinations of frequencies governing the nonlinear response will increase accordingly.

Table 4.1. Numerical values of the Duffing oscillator properties used for simulations.

m [kg]	k_1 [N/m]	k_3 [N/m^3]	c [Ns/m]
1.00	39.48	1000.0	0.38

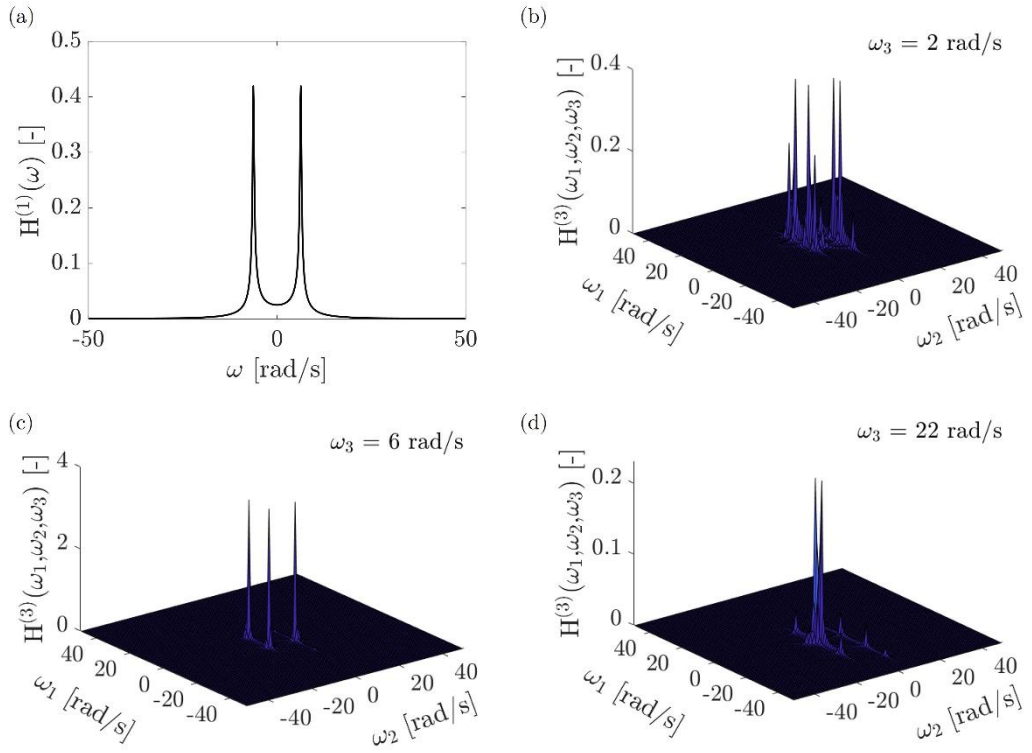

Figure 4.1. Volterra kernels of a classical Duffing oscillator: (a) linear kernel $H^{(1)}$, and cubic kernel $H^{(3)}(\omega_1, \omega_2, \omega_3)$ at the values (b) $\omega_3 = 2$ rad/s, (c) $\omega_3 = 6$ rad/s, and (d) $\omega_3 = 22$ rad/s.

4.3 Results

Numerical simulations were carried out considering a time step size $\Delta t = 0.005\ s$ and a time span $t_{max} = 200\ s$ through ODE23s in Matlab®. Figure 4.2 shows the linear, nonlinear, and total component of restoring force f_r, defined as:

$$f_r = k_1 y + k_3 y^3 \tag{4.28}$$

where the linear component is given by $k_1 y$ and the nonlinear component is given by $k_3 y^3$. It is clear that the nonlinear component is relatively small, given by the fact that the existence and the convergence of the Volterra series should be ensured.

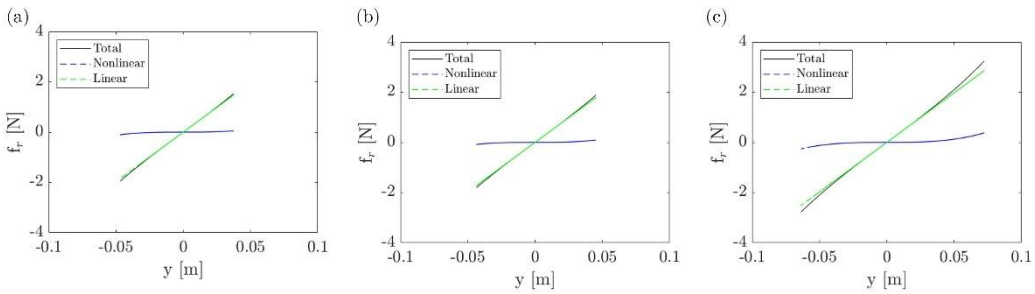

Figure 4.2. Linear, nonlinear, and total f_r for (a) $P = 1$, (b) $P = 1.25$, and (c) $P = 1.5$.

4.3.1 Validation of the time-frequency estimator

Validation of the correction factor

First, a validation of the correction factor due to the distortions of the windowing function γ was carried out. In particular, the process was repeated for three values of window length (WL):

$$\mathrm{WL} = \{15T_0, 30T_0, 50T_0\} \tag{4.29}$$

where T_0 is the period of the linearised Duffing oscillator. In this case:

$$T_0 = 2\pi\sqrt{\frac{m}{k_1}} = 2\pi\sqrt{\frac{1}{39.48}} = 1\ s \tag{4.30}$$

The validation is reported in Figure 4.3. The entire response signal is depicted in black, while the windowed one is in light blue. On the right, the time-frequency estimator w/o and with correction, S_{yy} and $\mathbf{T}_{y\gamma}$, is reported in orange and red, respectively, while the measured spectral density $\widetilde{\mathbf{T}}_{y\gamma}$ is reported in green.

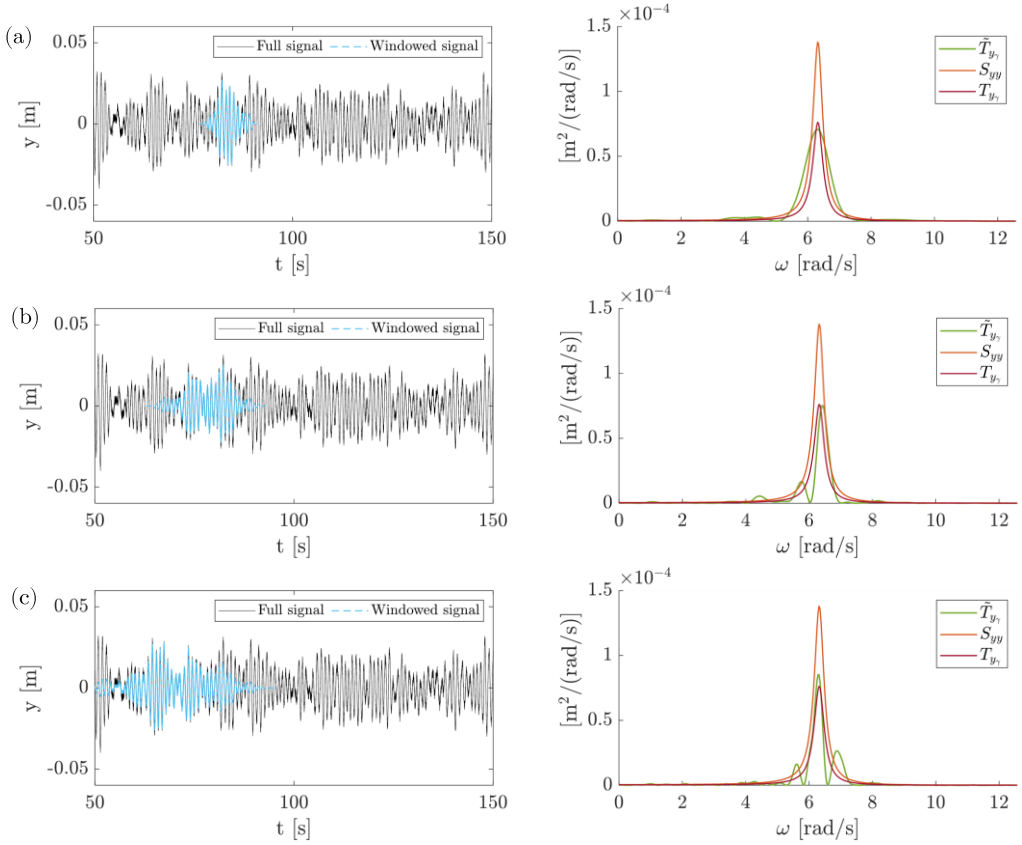

Figure 4.3. Validation of the correction factor for the windowing function γ.

The proposed correction systematically improves the correspondence between the measured and estimated spectral density. This reasoning is applicable to all the cases of WL. A residual discrepancy is observable, which can be ascribed to: (i) uncertainty in the measured spectral density $\widetilde{\mathbf{T}}_{y_\gamma}(\bar{t}, \omega)$; (ii) truncation order m; (iii) residual bias induced by the windowing function $\gamma(t - \bar{t})$.

Validation of the estimation procedure

Once the correction factor has been validated, one may focus on the validation of the estimation procedure reported in Algorithm 1. In particular, displacement response signals have been calculated and polluted with noise. The signal-to-noise ratio (SNR) is here defined as:

$$\mathrm{SNR} = \frac{\sigma_y^2}{\sigma_n^2} = \{10.0, 100\} \tag{4.31}$$

with σ_y^2 as the variance of the displacement response y without pollution (clean) and σ_n^2 as the variance of the added noise. The procedure has been repeated for two different truncation order of the Volterra series, $m = 3$ and $m = 5$, in order to prove that the procedure gives unbiased results independently from the truncation order m chosen. The procedure has been carried out on a system with time-invariant parameters.

In this first case, the input variance P is assumed to be known, along with the linear parameters m, c, and k_1. To further validate the proposed procedure, the estimation has been repeated using the UKF, as described in Chapter 3. The UKF has been augmented with the nonlinear parameter k_3 as quantity to be estimated additionally to the system states. The comparison with the UKF is presented in the time-invariant scenario in Figure 4.4, since, for rapidly time-varying parameters, such as those considered in this work, the standard UKF may require prior knowledge of the parameter variations or significant tuning of the process noise covariance to achieve accurate estimates. Similar observations have been reported in (Bisht and Singh, 2014; Zhang et al., 2023).

The procedure proves to be robust even for $\mathrm{SNR} = 10.0$, corresponding to high level of noise. By zooming in between $30\ s$ and $40\ s$, small variations occur around the theoretical value, less evident for higher truncation order. Nevertheless, the estimation remains reliable in all cases, particularly considering the inherent difficulty of identifying even the order of magnitude of parameters in nonlinear systems. Only in the case of a truncation order $m = 3$ a deviation from the theoretical values can be noticed $\mathrm{WL} = 50T_0$. This can be ascribed to the impossibility of longer WL of capturing the system behaviour, see time-frequency uncertainty principle, or to the need of repeating the procedure for several realisations of the system, as frequently happens under stochastic input excitation.

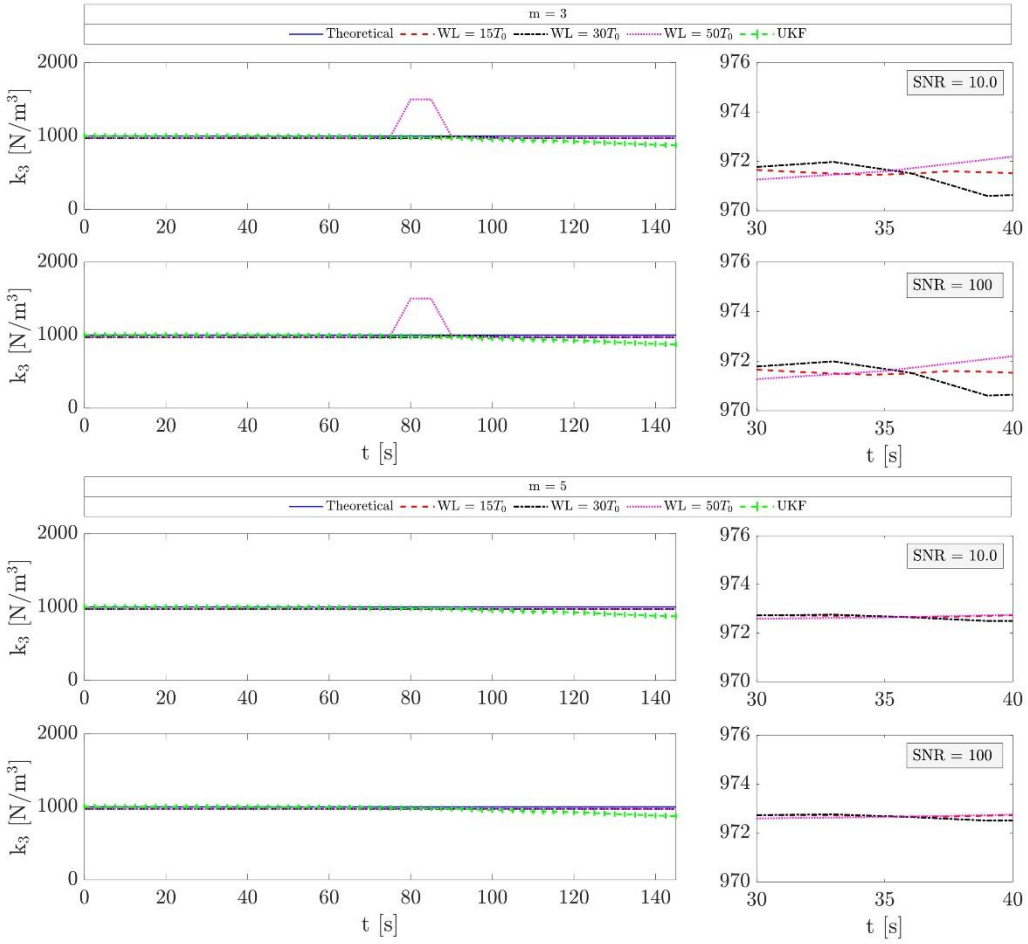

Figure 4.4. Time-invariant nonlinear parameter estimation results for different values of SNR.

A further validation was then carried out for a joint input-parameter estimation. In such a case, to avoid any outlier from the procedure, 20 realisations of the system response have been considered. Results representing k_3 and P are reported from Figure 4.5 to Figure 4.8.

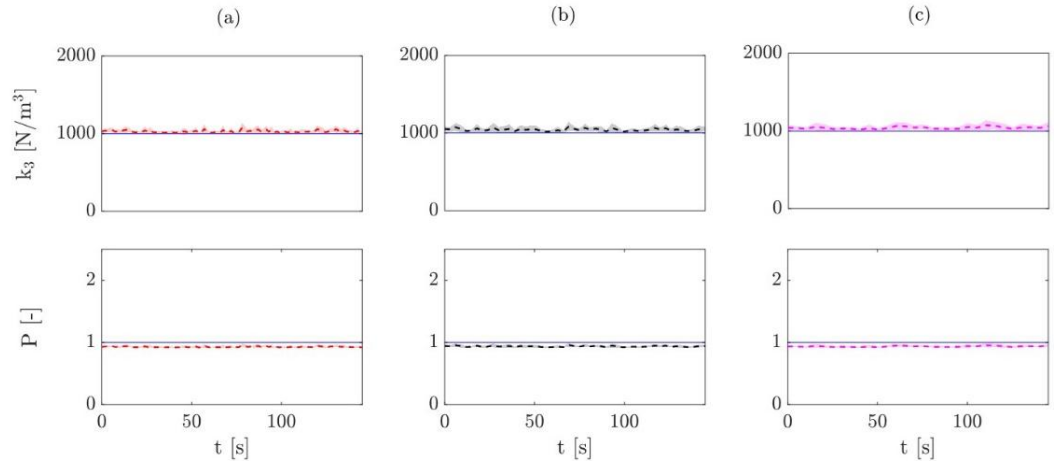

Figure 4.5. Joint input-parameter estimation for $m = 3$ in the case of SNR $= 10.0$ for (a) WL $= 15T_0$, (b) WL $= 30T_0$, and (c) WL $= 50T_0$. The theoretical values are the blue continuous line.

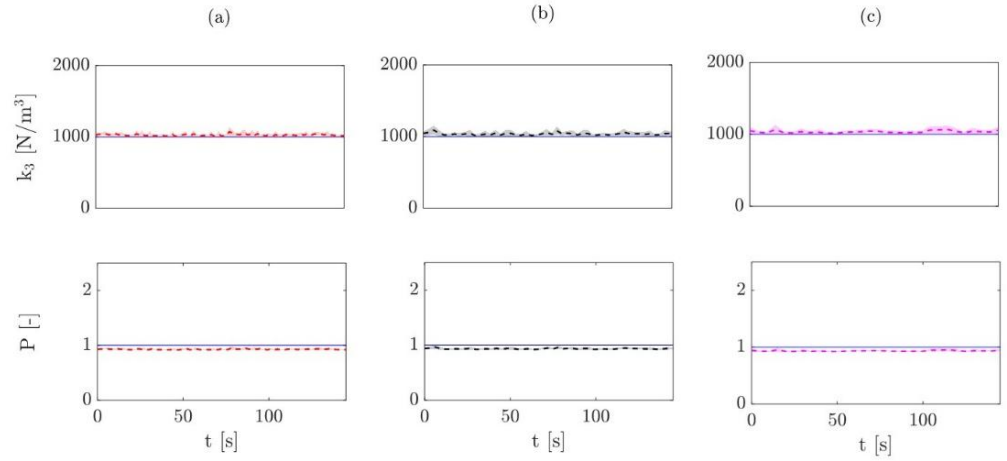

Figure 4.6. Joint input-parameter estimation for $m = 5$ in the case of SNR $= 10.0$ for (a) WL $= 15T_0$, (b) WL $= 30T_0$, and (c) WL $= 50T_0$. The theoretical values are the blue continuous line.

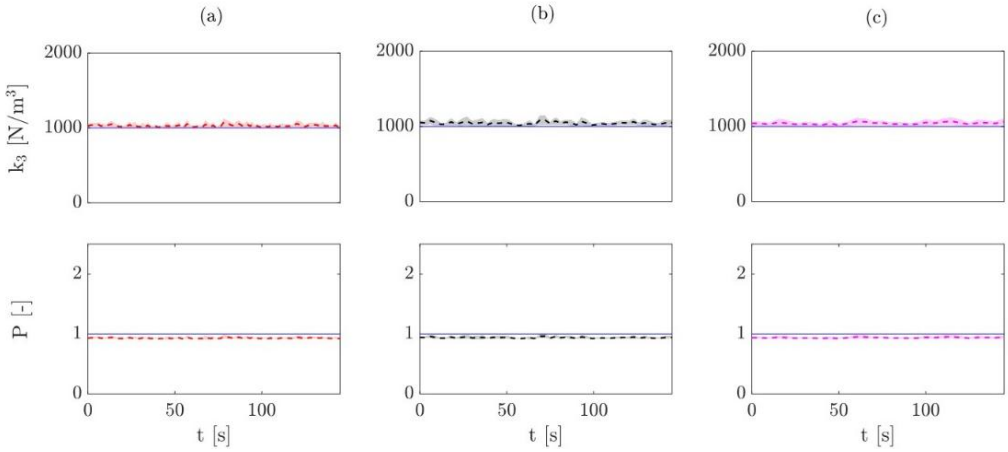

Figure 4.7. Joint input-parameter estimation for $m = 3$ in the case of SNR $= 100$ for (a) WL $= 15T_0$, (b) WL $= 30T_0$, and (c) WL $= 50T_0$. The theoretical values are the blue continuous line.

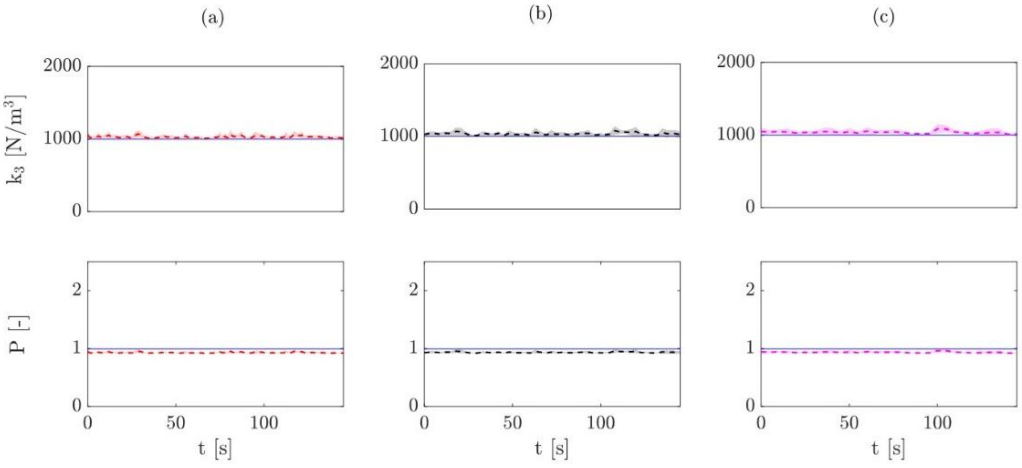

Figure 4.8. Joint input-parameter estimation for $m = 5$ in the case of SNR $= 100$ for (a) WL $= 15T_0$, (b) WL $= 30T_0$, and (c) WL $= 50T_0$. The theoretical values are the blue continuous line.

4.3.2 Benchmark on time-varying Volterra parameters

In this section, the procedure previously validated has been benchmarked considering a time-varying nonlinear parameter k_3 first, a time-varying input variance P, and finally both. The simulation was carried out on a system with the characteristics reported in Table 4.1 for the case of SNR $= 100$, a sampling time $\Delta t = 0.005\ s$ and a time span $t_{max} = 200\ s$. An overlap of 90% for the windowing function was considered for all the analyses. In all figures, the shaded region represents the 95% confidence bounds of the parameters.

Nonlinear parameter estimation

In the first case, the time-varying cubic stiffness is defined as:

$$k_3(t) = 1000 + 500\sin(0.1t) \tag{4.32}$$

and the parameter vector is actually a one-component vector as:

$$\mathbf{p} = k_3(t) \tag{4.33}$$

The results of the identification process for the two truncation orders considered are reported in Figure 4.9.

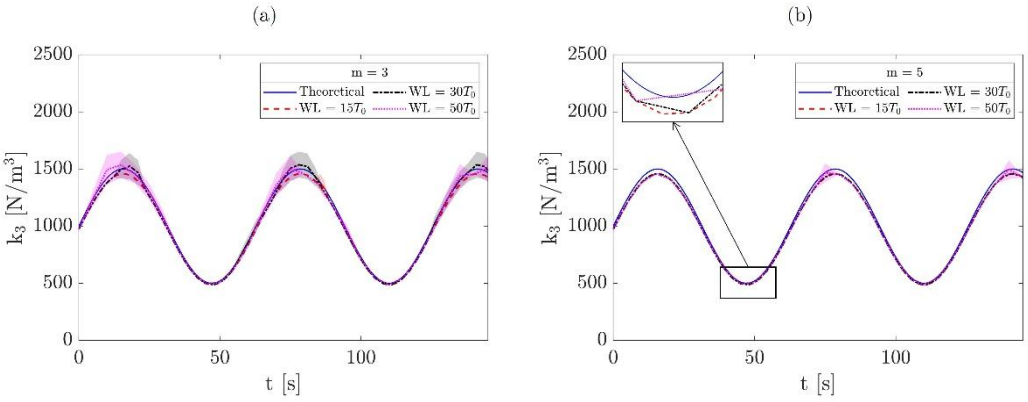

Figure 4.9. Estimated time-varying nonlinear parameter in the case of (a) $m = 3$ and (b) $m = 5$.

Shorter WL, such as WL $= 15T_0$, capture the variability of $k_3(t)$, with restricted confidence bounds for both $m = 3$ and $m = 5$. It is clear that for an higher truncation order, the results almost coincide for all the realisations, making the instantaneous identification of the parameter extremely accurate. Nevertheless, if the computational burden is a key aspect in the identification process (e.g., in the case the procedure is part of a bigger and more complex identification task), one can rely on the choice of $m = 3$ without losing of accuracy and precision. In general, longer WL yield a less accurate instantaneous estimation of the parameters, as the rate of change in the parameter exceeds the resolution of the window.

Input variance estimation

In this second case, the estimation involves a time-varying input variance $P(t)$, defined as:

$$P(t) = \begin{cases} 1.00 & 0 \leq t \leq t_1 \\ 1.25 & t_1 \leq t \leq t_2 \\ 1.50 & t_1 \leq t \leq t_{end} \end{cases} \tag{4.34}$$

and again, the parameter vector writes as one-component vector:

$$\mathbf{p} = P(t) \tag{4.35}$$

Results are reported in Figure 4.10.

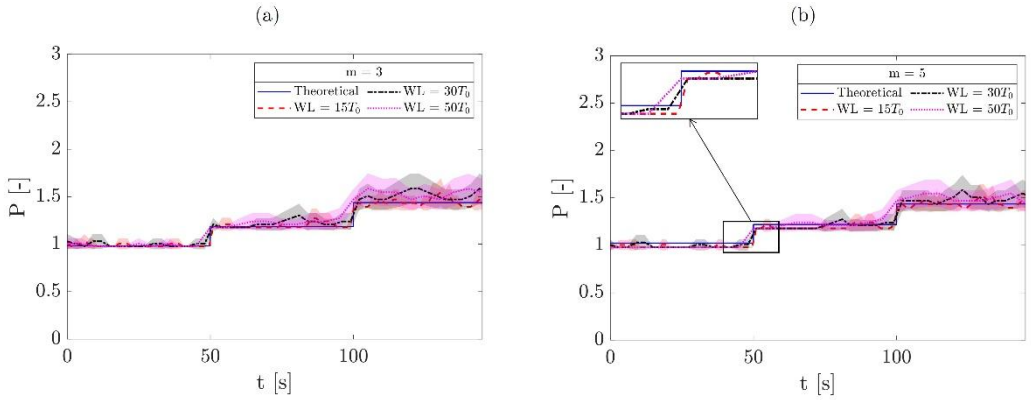

Figure 4.10. Estimated time-varying input variance in the case of (a) $m = 3$ and (b) $m = 5$.

For increasing values of the input variance P, there are evident fluctuations over time, independently on the windowing function (only for $\mathrm{WL} = 15T_0$ the bounds are smaller). The confidence bounds do not change increasing the truncation order m from 3 to 5: therefore, the validity of the proposed approach is restricted to lower input variances.

Joint input-parameter estimation

Finally, the proposed procedure is benchmarked on the case in which both the nonlinear parameter and the input variance are time-varying and defined according to Equation (4.32) and Equation (4.34), respectively. In this case, the parameter vector writes as a two-components vector:

$$\mathbf{p} = \{k_3(t), P(t)\} \tag{4.36}$$

The results of the joint input-parameter estimation are reported in Figure 4.11.

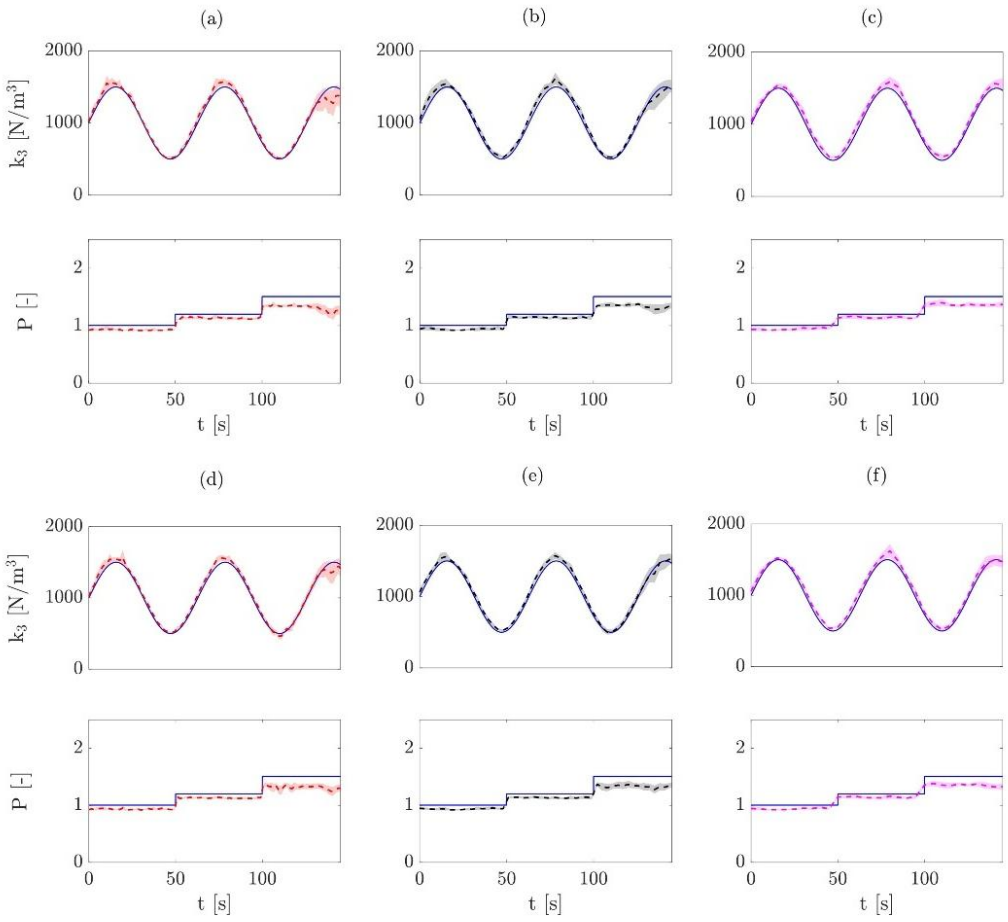

Figure 4.11. Time-varying joint input-parameter estimation for (a) $m = 3$ and $\mathrm{WL} = 15T_0$, (b) $m = 3$ and $\mathrm{WL} = 30T_0$, (c) $m = 3$ and $\mathrm{WL} = 50T_0$, (d) $m = 5$ and $\mathrm{WL} = 15T_0$, (e) $m = 5$ and $\mathrm{WL} = 30T_0$, and (f) $m = 5$ and $\mathrm{WL} = 50T_0$. The theoretical values are reported as a blue continuous line.

The estimates of k_3 and P show similar results in both cases of $m = 3$ and $m = 5$: when the WL is short, and the magnitude of the input variance increases, the results are noisy, and the confidence bounds of the estimation increase. Nevertheless, with respect to the case single estimation, the joint estimation seems to stabilise the value of the parameters and consequently decrease the confidence bounds, especially for the parameter P. In the transition regions, where the input variance suddenly increases, $\mathrm{WL} = 50T_0$ fails to capture these rapid variations. In all cases, when the input variance is $P = 1.5$, the estimation shows a bias, tending to underestimate its theoretical value.

The procedure is then repeated for the case of a common situation in real-world applications, i.e., the simultaneous estimation of linear and nonlinear parameters Thus,

$$\mathbf{p} = \{k_1(t), k_3(t), P(t)\} \tag{4.37}$$

with k_1 constant and defined according to Table 4.1. Results are reported for the case of $m = 3$ and $m = 5$ in Figure 4.12 and Figure 4.13, respectively.

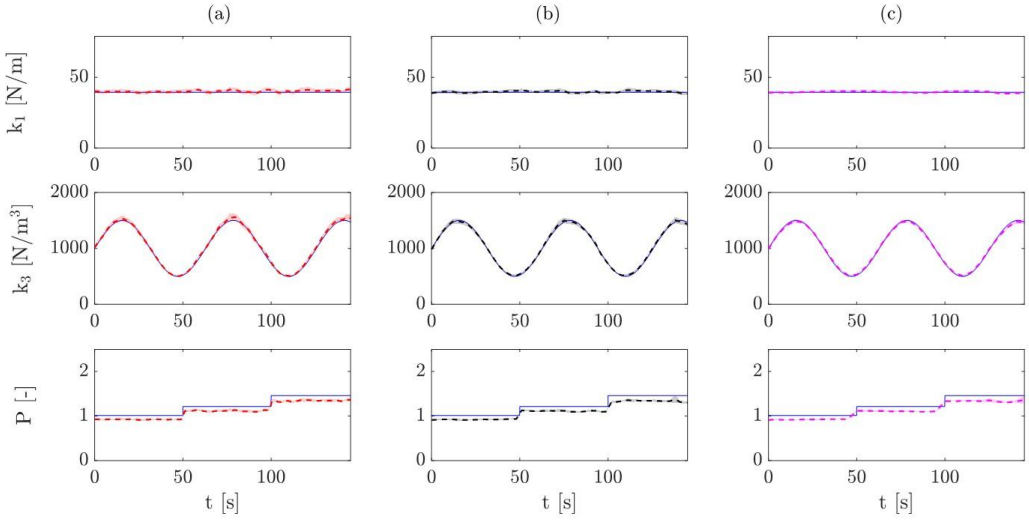

Figure 4.12. Time-varying joint input-parameter estimation in the case of $m = 3$ for (a) WL = $15T_0$, (b) WL = $30T_0$, and (c) WL = $50T_0$. The theoretical values are reported as a blue continuous line.

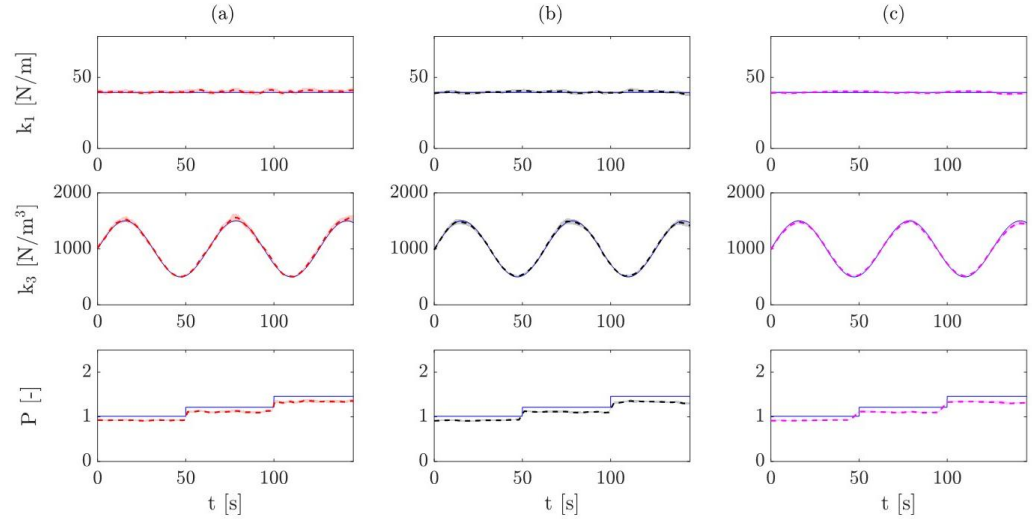

Figure 4.13. Time-varying joint input-parameter estimation in the case of $m = 5$ for (a) WL = $15T_0$, (b) WL = $30T_0$, and (c) WL = $50T_0$. The theoretical values are reported as a blue continuous line.

The estimation results in the case of $m = 3$ and $m = 5$ suggest that, when k_1 is included in the estimation process, the confidence bounds of k_3 become narrower compared with the case where only k_3 is estimated. A trade-off between bias and accuracy of the parameters can be observed, especially in the case of P.

4.4 Application to a chain-like system under simulated laboratory-testing conditions

To illustrate the applicability of the proposed methodology beyond the SDoF Duffing oscillator, a chain-like MDoF system is considered, as schematically shown in Figure 4.14. Such systems are commonly used as representative models of engineering structures exhibiting nonlinear dynamic behaviour, such as frame structures (Hernandez-Garcia et al., 2010).

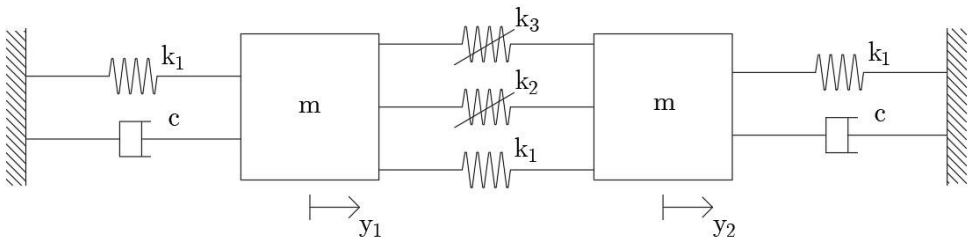

Figure 4.14. 2-DoFs chain-like structure with nonlinearity between the masses.

The system is composed by two equal masses m, linked by a linear, quadratic, and cubic stiffnesses, k_1, k_2, and k_3, respectively. Accordingly, the system dynamics is governed by the following equations:

$$\begin{cases} m\ddot{y}_1 + c\dot{y}_1 + k_1(2y_1 - y_2) + k_2(y_1 - y_2)^2 + k_3(y_1 - y_2)^3 = u_1(t) \\ m\ddot{y}_2 + c\dot{y}_2 + k_1(2y_2 - y_1) + k_2(y_2 - y_1)^2 + k_3(y_2 - y_1)^3 = u_2(t) \end{cases} \tag{4.38}$$

where y_1 and y_2 are the displacements of the two masses, while u_1 and u_2 are the external inputs applied on the two masses. A modal decomposition of the underlying linear system around the zero position reveals two vibration modes: the first mode, $\boldsymbol{\Phi}_1 = \{1,1\}^{\mathrm{T}}$, corresponding to in-phase motion of the masses, remains essentially linear, while the second mode, $\boldsymbol{\Phi}_2 = \{1,-1\}^{\mathrm{T}}$, representing out-of-phase motion, carries the nonlinear contributions. This is clear when transforming the system in modal coordinates q_1 and q_2:

$$\begin{cases} m\ddot{q}_1 + c\dot{q}_1 + k_1 q_1 = \dfrac{1}{\sqrt{2}}\left(u_1(t) + u_2(t)\right) \\ m\ddot{q}_2 + c\dot{q}_2 + 3k_1 q_2 + 2k_2 q_2^2 + \dfrac{1}{2}k_3 q_2^3 = \dfrac{1}{\sqrt{2}}\left(u_1(t) - u_2(t)\right) \end{cases} \tag{4.39}$$

with the modal coordinate transformation defined as:

$$\begin{bmatrix} y_1 \\ y_2 \end{bmatrix} = \frac{1}{\sqrt{2}} \begin{bmatrix} 1 & 1 \\ 1 & -1 \end{bmatrix} \begin{bmatrix} q_1 \\ q_2 \end{bmatrix} \tag{4.40}$$

Importantly for this application, Equation (4.39) shows that that the system can be decoupled into two equivalent SDoF systems. This property can be exploited for the purpose of nonlinear parameter estimation. Thus, although an analytical expression of the full MDoFs FRF can be achieved, it results impractical due to the fact that the linear kernel $H^{(1)}(\omega)$ should be multi-mode (Worden and Manson, 1999), the identification task can exploit the mode-specific response, greatly simplifying the analysis. The FRF associated with the nonlinear mode can then be used within the proposed framework to extract the nonlinear and input parameters, demonstrating that the methodology is also applicable to more complex systems relevant for SHM. In particular, in this case, where a quadratic nonlinearity is added to the cubic one, the composite FRF writes:

$$\begin{aligned} \Lambda(\omega) = H^{(1)}(\omega) + \frac{k_2^2 H^{(1)}(\omega)^2}{c k_1^2} P - \frac{3 k_3 H^{(1)}(\omega)^2}{2 c k_1} P \\ - \frac{2 k_2^2 H^{(1)}(\omega)^2 (\omega - 4 j \zeta \omega_{n,2})}{m c k_1 (\omega - 2 j \zeta \omega_{n,2})(\omega + 2\omega_{d,2} - 2 j \zeta \omega_{n,2})(\omega + 2\omega_{d,2} - 2 j \zeta \omega_{n,2})} P \end{aligned} \tag{4.41}$$

where $\omega_{n,2}$ and $\omega_{d,2}$ are the undamped and damped frequencies, respectively, referred to the second mode of vibration, ζ is the damping ratio, deducible from the damping c as reported in Table 4.1, and $H^{(1)}(\omega)$ can be easily deducted from the harmonic probing of the equivalent second mode SDoF system (Worden and Tomlinson, 2019). Due to the complexity of its explicit Volterra formulation for higher truncation orders, a truncation order of $m = 3$ has been imposed for the following analyses.

Joint-input parameter estimation under laboratory testing conditions

The estimation task addressed in this section considers the following parameter vector:

$$\mathbf{p} = \{k_2(t), k_3(t), P(t)\} \tag{4.42}$$

with the cubic stiffness k_3 and input variance P defined according to Equation (4.32) and Equation (4.34), and the quadratic stiffness k_2 defined as:

$$k_2(t) = 100 + 50\sin(0.5t) \tag{4.43}$$

By comparing the composite FRF of Equation (4.41) with the one obtained from the modal coordinate q_2, one can observe a good correspondence, proving the goodness of the analytical formulation as estimator. This comparison is reported in Figure 4.15.

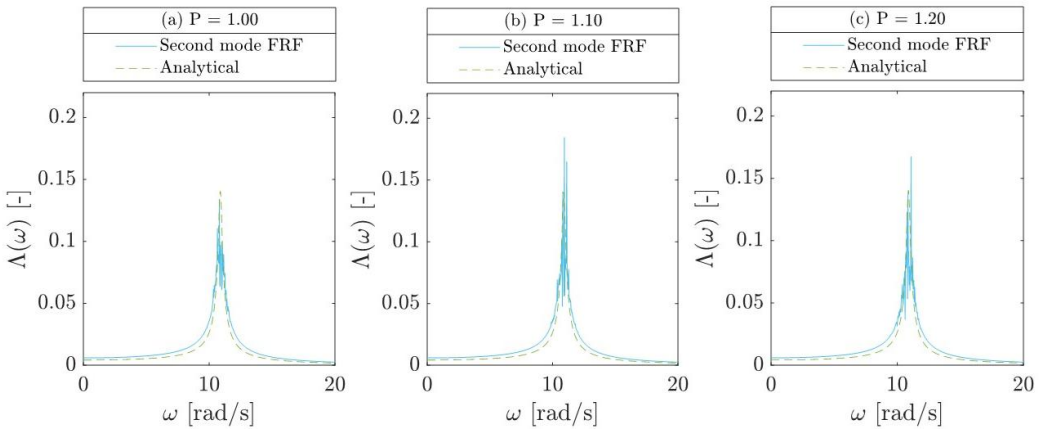

Figure 4.15. Composite FRF $\Lambda(\omega)$ for (a) $P = 1.00$, (b) $P = 1.10$, and (c) $P = 1.20$.

The following simulation includes a 50 Hz disturbance to reproduce the mains hum (Knapp and Anderson, 1994), which is one of the main sources of contamination in acquisition systems. This allows the evaluation of the procedure under realistic conditions. Figure 4.16 illustrates the results of joint input-parameter estimation in the case of time-varying input variance P.

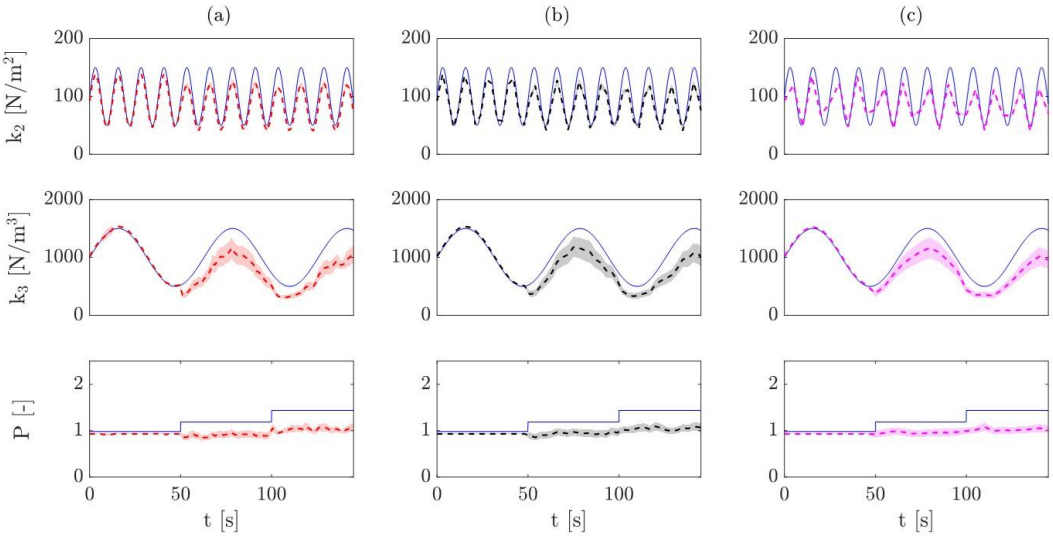

Figure 4.16. Time-varying joint input-parameter estimation of a 2-DoFs in the case of $m = 3$ for (a) $\mathrm{WL} = 15T_0$, (b) $\mathrm{WL} = 30T_0$, and (c) $\mathrm{WL} = 50T_0$. The theoretical values are reported as a blue continuous line.

In the case of time-varying P, the estimator can follow the evolution of the parameters, although the quality of the estimate deteriorates as P increases. This confirms that, for higher excitation levels, the bias observed in the 1-DoF case is still present. A positive aspect is that, even under realistic conditions, the estimate is generally reliable. It is also important to note that the estimate of k_2 deteriorates as the length of the analysis window increases, due to the impossibility of exceedingly long WL to capture the rapid parameter variations. As confirmation

of the above-mentioned results, a further analysis involving the case of time-invariant $P = 1$ was carried out. Results are reported in Figure 4.17.

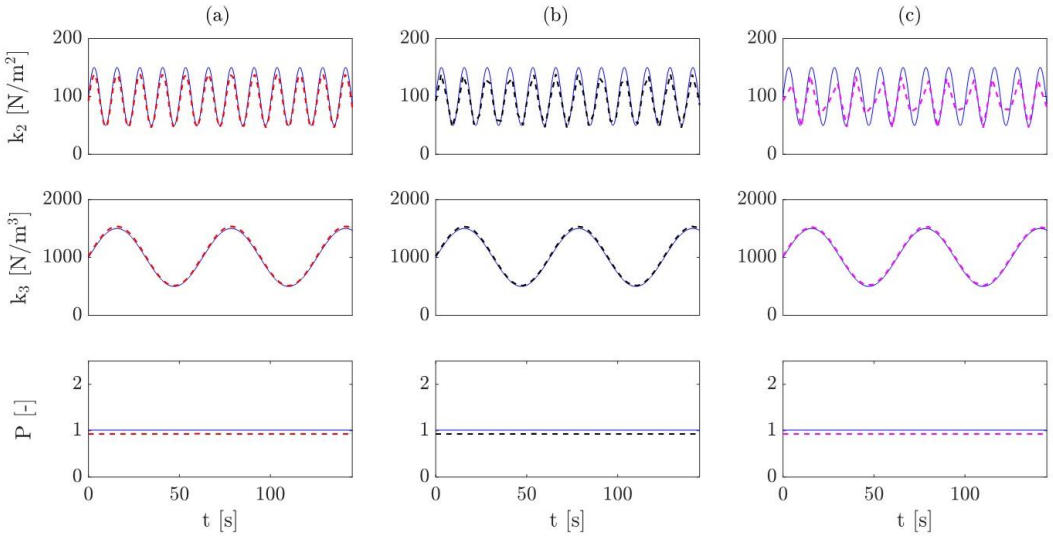

Figure 4.17. Joint input-parameter estimation for time-invariant P of a 2-DoFs in the case of $m = 3$ for (a) WL $= 15T_0$, (b) WL $= 30T_0$, and (c) WL $= 50T_0$. The theoretical values are reported as a blue continuous line.

4.5 Concluding remarks

This chapter aimed to develop a methodology for the estimation of the instantaneous value of the parameters of time-varying nonlinear dynamical systems admitting a Volterra representation. The estimation is conducted in the time-frequency domain. The instantaneous spectral density of the response of the dynamical system is obtained from a parametric model using Volterra theory. One of the main issues investigated is represented by the problem of distortion inducted by the windowing function, which is a crucial point for the definition of the time-frequency estimator, as already largely pointed out in Chapter 3. Here the distortions are numerically accounted by correcting the parametric model of spectral density, which here represents the time-frequency estimator.

The methodology is benchmarked numerically on a Duffing oscillator subjected to time-varying excitation and stiffness. To prove the validity of the procedure, the estimation is conducted for different WL and different SNR. The results reveal that the estimator is robust to noise in response signals. An additional numerical example involving a 2-DoFs system was also considered, simulating a laboratory-like scenario with realistic disturbances. The main drawback observed is that the bias of the estimate is larger for increasing levels of excitation, here accounted as input variance of the random noise.

References

Bendat, J.S., Piersol, A.G., 2011. Random data: analysis and measurement procedures. John Wiley & Sons.

Billings, S.A., 2013. Nonlinear system identification: NARMAX methods in the time, frequency, and spatio-temporal domains. John Wiley & Sons, Inc, Chichester, West Sussex, United Kingdom. https://doi.org/10.1002/9781118535561

Billings, S. A., Fakhouri, S.Y., 1978. Identification of a class of nonlinear systems using correlation analysis, in: Proceedings of the Institution of Electrical Engineers. IET, pp. 691–697.

Billings, S.A., Fakhouri, S.Y., 1978. Identification of a class of nonlinear systems using correlation analysis. Proc. Inst. Electr. Eng. UK 125, 691. https://doi.org/10.1049/piee.1978.0161

Billings, S.A., Tsang, K.M., 1989a. Spectral analysis for non-linear systems, Part I: Parametric non-linear spectral analysis. Mechanical Systems and Signal Processing 3, 319–339. https://doi.org/10.1016/0888-3270(89)90041-1

Billings, S.A., Tsang, K.M., 1989b. Spectral analysis for non-linear systems, Part II: Interpretation of non-linear frequency response functions. Mechanical Systems and Signal Processing 3, 341–359. https://doi.org/10.1016/0888-3270(89)90042-3

Bisht, S.S., Singh, M.P., 2014. An adaptive unscented Kalman filter for tracking sudden stiffness changes. Mechanical Systems and Signal Processing 49, 181–195.

Brillinger, D.R., 1970. The identification of polynomial systems by means of higher order spectra. Journal of Sound and Vibration 12, 301–313. https://doi.org/10.1016/0022-460X(70)90074-X

Ceravolo, R., Demarie, G.V., Erlicher, S., 2010. Instantaneous Identification of Degrading Hysteretic Oscillators Under Earthquake Excitation. Structural Health Monitoring 9, 447–464. https://doi.org/10.1177/1475921710368202

Chance, J.E., Worden, K., Tomlinson, G.R., 1998. FREQUENCY DOMAIN ANALYSIS OF NARX NEURAL NETWORKS. Journal of Sound and Vibration 213, 915–941. https://doi.org/10.1006/jsvi.1998.1539

Chatterjee, A., Vyas, N.S., 2003. Non-linear parameter estimation with Volterra series using the method of recursive iteration through harmonic probing. Journal of Sound and Vibration 268, 657–678. https://doi.org/10.1016/S0022-460X(02)01537-7

Cohen, L., 1989. Time-frequency distribution-a review. A. Instantaneous Frequency and Analytic Signal, Proc. IEEE 77, 968.

Collis, W.B., 1996. Higher order spectra and their application to nonlinear mechanical systems. University of Southampton.

Demarie, G.V., Ceravolo, R., Sabia, D., Argoul, P., 2011. Experimental identification of beams with localized nonlinearities. Journal of Vibration and Control 17, 1721–1732. https://doi.org/10.1177/1077546310385287

Doyle, F.J., Pearson, R.K., Ogunnaike, B.A., 2002. Identification and Control Using Volterra Models, Communications and Control Engineering. Springer London, London. https://doi.org/10.1007/978-1-4471-0107-9

Franz, M.O., Schölkopf, B., 2006. A unifying view of Wiener and Volterra theory and polynomial kernel regression. Neural computation 18, 3097–3118.

Gkikas, G.D., Athanassoulis, G.A., 2014. Development of a novel nonlinear system identification scheme for the pressure fluctuation inside an oscillating water column-wave energy converter Part I: Theoretical background and harmonic excitation case. Ocean Engineering 80, 84–99. https://doi.org/10.1016/j.oceaneng.2013.05.028

Goussard, Y., Krenz, W., Stark, L., 1985. An improvement of the Lee and Schetzen cross-correlation method. IEEE Trans. Automat. Contr. 30, 895–898. https://doi.org/10.1109/TAC.1985.1104086

Hawes, D.H., Langley, R.S., 2018. Analysis of the power flow in nonlinear oscillators driven by random excitation using the first Wiener kernel. Journal of Sound and Vibration 412, 256–269.

Hernandez-Garcia, M.R., Masri, S.F., Ghanem, R., Figueiredo, E., Farrar, C.R., 2010. An experimental investigation of change detection in uncertain chain-like systems. Journal of Sound and Vibration 329, 2395–2409.

Kalouptsidis, N., Koukoulas, P., 2000. Second-order Volterra system identification. IEEE Trans. Signal Process. 48, 3574–3577. https://doi.org/10.1109/78.887051

Kim, K.I., Powers, E.J., 1988. A digital method of modeling quadratically nonlinear systems with a general random input. IEEE Trans. Acoust., Speech, Signal Processing 36, 1758–1769. https://doi.org/10.1109/29.9013

Klein, S., Yasui, S., 1979. Nonlinear systems analysis with non-Gaussian white stimuli; General basis functionals and kernels (Corresp.). IEEE Trans. Inform. Theory 25, 495–500. https://doi.org/10.1109/TIT.1979.1056054

Knapp, R.W., Anderson, N.L., 1994. Digital hum filtering. Computers & Geosciences 20, 881–888.

Koukoulas, P., Kalouptsidis, N., 1997. Third order Volterra system identification, in: 1997 IEEE International Conference on Acoustics, Speech, and Signal Processing. Presented at the 1997 IEEE International Conference on Acoustics, Speech, and Signal Processing, IEEE Comput. Soc. Press, Munich, Germany, pp. 2405–2408. https://doi.org/10.1109/ICASSP.1997.599540

Laning, J.H., Battin, R.H., 1956. Random processes in automatic control. (No Title).

Lee, Y.W., Schetzen‡, M., 1965. Measurement of the Wiener Kernels of a Non-linear System by Cross-correlation†. International Journal of Control 2, 237–254. https://doi.org/10.1080/00207176508905543

Luo, W., Billings, S.A., 1995. Adaptive model selection and estimation for nonlinear systems using a sliding data window. Signal Processing 46, 179–202. https://doi.org/10.1016/0165-1684(95)00081-N

Mathews, V.J., Sicuranza, G., 2000. Polynomial signal processing. John Wiley & Sons, Inc.

Nordsjo, A.E., Zetterberg, L.-H., 2002. Identification of certain time-varying nonlinear Wiener and Hammerstein systems. IEEE transactions on signal processing 49, 577–592.

Palm, G., Poggio, T., 1977. The Volterra Representation and the Wiener Expansion: Validity and Pitfalls. SIAM J. Appl. Math. 33, 195–216. https://doi.org/10.1137/0133012

Papoulis, A., 1965. Random variables and stochastic processes. McGraw Hill.

Rugh, W.J., 1981. Nonlinear system theory: the Volterra/Wiener approach, Johns Hopkins series in information sciences and systems. Johns Hopkins University Press, Baltimore.

Sauder, T., 2021. Empirical estimation of low-frequency nonlinear hydrodynamic loads on moored structures. Applied Ocean Research 117, 102895.

Schetzen, M., 2006. The Volterra and Wiener theories of nonlinear systems. Krieger Pub, Malabar, Fla.

Schetzen, M., 2005. Nonlinear system modeling based on the Wiener theory. Proceedings of the IEEE 69, 1557–1573.

Schoukens, M., Tiels, K., 2017. Identification of block-oriented nonlinear systems starting from linear approximations: A survey. Automatica 85, 272–292.

Simpson, R.J., Power, H.M., 1972. Correlation Techniques for the Identification of Non-Linear Systems. Measurement and Control 5, 316–321. https://doi.org/10.1177/002029407200500802

Tawfiq, I., Vinh, T., 2003. CONTRIBUTION TO THE EXTENSION OF MODAL ANALYSIS TO NON-LINEAR STRUCTURE USING VOLTERRA FUNCTIONAL SERIES. Mechanical Systems and Signal Processing 17, 379–407. https://doi.org/10.1006/mssp.2002.1499

Tick, L.J., 1961. The Estimation of "Transfer Functions" of Quadratic Systems. Technometrics 3, 563–567. https://doi.org/10.1080/00401706.1961.10489976

Villani, L.G.G., Da Silva, S., Cunha, A., 2022. An optimizationless stochastic volterra series approach for nonlinear model identification. J Braz. Soc. Mech. Sci. Eng. 44, 260. https://doi.org/10.1007/s40430-022-03558-z

Weng, B., Barner, K., 2006. Time-Varying Volterra System Identification Using Kalman Filtering, in: 2006 40th Annual Conference on Information Sciences and Systems. Presented at the 2006 40th Annual Conference on Information Sciences and Systems, IEEE, Princeton, NJ, USA, pp. 1617–1622. https://doi.org/10.1109/CISS.2006.286394

Wiener, N., 1949. Extrapolation, Interpolation, and Smoothing of Stationary Time Series: With Engineering Applications. The MIT Press. https://doi.org/10.7551/mitpress/2946.001.0001

Worden, K., Manson, G., 1999. Random vibrations of a multi-degree-of-freedom non-linear system using the Volterra series. Journal of sound and vibration 226, 397–405.

Worden, K., Manson, G., 1998. Random vibrations of a Duffing oscillator using the Volterra series. Journal of Sound Vibration 217, 781–789.

Worden, K., Manson, G., Cross, E.J., 2014. On Gaussian Process NARX Models and Their Higher-Order Frequency Response Functions, in: Koziel, S., Leifsson, L., Yang, X.-S. (Eds.), Solving Computationally Expensive Engineering Problems, Springer Proceedings in Mathematics & Statistics. Springer International Publishing, Cham, pp. 315–335. https://doi.org/10.1007/978-3-319-08985-0_14

Worden, K., Manson, G., Tomlinson, G.R., 1997. A HARMONIC PROBING ALGORITHM FOR THE MULTI-INPUT VOLTERRA SERIES. Journal of Sound and Vibration 201, 67–84. https://doi.org/10.1006/jsvi.1996.0746

Worden, K., Tomlinson, G.R., 2019. Nonlinearity in Structural Dynamics: Detection, Identification and Modelling, 1st ed. CRC Press. https://doi.org/10.1201/9780429138331

Zhang, Y., Ding, Y., Bu, J., Guo, L., 2023. A Novel Adaptive Square Root UKF with Forgetting Factor for the Time-Variant Parameter Identification. Structural Control and Health Monitoring 2023, 4160146.

Chapter 5

Identification of nonlinear systems through Wigner-Ville transforms

The aim of this chapter is to introduce an instantaneous identification framework for nonlinear systems, based on time-frequency representations with an energetic interpretation, i.e., quadratic distributions (Loughlin, 1992). Focus is placed on the instantaneous spectrum derived from the Wigner-Ville transform, or WVD, which provides a physically meaningful description of the energy distribution of a signal in the time-frequency plane. Although the WVD is inherently non-causal (Boashash, 1987), it represents a natural theoretical reference for defining instantaneous spectral quantities.

The previous chapter demonstrated that combining linear time-frequency transforms with Volterra-based methods is effective in the estimation of nonlinear parameters for time-varying systems. However, this approach has largely relied on the assumption that for some classes of nonlinear systems an analytical expression of the Volterra spectral density is available, allowing for an extension of the local stationarity, developed for linear systems in Equations (3.21)-(3.28). Consequently, a more generalisable method is required to apply quadratic time-frequency transforms for the estimation of parameters in a broader class of nonlinear systems.

Accordingly, the main contribution of this chapter builds on the approach of the ALEs, first proposed in (Feijoo et al., 2004), and introduced in Chapter 2, and extends it to an instantaneous identification strategy based on the WVD. By exploiting the connection between Volterra series and perturbative approaches (Ibrahim and Pandya, 1990), the ALEs allow a greater applicability of Volterra series approaches, by reducing the computational burden typically associated with nonlinear convolution operators (Feijoo et al., 2010). Another important advantage is related to the fact that, in the case of structural dynamics problems,

where the level of nonlinearity activated depends on the intensity of the actions (Pinho, 2007), and multiple states of the response can coexist at the same time (Kougioumtzoglou and Spanos, 2009; Nayfeh and Serhan, 1990), it can be convenient to limit the number of terms in the Volterra series, thereby preventing the introduction of numerical artefacts in the calculated response.

5.1 Time-frequency nonlinear identification based on Wigner-Ville representations

5.1.1 Identification with quadratic time-frequency transforms

One of the main issues of dynamic identification is that structural response signals are intrinsically multicomponent, as they result from the superposition of several modal contributions (Bonato et al., 1997). In this context, quadratic time-frequency transforms hold some interesting properties which allow their treatment (Flandrin, 1984; Stanković et al., 2018). Chapter 3 discussed that quadratic time-frequency transforms make it possible to overcome limitations due to the time-frequency resolution of linear ones, since energetic and correlative transforms do not require signal windowing. Specifically, among the quadratic transforms, those belonging to the Cohen class are characterised by their invariance to time and frequency shifts (Cohen, 2002).

The WVD, for which one may refer to Equation (3.14), plays a central role within this class, due to its connection with the spectral density of stationary processes and its ability to preserve instantaneous spectral information. In particular, it convenient to recall some notions already discussed in Chapter 3. Introducing the auto-covariance function of a process F as the expectation of the instantaneous auto-correlation $r_F(t,\tau)$, i.e., $C_F(t,\tau) = \mathbb{E}[r_F(t,\tau)]$, the Wigner spectrum can be defined as follows (Carmona et al., 1998; Mecklenbräuker and Hlawatsch, 1997):

$$\mathbb{E}[\mathbf{WD}_F(t,\omega)] = \int_{-\infty}^{+\infty} C_F\left(t+\frac{\tau}{2}, t-\frac{\tau}{2}\right) e^{-j\omega\tau} d\tau \tag{5.1}$$

In the stationary case, the quantity of Equation (5.1) is independent of t and reduces to the usual spectral density $\mathbb{E}[\mathbf{WD}_F(t,\omega)] = S_F(\omega)$. As already said, the covariance operator is nothing more than a convolution operator in this case, which is known to be diagonalised by the complex exponential functions. In practical applications, where a limited number of process realisations is available, this is not inherently true. If the process is ergodic, a Wigner Distribution estimate of the spectral density V_B can be obtained from a single realisation Y by averaging over the finite bandwidth B of the time instantaneous spectrum (Flandrin and Martin, 1997) as:

$$V_B(\omega) = \frac{1}{B} \int_{-B/2}^{+B/2} |\mathbf{WD}_Y(t, \omega)| dt \tag{5.2}$$

However, in multi-component signals, the Wigner representation of a single realisation of the process is affected by interference terms, which can be filtered out in the ambiguity function domain but at the cost of reducing resolution. There is, in fact, a trade-off between cross term filtering and time-frequency resolution, hence the representation is kernel dependent. Another problem is that the Wigner transform of a single signal misses the desirable property of non-negativity over the time-frequency plane (Janssen, 1997). These two aspects may have some negative implications in the definition of instantaneous estimators to be used in the analysis of deterministic signals.

A fundamental formalism which favours the practical use of WVD in structural identification is provided by the formulation of distribution in the ambiguity domain. In the ambiguity domain, signal-related auto-terms associated with individual modal components are generally concentrated near the coordinate axes, whereas interference cross-terms are distributed away from them. This separation allows interference effects to be selectively attenuated by means of suitable filtering in the ambiguity plane. Kernel-based distributions of the Cohen class exploit this property by introducing a filtering function that controls the trade-off between time-frequency resolution and cross-term suppression. In particular, the Choi-Williams (Choi and Williams, 1989) distribution provides a convenient parametrisation of this trade-off through a single tuning parameter.

From a computational standpoint, ambiguity-domain filtering naturally leads to alias-free discrete implementations of quadratic time-frequency transforms (Morris and Wu, 1996). The adoption of smoothed or kernel-based Wigner-Ville representations mitigates spurious interference effects while preserving sufficient resolution to identify and track modal contributions in the time-frequency plane. Modal frequencies appear as well-defined ridges whose temporal evolution can be followed, providing direct insight into time-varying structural behaviour. The use of quadratic time-frequency transforms for structural identification has been previously investigated in the literature from a qualitative point of view by (Bonato et al., 1997). Ambiguity-domain has been exploited to identify modal parameters from structural responses under ambient or transient excitation.

5.1.2 Numerical implementation of the time-frequency estimation procedure

Let's consider the discrete time instant $n\Delta t$ and the discrete frequency $m\Delta f$. The identification relies on the minimisation of the distance between the measured and the analytical (model) time-frequency transform at the time instant $\bar{t} = \bar{n}\Delta t$ to

have an instantaneous tracking of the desired parameters. Specifically, in this work the objective function to minimise writes:

$$J(n,\mathbf{p}) = \sum_{m=0}^{M-1} \left\| \mathbf{T}_y(n,m) - \widetilde{\mathbf{T}}_y(n,m;\mathbf{p}) \right\|_2 \tag{5.3}$$

with the instantaneously identified parameter vector $\mathbf{p}_{id}$:

$$\mathbf{p}_{id}(\bar{t}) = \arg[\min J(n,\mathbf{p})] \tag{5.4}$$

The values of the measured and the analytical quadratic time-frequency transforms, $\mathbf{T}_y(n,m)$ and $\widetilde{\mathbf{T}}_y(n,m;\mathbf{p})$, respectively, write:

$$\mathbf{T}_y(n,m) = \sum_{k=-N}^{N} \tilde{y}\left(n+\frac{k}{2}\right)\tilde{y}^*\left(n-\frac{k}{2}\right)e^{-\frac{j2\pi mk}{N}} \tag{5.5}$$

$$\widetilde{\mathbf{T}}_y(n,m;\mathbf{p}) = \sum_{k=-N}^{N} \tilde{y}\left(n+\frac{k}{2};\mathbf{p}\right)\tilde{y}^*\left(n-\frac{k}{2};\mathbf{p}\right)e^{-\frac{j2\pi mk}{N}} \tag{5.6}$$

Where the index k denotes the discrete time lag. The analytical expression of the WVD of Equation (5.6) is nothing else than the parametric version of Eq. (5.5), which is on the contrary calculated on the measured response y.

The problem of interference reported above may take place also in the case where the response exhibits sudden transitions (e.g., between two states of the system). A convenient approach to deal with these cross-terms relies on introducing independent smoothing windows in time and frequency domain, $w(n)$ and $W(m)$, respectively. The time-frequency transform is thus called S-WVD, and the quantities $\mathbf{T}_y(n,m)$ and $\widetilde{\mathbf{T}}_y(n,m;\mathbf{p})$ write:

$$\mathbf{T}_y(n,m) = \sum_{k=-N}^{N} w(n)W(m)\tilde{y}\left(n+\frac{k}{2}\right)\tilde{y}^*\left(n-\frac{k}{2}\right)e^{-\frac{j2\pi mk}{N}} \tag{5.7}$$

$$\widetilde{\mathbf{T}}_y(n,m;\mathbf{p}) = \sum_{k=-N}^{N} w(n)W(m)\tilde{y}\left(n+\frac{k}{2};\mathbf{p}\right)\tilde{y}^*\left(n-\frac{k}{2};\mathbf{p}\right)e^{-\frac{j2\pi mk}{N}} \tag{5.8}$$

The introduction of smoothing windows has a double effect: on the one hand, it suppresses the interference terms; on the other hand, it also reduces the sharpness of the patterns in the time-frequency representation. By referring to classical deterministic optimisation procedures, one can minimise the objective function $J(n,\mathbf{p})$ reported in Equation (5.3) at every instant. Here, a constrained nonlinear optimisation algorithm (*fmincon* in Matlab) has been used.

5.2 Benchmarks

5.2.1 Benchmark #1: Duffing oscillator with time-invariant parameters

The time-frequency estimator of Section 5.2 is first benchmarked on a time-invariant Duffing oscillator. In the case of the classical Duffing oscillator, the ALEs can be written as:

$$m\sum_{p=1}^{+\infty}\ddot{y}^{(p)}(t)+c\sum_{p=1}^{+\infty}\dot{y}^{(p)}(t)+k_1\sum_{p=1}^{+\infty}y^{(p)}(t)=u(t)-k_3\left[\sum_{p=1}^{+\infty}y^{(p)}(t)\right]^3 \quad (5.9)$$

where the order $p=0$ is neglected without losing of generality (the steady-state solution $y^{(0)}=0$ is the only existing solution for this kind of oscillator). By developing Equation (5.9) and assuming a truncation order $m=3$ one has:

$$\begin{aligned} m\left(\ddot{y}^{(1)}(t)+\ddot{y}^{(3)}(t)\right)+c\left(\dot{y}^{(1)}(t)+\dot{y}^{(3)}(t)\right)+k_1\left(y^{(1)}(t)+y^{(3)}(t)\right)= \\ =u(t)-k_3\left(y^{(1)}(t)+y^{(3)}(t)\right)^3 \end{aligned} \quad (5.10)$$

where the even-order terms vanish as expected. By developing the squared and the cubic terms of Equation (5.10) and grouping the terms by their order, the first two ALEs can be written as:

$$\begin{cases} m\ddot{y}^{(1)}(t)+c\dot{y}^{(1)}(t)+k_1y^{(1)}(t)=u(t) \\ m\ddot{y}^{(3)}(t)+c\dot{y}^{(3)}(t)+k_1y^{(3)}(t)=-k_3y^{(1)}(t)^3 \end{cases} \quad (5.11)$$

The system reported in Equation (5.11) was solved employing the numerical values reported in Table 5.1. The values of linear and cubic stiffness k_1 and k_3 were considered as time-invariant and were chosen to ensure a pronounced nonlinear behaviour, i.e. $k_3 \gg k_1$, consistently with the objective of this chapter. For this purpose, as external input a bi-harmonic excitation $u(t)=A_1\omega_1+A_2\omega_2$ with excitation frequencies ω_1 and ω_2 equal to 80 rad/s and 120 rad/s and amplitudes A_1 and A_2 equal to $1e^{-1}$ N and $2e^{-1}$ N was employed. A time span $t_{max}=6.92\,s$ and a sampling time $\Delta t=0.0157\,s$ were considered. Consequently, the sampling frequency assumed a value of $f_s=63.33\,Hz$ much higher than the natural frequency of the system, i.e., $f_n=15.91\,Hz$.

Table 5.1. Values assigned to Benchmark #1 for the numerical simulations.

m [kg]	c [Ns/m]	k_1 [N/m]	k_3 [N/m^3]
1	20	1×10^4	5×10^9

In order to demonstrate the validity of the proposed procedure, the response of the system was simulated both with the system of Equation (5.11) and then directly solving the equation of motion, using a modified Rosenbrock formula of order 2 algorithm (*ODE23s* in Matlab®). The displacement response y calculated directly solving the equation of motion and then solving the system of Equation (5.11) is shown in Figure 5.1. A zoom on the first seconds of the response signal is also shown to demonstrate the validity of the procedure even for transient parts of the response.

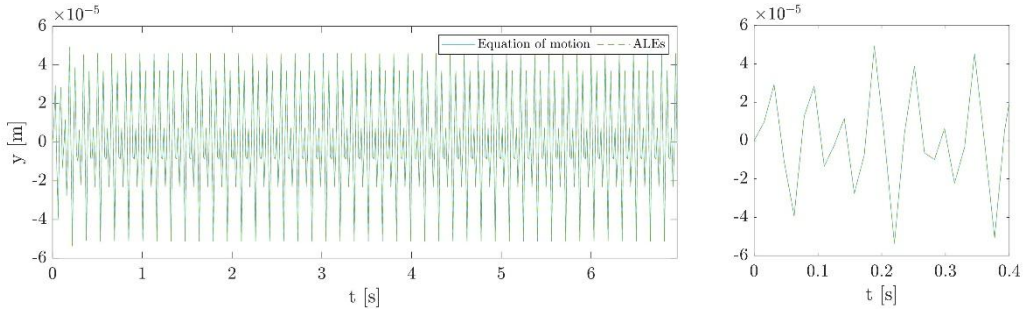

Figure 5.1. Validation of the proposed approach for a time-invariant Duffing oscillator.

The subsequent step was the calculation of the WVD and the smoothed WVD. The displacement response y obtained from the ALEs was employed in the calculation of both distributions. For the smoothed one, an Hanning window with a number of samples equal to the length of the signal was employed. Figure 5.2 depicts both distributions.

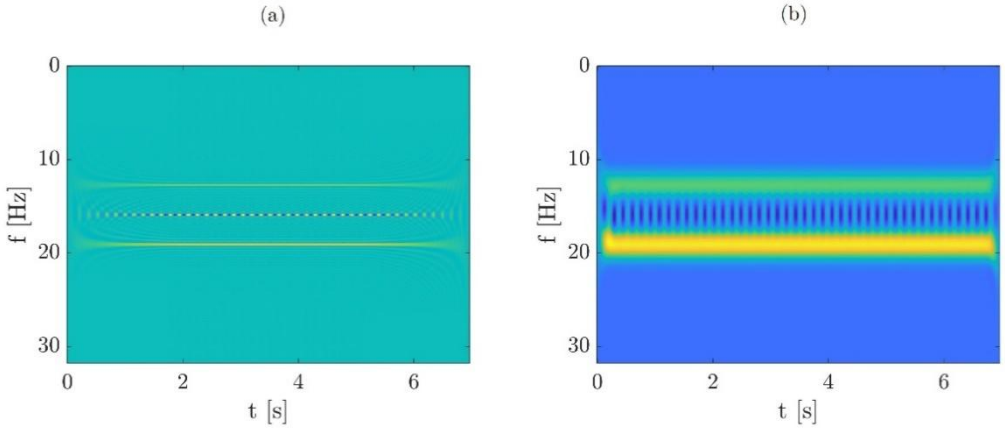

Figure 5.2. (a) WVD and (b) S-WVD distributions for a classical Duffing oscillator under bi-harmonic excitation.

It is clear that the WVD exhibits higher time-frequency resolution with respect to its smoothed counterpart, however it suffers from cross-term interference. Contrarily, the use of a smoothing window mitigates these interference effects at the cost of reduced resolution, resulting in a smoother but less detailed representation. Since the aim of this work is to prove the goodness of

the identification procedure, both distributions have been employed to perform the identification task. In this case, the parameter vector to be identified writes:

$$\mathbf{p} = k_3 \tag{5.12}$$

Results of the identification procedure are reported in Figure 5.3. The effectiveness of the identification process is clearly visible for both the WVD and the S-WVD. The main difference between the two distributions is the time required for the estimation to stabilise, as can be observed from the zoomed-in region between 0 s and 0.4 s. Specifically, the S-WVD stabilises earlier than the WVD, demonstrating slightly more robust results.

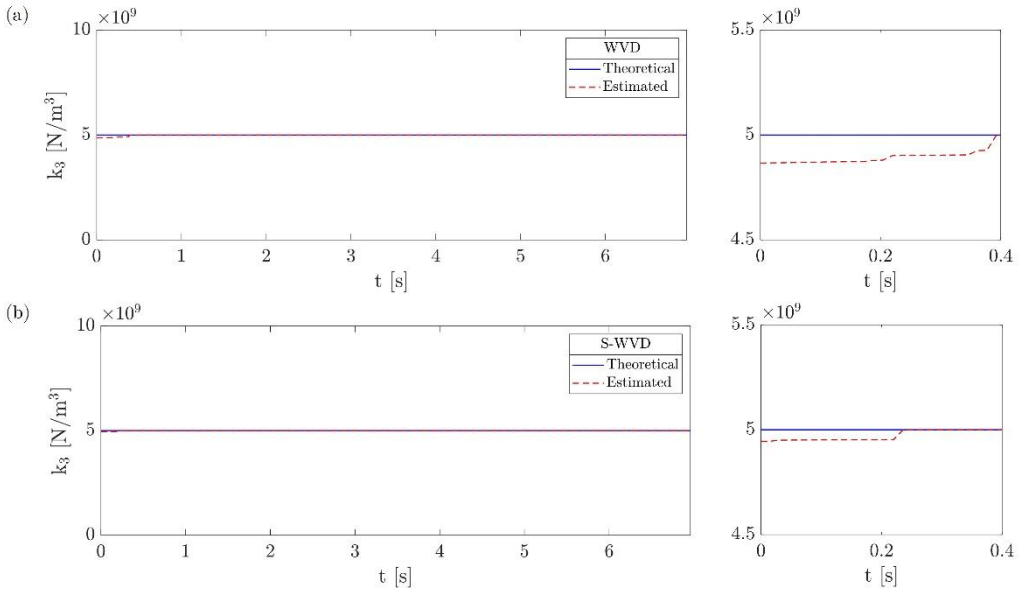

Figure 5.3. Results of the estimation of the parameter k_3 in the case of (a) WVD and (b) PSWVD.

5.2.2 Benchmark #2: bistable oscillator with time-invariant parameters

The Benchmark #2 is carried out on a Duffing oscillator that show a double-well potential. These kind of systems, namely bistable systems, are characterised by two stable configurations and one unstable configuration. Under dynamic excitation, the bistable oscillator operates in two distinct regimes: *intrawell*, occurring around one of the stable equilibrium points, and *interwell*, involving the crossing of the unstable equilibrium point. The continuous equation of motion for a SDOF bistable oscillator writes (Perkins, 2025; Wu et al., 2015):

$$m\ddot{y}(t) + c\dot{y}(t) - k_1 y(t) + k_3 y^3(t) = u(t) \tag{5.13}$$

where the mass m, the linear damping c, and the cubic stiffness k_3 recall the equation of motion of a classical Duffing oscillator. Conversely to the case of the

Duffing oscillator, the stiffness k_1 assumes a negative sign, governing the nonlinear behaviour, especially when the system crosses the equilibrium position. It is clear that this kind of systems show a type of nonlinearity which can ultimately result in a chaotic behaviour (Bonthron and Tubaldi, 2024).

Chapter 2 introduced the problem of existence and convergence for Volterra series. To briefly recall some basic notions, the existence of the Volterra series is guaranteed for smooth systems, i.e., systems that are sufficiently differentiable. In particular, a Volterra representation is always valid for polynomial nonlinearities, which are infinitely differentiable, including the one described by Equation (5.13). This means that even a bistable system, despite the presence of two stable and one unstable configuration (in total, three equilibrium points), may, at least in principle, satisfy the smoothness assumptions locally around a configuration. Consequently, a Volterra series exists for a bistable system when the input-output relationship is expanded in a neighbourhood admitting the Fréchet differentiability property, i.e., the stable equilibrium points. However, it was also stressed that, for the Volterra series representation to be meaningful, a convergence condition must be defined. In the case of a bistable oscillator, when $y = 0$ (i.e., unstable configuration), the Volterra kernels may diverge, and the Volterra series fails to exist. This is not inherently true when the system reaches one of the two stable configurations. In this case, the Volterra expansion may accurately describe the response of the system around the equilibrium states.

The reason behind that stems from the perturbation methods (Nayfeh, 2000), which clarify the need of analysing separately intrawell and interwell oscillations. For bistable systems, a direct application of a perturbation method requires selecting which terms are assumed to be small, thus of ε^1 order. One may normalise Equation (5.13) by the mass, obtaining non-dimensional damping, linear, and cubic stiffness, γ, α, and β. Since γ, β, and the external excitation $u(t)$ are typically considered small contributors to the nonlinear dynamics, one has:

$$\ddot{y}(t) + \varepsilon\gamma\dot{y}(t) - \alpha y(t) + \varepsilon\beta y^3(t) = \varepsilon u(t) \tag{5.14}$$

If $\varepsilon = 0$, the formulation of Equation (5.14) is not the one of a linear oscillator. This indicates perturbation methods are not ordinarily suitable to predict the interwell dynamics of bistable structures since such behaviours involve responses inherently far from equilibrium (Harne and Wang, 2017). On the other hand, with appropriate transformations and considerations, approaches similar to perturbation ones can be applied for analysing the intrawell dynamics.

At the beginning of this chapter, it was explicated that the derivation of the ALEs lies its foundation precisely in perturbation methods. Thus, exploiting the connection between the Volterra series and the perturbation methods, a similar

approach to the one of ALEs can be used to develop the intrawell dynamics of bistable oscillators. In particular, by using the variational approach (Rugh, 1981), and collecting the same-order terms, the following adaptation of ALEs can be developed (Belousov et al., 2019):

$$\begin{cases} m\ddot{y}^{(0)} + c\dot{y}^{(0)} - k_1 y^{(0)} = k_3\left(y^{(0)}\right)^3 \\ m\ddot{y}^{(1)} + c\dot{y}^{(1)} - k_1 y^{(1)} = u + 3k_3\left(y^{(0)}\right)^2 y^{(1)} \\ m\ddot{y}^{(2)} + c\dot{y}^{(2)} + k_1 y^{(2)} = 3k_3\left(\left(y^{(0)}\right)^2 y^{(1)} + \left(y^{(1)}\right)^2 y^{(0)}\right) \\ m\ddot{y}^{(3)} + c\dot{y}^{(3)} + k_1 y^{(3)} = 3k_3\left(\left(y^{(0)}\right)^2 y^{(2)} + \frac{1}{3}\left(y^{(1)}\right)^3 + 2y^{(0)}y^{(1)}y^{(3)}\right) \end{cases} \tag{5.15}$$

The steady-state solution $y^{(0)}$ is constant and equal to the two stable roots of the system, given by $y^{(0)} = \pm\sqrt{(k_1/k_3)}$. Unlike the case of the classical Duffing oscillator, the even-order terms do not vanish in the Volterra series of bistable oscillators around $y^{(0)}$ because the potential wells surrounding these points are asymmetric. However, the symmetry, at least in principle, of the double-well potential ensures opposite signs for the even-order terms.

For identification purposes, the system of Equation (5.15) was exploited to calculate the intrawell response of the bistable oscillator with the same characteristics reported in Table 5.1. Also, $u(t)$ was assumed to be a white Gaussian noise $n(\mu, \sigma)$ with null mean μ with the same simulation steps of Benchmark #1. Figure 5.4 shows the dynamics of the bistable oscillator for two distinct values of standard deviation σ. In the case of $\sigma = 2$ only the intrawell oscillations are visible, while for $\sigma = 3$ the system clearly enters in interwell regime, leading to the jump between the two stable conditions. In this second case, the system oscillates between the two stable equilibrium points, corresponding to $\pm 1.5 \times 10^{-3}$ m.

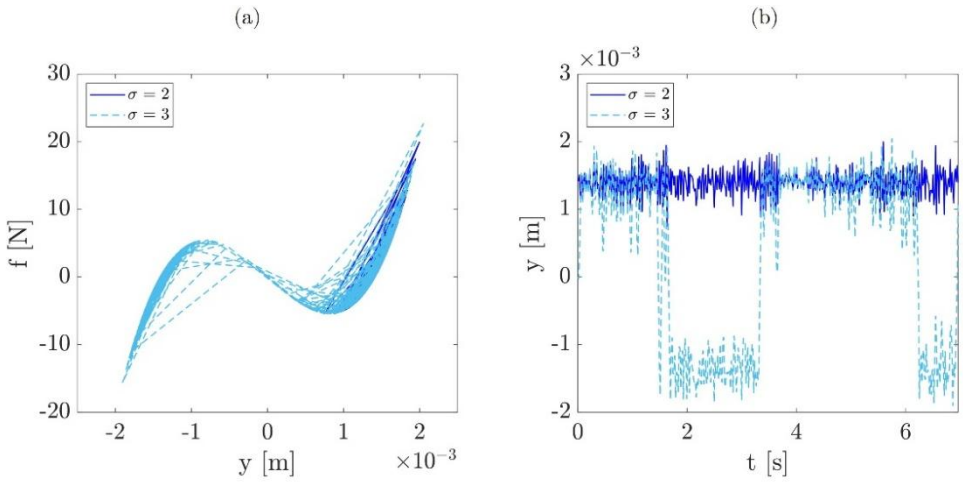

Figure 5.4. Dynamics of a bistable oscillator under white noise: (a) restoring force and (b) displacement response.

The case $\sigma = 2$ was considered for further analyses. Figure 5.5 reports the validation of Equation (5.15) with respect to the direct resolution of Equation (5.13). As can be observed, the correspondence between the two methods is almost identical, with the computational advantage of ALEs.

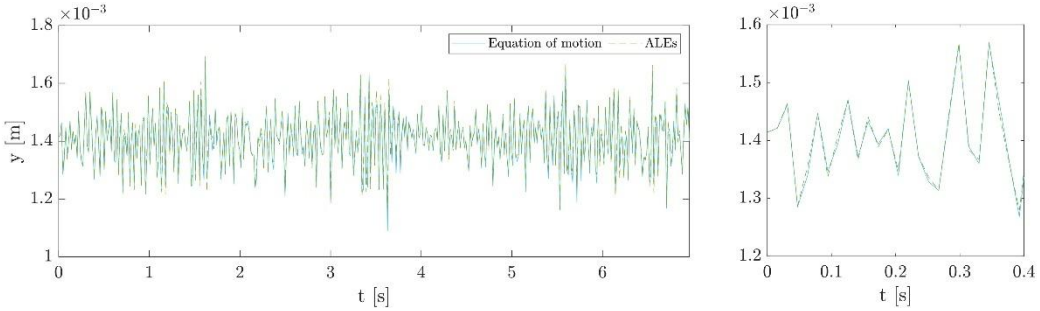

Figure 5.5. Validation of the proposed approach for a time-invariant bistable oscillator.

Finally, the parameter estimation task was performed considering both the WVD and the S-WVD distribution. In this case, the parameter vector writes:

$$\mathbf{p} = \{k_1, k_3\} \tag{5.16}$$

Results of the identification are reported in Figure 5.6 and in Figure 5.7 for the WVD and the S-WVD case, respectively.

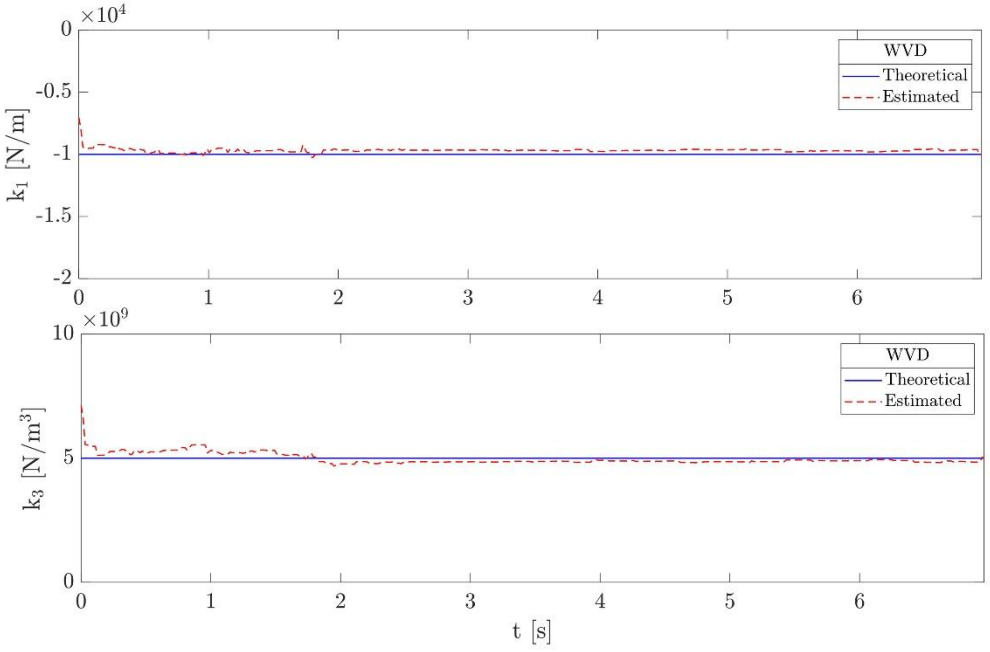

Figure 5.6. Estimated parameters k_1 and k_3 for a bistable oscillator using WVD.

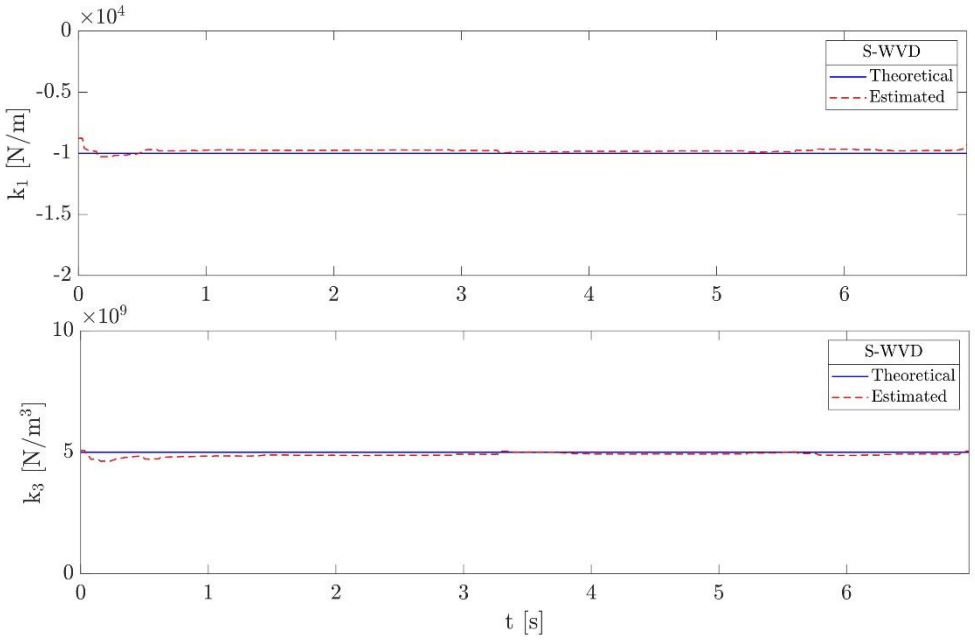

Figure 5.7. Estimated parameters k_1 and k_3 for a bistable oscillator using S-WVD.

In the case of time-invariant parameters, both the WVD and the S-WVD proved effective in the identification task. However, a small bias in the estimation of the parameters can be appreciated. This can be possibly ascribed to the presence of a smoothing window in both time- and frequency-domain.

5.2.3 Benchmark #3: bistable oscillator with time-varying parameters

Finally, a third benchmark considering a time-varying parameter for the bistable oscillator has been introduced. In particular, the cubic stiffness k_3 can be defined as:

$$k_3(t) = 5 \times 10^9 + 1 \times 10^9 \sin(10t) \tag{5.17}$$

thus, providing a sinusoidal variation of the parameter over time. In this case, the parameter vector writes:

$$\mathbf{p} = \{k_1, k_3(t)\} \tag{5.18}$$

The estimation was carried out with the same simulation details reported for Benchmark #1 and Benchmark #2. The results are reported in Figure 5.8 and Figure 5.9 for WVD and S-WVD, respectively.

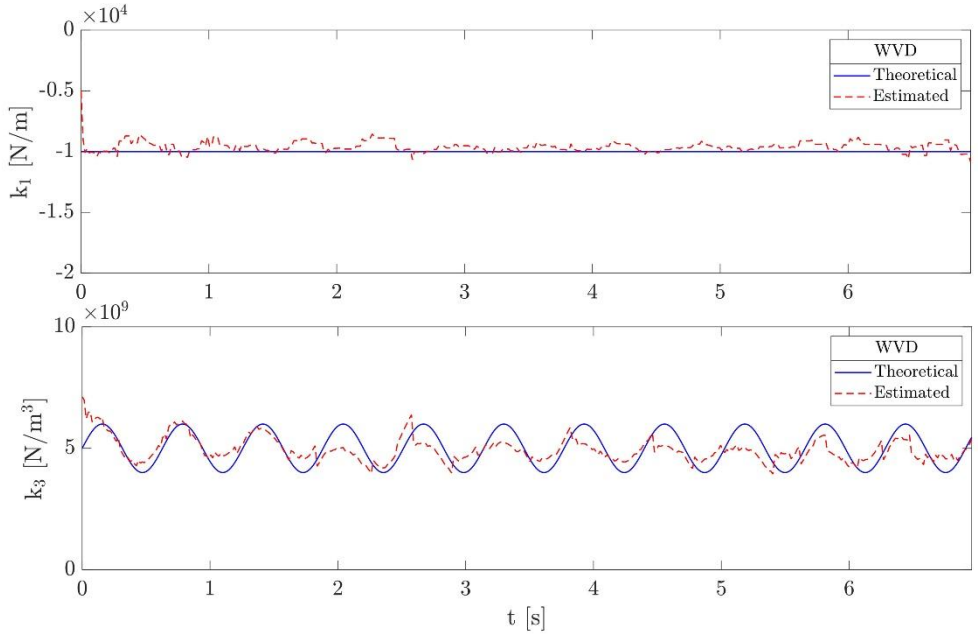

Figure 5.8. Estimated parameters k_1 and k_3 (time-varying) for a bistable oscillator using WVD.

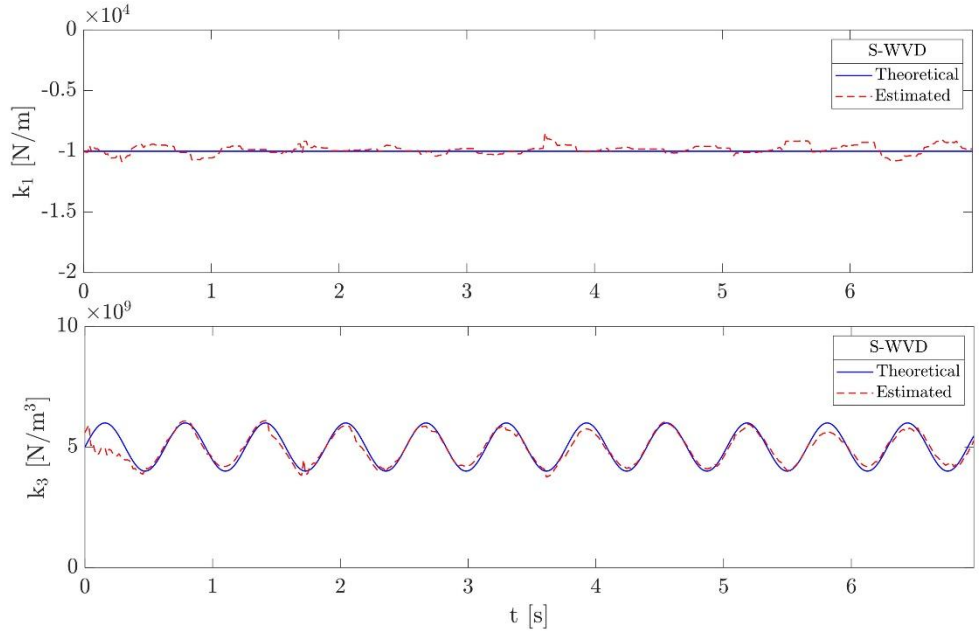

Figure 5.9. Estimated parameters k_1 and k_3 (time-varying) for a bistable oscillator using S-WVD.

By comparing Figure 5.8 and Figure 5.9 it is clear that the case of S-WVD estimation outperforms the WVD without smoothing window. Indeed, the estimation is able to follow the trend of the sinusoidal parameter. This is particularly valuable also for real applications. To prove these results, a further validation was carried out. In particular, the parameters estimated in Figure 5.8 and Figure 5.9 have been substituted to numerically simulate the response of the system by using Equation (5.13). The response in the two cases is reported in Figure 5.10.

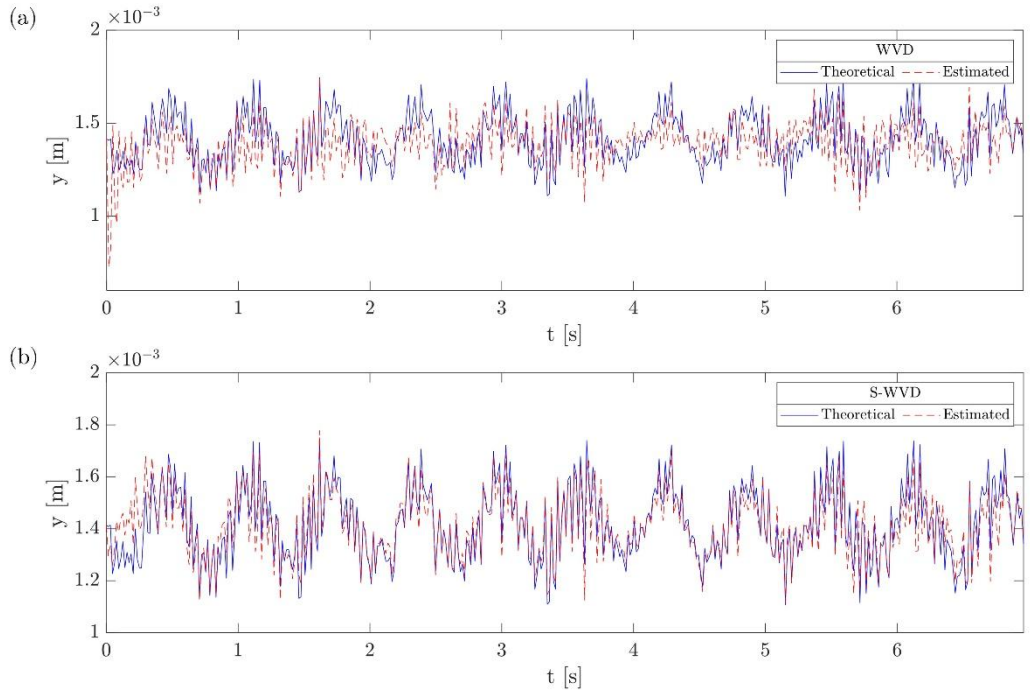

Figure 5.10. Theoretical and estimated response for (a) WVD and (b) S-WVD estimation.

5.3 Discussion and concluding remarks

Conversely to the case of time-invariant parameters, where the use of the WVD and S-WVD is almost interchangeable, these results confirm that in the case of even just one time-varying parameter, the S-WVD is more suitable for the estimation task, due to the fact it is alias-free. A quantification of this is possible by using the root mean squared error (RMSE) normalised by the mean value of the measured signal and expressed as percentage. In particular, the RMSE has been calculated as:

$$\text{RMSE} = \frac{\sqrt{\frac{1}{N}\sum_{n=1}^{N}\left(y_n - y_{Ess,n}\right)^2}}{\bar{y}} \tag{5.19}$$

with y_n and $y_{Ess,n}$ as the n-th component of the theoretical and estimated response, respectively, over a total number of samples N, and $\bar{y}$ as the mean value of the theoretical response y. The normalised RMSE for Benchmark #1, Benchmark #2, and Benchmark #3 are reported in Table 5.2.

Table 5.2. Normalised RMSE calculated on the displacements for the three benchmarks.

Benchmark	WVD	S-WVD
#1	0.42 %	0.31 %
#2	2.54 %	1.41 %
#3	7.29 %	4.03 %

In all cases, the S-WVD case outperforms the WVD. If the difference is almost negligible in Benchmark #1, it becomes more evident in the case of Benchmark #2, up to almost half the value of RMSE in the case of Benchmark #3, corresponding to the time-varying bistable Duffing. Nevertheless, both transforms give good results, especially given the inherent difficulty of estimating nonlinear parameters. This proves the effectiveness of the proposed procedure on all the benchmarks considered.

Part of the work described in this chapter has been published in a paper (Scussolini et al., 2025).

References

Belousov, R., Berger, F., Hudspeth, A.J., 2019. Volterra-series approach to stochastic nonlinear dynamics: The Duffing oscillator driven by white noise. Phys. Rev. E 99, 042204. https://doi.org/10.1103/PhysRevE.99.042204

Boashash, B., 1987. Theory, implementation and application of time-frequency signal analysis using the Wigner-Ville distribution.

Bonato, P., Ceravolo, R., Stefano, A.D., 1997. Time-Frequency and Ambiguity Function Approaches in Structural Identification. J. Eng. Mech. 123, 1260–1267. https://doi.org/10.1061/(ASCE)0733-9399(1997)123:12(1260)

Bonthron, M., Tubaldi, E., 2024. Dynamic Behavior of Bistable Shallow Arches: From Intrawell to Chaotic Motion. Journal of Applied Mechanics 91, 021010. https://doi.org/10.1115/1.4064208

Carmona, R., Hwang, W.-L., Torresani, B., 1998. Practical Time-Frequency Analysis: Gabor and wavelet transforms, with an implementation in S. Academic Press.

Choi, H.-I., Williams, W.J., 1989. Improved time-frequency representation of multicomponent signals using exponential kernels. IEEE Transactions on Acoustics, Speech, and Signal Processing 37, 862–871.

Cohen, L., 2002. Time-frequency distributions-a review. Proceedings of the IEEE 77, 941–981.

Feijoo, J.V., Worden, K., Garcia, P.M., Rivera, L.L., Rodriguez, N.J., Perez, A.P., 2010. Analysis of MDOF nonlinear systems using associated linear equations. Mechanical systems and signal processing 24, 2824–2843.

Feijoo, J.V., Worden, K., Stanway, R., 2004. System identification using associated linear equations. Mechanical Systems and Signal Processing 18, 431–455.

Flandrin, P., 1984. Some features of time-frequency representations of multicomponent signals, in: ICASSP'84. IEEE International Conference on Acoustics, Speech, and Signal Processing. IEEE, pp. 266–269.

Flandrin, P., Martin, W., 1997. The Wigner-Ville spectrum of nonstationary random signals. The Wigner Distribution—Theory and Applications in Signal Processing 211–267.

Harne, R.L., Wang, K.-W., 2017. Harnessing bistable structural dynamics: for vibration control, energy harvesting and sensing. John Wiley & Sons.

Ibrahim, R.A., Pandya, A., 1990. Functional-perturbational analysis of non-linear systems under random external and parametric excitations. Journal of sound and vibration 137, 443–455.

Janssen, A., 1997. Positivity and spread of bilinear time-frequency distributions. The Wigner Distribution, Elsevier, Amsterdam 1–58.

Kougioumtzoglou, I.A., Spanos, P.D., 2009. An approximate approach for nonlinear system response determination under evolutionary stochastic excitation. Current science 1203–1211.

Loughlin, P.J., 1992. Time-frequency energy density functions: Theory and synthesis. University of Washington.

Mecklenbräuker, W.F., Hlawatsch, F., 1997. The Wigner distribution-theory and applications in signal processing. Elsevier.

Morris, J.M., Wu, D., 1996. On alias-free formulations of discrete-time Cohen's class of distributions. IEEE transactions on signal processing 44, 1355–1364.

Nayfeh, A.H., 2000. Perturbation methods, Wiley classics library ed. ed, Wiley classics library. John Wiley & Sons, New York.

Nayfeh, A.H., Serhan, S.J., 1990. Response statistics of non-linear systems to combined deterministic and random excitations. International Journal of Non-Linear Mechanics 25, 493–509. https://doi.org/10.1016/0020-7462(90)90014-Z

Perkins, E., 2025. The Duffing adaptive oscillator. Nonlinear Dyn 113, 2987–3000. https://doi.org/10.1007/s11071-024-10417-0

Pinho, R., 2007. Nonlinear dynamic analysis of structures subjected to seismic action, in: Advanced Earthquake Engineering Analysis. Springer, pp. 63–89.

Rugh, W.J., 1981. Nonlinear system theory: the Volterra/Wiener approach, Johns Hopkins series in information sciences and systems. Johns Hopkins University Press, Baltimore.

Scussolini, L., Cavanni, V., Ceravolo, R., 2025. Volterra System Identification Using Wigner-Ville Representations, in: International Conference on Experimental Vibration Analysis for Civil Engineering Structures. Springer, pp. 281–290.

Stanković, L., Mandić, D., Daković, M., Brajović, M., 2018. Time-frequency decomposition of multivariate multicomponent signals. Signal Processing 142, 468–479.

Wu, Z., Harne, R.L., Wang, K.W., 2015. Excitation-Induced Stability in a Bistable Duffing Oscillator: Analysis and Experiments. Journal of Computational and Nonlinear Dynamics 10, 011016. https://doi.org/10.1115/1.4026974

Chapter 6

Experimental testing on nonlinear systems: probabilistic identification of bistable oscillators

In the previous chapters the identification of nonlinear and time-varying systems has been addressed from a theoretical and numerical point of view. However, the difficulty of performing, and above all interpreting, experimental tests on these systems is well known, especially in light of the many uncertainties that govern the problem. In this regard, the aim of this chapter is to introduce efficient approaches to experimental dynamic identification, both in the sense of test setup optimisation and probabilistic treatment of uncertainties. The experimental procedures will be validated on a bistable anti-seismic device, characterised by a complex response.

For the identification of nonlinear dynamical systems, an effective approach consists of decoupling the rate-dependent from the rate-independent component as two sequential separate steps (Liu et al., 2023; Rogers and Friis, 2022). In the presence of linear viscous damping, the rate-dependent contribution can be preliminarily identified with classical methods based on free-decay response (Ceravolo, 2004; Liu et al., 2023; Magalhães et al., 2010; Nogueira and Barbosa, 2024). This approach is applicable also to bistable oscillators (with possible generalisation to multiple ones) provided that low-amplitude intrawell oscillations are considered. Then, the main focus of the nonlinear identification task is on the rate-independent component, which characterises the stiffness restoring force governing the potential energy topology and the existence of multi-stable states.

While stiffness coefficients are generally assumed to be time-invariant in the case of bistable systems, this assumption appears restrictive in some real-world

cases, especially those involving energy absorption/dissipation (Zeng et al., 2025). Even though bistable systems are stationary around their equilibrium points, when subject to strong excitations, such as earthquakes, the activation of the snap-through mechanism leads to a markedly non-stationary response (Cheng et al., 2015; Hammond and White, 1996). As a result, the bistable dynamics in the interwell regime can be effectively described by time-varying parameters, at least for identification purposes. According to the previous chapters, an appealing approach is to assume the signal as a realisation of a process whose statistical properties, i.e., mean, variance, higher moments, change slowly over time, this allowing the parameters to be identified from short analysing windows, i.e. from time-frequency representations (Ceravolo, 2008; Mallat et al., 1998).

Another issue to address is the statistical variability of some characteristics and factors which, especially in bistable systems, can influence the dynamic behaviour and, therefore, the performance of the device (Fadel Miguel et al., 2025; Norenberg et al., 2023; Yang and Zhou, 2019). In this sense, a Bayesian framework allows model parameters to be treated as random variables and their probability distributions to be updated as new information becomes available (Beck and Katafygiotis, 1998; Huang et al., 2019).

It is known that, under nonlinear model uncertainty, Bayesian approaches outperform deterministic ones (Lye et al., 2023). Some contributions, which provide useful insights for this research, have focused on the problem of high uncertainty in parameter estimation, typical of nonlinear systems (Beck and Katafygiotis, 1998), including Markov chain Monte Carlo simulations (Green and Worden, 2015; Luengo et al., 2020; Schön et al., 2015) and, more generally, Bayesian inference (Ben Abdessalem et al., 2018; Huang et al., 2019; Worden and Hensman, 2012). In the task of identification of nonlinear time-varying parameters, one may combine these techniques with other methods suitable for an instantaneous implementation, such as Kalman filtering techniques (Ding et al., 2021; Erazo and Nagarajaiah, 2017), reinforcement learning (Ritto et al., 2023), and stochastic simulation-based approaches, e.g., particle filters (Jasra et al., 2012).

The need for a technique capable of capturing the instantaneous behaviour of highly nonlinear systems characterised by uncertainty in parameters, i.e. the bistable ones, is fundamental. This requirement is even more pressing when considering the possible use of these systems in seismic devices, namely the instantaneous dissipation and/or absorption, which is critical in real-world applications (Chen et al., 2023; Vakakis et al., 2022; Zuo and Zhu, 2022). For the purposes of this work, approximate Bayesian computation (ABC) (Csilléry et al., 2010) is combined with a time-frequency estimator in order to obtain an instantaneous probabilistic evaluation of the nonlinear parameters governing the bistable response and, consequently, of the instantaneous dissipated energy. This

technique has been verified on experimental recordings obtained by testing a 3D-printed cosine shaped beam bistable sample. Both the Bayesian and the intrinsically time-varying approaches, which are desirable for the nonlinear identification procedure of bistable systems, will be discussed in more detail in the following paragraphs.

6.1 A new bistable energy dissipation device

The type of energy dissipation devices experimentally investigated and identified in this work is designed to exploit bistable dynamics for passive seismic control. As stated in Chapter 5, in the case of bistable systems, two characteristic regimes of oscillations can be identified: (i) intrawell oscillations, around one of the two stable equilibrium points, and (ii) interwell oscillations, around the unstable equilibrium point. Consequently, the potential energy of bistable systems is referred to as double-well potential, whose shape dictates both the threshold for the activation of snap-through and the elevated velocities linked to interwell oscillations. Conceptually, the device can be described as a nonlinear extension of the tuned mass damper (TMD) (Pinkaew et al., 2003; Soong and Dargush, 1997), but, differently from classical TMDs, it does not operate as a traditional absorber, since its dissipation capabilities come from the high-velocity transitions during the interwell phase of oscillations rather than the viscous damping coefficient (Habib and Romeo, 2018; Parseh et al., 2015).

Bistable dynamics can be obtained by exploiting the unit cells of mechanical metamaterials, i.e., engineered materials whose nonlinear properties are determined by specific geometries rather than the constitutive material itself (Bertoldi et al., 2017; Dykstra et al., 2023; Zadpoor, 2016). An attractive typology of metamaterials is given by the ones characterised by a negative stiffness behaviour consisting of an increase in deformation resulting in a decrease in load (Zhang and Xu, 2015). The occurrence of negative stiffness behaviour is conveniently achieved by the snap-through phenomenon, linked to the bistable behaviour. An extensive literature review on negative stiffness mechanical metamaterials can be found in (Tan et al., 2024).

Curved beams, or cosine-shaped beams (CSB), and inclined beams, or V-shaped beams, can achieve a negative-stiffness behaviour due to their buckling instability property. Also, they are relatively simple to design and implement. In this research, a curved CSB geometry was selected given its greater energy trapping capacity compared to similar tilted configurations (Tan et al., 2022). A 3D representation of the device is reported in Figure 6.1.

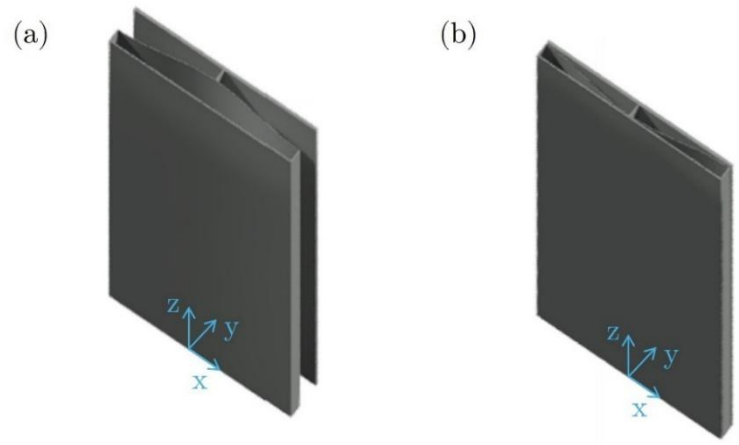

Figure 6.1. Bistable device for energy dissipation: (a) fist equilibrium position (open) and (b) second equilibrium position (closed).

The device architecture has two main features:

(i) a distributed mass attachment, where the inertial mass is spread across part of the host structure instead of being concentrated in a single point.

(ii) the nonlinear bistable mechanism achieved by the snap-through activation of the CSB unit cell.

The interaction between these two components ensures that seismic energy is efficiently transferred and dissipated through successive snap-through events. From the point of view of the system dynamics, it is clear that the critical parameter for the performance of the device is not so much the linear viscous damping itself, but rather the interwell transitions, which, thanks to the high velocities at which they occur, are responsible for the energy dissipation.

In this chapter, the formulation of the bistable dynamics in Equation (5.13) is modified to take into account the separation of the rate-dependent and the rate-independent component. The equation of motion of the bistable oscillator with mass m and viscous damping c reads:

$$\begin{cases} m\ddot{y} + f_{r,d}(\dot{y}) + f_{r,s}(y) = u(t) \\ f_{r,d} = c\dot{y} \\ f_{r,s} = \sum_{l=0}^{L} k_l y^l \end{cases} \tag{6.1}$$

where y, $\dot{y}$, and $\ddot{y}$ are the displacement, velocity, and acceleration of the system and $u(t)$ is the generic external excitation. The restoring force, $f_{r,s}$, is described by the system stiffness coefficients k_l, and the maximum polynomial order L. Conversely, $f_{r,d}$ is the rate-dependent contribution, in the form of linear

viscous damping. If the stiffness restoring force $f_{r,s}$ is an odd function of y, i.e., it shows a symmetric potential, then all the even coefficients vanish. The governing equation of motion for the majority of bistable systems is a direct consequence of Equation (6.1) truncated up to the third order. In such a case, the stiffness restoring force writes:

$$f_{r,s} = k_1 y + k_3 y^3 \tag{6.2}$$

with $k_1 < 0$, differently from the classical Duffing oscillator case. From a modelling perspective, under the assumption of negligible mass, the two sides of the CSB, employed in the device as bistable metalayer, are schematised as two inclined springs, each with stiffness k and initial length l_0, attached to a vibrating mass m. Figure 6.2 reports a schematic of the CSB and the corresponding SDoF bistable oscillator, while the typical shape of the potential energy and force-displacement profile is shown in Figure 6.3. It is worth noting that this configuration forces the linear stiffness k_1 to be negative, that is the fundamental condition for achieving bistability, as already explained in Chapter 5.

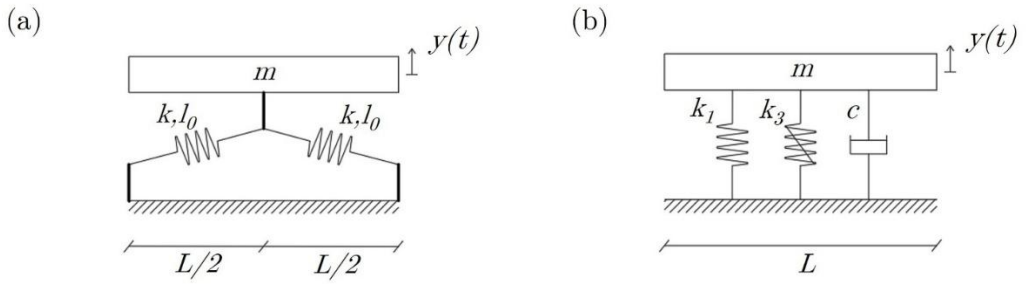

Figure 6.2. Schematic of the (a) CSB and the corresponding (b) SDoF bistable oscillator.

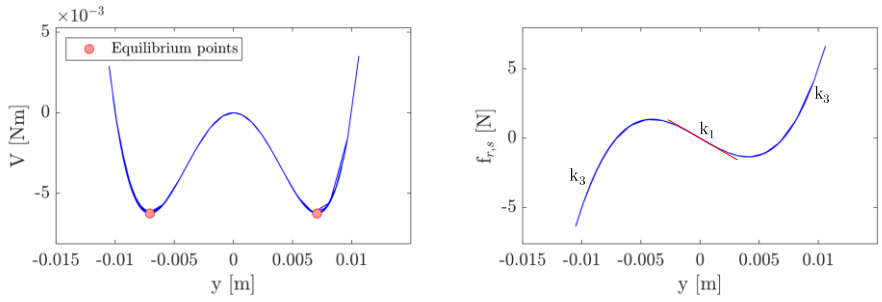

Figure 6.3. Potential energy and force-displacement profile of a bistable oscillator with $m = 1\ kg$, $k_1 = -5e^2\ N/m$, $k_3 = 1e^7\ N/m^3$, and $c = 10\ Ns/m$ for a white noise input with null mean and standard deviation equal to 2.

Finally, it should be noted that this simple SDoF formulation, which only considers the mass displacement in the snap-through direction, does not account for possible rotations of the distributed mass attachment. It is worth noting that parasitic rotations can be observed, and possibly controlled, during experiments on the real device.

6.2 Bayesian instantaneous identification of nonlinear time-varying parameters

6.2.1 Bayesian inference for nonlinear system identification

If a dynamic model of input $u(t)$ and output $y(t)$ is introduced, one may infer a mathematical model describing their relationship (i.e., identification task). In practice, one can refer to a set of data $\widetilde{D} = \{(u_i, y_i), i = 1, \dots, Z\}$, where (u_i, y_i) represents the set of sampled input and output at the i-th sample. By considering the parameter vector $\mathbf{p} = \{p_1, p_2, \dots, p_{N_{par}}\}$, where N_{par} is the total number of parameters describing the dynamic model, a probabilistic estimate of the parameter vector $\mathbf{p}$ may be given by (Green and Worden, 2015):

$$\mathbf{p} \sim P\left(\mathbf{p}\middle|\widetilde{D}, \mathcal{M}\right) \tag{6.3}$$

where $\mathcal{M}$ is nothing else than the chosen model. A classical approach to estimate the probability function P is given by the Bayes one, that basically includes estimating a posterior distribution from a priori probability function of the parameters $\mathbf{p}$ considering the observed data $\widetilde{D}$. The objective is therefore to find a good approximation, and also computationally affordable, of the posterior distribution:

$$P\left(\mathbf{p}\middle|\widetilde{D}, \mathcal{M}\right) \propto P\left(\widetilde{D}\middle|\mathbf{p}, \mathcal{M}\right) P(\mathbf{p}|\mathcal{M}) \tag{6.4}$$

where the quantities $P\left(\widetilde{D}\middle|\mathbf{p}, \mathcal{M}\right)$ and $P(\mathbf{p}|\mathcal{M})$ represent the likelihood of the observed data $\widetilde{D}$ for a given parameter vector $\mathbf{p}$ and the prior distribution over parameter space, respectively. In the ABC algorithm, a good approximation may be given by (Abdessalem et al., 2018; Chiachio et al., 2014; Worden and Cross, 2025):

$$P\left(\mathbf{p}\middle|\widetilde{D}, \mathcal{M}\right) \approx P_{\varepsilon}\left(\mathbf{p}\middle|\widetilde{D}, \mathcal{M}\right) = \int_{D} f\left(\widetilde{D}\middle|\mathbf{p}, \mathcal{M}\right) \mathbf{I}\left(\Delta\left(D, \widetilde{D}\right)\right) P(\mathbf{p}|\mathcal{M}) dD \tag{6.5}$$

with $\mathbf{I}\left(\Delta\left(D, \widetilde{D}\right)\right)$ as indicator function depending on the distance between the observed and simulated data $\widetilde{D}$ and D. The latter can assume the following values:

$$\mathbf{I}\left(\Delta\left(D, \widetilde{D}\right)\right) = \begin{cases} 1 & if \Delta\left(D, \widetilde{D}\right) \leq \varepsilon \\ 0 & if \Delta\left(D, \widetilde{D}\right) > \varepsilon \end{cases} \tag{6.6}$$

From Equation (6.6) it is clear that the ABC algorithm has the main assumption that the distance between the observed and simulated data should be lower than a certain threshold ε. This threshold can be defined by the user,

depending on the identification task and on the observed data $\widetilde{D}$. The main advantage of using ABC is that for nonlinear models, it might be difficult to formulate an analytical expression of the prior distribution, relying on restrictive assumptions. This step is bypassed if ABC is employed (Huang et al., 2019).

6.2.2 Proposed combined Bayesian time-frequency estimator

Chapter 3 showed that when the system admits a spectral localisation of its components, a compelling approach to obtain an instantaneous estimate of the parameter vector $\mathbf{p}$ is using time-frequency representations (Ceravolo, 2008). For a generic signal s, its time-frequency transform $\mathbf{T}_s(t,f)$ allows a simultaneous representation of the signal in the joint time-frequency domain (t,f). In particular, if y is the response of a generic dynamical system, possibly described by the parameter vector $\mathbf{p}$, one may minimise the following error function in order to obtain an optimal parameter vector estimate $\mathbf{p}_{\text{opt}}$:

$$\begin{gathered} J(\mathbf{p}) = ||\mathbf{T}_y(t,f;\mathbf{p}) - \widetilde{\mathbf{T}}_y(t,f)||_2^2 \\ \mathbf{p}_{\text{opt}} = \arg\left[\min_{\forall \mathbf{p}} J(\mathbf{p})\right] \end{gathered} \tag{6.7}$$

with $\widetilde{\mathbf{T}}_y$ and $\mathbf{T}_y$ as the observed and simulated time-frequency transforms of the response y. It was shown in Chapter 3 that Equation (6.7) aims to minimise the energy between the two transforms. To preserve the instantaneous energy, one may adapt Equation (6.7) to be minimised instant by instant. Therefore, if the excitation is known, for a generic time instant $\bar{t}$ one has:

$$\begin{gathered} J(\bar{t},\mathbf{p}) = ||\mathbf{T}_y(t,f;\mathbf{p}) - \widetilde{\mathbf{T}}_y(t,f)||_{2,t=\bar{t}}^2 \\ \mathbf{p}_{\text{opt}}(\bar{t}) = \arg\left[\min_{\forall \mathbf{p}} J(\bar{t},\mathbf{p})\right] \end{gathered} \tag{6.8}$$

This is nothing more than the time-frequency approach already adopted in Chapter 4 and Chapter 5. The choice of the time-frequency transform depends on several factors, such as the possibility of an online implementation, largely discussed in (Ceravolo, 2008). The spectrogram, which is nothing else than the squared modulus of the STFT, proved to be effective in the identification of nonlinear systems, also in presence of hysteresis and degradation (Ceravolo et al., 2013). In this work, a spectrogram has been chosen as time-frequency representation. BY introducing the discrete frequency m and the discrete time n, a possible form of Equation (6.8) writes:

$$J(n,\mathbf{p}) = \frac{\sqrt{\frac{1}{M}\sum_{m=0}^{M-1}\left|\mathrm{SPEC}_y^{\gamma}(n,m;\mathbf{p}) - \widetilde{\mathrm{SPEC}}_y^{\gamma}(n,m)\right|^2}}{\sqrt{\frac{1}{M}\sum_{m=0}^{M-1}\left|\widetilde{\mathrm{SPEC}}_y^{\gamma}(n,m)\right|^2}} \tag{6.9}$$

where SPEC_y^{γ} and $\widetilde{\mathrm{SPEC}}_y^{\gamma}$ are the spectrogram of the simulated and measured response signal y analysed with a running window γ (the dependence on time of the running window has been omitted for brevity's sake) at the time instant $n\Delta t$ and frequency $m\Delta f$.

The objective function J reported in Equation (6.9) has traditionally been solved using least squares or optimisation algorithms (Ceravolo et al., 2013). In this work, an extension of its solution that accounts for uncertainties by integrating probabilistic approaches is proposed. The main issue is therefore to obtain an instantaneous distribution of the parameter vector $\mathbf{p}$. More specifically, by considering the probabilistic formulation reported in Equations (6.4)-(6.6), the deterministic optimisation problem of Equation (6.9) can be reformulated in terms of the posterior distribution of the parameter vector. Instead of identifying a deterministic optimal parameter vector, $\mathbf{p}_{\mathrm{opt}}$ at the time instant $\bar{t} = n\Delta t$ writes:

$$\mathbf{p}_{\mathrm{opt}}(\bar{t} = n\Delta t) = P_{\varepsilon}\left(\mathbf{p}\middle|\widetilde{D},\mathcal{M}\right)_{\bar{t}=n\Delta t} \tag{6.10}$$

where $P_{\varepsilon}\left(\mathbf{p}\middle|\widetilde{D},\mathcal{M}\right)_{\bar{t}=n\Delta t}$ is nothing more than the posterior distribution calculated with ABC method for a certain threshold ε at the time instant $\bar{t} = n\Delta t$.

6.2.3 Numerical implementation of the estimator

In this section the numerical implementation of the ABC time-frequency estimator is reported. Since it is not possible to obtain a closed solution of Equation (6.10), a kernel density estimation (KDE) has been employed to obtain the posterior distribution of the optimal parameters $\mathbf{p}_{\mathrm{opt}}$ for each time instant. For any real values of $\mathbf{p}$, the KDE (Peter D., 1985) is given by:

$$P_{\varepsilon}\left(\mathbf{p}\middle|\widetilde{D},\mathcal{M}\right)_{\bar{t}=n\Delta t} \cong \mathrm{KDE}_{\mathrm{post}}(\mathbf{p}) = \frac{1}{N_s h}\sum_{j=0}^{N_s-1} K\left(\frac{\mathbf{p}-\mathbf{p}_m}{h}\right) \tag{6.11}$$

where $\mathbf{p}_1, \mathbf{p}_2, \ldots, \mathbf{p}_m$ are random sample vectors from un unknown distribution, $K(\cdot)$ is the kernel smoothing function, N_s is the total number of samples, and h is the bandwidth of the smoothing window. Algorithm 1 reports the pseudocode for the implementation of Equation (6.11). In this work, Algorithm 1 has been implemented in Matlab®. The bandwidth h has been calculated using the normal approximation method. The threshold ε has been chosen to be a vector composed of decreasing values for the objective function

$\mathbf{J}_{thresh}$, in order to refine the search at each optimisation cycle k. The optimisation has been carried out for a total number of cycles K_{opt} as required from the ABC methods. The parameters have been initially chosen by using a Latin hypercube sampling (LHS) between the minimum and maximum parameter vector $\mathbf{p}_{min}$ and $\mathbf{p}_{max}$.

Algorithm 2: ABC time-frequency estimator.

1:	Threshold objective function vector $\mathbf{J}_{thresh}$	
2:	for $n = 1{:}\,N$	
3:	for $k = 1{:}\,K_{opt}$	
4:	$\mathbf{p} \sim \mathrm{LHS}(\mathbf{p}_{min}, \mathbf{p}_{max})$	*Generate N_s samples*
5:	for $j = 1{:}\,N_s$	
6:	Obtain discrete response $y_j[k;\mathbf{p}]$	
7:	$X_j(k,n) = \Sigma\, y_j[n]w[n-mR]e^{-\frac{i2\pi kn}{L}}$	*Compute STFT at frame n*
8:	$S_j(k,n) = \lvert X_j(k,n)\rvert^2$	*Compute spectrogram at frame n*
9:	$J_j(k,n;\mathbf{p}) = \dfrac{\sqrt{\frac{1}{M}\sum_{m=0}^{M-1}\left\lvert \mathrm{SPEC}_y^{\gamma}(n,m;\mathbf{p}) - \widehat{\mathrm{SPEC}}_y^{\gamma}(n,m)\right\rvert^2}}{\sqrt{\frac{1}{M}\sum_{m=0}^{M-1}\left\lvert \widehat{\mathrm{SPEC}}_y^{\gamma}(n,m)\right\rvert^2}}$	*Objective function at frame n*
10:	$J(k,n;\mathbf{p}) = [J(k,n;\mathbf{p}),\ J_j(k,n;\mathbf{p})]$	
11:	end	
12:	$J_{tot}(k,n;\mathbf{p}) = [J_{tot}(k,n;\mathbf{p}),\quad J(k,n;\mathbf{p})]$	*Thresholding*
13:	if $J_{tot}(k,n;\mathbf{p}) < J_{thresh}(k)$	
14:	$\mathrm{KDE}_{\mathrm{post}}(\mathbf{p}) = \dfrac{1}{N_s h}\sum_{j=0}^{N_s-1} K\left(\dfrac{\mathbf{p}-\mathbf{p}_m}{h}\right)$	*Calculate posterior KDE*
15:	end	
16	end	
17:	end	

6.3 Experimental testing campaign

6.3.1 Sample design and construction

The first step for setting up the experiments consisted of the design and fabrication of specimens, able to describe the bistable dynamics. The Bambu Lab X1 Carbon printer (https://bambulab.com/en/x1) was used for this purpose, and the material selected for printing was PLA Basic (https://files.bbystatic.com/), a common thermoplastic polyester, due to its due to its ease of processing and relatively low cost (Vorkapić et al., 2025). Also, PLA Basic is formulated for high-speed printing, readily supporting print speeds of approximately 250–300

mm/s while exhibiting enhanced toughness and improved interlayer adhesion. Its elastic modulus and density are equal to $E_{PLA} = 2580 \pm 220$ MPa and $\rho_{PLA} = 1240\ \mathrm{kg/m^3}$. However, it is important to highlight that the actual 3D printing mechanical model performance can be influenced from several factors, including printers, printing conditions, printing models, printing parameters (e.g., infill density), as recently reported in (Ambati and Ambatipudi, 2022).The fabrication of the sample is reported in Figure 6.4. The sample measures are reported in Table 6.1.

Table 6.1. Geometrical values of the 3D-printed CSB.

h [m]	t [m]	L [m]	m [kg]
5×10^{-3}	0.5×10^{-3}	9×10^{-2}	47×10^{-3}

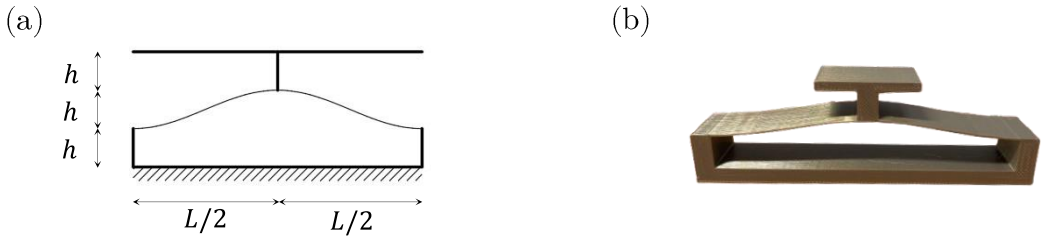

Figure 6.4. From schematisation to fabrication: (a) drawing of the CSB and (b) 3D-printed sample.

The fabricated sample with the attached mass is reported in Figure 6.5. In order to simulate the bistable behaviour, the sample was designed to be mechanically clamped in a steel support. The support as well its geometrical dimensions are reported in Figure 6.6.

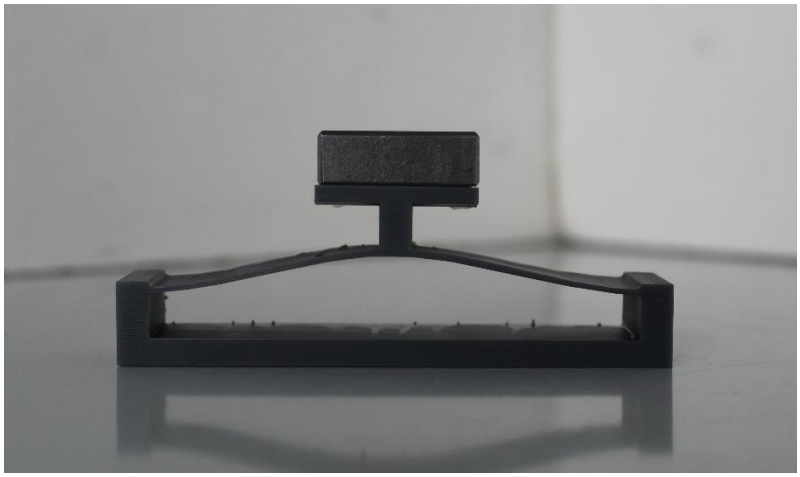

Figure 6.5. Bistable sample with attached mass.

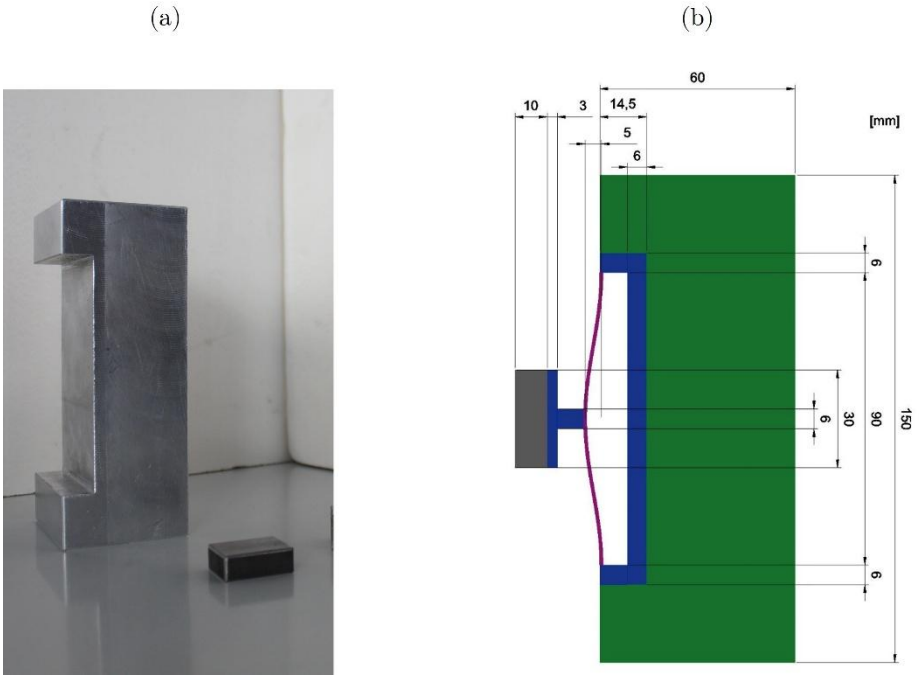

Figure 6.6. (a) Fabrication and (b) schematic of the support (dimension in millimetres).

6.3.2 Prototype testing machine description

The prototype testing machine is shown in Figure 6.7 and consists of an electromagnetic actuation system and a laser measurement chain.

Figure 6.7. Prototype testing machine.

The laser measurement system is composed by HeNe gas laser (https://www.thorlabs.com) that features a fluctuating output beam polarisation of 0.48 mm in diameter and with a noise RMSE lower than 1.0%. The laser beam is first focused by a converging cylindrical rod-lens (ϕ = 10 mm) to make a vertical

flat light beam, which is subsequently redirected by two mirrors (ϕ = 25 mm) at 45° toward a convergent lens (50 × 50 × 5 mm), focusing the flat beam on a linear position-sensitive detector. The light pattern is reported in Figure 6.8.

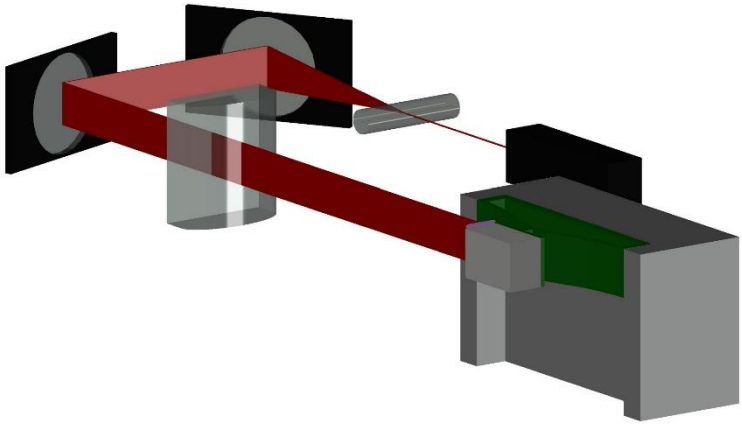

Figure 6.8. Schematic of the prototype testing setup with the light pattern in red.

The displacement is measured using 12 mm long position-sensitive detector, which is placed horizontally on the vibrating mass, and detects the position at which the light beam hits the sensitive area, enabling high-precision motion tracking, see Figure 6.9(a). When a light spot strikes the position-sensitive detector, it generates an electric charge proportional to the light intensity at the point of incidence. This charge flows as photocurrent through the resistive layer and is extracted from the output electrodes. The current is divided between the electrodes in inverse proportion to the distance from the incident point, allowing the position to be determined.

However, the calculated position typically exhibits slight deviations from the actual light incidence point. This discrepancy is known as *position detection error*, which is typically within ±20 μm, with a maximum of ±60 μm. The *position resolution*, defined as the minimum detectable displacement of the light spot on the sensor photosensitive area, is determined by the noise components in the output current when positional changes are infinitesimally small. The noise current originates from dark current, that is typically 0.1 nA and at maximum 2 nA. Considering the thickness of the light blade, the linearity of the sensor, and the noise generated by the dark current of the position-sensitive detector and the interface electronics, it is possible to conclude that the uncertainty on the calculated position is throughout lower than 50 μm.

On the other hand, the actuation system, mechanically connected to the specimen via a cylindrical plexiglass beam with a diameter of 10 mm, constraints the system against rotation and thus prevents the activation of rotational vibration modes. Under these conditions, the response is dominated by the SDoF oscillator

dynamics. The length of the plexiglass rod is specifically chosen to minimise the magnetic attraction between the steel vibrating mass and the permanent magnets. The actuator itself consists of a cardboard substrate with a copper coil on top. The copper wire has a diameter of 1 mm, and 20 turns for each side show resistance of 0.2 Ω, see Figure 6.9(b).

Initially, tracks were added to maintain the position of the actuator. However, due to high friction, it was decided to remove them and support the actuator with rollers. Motion is induced by the interaction between the coil and the magnetic field generated by two permanent magnets. A representation of the magnetic circuit, easily confined within the circuit, is given in Figure 6.9(b). The extra-strong neodymium (NdFeB) rectangular bar magnets have dimensions of 30 × 10 × 4 mm and a magnetic flux density of 1 T.

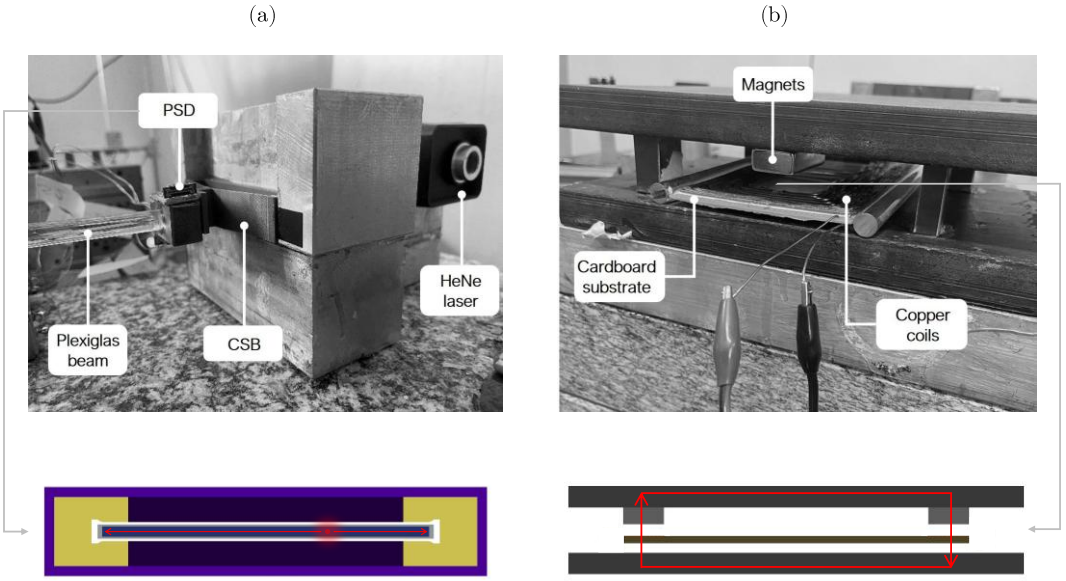

Figure 6.9. Significant components in the prototype machine: (a) positioning of position-sensitive detector (in the figure indicated as PSD for brevity's sake) and (b) actuator.

The apparatus can be used for both free-decay and forced tests. Indeed, the input signal is generated by the function generator embedded in the oscilloscope and is delivered to the actuator through a 20 A current amplifier. Both systems are anchored on a solid granite base measuring 600 × 600 × 145 mm to ensure stability and vibration isolation.

6.3.3 Nonlinear data gathering

The prototype testing machine described above has three main advantages for the nonlinear data gathering in the case of bistable systems, which can be summarised as follows:

(i) First, it allows the direct measurement of displacement. In bistable behaviour, displacements are the key variables. Measuring

accelerations directly would lead to imprecise motion due to numerical integration errors, whereas accelerations can be reliably obtained from displacement data through differentiation.

(ii) Electromagnetic actuators, exerting lower forces than mechanical ones, introduce less interference during jump-induced instabilities, allowing more precise control of the measured quantities.

(iii) The setup is highly cost-effective and reproducible using lasers, lens, oscilloscopes, and position-sensitive detector sensors.

Figure 6.10 represents the steps carried out for the recording of the displacements in the experimental testing. First, the input shape is defined in the control module through the function generator. Then, an electro-magnetic field is created through the system of magnets as described above and directly implies the force on the bistable 3D printed sample. Nonlinear displacements are then recorded through the laser-lenses system.

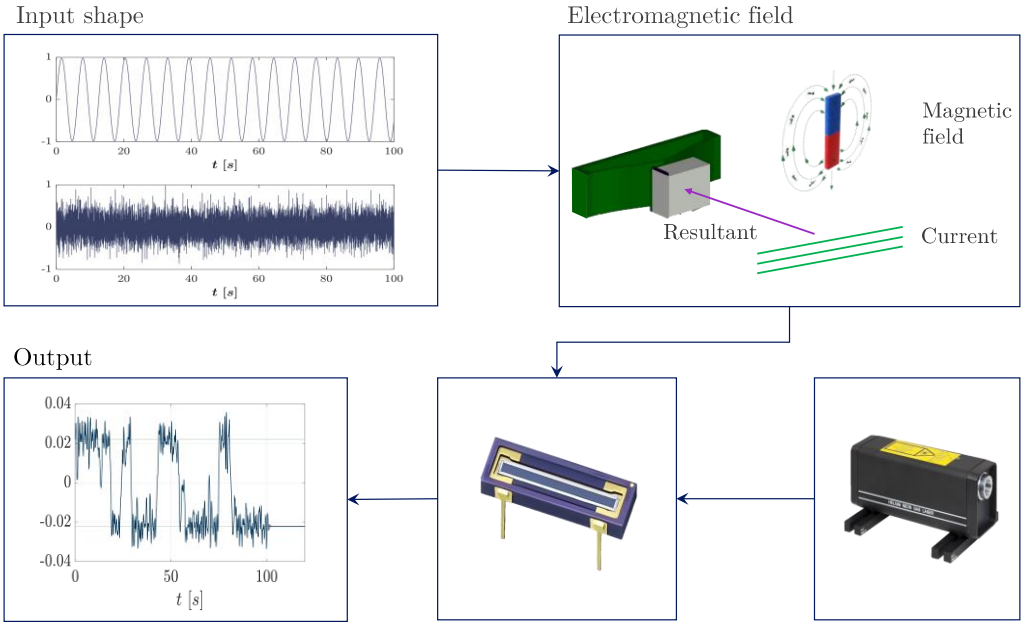

Figure 6.10. Workflow of the nonlinear data gathering.

6.4 Identification results

6.4.1 Rate-dependent component

The first step was to identify the rate-dependent component of the response, composed by the viscous, or viscous equivalent, damping. This choice was made also due to the fact that damping represents one of the parameters with higher uncertainty in experimental identification. Indeed, the assumption of linear viscous damping may not be fully verified. Furthermore, it should be noted that,

even under ideal conditions, identification algorithms can be quite inaccurate; for example, in output-only identification techniques, errors of 20% are common, sometimes even higher depending on the technique used and the stationary conditions (Ceravolo and Abbiati, 2013). When the bistable system oscillates in intrawell regime, its dynamic parameters can be considered slowly time-varying, and therefore one may consider exploiting the free decay oscillations in order to estimate the instantaneous frequency, and, consequently, instantaneous relative damping. To this aim, the FREEVIB method (Feldman, 2014, 1997), as described in Chapter 2, has been employed on the experimental free decay response of the system in one of the two stable positions, after an impulse excitation. The free decay response as well as the input which generated it are reported in Figure 6.11.

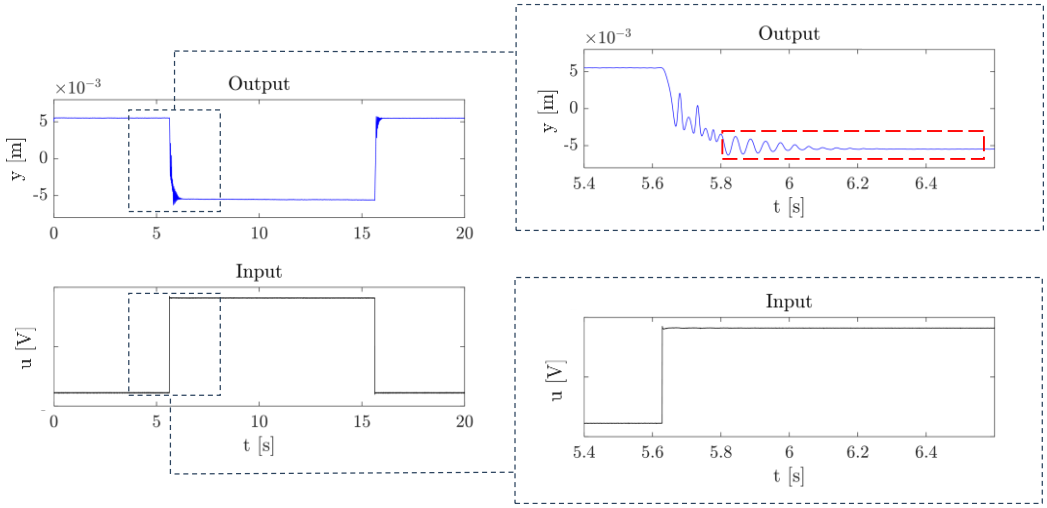

Figure 6.11. Free decay response: input and output.

The instantaneous frequency has been obtained directly from the analytic signal formulation, as described for classical applications of the FREEVIB method. Conversely, the instantaneous damping ratio has been obtained by the rate-dependent component $f_{r,d}$, provided by FREEVIB, through a classical least-square fitting. For theory on this matter, one may refer to (Worden and Tomlinson, 2019). The problem has been solved using the *lsqlin* algorithm in Matlab®. The instantaneous frequency and damping identification results are reported in Figure 6.12. As can be observed, both the instantaneous frequency and damping ratio show small oscillations in time. This can be attributed to the nonlinear nature, at least up to certain limits, of the intrawell oscillations, corresponding to the case of a classical Duffing oscillator, which may present multiple components, small in amplitude but high in frequency, besides the principal ones. As a consequence, all the instantaneous functions extracted using Hilbert transform based methods can be classified as fast oscillating functions (Feldman and Braun, 2017). In order to highlight the trend of estimation, a third-order polynomial fitting has been carried out for both the instantaneous frequency and damping ratio. As can be observed, for fairly small values of amplitude, the instantaneous damping estimate tends to stabilise to a value of 1.9%.

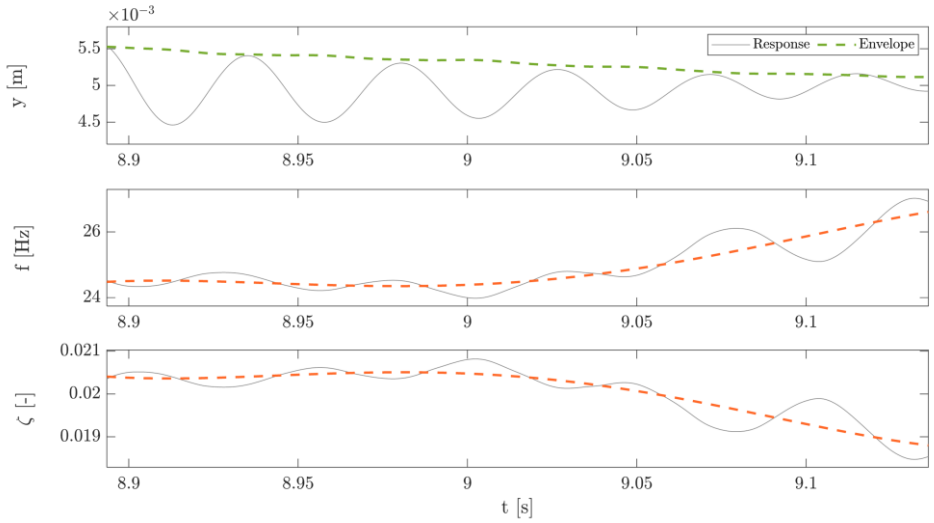

Figure 6.12. Instantaneous frequency and damping identification using Hilbert transform (FREEVIB method). For what concerns f and ζ, the dashed orange line represents their polynomial trend, while their instantaneous estimated value is represented by the continuous light grey line.

One of the advantages of using this method is the possibility to obtain a rough estimate of k_1 and k_3 through a least-square fitting starting from the rate-independent component $f_{r,s}$. This allowed the definition of the order of magnitude of parameters, exploited in the next sections to define the boundaries for the more refined time-frequency probabilistic identification task. In particular, the values estimated from FREEVIB are $k_1 = -1.1 \times 10^3$ N/m and $k_3 = 3.6 \times 10^7$ N/m^3.

6.4.2 Rate-independent component

For what concerns the rate independent components, the identification has been carried out considering as model assumption a perfectly elastic behaviour and using the probabilistic time-frequency method as implemented in Algorithm 2 for two different types of excitations: white noise and earthquake loading. This is justified by the fact of verifying the device effectiveness under earthquake excitation rather than ambient vibrations.

White-noise excitation

First, a white noise input with null mean was considered as external excitation $u(t)$. In order to obtain the interwell response, the standard deviation of the white noise was scaled to 5 V by means of the acquisition system oscilloscope. The acquired experimental signals were pre-processed and filtered using a low-pass Butterworth filter of order 2. The output, used as observed data, $\widetilde{D}$, and the input are reported in Figure 6.13 for reference. For the spectrogram calculation an Hanning analysis window, γ (time length: 0.5 s; 90% overlap), was used.

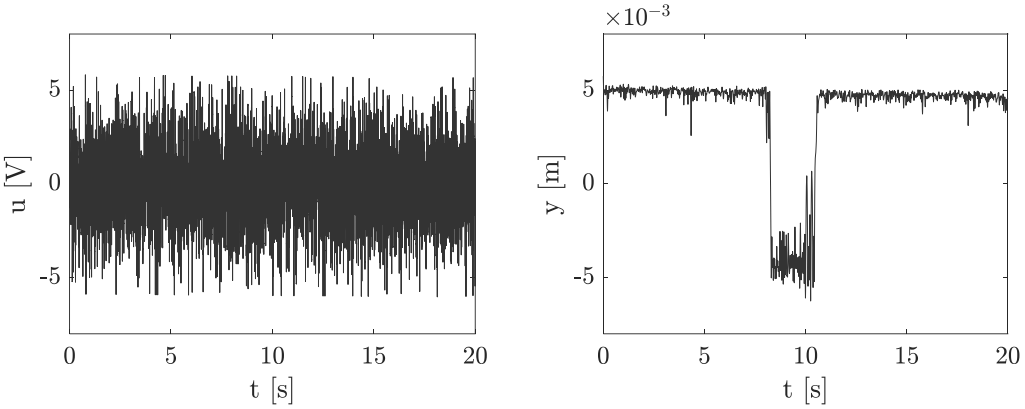

Figure 6.13. Input white noise and corresponding displacement response.

The identification was then carried out using the experimental signals depicted in Figure 6.13. In particular, the values reported in Table 6.2 were used for the estimation procedure. The results are reported in Figure 6.14.

Table 6.2. Values of the parameters used for the identification procedure under white noise.

Parameter	Initial value	Lower boundary	Upper boundary
m [kg]	47×10^{-3}	Fixed	Fixed
ζ [−]	1.9×10^{-2}	Fixed	Fixed
k_1 [N/m]	-1.1×10^{3}	-2.2×10^{3}	0
k_3 [N/m^3]	3.6×10^{7}	0	9.0×10^{7}

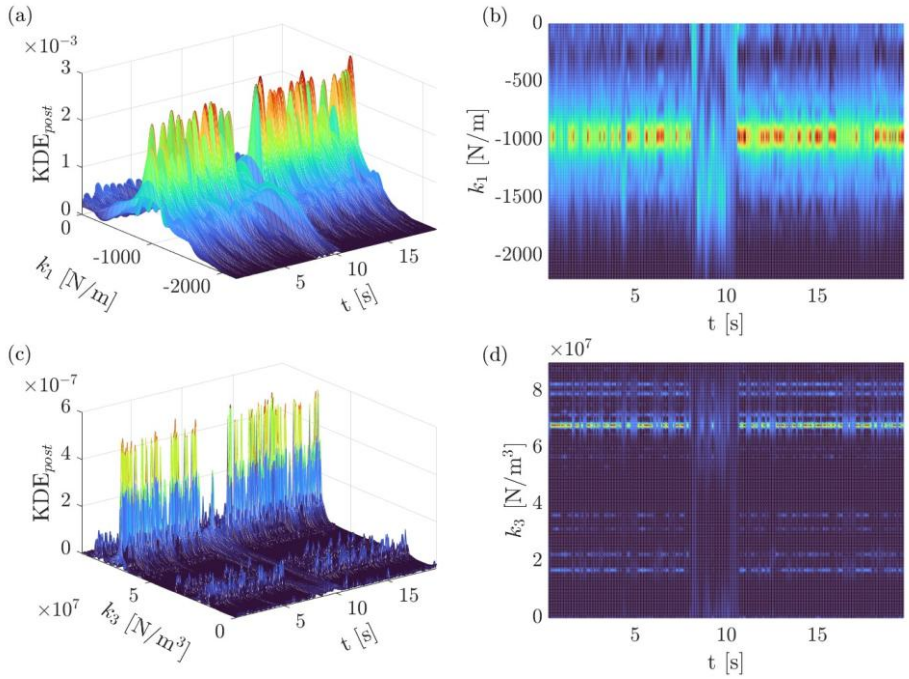

Figure 6.14. Identification results under white noise: 3D view of the posterior kernel density estimated for k_1 (a) and k_3 (c), and top view of the tracking of the mode during time of k_1 (b) and k_3 (d).

Figure 6.14 clearly shows the goodness of the procedure for experimental signals under white noise vibration. In particular, the parameter k_1 has a mode, i.e., the most frequent values in a distribution, of nearly -1×10^3 N/m for every time instant considered, leading to a confirmation of what already achieved with the FREEVIB procedure. On the other hand, the parameter k_3, governing the intrawell oscillation, showed a higher value with respect to the one used for the initialisation of the procedure, with a mode of 6.7×10^7 N/m^3. This discrepancy is consistent with the excitation level selected for the experiments, which was calibrated to activate snap-through between the two stable equilibrium points. Indeed, in the interwell regime, the response is primarily controlled by the negative linear stiffness term k_1, whereas the positive cubic stiffness k_3 mainly affects the local curvature of the potential within each well. A dispersion of both parameters can be observed in Figure 6.14(b)-(d) during snap-through events, where the response is markedly non-stationary. Nevertheless, the proposed approach demonstrates robustness, especially considering the intrinsic difficulty of identifying nonlinear parameters in non-stationary systems.

Earthquake loading

The second identification task involved the case of the system under earthquake excitation. The Aquila earthquake (https://www.ont.ingv.it/) scaled at 5 V was chosen as input excitation. Again, the acquired experimental signals were pre-processed and as in the case of white noise excitation. The earthquake as well as the output response of the system are reported in Figure 6.15.

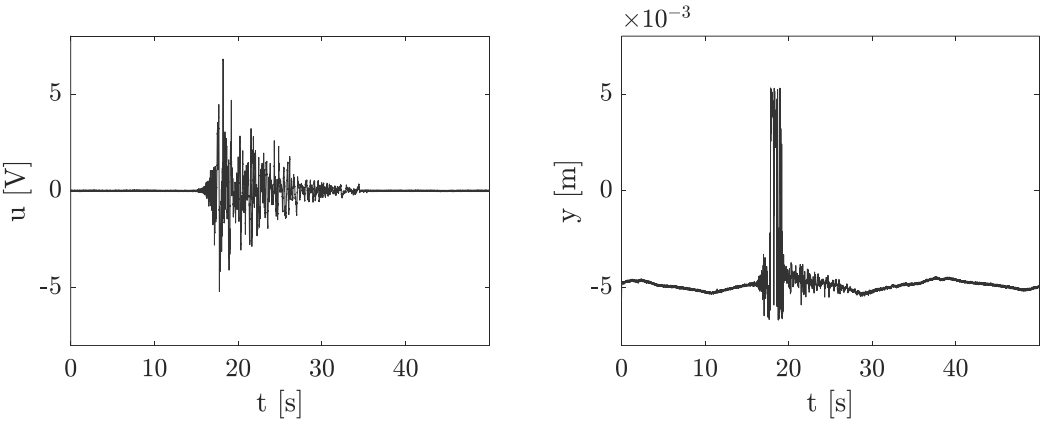

Figure 6.15. Input earthquake and corresponding displacement response.

Figure 6.16 shows the estimation results. The values used for the identification are reported in Table 6.3.

Table 6.3. Values of the parameters used for the identification procedure under seismic excitation.

Parameter	Initial value	Lower boundary	Upper boundary
m [kg]	47×10^{-3}	Fixed	Fixed
ζ [−]	1.9×10^{-2}	Fixed	Fixed
k_1 [N/m]	-1.1×10^{3}	-8.2×10^{3}	0
k_3 [N/m^3]	3.6×10^{7}	0	2.6×10^{8}

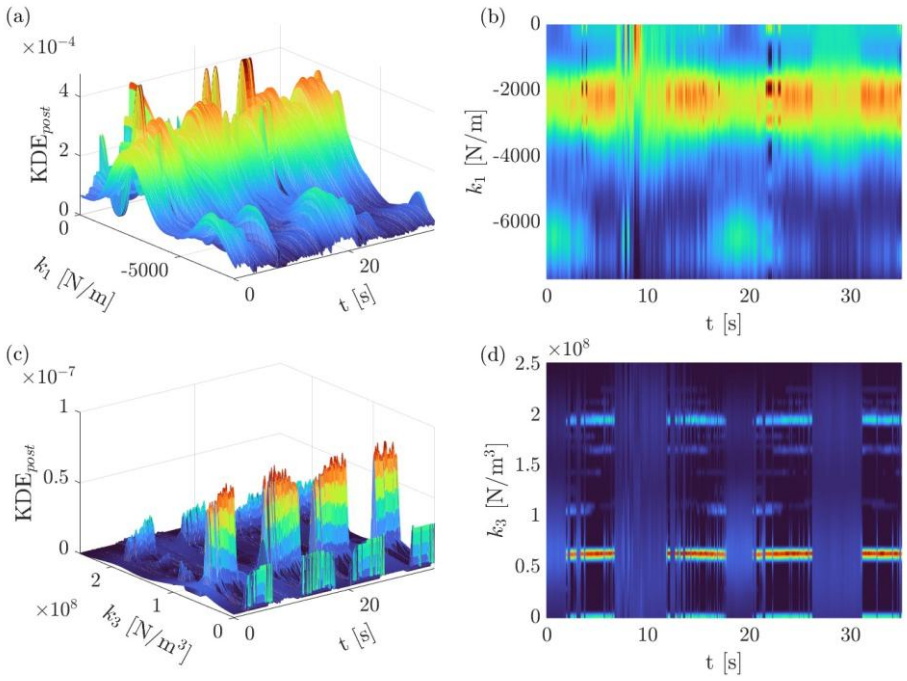

Figure 6.16. Identification results under seismic excitation: 3D view of the posterior kernel density estimated for k_1 (a) and k_3 (c), and top view of the tracking of the mode during time of k_1 (b) and k_3 (d).

Again, both the negative linear stiffness k_1 and the positive cubic stiffness k_3 are accurately identified under seismic excitation. The estimate of the negative linear stiffness k_1 appears significantly more stable than that of the positive cubic stiffness k_3, further reflecting the predominant role of k_1 in governing the interwell response. A comparison between Figure 6.14 and Figure 6.16 reveals that the magnitude of the negative linear stiffness k_1 identified under seismic excitation, with a mode value of -2.1×10^3, is approximately twice as large as the corresponding estimate obtained under white noise, with a mode of -1×10^3. This discrepancy reflects the influence of the excitation characteristics on the bistable mechanism. Of particular interest for this research, in bistable systems larger negative values of k_1 can be related to improved dissipation properties (Wu et al., 2022). Consequently, from a quantitative standpoint, the higher magnitude of k_1 observed under seismic excitation is expected to result in higher values of dissipated energy. The dissipation efficiency of the device under different types of excitations will be further discussed in Section 6.5.

6.5 Discussion on the efficiency of the device

Once the parameters were identified, the next step was to evaluate the dissipation capacity of the device. In the identification task, the parameters k_1 and k_3 were identified independently, leading to mono-dimensional distributions, mainly for computational reason. However, in order to calculate the dissipated energy, one should make a step forward. In particular, 1000 samples of k_1 and k_3 were extracted from the corresponding distributions (reported in Figure 6.14 and Figure 6.16). A bi-dimensional distribution was then calculated as KDE according to Eq. (6.11) over a grid of parameters $[k_1, k_3]$. From this bi-dimensional distribution, 200 samples of the couple (k_1, k_3) were extracted and used for the resolution of the bistable dynamics employing ODE45 solver in Matlab®. Finally, the dissipated energy $E_{d,cum}$ has been calculated as a cumulative function over time as:

$$E_{d,cum} = c \int \dot{y}(t)^2 dt \tag{6.12}$$

where c is the viscous damping coefficient, calculated on the basis of the damping ratio ζ, and kept constant, and $\dot{y}(t)$ is the velocity response of the system retrieved from the ODE resolution. Finally, the values of $E_{d,cum}$ have been fitted as KDE. The process has been repeated for the two external excitations considered, i.e., white noise and Aquila earthquake. Results for both input excitations are reported in Figure 6.17.

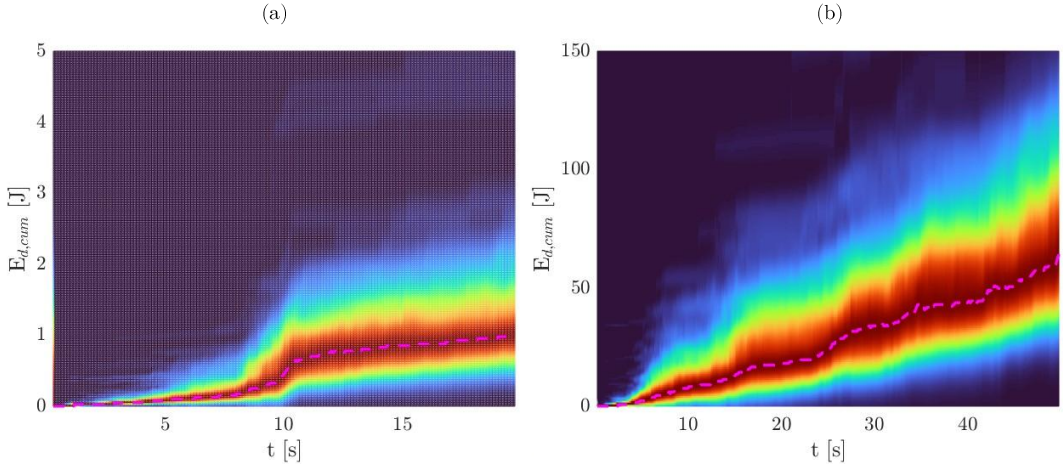

Figure 6.17. Cumulative dissipated energy under (a) white noise and (b) earthquake excitation and its mean value (pink dashed line).

When dealing with bistable systems, one should expect a sort of step in the increase of energy over time, due to the activation of the snap-though mechanism. This is clearly visible in both cases, looking at the mean value of the dissipated energy (i.e., the dashed pink line in Figure 6.17) for each instant. However, one

can make a distinction: in the case of white noise, one single step around 10 seconds is observable and a mean value of around $1\,J$ represents the maximum energy reachable under this kind of dissipation; in the case of the earthquake, there are several steps over time, given by the fact that the dissipation is continuously increasing, up to a dissipated energy of $64.82\,J$, that is more than 60 times the value obtained with white noise.

It is important to highlight that since the dashed pink line represents a mean value the confidence bounds should be carefully evaluated. In this respect, a difference in the confidence bounds of the dissipated energy is observable for the two excitations: the energy dissipated under seismic excitation presents larger confidence bounds (given by the red area and delimitated by the smaller green area) than the white noise case. This may be ascribed to the larger uncertainty of the parameters k_1 and k_3 in the identification task.

6.6 Conclusions

This chapter addressed the delicate problem of experimental identification of nonlinear systems, designing a specific setup for the controlled excitation and accurate measurement of the dynamic response of nonlinear oscillators. In this context, a new probabilistic instantaneous identification tool for bistable systems characterised by parameter uncertainty is proposed that combines time-frequency and probabilistic approaches. The estimation was validated experimentally on the signals recorded from a laboratory testing on a bistable sample, engineered for seismic energy dissipation. The identification proved robust under different types of excitations, and the cumulative instantaneous energy showed the effectiveness of the device, which represents a critical aspect in real-world applications.

This specific application was considered valid under the specific assumption of a perfectly elastic bistable model, with the rate-independent component, i.e., the stiffness restoring force, of the form reported in Equation (6.2). However, when dealing with experimental testing, especially under repeated loadings, this assumption may be restrictive. In this regard, Chapter 7 will explore different models and probabilistic identification techniques for considering the situation when the model describing the bistable dynamics is not perfectly elastic.

References

Abdessalem, A.B., Dervilis, N., Wagg, D., Worden, K., 2018. Model selection and parameter estimation in structural dynamics using approximate Bayesian computation. Mechanical Systems and Signal Processing 99, 306–325.

Ambati, S., Ambatipudi, R., 2022. Effect of infill density and infill pattern on the mechanical properties of 3D printed PLA parts. Materials Today: Proceedings 64, 804–807. https://doi.org/10.1016/j.matpr.2022.05.312

Beck, J.L., Katafygiotis, L.S., 1998. Updating Models and Their Uncertainties. I: Bayesian Statistical Framework. J. Eng. Mech. 124, 455–461. https://doi.org/10.1061/(ASCE)0733-9399(1998)124:4(455)

Ben Abdessalem, A., Dervilis, N., Wagg, D., Worden, K., 2018. Model selection and parameter estimation in structural dynamics using approximate Bayesian computation. Mechanical Systems and Signal Processing 99, 306–325. https://doi.org/10.1016/j.ymssp.2017.06.017

Bertoldi, K., Vitelli, V., Christensen, J., Van Hecke, M., 2017. Flexible mechanical metamaterials. Nature Reviews Materials 2, 1–11.

Ceravolo, R., 2008. Time–Frequency Analysis, in: Boller, C., Chang, F., Fujino, Y. (Eds.), Encyclopedia of Structural Health Monitoring. Wiley. https://doi.org/10.1002/9780470061626.shm047

Ceravolo, R., 2004. Use of instantaneous estimators for the evaluation of structural damping. Journal of Sound and Vibration 274, 385–401. https://doi.org/10.1016/j.jsv.2003.05.025

Ceravolo, R., Abbiati, G., 2013. Time Domain Identification of Structures: Comparative Analysis of Output-Only Methods. J. Eng. Mech. 139, 537–544. https://doi.org/10.1061/(ASCE)EM.1943-7889.0000503

Ceravolo, R., Erlicher, S., Zanotti Fragonara, L., 2013. Comparison of restoring force models for the identification of structures with hysteresis and degradation. Journal of Sound and Vibration 332, 6982–6999. https://doi.org/10.1016/j.jsv.2013.08.019

Chen, Y., Su, W., Tesfamariam, S., Qian, Z., Zhao, W., Yang, Z., Zhou, F., 2023. Experimental study of magnetic bistable nonlinear energy sink for structural seismic control. Soil Dynamics and Earthquake Engineering 164, 107572. https://doi.org/10.1016/j.soildyn.2022.107572

Cheng, C., Sa-Ngasoongsong, A., Beyca, O., Le, T., Yang, H., Kong, Z. (James), Bukkapatnam, S.T.S., 2015. Time series forecasting for nonlinear and non-stationary processes: a review and comparative study. IIE Transactions 47, 1053–1071. https://doi.org/10.1080/0740817X.2014.999180

Chiachio, M., Beck, J.L., Chiachio, J., Rus, G., 2014. Approximate Bayesian computation by subset simulation. SIAM Journal on Scientific Computing 36, A1339–A1358.

Csilléry, K., Blum, M.G.B., Gaggiotti, O.E., François, O., 2010. Approximate Bayesian Computation (ABC) in practice. Trends in Ecology & Evolution 25, 410–418. https://doi.org/10.1016/j.tree.2010.04.001

Ding, D., He, K.F., Qian, W.Q., 2021. A Bayesian Adaptive Unscented Kalman Filter for Aircraft Parameter and Noise Estimation. Journal of Sensors 2021, 9002643. https://doi.org/10.1155/2021/9002643

Dykstra, D.M., Lenting, C., Masurier, A., Coulais, C., 2023. Buckling metamaterials for extreme vibration damping. Advanced materials 35, 2301747.

Erazo, K., Nagarajaiah, S., 2017. An offline approach for output-only Bayesian identification of stochastic nonlinear systems using unscented Kalman filtering. Journal of Sound and Vibration 397, 222–240. https://doi.org/10.1016/j.jsv.2017.03.001

Fadel Miguel, L.F., Lopez, R.H., Ambrosini, D., 2025. Performance-based optimization of inerter-assisted T-NESs considering SSI effects. Mechanical Systems and Signal Processing 225, 112277. https://doi.org/10.1016/j.ymssp.2024.112277

Feldman, M., 2014. Hilbert transform methods for nonparametric identification of nonlinear time varying vibration systems. Mechanical Systems and Signal Processing 47, 66–77. https://doi.org/10.1016/j.ymssp.2012.09.003

Feldman, M., 1997. NON-LINEAR FREE VIBRATION IDENTIFICATION VIA THE HILBERT TRANSFORM. Journal of Sound and Vibration 208, 475–489. https://doi.org/10.1006/jsvi.1997.1182

Feldman, M., Braun, S., 2017. Nonlinear vibrating system identification via Hilbert decomposition. Mechanical Systems and Signal Processing 84, 65–96. https://doi.org/10.1016/j.ymssp.2016.03.015

Green, P.L., Worden, K., 2015. Bayesian and Markov chain Monte Carlo methods for identifying nonlinear systems in the presence of uncertainty. Phil. Trans. R. Soc. A. 373, 20140405. https://doi.org/10.1098/rsta.2014.0405

Habib, G., Romeo, F., 2018. Comparative analysis of NES and TMD performance via high-dimensional invariant manifolds, in: IUTAM Symposium on Exploiting Nonlinear Dynamics for Engineering Systems. Springer, pp. 143–153.

Hammond, J.K., White, P.R., 1996. THE ANALYSIS OF NON-STATIONARY SIGNALS USING TIME-FREQUENCY METHODS. Journal of Sound and Vibration 190, 419–447. https://doi.org/10.1006/jsvi.1996.0072

Huang, Y., Shao, C., Wu, B., Beck, J.L., Li, H., 2019. State-of-the-art review on Bayesian inference in structural system identification and damage assessment. Advances in Structural Engineering 22, 1329–1351. https://doi.org/10.1177/1369433218811540

Jasra, A., Singh, S.S., Martin, J.S., McCoy, E., 2012. Filtering via approximate Bayesian computation. Stat Comput 22, 1223–1237. https://doi.org/10.1007/s11222-010-9185-0

Liu, Q., Zhang, Y., Hou, Z., Qiao, Y., Cao, J., Lei, Y., 2023. Optimal Hilbert transform parameter identification of bistable structures. Nonlinear dynamics 111, 5449–5468.

Luengo, D., Martino, L., Bugallo, M., Elvira, V., Särkkä, S., 2020. A survey of Monte Carlo methods for parameter estimation. EURASIP J. Adv. Signal Process. 2020, 25. https://doi.org/10.1186/s13634-020-00675-6

Lye, A., Marino, L., Cicirello, A., Patelli, E., 2023. Sequential Ensemble Monte Carlo Sampler for On-Line Bayesian Inference of Time-Varying Parameter in Engineering Applications. ASCE-ASME Journal of Risk and Uncertainty in Engineering Systems, Part B: Mechanical Engineering 9, 031202. https://doi.org/10.1115/1.4056934

Magalhães, F., Cunha, Á., Caetano, E., Brincker, R., 2010. Damping estimation using free decays and ambient vibration tests. Mechanical Systems and Signal Processing 24, 1274–1290.

Mallat, S., Papanicolaou, G., Zhang, Z., 1998. Adaptive covariance estimation of locally stationary processes. Ann. Statist. 26. https://doi.org/10.1214/aos/1030563977

Nogueira, F.M., Barbosa, F.S., 2024. Novel approach for precise identification of vibration frequencies and damping ratios from free vibration decay time histories data of nonlinear single degree of freedom models. International Journal of Non-Linear Mechanics 167, 104867.

Norenberg, J.P., Cunha Jr, A., da Silva, S., Varoto, P.S., 2023. Probabilistic maps on bistable vibration energy harvesters. Nonlinear Dynamics 111, 20821–20840.

Parseh, M., Dardel, M., Ghasemi, M.H., 2015. Performance comparison of nonlinear energy sink and linear tuned mass damper in steady-state dynamics of a linear beam. Nonlinear Dynamics 81, 1981–2002.

Peter D., H., 1985. Kernel estimation of a distribution function. Communications in Statistics - Theory and Methods 14, 605–620. https://doi.org/10.1080/03610928508828937

Pinkaew, T., Lukkunaprasit, P., Chatupote, P., 2003. Seismic effectiveness of tuned mass dampers for damage reduction of structures. Engineering Structures 25, 39–46.

Ritto, T.G., Beregi, S., Barton, D.A.W., 2023. Reinforcement learning and approximate Bayesian computation (RL-ABC) for model selection and parameter calibration of time-varying systems. Mechanical Systems and Signal Processing 200, 110458. https://doi.org/10.1016/j.ymssp.2023.110458

Rogers, T.J., Friis, T., 2022. A latent restoring force approach to nonlinear system identification. Mechanical Systems and Signal Processing 180, 109426. https://doi.org/10.1016/j.ymssp.2022.109426

Schön, T.B., Lindsten, F., Dahlin, J., Wågberg, J., Naesseth, C.A., Svensson, A., Dai, L., 2015. Sequential Monte Carlo Methods for System Identification**This work was supported by the projects Learning of complex dynamical systems (Contract number: 637-2014-466) and

Probabilistic modeling of dynamical systems (Contract number: 621-2013-5524), both funded by the Swedish Research Council. IFAC-PapersOnLine 48, 775–786. https://doi.org/10.1016/j.ifacol.2015.12.224

Soong, T.T., Dargush, G.F., 1997. Passive energy dissipation systems in structural engineering. (No Title).

Tan, X., Cao, B., Liu, X., Zhu, S., Chen, S., Kadic, M., Wang, B., 2024. Negative stiffness mechanical metamaterials: a review. Smart Materials and Structures.

Tan, X., Wang, B., Wang, L., Zhu, S., Chen, S., Yao, K., Xu, P., 2022. Effect of beam configuration on its multistable and negative stiffness properties. Composite Structures 286, 115308. https://doi.org/10.1016/j.compstruct.2022.115308

Vakakis, A.F., Gendelman, O.V., Bergman, L.A., Mojahed, A., Gzal, M., 2022. Nonlinear targeted energy transfer: state of the art and new perspectives. Nonlinear Dyn 108, 711–741. https://doi.org/10.1007/s11071-022-07216-w

Vorkapić, M., Baltić, M., Fidanovski, B., Vasić, M., Bajić, D., 2025. Thermo-mechanical resistance of additively manufactured carbon fiber-reinforced PLA. Procedia Structural Integrity 72, 470–478.

Worden, K., Cross, E.J., 2025. A Tutorial on Data-Driven Methods in Nonlinear Dynamics, in: Nonlinear Structures & Systems, Volume 1. River Publishers, New York, pp. 51–70. https://doi.org/10.1007/978-3-031-36999-5_8

Worden, K., Hensman, J.J., 2012. Parameter estimation and model selection for a class of hysteretic systems using Bayesian inference. Mechanical Systems and Signal Processing 32, 153–169. https://doi.org/10.1016/j.ymssp.2012.03.019

Worden, K., Tomlinson, G.R., 2019. Nonlinearity in Structural Dynamics: Detection, Identification and Modelling, 1st ed. CRC Press. https://doi.org/10.1201/9780429138331

Wu, Z., Seguy, S., Paredes, M., 2022. Qualitative analysis of the response regimes and triggering mechanism of bistable NES. Nonlinear Dynamics 109, 323–352.

Yang, K., Zhou, Q., 2019. Robust optimization of a dual-stage bistable nonlinear vibration energy harvester considering parametric uncertainties. Smart Materials and Structures 28, 115018.

Zadpoor, A.A., 2016. Mechanical meta-materials. Materials Horizons 3, 371–381.

Zeng, Y.-C., Ding, H., Ji, J.-C., Mao, X.-Y., Chen, L.-Q., 2025. A tristable nonlinear energy sink with time-varying potential barriers. Communications in Nonlinear Science and Numerical Simulation 142, 108559.

Zhang, L.-Y., Xu, G.-K., 2015. Negative stiffness behaviors emerging in elastic instabilities of prismatic tensegrities under torsional loading. International Journal of Mechanical Sciences 103, 189–198.

Zuo, H., Zhu, S., 2022. Bistable track nonlinear energy sinks with nonlinear viscous damping for impulsive and seismic control of frame structures. Engineering Structures 272, 114982. https://doi.org/10.1016/j.engstruct.2022.114982

Chapter 7

Using the Bouc-Wen model for simulating bistable oscillators: numerical and experimental results

Chapter 6 illustrated the identification results obtained for a prototype of a bistable device for seismic energy dissipation subject to two different types of external excitations, namely white noise, and earthquake loading. In that case, the main assumption was that the system shows a bistable behaviour that, under ideal conditions and for excitations applied at the mid-span of the sample (Cazottes et al., 2009), can be described as perfectly elastic. However, when dealing with real world devices, this assumption does not always hold. In particular, when the external excitation reaches a high level of intensity, the response of the system rarely remains perfectly elastic, possibly due to some residual plastic deformation or other irreversible mechanisms. Even bistable devices that are explicitly designed to behave elastically may exhibits hysteretic loops during experimental cycles of snap-through, mainly as a consequence of non-ideal fabrication conditions. In this regard, Pan et al. (Pan et al., 2020) experimentally demonstrated that a compliant bistable device showed a clear hysteresis loop in the force-displacement profile with non-negligible loss of effective energy.

Deviations from elastic behaviour motivate the adoption of more sophisticated modelling strategies able to simulate these effects. Among others the Bouc-Wen model represents one of the most widely used formulations for the description of hysteretic phenomena. Originally introduced by the pioneering work of Bouc (Bouc, 1971, 1967) for ferromagnetic applications, it differed from the Volterra hereditary model (Volterra, 1928) in terms of the time used, shifting from the 'conventional' time (i.e., the clock one) to an internal (or intrinsic) time. This simple modification made it possible to effectively represent the dissipative evolution of nonlinear systems. The original work of Bouc was then the subject of

several extensions throughout the years. The most significant one is perhaps the one defined by Wen (Wen, 1976). This led to the large family of Bouc-Wen models, which nowadays serves as a standard for the modelling of hysteresis. A classification of different types of Bouc-Wen models based on the presence or absence of degradation is suggested in (Erlicher and Bursi, 2008). In particular, among degrading models, one may consider the case of strength degradation only, or strength/stiffness degradation. Also, a distinction between the models formulated for describing the material behaviour through stress-strain relationship (Casciati, 1989) and the structural behaviour by generalised force-displacement laws (Erlicher and Point, 2008) is carried out.

The classical Bouc-Wen model is a particular case of a single-valued restoring force defined as $\dot{f}_r = g(\dot{y}, f_r)$. The latter characterises a time-history dependent force, with the property of causality. The memory property is conversely associated with the state function g. In particular, the restoring force described by a Bouc-Wen model writes:

$$\dot{f}_r = A\dot{y} - \beta f_r |f_r|^{N-1}|\dot{y}| - \gamma |f_r|^N \dot{y} \tag{7.1}$$

with A as the linear stiffness parameter, and β, γ, and N constants affecting the shape of the hysteresis loop. Equation (7.1) can be rewritten as:

$$\begin{cases} f_r = A(y - y_h) \rightarrow \dot{f}_r = A(\dot{y} - \dot{y}_h) \\ \dot{y}_h = \beta(y - y_h)|A(y - y_h)|^{N-1}|\dot{y}| + \dfrac{\gamma}{A}|A(y - y_h)|^N \dot{y} \end{cases} \tag{7.2}$$

with y_h as an internal state variable representing the physical inelastic part of the response y. The use of y_h or f_r as internal state variable equivalently generates the memory effect. More importantly for this study, the Bouc-Wen model is rate independent, and it can be easily proved for each $p > 0$ (Visintin, 2013):

$$g(p \cdot \dot{y}, f_r) = p \cdot g(\dot{y}, f_r) \tag{7.3}$$

i.e., rate independence occurs only if the state function g is positively homogeneous of order 1 with respect to $\dot{y}$.

7.1 A modified Bouc-Wen model for simulating bistable dynamics

As stated before, the plasticisation effect on bistable systems needs to be explored in the cases where their dynamics cannot be described as perfectly elastic. Therefore, a classical Bouc-Wen model of Equation (7.1) modified to account for bistability is proposed here, forming the bistable Bouc-Wen (BBW)

model. This coupling is possible because the Bouc-Wen model is rate independent, and as introduced in Chapter 6, the bistable restoring force represents the rate independent component of the system, and the rate dependent one is related solely to the linear viscous damping. Accordingly, an equivalent nonlinear restoring force r_{BBW} considering both bistability and hysteresis can be defined as:

$$\begin{cases} r_{BBW} = r(y,\dot{y}) + k_3 y^3 \\ \dot{r} = g(\dot{y}, r, \boldsymbol{\theta}) \end{cases} \tag{7.4}$$

where r is the restoring force from the Bouc-Wen model as defined in Equation (7.1), slightly modified to account for the negative linear stiffness k_1 of a bistable system. The derivative of this restoring force component depends on the gradient of the displacement $\dot{y}$, corresponding to the velocity, the restoring force r, and a vector of model parameters $\boldsymbol{\theta}$. The latter can be expressed as:

$$\dot{r} = \dot{r}_L + \dot{r}_H = k_1\dot{y} + k_{BW}\dot{y} = [k_1 + k_{BW}]\dot{y} \tag{7.5}$$

where k_{BW} is an equivalent stiffness accounting for the hysteretic behaviour and is a function of the modal parameters $\theta = [\beta, \gamma, N]$, the velocity $\dot{y}$, and the restoring force r. It is defined as:

$$k_{BW} = -[\beta \cdot sign(\dot{u} \cdot r) + \gamma]|r|^N \tag{7.6}$$

The equation of motion that governs the combined BBW oscillator reads:

$$\begin{cases} m\ddot{y} + c\dot{y} + r_{BBW}(y,\dot{y}) = u(t) \\ r_{BBW} = r(y,\dot{y}) + k_3 y^3 \\ \dot{r} = \{k_1 - [\beta \cdot sign(\dot{y} \cdot r) + \gamma]|r|^N\}\dot{y} \end{cases} \tag{7.7}$$

where m is the mass, c the linear viscous damping, k_1 is the negative linear stiffness, and k_3 the positive cubic stiffness, as represented in Figure 7.1.

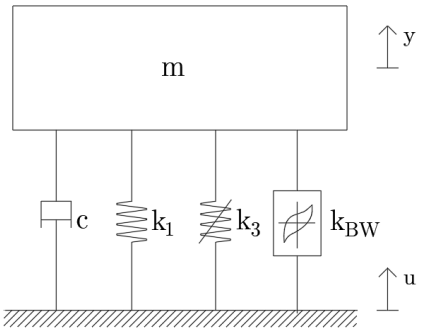

Figure 7.1. BBW model for a SDoF.

When dealing with Bouc-Wen model and/or its variations, it is fundamental to verify the thermodynamic admissibility conditions of the model considered (Ahmadi et al., 1997; Erlicher and Point, 2003). According to (Erlicher and Bursi, 2008), the thermodynamic admissibility is guaranteed when the dissipation associated with the hysteretic variable is non-negative, consistently with the second principle of thermodynamics. Chapter 6 identified the restoring force coming from the bistable dynamics as rate-independent and purely conservative, in the sense that it is derivable from an elastic potential. As a consequence, in the BBW model the thermodynamic admissibility depends only on the Bouc-Wen parameters, while the bistable component does not alter the dissipative balance of the system. Thus, the standard constraints of $\beta > 0$ and $-\beta < \gamma < \beta$ can be imposed without loss of generality (Erlicher and Bursi, 2008).

7.2 Numerical investigation

First, a parametric analysis was carried out to investigate the influence of Bouc-Wen parameters on the bistable dynamics. The linear and cubic stiffnesses k_1 and k_3 were fixed to $-693.08\ \mathrm{N/m}$ and $6.34 \times 10^5\ \mathrm{N/m^3}$, respectively. For what concerns the Bouc-Wen parameters, N was fixed equal to 2, in order to balance stability with physical relevance (Park et al., 1986). Six combinations of the model parameters $\boldsymbol{\theta}$ were considered, as reported in Table 7.1. Results of the parametric study are shown in Figure 7.2 and Figure 7.3.

Table 7.1. Numerical values assumed for the Bouc-Wen model parameters.

Model set	β	γ	N
$\boldsymbol{\theta}_1$	0.5	-0.4	2
$\boldsymbol{\theta}_2$	0.5	0.4	2
$\boldsymbol{\theta}_3$	10	-9	2
$\boldsymbol{\theta}_4$	10	9	2
$\boldsymbol{\theta}_5$	100	-99	2
$\boldsymbol{\theta}_6$	100	99	2

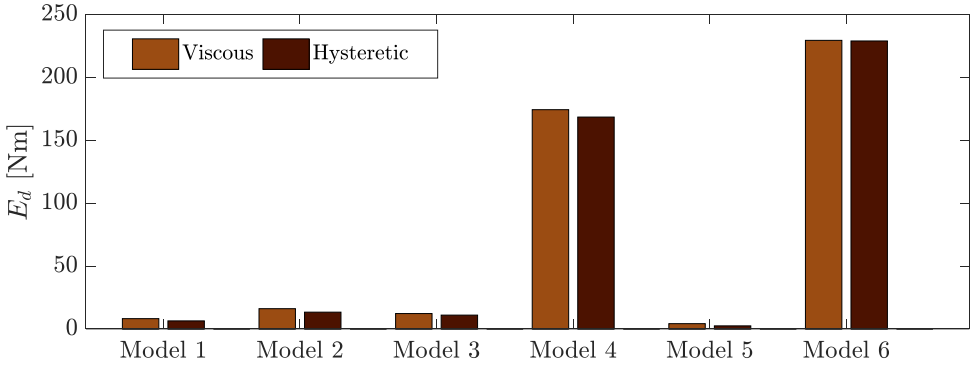

Figure 7.2. Viscous and hysteretic dissipated energy for each model set.

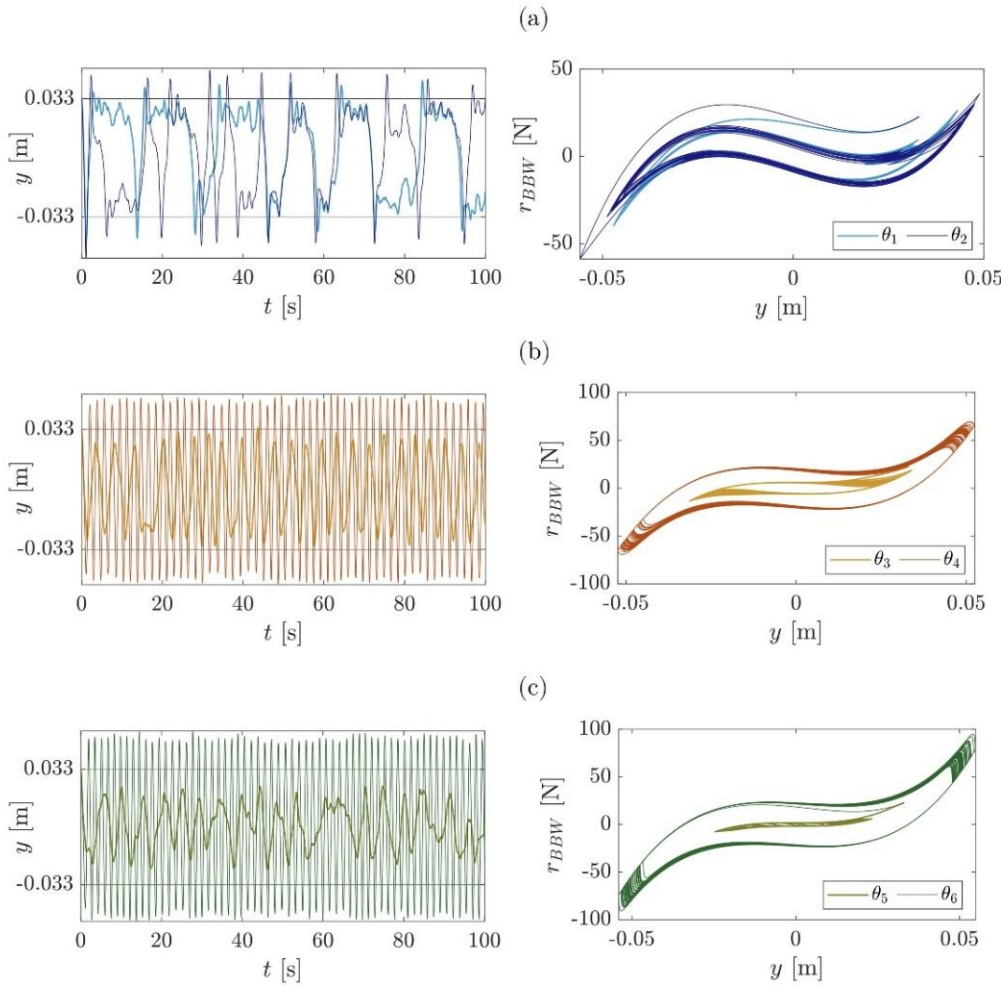

Figure 7.3. Results of the parametric study for the BBW model for the set of model parameters (a) $\boldsymbol{\theta}_1$ - $\boldsymbol{\theta}_2$, (b) $\boldsymbol{\theta}_3$ - $\boldsymbol{\theta}_4$, and (c) $\boldsymbol{\theta}_5$ - $\boldsymbol{\theta}_6$.

The parametric study aimed to explore bistability-hysteresis interplay for energy dissipation: the higher are the Bouc-Wen parameters, the less the bistable dynamics influences the response of the system. A good trade-off can be found in the case of the models $\boldsymbol{\theta}_1$ - $\boldsymbol{\theta}_2$, see Figure 7.3(a). These results allowed the determination of an equivalent damping ratio ζ_{eq} for each of the six proposed model sets, as reported in Table 7.2, demonstrating that the hysteresis nearly doubles the viscous dissipation.

Table 7.2. Equivalent damping ratio for each model set.

Model	$\boldsymbol{\theta}_1$	$\boldsymbol{\theta}_2$	$\boldsymbol{\theta}_3$	$\boldsymbol{\theta}_4$	$\boldsymbol{\theta}_5$	$\boldsymbol{\theta}_6$
ζ_{eq}	5.3 %	5.5 %	5.7 %	5.9 %	4.7 %	6.0 %

As subsequent step of the numerical validation, the procedure proposed in Chapter 5 employing a WVD has been applied in order to identify both the bistable and Bouc-Wen parameters. The results of the procedure for the model set $\boldsymbol{\theta}_2$ under a unitary white Gaussian noise are reported in Figure 7.4.

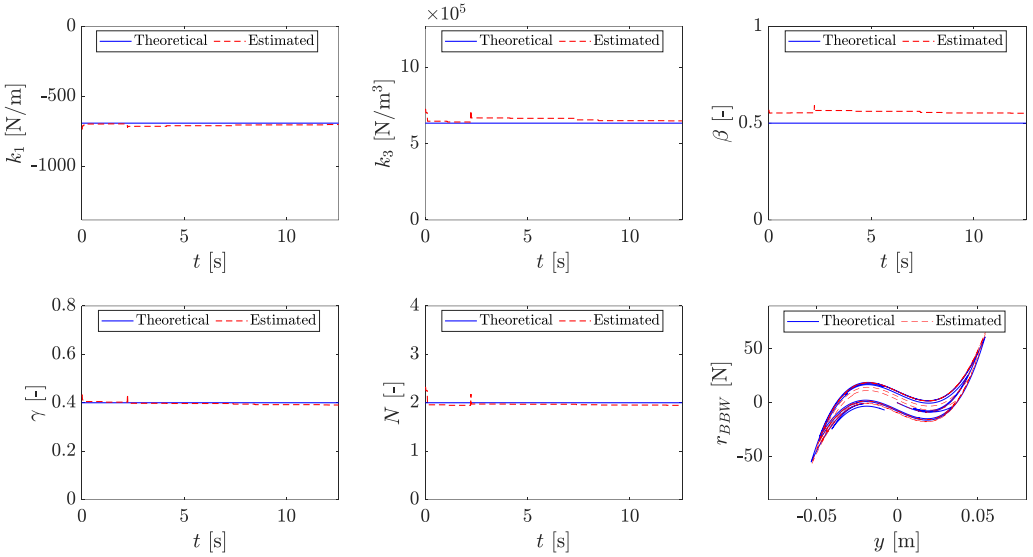

Figure 7.4. Bistable and Bouc-Wen parameters estimation results for the proposed model using the time-frequency procedure of Chapter 5.

7.3 Experimental validation

The testing campaign, as extensively described in Chapter 6, allowed the acquisition of different kinds of response signals of the bistable sample. In particular, for the purposes of validating the model of Equation (7.7), the response signal obtained from a sinusoidal input excitation scaled at 3.3 V has been employed, as reported in Figure 7.5.

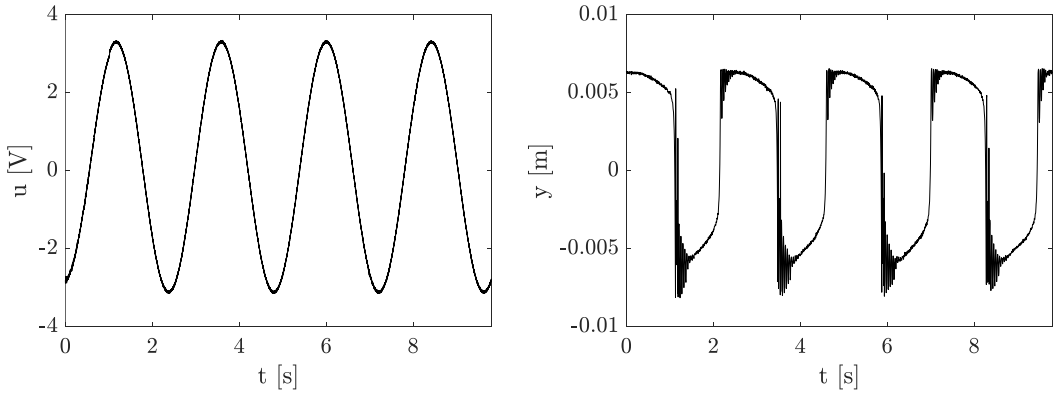

Figure 7.5. Input excitation and displacement response of the bistable sample.

The presence of hysteretic components of the dynamic response is made it clear from Figure 7.6. In particular the stiffness restoring force $f_{r,s}$ is calculated in three different cases: (i) the experimental case, (ii) the bistable case which assumes a purely elastic behaviour (i.e., the Bouc-Wen parameters are equal to zero) and (iii) using the BBW model proposed here. In particular, the purely elastic model is calculated using the values of $k_1 = -1.96 \times 10^3$ N/m and $k_3 = 7.79 \times 10^7$ N/m^3 as estimated from the identification procedure based on the

Hilbert transform (for reference, see Chapter 2) in Chapter 6. The same values have been employed to calculate the stiffness restoring force of the BBW model with the following Bouc-Wen parameter set $\boldsymbol{\theta} = [0.5,\ 0.4,\ 2]$, corresponding to the model set $\boldsymbol{\theta}_2$. Two main considerations can be derived from Figure 7.6. First, the bistable behaviour is clearly asymmetric. A bistable system is said to be asymmetric when one direction of actuation requires less energy than the other, facilitating the activation of snap-through in that direction, and this is reflected in the force-displacement curve (Chang et al., 2020). Asymmetry is a crucial parameter in mechanism design as it influences the onset of hysteresis during activation (Megret et al., 2025). Second, one should consider that this asymmetry may stem from multiple sources, starting from the geometry itself (Shan et al., 2015). Moreover, when dealing with 3D printed samples, as in this case, the mechanical properties of the sample can be influenced by several factors, such as the infill density and the light exposure of the material.

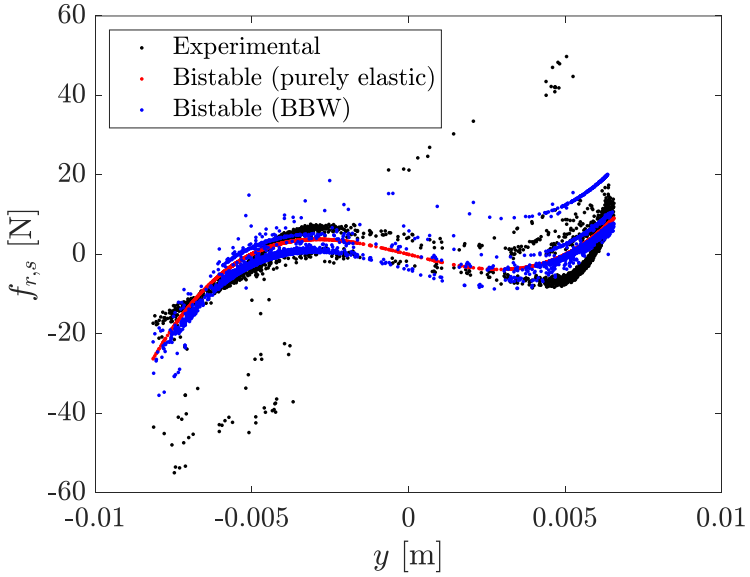

Figure 7.6. Stiffness restoring force: experimental, purely elastic bistable, and BBW model.

7.3.1 A probabilistic version of UKF to deal with uncertainties in complex models

As already stated in Chapter 6, Bayesian approaches do not provide an exact analytic form of the posterior distribution of parameters, rather its approximate form based on the observed data. If the number of parameters increases and the model structure becomes more complex, as in the case of the BBW model, the poster distribution may assume irregular shapes, making impractical not to assume a prior distribution.

In this case, the use of the Markov Chain Monte Carlo (MCMC) methods (Geyer, 1992) represents a good compromise making it possible to numerically

approximate the posterior distribution even for complex cases. The MCMC method basically relies on the idea of building a chain of values progressively exploring the parameter space in such a way that, after a certain number of iterations, the sample distribution coincides with the desired posterior distribution. It is therefore a stochastic and iterative process, in which every state depends only on the previous state, based on the Markov principle.

The Metropolis-Hastings is one of the most common MCMC algorithms to generate samples from a target distribution (Chib and Greenberg, 1995; Yildirim, 2012). Differently from traditional Monte Carlo methods, the Metropolis-Hastings algorithm employs a density depending on the current state of the chain, avoiding the loss of efficiency typical of such methods. The Metropolis-Hastings method can be schematised as follows:

1. Initialisation of parameters and proposed density.

2. Iteration on each step where: (i) a candidate is generated for the next sampling; (ii) calculation of acceptance probability; (iii) extraction of a random number; (iv) if the random number is lower than the acceptance probability, it is accepted.

By repeating this procedure, one can obtain the sequence of points constituting a Markov Chain. However, the MCMC method, as in the case of ABC, does not include an instantaneous evaluation of the parameters to estimation. Therefore, it should be combined with one of the methods allowing an instantaneous implementation, and thus suitable for time-varying responses, such as the ones reported in Chapter 3. In particular, here, starting from the work of (Erazo and Nagarajaiah, 2017), a similar algorithm, which combines the UKF (Julier et al., 2002) and MCMC of type Metropolis-Hastings, has been implemented. This sequential UKF-MCMC algorithm produces a temporal distribution of parameters with an automatic adaptive step MCMC as a function of a predefined acceptance rate.

A pseudocode of the algorithm is reported in Algorithm 3. To summarise, at each time step t_k, the UKF predicts and corrects the system state $\mathbf{x}_k = [y_k, \dot{y}_k]$, while the logarithmic parameters ϕ_1 and ϕ_3 are updated through a local MCMC chain, which provides a posterior distribution estimate $p(\phi \mid y_{1:k})$.

Algorithm 3: UKF-MCMC numerical implementation

Initialisation:
Log-parameters ϕ
Augmented state vector $\mathbf{x}_k$
Gaussian prior on log-parameters $\phi \sim N(\mu_\phi, \sigma_\phi)$
for $t_k = 1{:}\,t_N$
  $\mathbf{x}_{k\,|\,k-1} = f(\mathbf{x}_{k-1\,|\,k-1}, u_k)$ — *Prediction*
  $\hat{y}_k = h(\mathbf{x}_{k\,|\,k-1}), \mathbf{x}_{k\,|\,k} = \mathbf{x}_{k\,|\,k-1} + K_k(y_k - \hat{y}_k)$ — *Updating*
  For $s = 1, \dots, N_{MCMC}$
    $\phi^* = \phi^{(s-1)} + \varepsilon_s$ with $\varepsilon_s \sim N(0, \sum_q)$ — *Proposed distribution*
    $\log p^* = \log p\,(\phi^* | y_{1:k})$ — *Proposed log-posterior*
    $\log p^{(s-1)} = \log p\,(\phi^{(s-1)} | y_{1:k})$ — *Current log-posterior*
    $\alpha = min\{1, \exp(\log p^* - \log p^{(s-1)})\}$ — *Acceptance coefficient*
    $u \sim U(0,1)$
    If $u < \alpha$
      $\phi^{(s)} = \phi^*$
    else
      $\phi^{(s)} = \phi^{(s-1)}$
    end
    $p^{(s)}(t_k) = -e^{\phi^{(s)}}$
  end
  $\bar{p}(t_k) = \frac{1}{N_{MCMC}} \sum_{s=1}^{N_{MCMC}} p^{(s)}(t_k)$ — Posterior mean
  $\phi_k = log(-\bar{p}(t_k))$ — Update initial state
end

7.3.2 Results

The procedure described by Algorithm 3 has been implemented in Matlab® for identifying the parameters describing the system with the experimental response of Figure 7.5. In Chapter 4, an augmented version of the UKF has been implemented to consider the parameters to estimate along with the states of the system. The same has been done here, where the parameters to be estimated include the negative linear stiffness k_1, the positive cubic stiffness k_3, and the Bouc-Wen parameters β and γ. In this case, the parameter N is assumed to be known and equal to 2, since the previous numerical analysis proved a good correspondence for a fixed value of $N = 2$. Chapter 3 highlighted the importance of choosing the proper parameters for having reliable results from filtering. Accordingly, the process covariance matrix has been built to give to the filter the possibility of exploring the parameter space, given the logarithmic nature of the log-parameters. The same reasoning was carried out for measurement noise, calculated directly from the observed data, and regularised with a value of 10^{-4}.

Figure 7.7 shows the MCMC realisations over time of k_1, k_3, β and γ estimated using the UKF-MCMC algorithm. Basically, these realisations are based on 100 samples for each parameter and are formed starting from a likelihood-function on the data and a Gaussian log-prior distribution centred on the measured values.

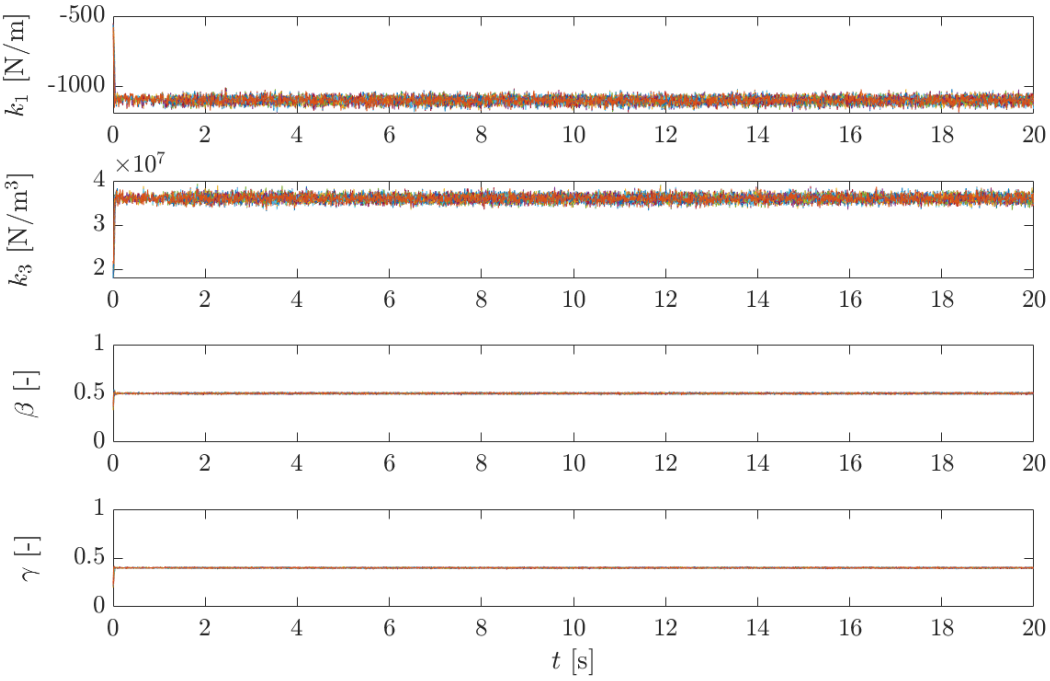

Figure 7.7. MCMC realisations of BBW model parameters in time.

It can be deducted that all the parameters tend to converge to the real value. However, this kind of representation has two major drawbacks: (i) first, it is complex to read, since it is substantially a superposition of different curves; (ii) it does not provide a real distribution of the parameters over time, complicating the evaluation of the confidence bounds of the parameters, as already successfully done in Chapter 6.

Thus, a second more insightful representation can be found in Figure 7.8, Figure 7.9, Figure 7.10, and Figure 7.11. An approximation of the posterior distribution can be found, allowing the evaluation of the confidence interval and the tails for each parameter. Generally, it can be said that the estimation proves to be reliable in all case, leading to stable estimates over time. Going into greater detail for each parameter:

- The negative linear stiffness k_1 shows limited confidence bounds around its mean value, corresponding to the true value of the parameter already identified. This confirms what already found in Chapter 6: this is the most important parameter for the *interwell* dynamics, and thus it is the most stable.

- Conversely, the positive cubic stiffness k_3 holds extended confidence bounds. Indeed, the latter governs the *intrawell* dynamics, and its impact is less pronounced. Practically speaking, this means that variations of k_3 do not crucially influence the bistable dynamics, especially when the interwell motion is repeated over time.

- Finally, for what concerns the Bouc-Wen parameters, it is clear that the values chosen as initial guesses are a good trade-off, as already noticed from the parametric analysis. In this case the confidence bounds remain narrower than the ones observed for the k_3 parameter, proving the validity of the proposed model in the identification procedure.

An important observation that can be derived from these results is that in all cases, except for k_1, a transitory phase where the parameter is unstable is present. This aspect was not clear from Figure 7.7.

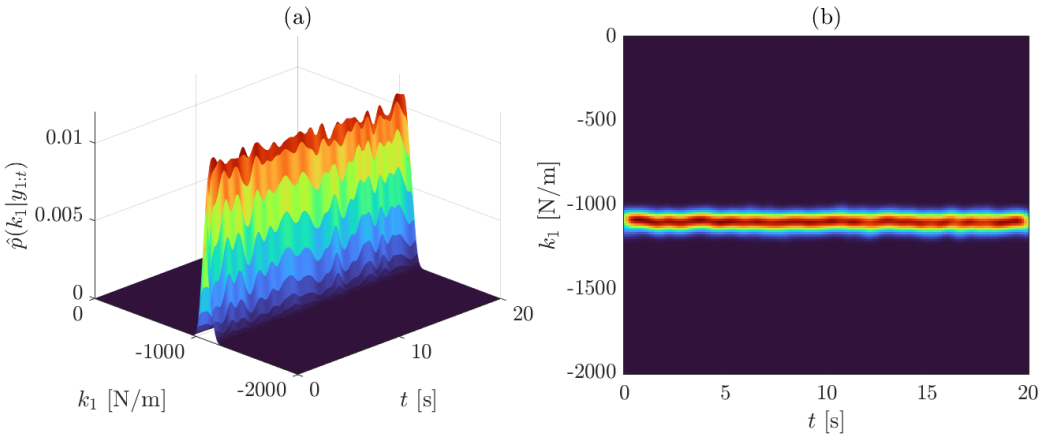

Figure 7.8. UKF-MCMC estimated negative linear stiffness k_1: (a) instantaneous posterior distribution estimate and (b) top-view of the distribution over time.

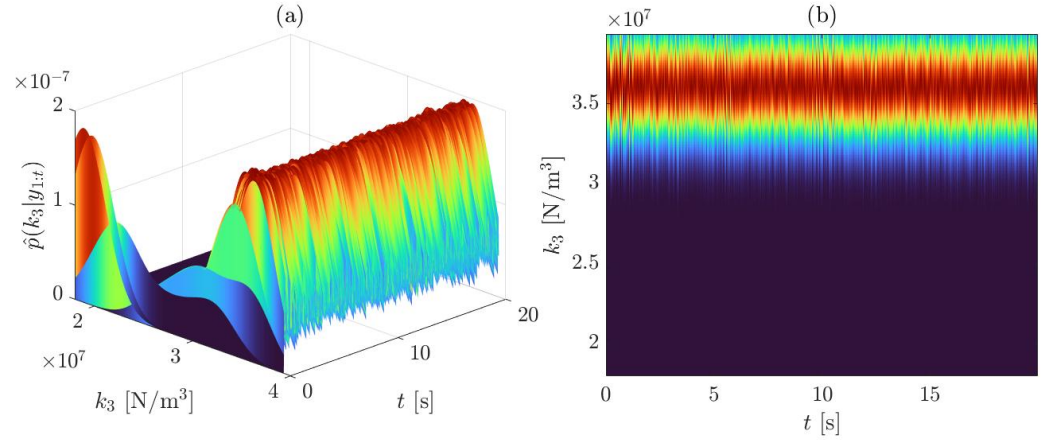

Figure 7.9. UKF-MCMC estimated positive cubic stiffness k_3: (a) instantaneous posterior distribution estimate and (b) top-view of the distribution over time.

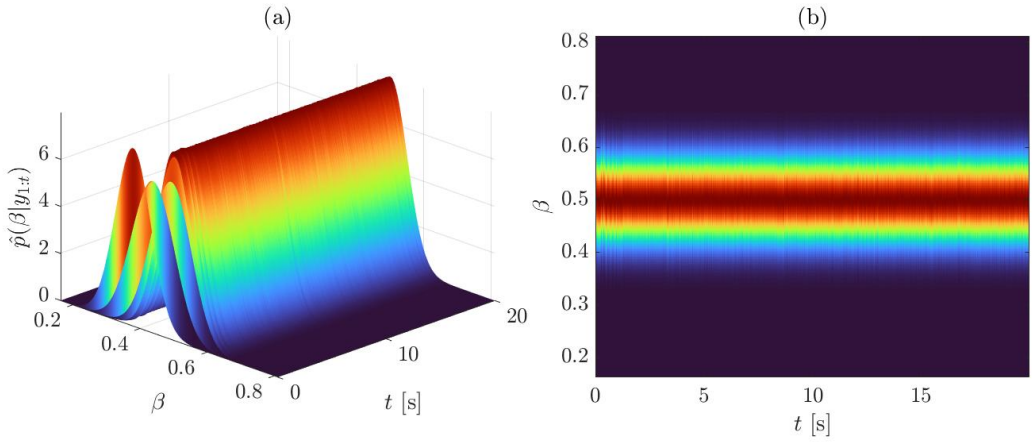

Figure 7.10. UKF-MCMC estimated Bouc-Wen parameter β: (a) instantaneous posterior distribution estimate and (b) top-view of the distribution over time.

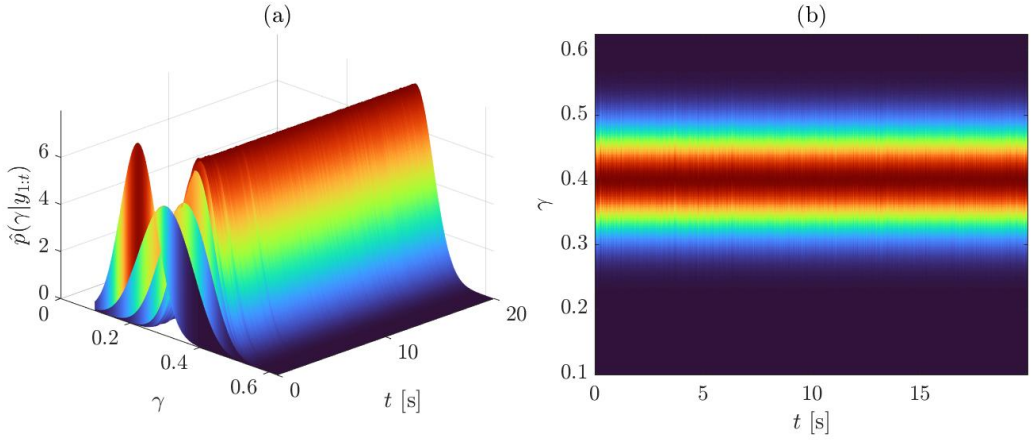

Figure 7.11. UKF-MCMC estimated Bouc-Wen parameter γ: (a) instantaneous posterior distribution estimate and (b) top-view of the distribution over time.

7.4 Discussion and conclusions

This chapter aimed to propose and validate, through a customised nonlinear identification procedure, a BBW model for representing bistable dynamics when the system response is not perfectly elastic. This issue is of particular significance in real-world cases, where high-intensity excitations or non-ideal fabrication conditions can induce hysteretic-like force-displacement profiles. In those cases, it can be convenient to assume a priori distribution for each parameter involved in the nonlinear identification task, due to its higher computational complexity. Thus, an instantaneous algorithm based on MCMC has been specifically designed and implemented.

The simulations performed in this chapter were designed to investigate the behaviour of the novel Bouc-Wen model incorporating bistable dynamics under such non-ideal conditions. In particular, the experimental response of the 3D-

printed bistable sample as introduced and described in Chapter 6 was employed for this purpose. More specifically:

(i) A numerical parametric simulation was carried out to investigate the effects of the Bouc-Wen parameters on the system dynamics. It was proved that, for a constant value of $N = 2$, a trade-off between bistable and Bouc-Wen parameters is always present. A further numerical validation was provided employing the methodology relying on quadratic time-frequency transform proposed in Chapter 5, proving the goodness of the model for an identification procedure whose parameters were known a-priori.

(ii) A probabilistic identification procedure, namely UKF-MCMC, was performed on the experimental response of the sample subject to harmonic excitation. The UKF-MCMC proved robust and reliable, compared also with the previous deterministic identification results employing a quadratic time-frequency transform.

Part of the work described in this chapter was also published in a paper (Cavanni et al., 2025).

References

Ahmadi, G., Fan, F.C., Noori, M., 1997. A thermodynamically consistent model for hysteretic materials. Iranian Journal of Science and Technology 21, 257–278.

Bouc, R., 1971. Modele mathematique d'hysteresis. Acustica 21, 16–25.

Bouc, R., 1967. Forced vibrations of mechanical systems with hysteresis. Presented at the Proc. of the Fourth Conference on Nonlinear Oscillations, Prague, 1967.

Casciati, F., 1989. Stochastic dynamics of hysteretic media. Structural Safety 6, 259–269. https://doi.org/10.1016/0167-4730(89)90026-X

Cavanni, V., Scussolini, L., Bursi, O.S., Coulais, C., Ceravolo, R., 2025. Simulation and Identification of a Seismic Bistable Device with Hysteresis, in: 2025 Nineteenth International Congress on Artificial Materials for Novel Wave Phenomena (Metamaterials). IEEE, p. X-055-X–057.

Cazottes, P., Fernandes, A., Pouget, J., Hafez, M., 2009. Bistable buckled beam: modeling of actuating force and experimental validations.

Chang, P.-L., Chi, I.-T., Tran, N.D.K., Wang, D.-A., 2020. Design and modeling of a compliant gripper with parallel movement of jaws. Mechanism and Machine Theory 152, 103942.

Chib, S., Greenberg, E., 1995. Understanding the metropolis-hastings algorithm. The american statistician 49, 327–335.

Erazo, K., Nagarajaiah, S., 2017. An offline approach for output-only Bayesian identification of stochastic nonlinear systems using unscented Kalman filtering. Journal of Sound and Vibration 397, 222–240.

Erlicher, S., Bursi, O.S., 2008. Bouc–Wen-Type Models with Stiffness Degradation: Thermodynamic Analysis and Applications. J. Eng. Mech. 134, 843–855. https://doi.org/10.1061/(ASCE)0733-9399(2008)134:10(843)

Erlicher, S., Point, N., 2008. Pseudopotentials and Loading Surfaces for an Endochronic Plasticity Theory with Isotropic Damage. J. Eng. Mech. 134, 832–842. https://doi.org/10.1061/(ASCE)0733-9399(2008)134:10(832)

Erlicher, S., Point, N., 2003. Thermodynamic admissibility of Bouc–Wen type hysteresis models. Comptes Rendus. Mécanique 332, 51–57. https://doi.org/10.1016/j.crme.2003.10.009

Geyer, C.J., 1992. Practical markov chain monte carlo. Statistical science 473–483.

Julier, S., Uhlmann, J., Durrant-Whyte, H.F., 2002. A new method for the nonlinear transformation of means and covariances in filters and estimators. IEEE Transactions on automatic control 45, 477–482.

Megret, K., Dirrenberger, J., Monnoyer, J., Sollogoub, C., Goislard de Monsabert, B., Fernandez, L., Delalande, S., Viollet, S., 2025. An energetic approach

for comparing monomaterial compliant bistable mechanisms. Journal of Mechanical Design 147, 123301.

Pan, D., Wu, Z., Dai, F., Tolou, N., 2020. A novel design and manufacturing method for compliant bistable structure with dissipated energy feature. Materials & Design 196, 109081.

Park, Y.J., Wen, Y.K., Ang, A.H., 1986. Random vibration of hysteretic systems under bi-directional ground motions. Earthq Engng Struct Dyn 14, 543–557. https://doi.org/10.1002/eqe.4290140405

Shan, S., Kang, S.H., Raney, J.R., Wang, P., Fang, L., Candido, F., Lewis, J.A., Bertoldi, K., 2015. Multistable architected materials for trapping elastic strain energy. Adv. Mater 27, 4296–4301.

Visintin, A., 2013. Differential models of hysteresis. Springer Science & Business Media.

Volterra, V., 1928. Sur la théorie mathématique des phénomènes héréditaires. Journal de mathématiques pures et appliquées 7, 249–298.

Wen, Y.-K., 1976. Method for random vibration of hysteretic systems. Journal of the engineering mechanics division 102, 249–263.

Yildirim, I., 2012. Bayesian inference: Metropolis-hastings sampling. Dept. of Brain and Cognitive Sciences, Univ. of Rochester, Rochester, NY.

Conclusions

The identification of nonlinear systems benefits from a considerable amount of research and studies conducted by the scientific community over the last decades. As known from literature, a first key challenge is ensuring that in experimental tests nonlinearity is sufficiently activated to be observable. This limits the potential of nonlinear identification to all applications, primarily industrial, where it is possible to perform tests specifically designed for controlled laboratory environments and, above all, where human safety is not at stake. Nonetheless, in the specific field of earthquake engineering, advancing the performance-based approach requires: (i) data obtained from experimental tests, particularly those related to collapse, rate-of-loading, full-scale and structural systems, where data are scarce; (ii) nonlinear and hysteretic models, often time-varying (e.g., with stiffness degradation, strength deterioration, slip, etc.), simple enough to allow extensive parametric simulations. Furthermore, the availability of nonlinear mathematical models easily allows the development of passive and active control laws for nonlinear systems. In this context, research should combine the advantages of: (i) efficient and specifically designed test techniques, and (ii) nonlinear identification techniques capable of capturing the nonlinear, time-varying, and hereditary characteristics of the inelastic restoring forces and damping.

Even in the field of nonlinear identification, there are well-established techniques that, when applied under controlled conditions, have demonstrated their effectiveness. However, when applied to full-scale structures, they suffer from limitations stemming from the inability to fully measure the excitations (e.g., environmental actions, wind, etc.). Methods based on statistical response assumptions, so developed and successful in civil structures (e.g., operational modal analysis), suffer from the difficulty of disentangling nonlinearity from non-stationarity. To overcome these limitations, it is often appropriate to consider and, ultimately, tailor procedures for signals that usually allow temporal localisation of the spectral components. Along with this aspect, what emerges from the scientific literature is that nonlinear identification is strictly case-dependent and, eventually, user-oriented, leading to the impossibility of defining a unique technique valid for all the possible scenarios.

Within this framework, the present thesis work aims to propose some novel tools for the identification of nonlinear and time-varying systems when these are subject to earthquakes or, more generally, dynamic actions of interest for civil engineering structures.

The main original contributions of this thesis can be summarised as follows:

- An instantaneous identification method for nonlinear and time-varying structural systems under random excitation was formulated using Volterra-based modelling and linear time-frequency representations, extending local stationarity to nonlinear systems through a composite FRF, and validated numerically on Duffing-type systems.

- The energetic nature of quadratic time-frequency transforms, in particular the Wigner-Ville distribution, was exploited in combination with perturbative Volterra approaches, i.e., ALEs, to generalise the identification problem to markedly non-stationary responses, including those typical of bistable dynamics.

- Experimental identification was carried out on a bistable seismic energy dissipation device using a dedicated prototype testing machine and instantaneous probabilistic formulations under both perfectly elastic and Bouc-Wen modelling assumptions, demonstrating robust parameter estimation even at large response amplitudes.

Despite the novel contributions of this thesis, the systematic application of nonlinear identification tools in real-world SI tasks still faces challenges. These include increased computational complexity when identifying linear and nonlinear parameters simultaneously, limitations in observability and identifiability, and practical constraints on large-scale experimental datasets. Future research should focus on extending the modelling framework to include nonlinear damping and formalising observability and identifiability requirements, while the results of this thesis provide an encouraging foundation for reliable applications in earthquake engineering.